Development of Novel CO_2-Selective Chitosan Membrane Blended with Synthetic Amines and Natural Amines of Silk Fibroin and Sericin

A Thesis

Submitted in Partial

Fulfilments of the Requirements for the Degree of

DOCTOR OF PHILOSOPHY

by

Babul Prasad
(136107008)

Department of Chemical Engineering

Indian Institute of Technology Guwahati

Guwahati, Assam 781039

January 2019

Dedicated

To

My Parents and My Mentor

Department of Chemical Engineering
Indian Institute of Technology Guwahati
Guwahati, Assam 781039

STATEMENT

I hereby declare that the content embodied in this thesis entitled "**Development of Novel CO_2-Selective Chitosan Membrane Blended with Synthetic Amines and Natural Amines of Silk Fibroin and Sericin**" is the result of investigations carried out by me at the Department of Chemical Engineering, Indian Institute of Technology Guwahati, Guwahati, India, under the guidance of Prof. Bishnupada Mandal. In keeping with the general practice of reporting scientific observations, due acknowledgements have been made wherever the work described is based on the findings of other investigators.

January, 2019 Babul Prasad

Department of Chemical Engineering
Indian Institute of Technology Guwahati
Guwahati, Assam 781039

CERTIFICATE

It is certified that the work described in this thesis, entitled "**Development of Novel CO_2-Selective Chitosan Membrane Blended with Synthetic Amines and Natural Amines of Silk Fibroin and Sericin**", done by **Mr. Babul Prasad** (Roll No. 136107008) for the award of degree of Doctor of Philosophy is an authentic record of the results obtained from the research work carried out under my supervision in the Department of Chemical Engineering, Indian Institute of Technology Guwahati, India and this work has not been submitted elsewhere for the award of any other degree or diploma.

This thesis in my opinion, has reached the standard fulfilling the requirements for the award of the degree of Doctor of Philosophy in accordance with the regulations of the institute.

January, 2019

(**Prof. Bishnupada Mandal**)
Professor & Head
Department of Chemical Engineering
Indian Institute of Technology Guwahati
Guwahati 781039, India

ACKNOWLEDGEMENTS

The completion of this thesis would have not been possible without the support and encouragement of various people and institution. I take this opportunity to thank all those people and institution who have been an integral part in successful completion of this thesis.

At the onset, I would like to express my sincere thanks to my research supervisor ***Prof. Bishnupada Mandal*** *for his valuable guidance which allowed me to grow as a researcher. His approval for adequate freedom to think, plan and execute the research ideas provided a good basis for the present thesis. His positive attitude, encouragement, valuable guidance towards the research helped me to perform and complete the research objectives. His support in doing the experiments, analysis of the data and preparing the manuscripts are invaluable. I am fortunate enough to complete my thesis under his supervision. It has really been a notable working experience with him.*

I shall always be obliged to my doctoral committee chairman ***Prof. G. Pugazhenthi,*** *Department of Chemical Engineering, for his valuable suggestions, evaluation and proper direction during my progress review seminars. I would also like to thank* ***Prof. Vimal Katiyar,*** *Department of Chemical Engineering and* ***Prof. Parameswar K. Iyer,*** *Department of Chemistry, for their valuable suggestions, time and efforts.*

My special thanks to ***Prof. Sasidhar Gumma*** *for helping me during GC operation.*

The Department of Science and Technology (DST), New Delhi, Government of India, INDIA (Grant No. DST/TSG/NTS/2015/73), is acknowledged here for their financial support.

Various instruments used for characterization during the research work carried at IIT Guwahati specifically, Analytical Lab Facility (Department of Chemical Engineering), Centre of Excellence for Sustainable Polymers (CoE-SusPol), Central Instrument Facility (CIF) and Centre for Nanotechnology for AFM analysis.

Further, I would like to acknowledge Robin Simpson from Thermofisher Scientific, for his kind help in performing and analysis of the XPS data in the thesis.

I am also grateful to all the ***staff and faculty members*** *of Department of Chemical Engineering for helping and providing the necessary facilities.*

*I would like to thank all my **seniors (**Dr. Arijit Mondal, Dr. Sanjib Barma. Dr. Bisweswar Das, Dr. Rupak Kishor, Abhik, Satya**)**, **Colleagues (**Rajashree, Pradip, Mridusmita, Baite, Ramesh, Arun, Himali, Ankur, Lokesh, Bhargavi**)**, **friends (**Shasanka, Dibyajyoti, Ram, Jiten, Randeep, Dibakar**)** and other **well-wishers** who helped me to complete my research.*

*I express my gratitude to my beloved **parents, brother, sister, mother-in law** for showering their love, care, sacrifices and encouragement which have made it possible for me to come so far. Finally, and most importantly, I would like to thank my wife **Sharbani Kaushik** who has been with me all these years with her love, support, encouragement, and appreciations. She stands with me personally as well as professionally. Thank you for being my muse, editor, proof-reader, and sounding board. But most of all, thank you for being my best friend. I owe you everything.*

Babul Prasad

Contents

CHAPTER 3

CHAPTER 4

CHAPTER 5

Abstract

The major objective of the present work is to develop a thermally stable biopolymer-based membrane for CO_2 separation using facilitated transport mechanism. The biopolymer chitosan (CS) enables facilitated transport of CO_2 by dint of the amine group present in its structure, is thermally stable in absence of crosslinking and possess good film forming ability. The CO_2 permeance of the CS membrane with poly(ether sulfone) (PES) as a support, was 12.5 GPU and CO_2/N_2 selectivity was 54 at 90 °C with water flow rate of 0.03/0.05 ml/min (feed/sweep) and absolute pressure of 2/1.21 bar (feed/sweep) for binary gas mixture. The pristine CS membrane proved to be thermally stable under the operating conditions. Hence, the CS membrane was further explored by incorporation of synthetic and natural amines as carriers for improving and facilitating the transport of CO_2 gas molecules. There exists only one amine group per monomer of the CS polymer that can act as carrier. In order to increase the total amine content in the active layer, tetraethylenepentamine (TEPA) was blended and the CO_2 separation performance was evaluated. The CO_2 permeance increased two fold as compared to pure CS membrane to 24.7 GPU and CO_2/N_2 selectivity reached to 80 by blending 30 wt % of TEPA, at similar operating conditions. The poly(allylamine) (PAA) consists of mainly primary amine groups which is very brittle in the dry state with inability to form stable films alone. The blending of PAA with CS at optimized content of 70 wt % of CS and 30 wt % of PAA (PAA30) resulted in further improvement in the CO_2 separation performance. However, CO_2 separation with long-term stability, simultaneously with high permeance through eco-friendly and cost-effective materials is of utmost concern. Hence, a novel approach was undertaken to substitute the synthetic amines by the inherent amines of another versatile biopolymer silk fibroin (SF). In the rational blend of the two biopolymers (CS/SF): CS acted as a matrix and SF aided CS as a carrier for CO_2 facilitated transport. The optimum CO_2 permeance of 140 GPU and CO_2/N_2 selectivity of 103 for binary gas were observed at 90 °C. An unprecedented stability of 30 days was demonstrated by the SF induced CS membrane under the applied conditions. Sericin (SC) a polymeric protein has to be removed during extraction of SF from the silk cocoons by dissolving in sodium carbonate (Na_2CO_3). Further, this SC solution was exploited as fixed natural carrier along with the aid of Na_2CO_3 as a mobile carrier inside the CS matrix and the membrane (M3) was tested for CO_2 separation

performance. The XPS depth profiling revealed evenly distributed elemental composition across the depth of the M3 membrane which confirmed the formation of homogenously blend membrane. The M3 membrane displayed encouraging CO_2/N_2 selectivity of 73 at 0.05 ml/min of feed sweep water flow rate. The selectivity was least affected at 90 °C temperature. This selectivity was higher than the CS membranes prepared with only SC or Na_2CO_3 in the matrix. CO_2/N_2 and CO_2/H_2 selectivity were found to be 43 and 10, respectively at 2 bar. An initial drop perceived in the CO_2 permeance was due to increase in the effective thickness of the active layer by support pore filling phenomena that adversely affected the overall permeance. Hence, a novel strategy was designed by preparing a mixed matrix nanocomposite membrane by incorporating graphene nanoparticles (GNP) into the CS/SF matrix (CS/SF/GNP) to counteract the support pore blockage during gas separation test. The positive effect of GNP in the CS/SF/GNP was apparent in the CO_2 permeance inconsequential drop of ~ 7 % during the initial 12 h, in the presence of moisture and pressure. The CS/SF/GNP membrane exhibited CO_2 permeance of 159 GPU and CO_2/N_2 selectivity of 93 at 90 °C. The thermogravimetric analysis (TGA) isotherm specified the thermal stability of CS/SF/GNP membrane up to 150 °C even in absence of any crosslinking within the membrane. X-ray photoelectron spectroscopy (XPS) specified that the surface chemistry of the membrane remained consistent at temperature up to 120 °C. This encouraging work enabled us to distinctively envision the utilization of the whole of the raw silk for CO_2 separation.

List of Figures

List of Tables

CHAPTER 1

CO_2 Capture Overview, Literature Review and Research Objectives

CHAPTER 1

CO_2 Capture Overview, Literature Review and Research Objectives

This chapter provides an overview of the importance of CO_2 separation and its impact on climate change. It also emphasizes on various CO_2 capture technologies presently available. This chapter highlights the importance of membrane technology over other existing technologies. This section also reviews various membranes employed for CO_2 separation, elaborating different CO_2 capture methods, specifically membrane technologies for CO_2 separation using facilitated transport mechanism. Based on the gaps and challenges, the research objectives were defined.

1.1 Introduction and CO_2 emission overview

In today's era, controlling and regulating the emission of carbon dioxide (CO_2) in the atmosphere is the biggest challenge faced by the industrialized countries across the world as it has major detrimental effects on the global climate [1]. The advent of industries disrupted the total carbon distribution in the lithosphere, atmosphere and biosphere [2]. The potential adverse effects on the environment have a great impact on the common lives and is commonly referred as greenhouse effect. The primary cause for the greenhouse effect is increasing the level of CO_2 in the atmosphere due to the burning of fossil fuel. The energy demand is fulfilled mainly by running power plants based on coal (that emits ~ 12-15 vol % of CO_2) and natural gas (that emits ~ 4-8 vol % of CO_2) in post-combustion process [3]. Further, CO_2 is formed during H_2 production via water gas shift reaction. The increased level of CO_2 resulted in some deleterious effects which include melting of polar ice-caps leading to rise of sea levels, serious climatic changes and loss of biodiversity to name a few [4]. The presence of CO_2 currently contributes to ~ 60 % of the total climatic changes contributing to the greenhouse effect [5]. The global population is estimated to be around 9.2 billion by 2050 and dependency on the fossil fuel will increase in absence of alternative renewable energy source [6]. This will lead to higher CO_2 emission in the near future and is expected to reach up to 570 ppmv level by

2100 which may increase the overall temperature by 1.9 °C [2]. Hence, there is a pressing demand to reduce the CO_2 level using different techniques.

In the pre-industrial period, the CO_2 present in the environment was mainly removed by plants via the process of photosynthesis where plants naturally take CO_2 in presence of sunlight to release oxygen [7]. However, with such a rapid rise of carbon concentration and deforestation, plants alone are not sufficient to control CO_2 level in the environment. At present, there are three alternatives to minimize the CO_2 emission to the environment [2]. The first one is to reduce the fuel consumption by adopting more energy efficient techniques. The second is by embracing renewable sources of energy rather than conventional fossil fuels. The third alternative is to develop techniques which can sequestrate, capture and separate CO_2 easily and economically. Carbon sequestration or capture can be elucidated as direct containment of the CO_2 released from industrial units and storing it by using suitable means. However, the storage time must be long enough to ensure that the CO_2 will not release back into the atmosphere [8]. It comprises of three steps including CO_2 capture, transportation and storage [9]. Usually CO_2 is transported similarly to the other gases such as through pipelines, ship, tanker and trucks. Pipelines are the most economically feasible option as they enable transport of huge amount of CO_2 [10]. Even the disposal option should not be confined to the geologic or oceanic sink. Conversion of CO_2 using photosynthetic microorganisms in the bioreactor may be adopted as a sustainable and economical route [11]. The power plant based CO_2 separation and capture was achieved using three main processes (Figure 1.1), namely post-combustion capture, pre-combustion capture, and capture in oxyfuel combustion.

Post-combustion involves treatment of the exhaust gases containing CO_2 on the product side with most of the CO_2 getting separated before releasing to the atmosphere. In this method, the CO_2 has low partial pressure as it uses air for combustion which has high nitrogen content and hence low CO_2 (~ 15 %) concentration [12]. The energy requirement for the CO_2 capture in pre-combustion method is less than the post-combustion method, as along with CO_2, excess dust and impurities (SOx, NOx and incondensable gases) are also produced which again needs to be separated before using for CO_2 separation [2,8]. However, the main advantage of post-combustion process is that it can be used in the existing industrial plants (e.g., power plant, steel production industries, cement, iron industries etc.) [12]. Further, it can be fitted to the

power plants and has the liberty to connect/disconnect or upgrade according to requirement [13]. Hence, post-combustion process has great suitability for CO_2 reduction from various fossil fuel burning industries.

1.2 CO_2 capture processes

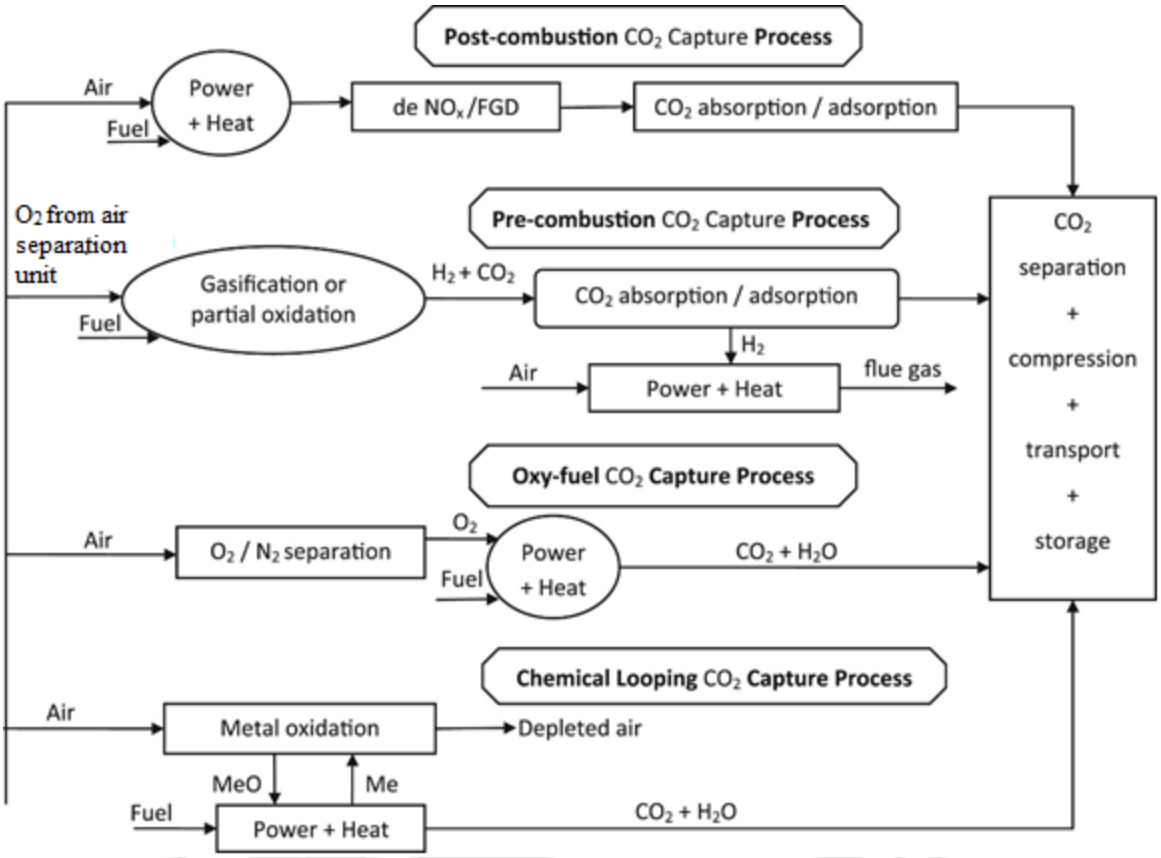

Figure 1.1 Principle of CO_2 capturing processes [14].

Pre-combustion capture refers to the treatment of gas mixture mainly containing carbon monoxide (CO) and hydrogen (H_2) [15]. Coal is gasified to produce the mixture of CO and H_2 (synthetic gas) which are then converted to CO_2 and H_2 via water-gas shift (WGS) reaction. Here, CO_2 is separated from the CO_2/H_2 gas mixture. This process generates more concentrated CO_2 than post-combustion process which increases the driving force for the separation [12]. However, this method is not commercially feasible due to high initial investments and complications to fit in the existing power plants [13].

In Oxy combustion method, only O_2 is supplied for combustion purpose instead of air as discussed in the above methods. The principal difference with the oxy-combustion method is the high partial pressure of CO_2 in the exhaust gas [13,16]. This method has some disadvantages like purification of O_2 from the air which increases the cost and use of this process in large scale is a challenge [13].

Another CO_2 capture process known as chemical-looping combustion (CLC) is also under consideration [17]. CLC is a two-step process as two reactors are used (one for air and one for fuel) [18]. There is no direct contact between fuel and air in CLC. Suitable oxygen carriers (metal oxide such as Fe_2O_3, Mn_2O_3, CuO) is used to bring O_2 to fuel [18]. However, long term stability of oxygen carriers, and large-scale CLC systems to treat high volume is still a prime challenge [19].

1.3 CO_2 separation technologies

The techniques used for CO_2 capture are: a) absorption b) adsorption c) gas separation using membrane technology d) cryogenic distillation. However, for higher efficiency hybrid systems can also be employed such as membrane system integrated with solvent absorption [20]. A brief description of these technologies are discussed below.

1.3.1 Absorption

In absorption process, the molecules or ions are dissolved in a bulk phase. The dissolving of CO_2 in amine solution is a similar process and industrially used for CO_2 separation [21]. The most common absorbent are the alkanolamines such as the MEA (monoethanolamine), diethanolamine (DEA) and methyldiethanolamine (MDEA) as solvents [22]. Moreover, mixed amines have proven to be more efficient than individual amines [2]. Amines have high rate of reaction but requires high energy during regeneration. Chilled ammonia process can be another option for absorption process at low temperature (2–10 °C) [23]. Also, carbonate based systems provide an alternative option in which CO_2 is reacted with soluble carbonates to form bi-carbonate and regeneration requires less energy as compared to amine based system, but has low reaction rate [24–26]. Further amino acid salts were also used in the absorption process due to their less corrosive nature than amine, greater stability in presence

of oxidative compounds, low volatility, and high reactivity towards CO_2 [27]. Though, absorption is a matured process, but it has some limitation based on solution used such as restricted CO_2 loading capacity, huge energy consumption for solvent recovery, equipment corrosion problem, solvent loss due to evaporation, and degradation of solvent in oxygen rich environment [28].

1.3.2 Adsorption

Adsorption is a process where the molecules present in the liquid or gaseous mixture cohere to the adsorbent. This process is recognized as one of the commercially viable methods for CO_2 capture [29]. For desired adsorption, the adsorbent should have large surface area, fast adsorption/desorption kinetics, high selectivity and absorptivity, high thermal and mechanical stability, regenerability [30]. The polarity and pore size of the adsorbent also play a very crucial role in the adsorption process [30]. The regeneration of the adsorbents for further use can be achieved by either increasing the temperature or decreasing the pressure [29]. In the pressure swing adsorption, the adsorption process occurs at above atmospheric pressure while desorption takes place at around atmospheric pressure. However, the adsorbent used at low pressure can be regenerated by maintaining vacuum [31]. Moreover, the temperature swing process is used when pressure is low such as flue gas generated in post-combustion process [30].

Adsorbents can be also classified as physical and chemical adsorbents [32]. Carbonaceous materials such as activated carbon are the commonly used physical adsorbents as these materials have excellent thermal stability, little sensitivity towards moisture, low cost, easy availability [33]. The performance of absorbents like zeolites is largely affected by size, chemical composition and charge density [34]. Mesoporous ordered silica is also a suitable adsorbent candidate having excellent thermal and mechanical stability, large pore volume, and tunable pore size properties but is limited by inadequate adsorption capacity [35,36]. Another currently prevalent absorbent is the metal-organic frameworks (MOFs) due to its exceptional adsorption capacity, high surface area and pore structures which can be easily controlled by changing the metallic clusters or organic ligands [37,38]. Poor selectivity and non-compatibility at high temperature are some of the major drawbacks of the physical adsorbents

that make it unfit for post-combustion CO_2 capture [32]. Chemical adsorbents are chemically modified to create basic active sites to improve the interaction between acidic CO_2 molecules and the surface [32]. Amine based adsorbents though broadly used but low capacity and high cost add to their utility limitations.

1.3.3 Cryogenic distillation

Cryogenic distillation is a separation method where the components in a gaseous mixture are separated by condensation. The system is typically a closed cycle operation consisting of cold trap filters to obtain different condensation temperatures for different air components [39]. In this method, CO_2 can be obtained in the liquefied form making CO_2 capture and transportation comparatively easier than the other techniques [40]. This technology is preferred for oxyfuel combustion process. However, post-combustion CO_2 capture is also possible using cryogenic distillation via application of dynamically operated packed beds [41]. Cryogenic distillation is a complex process, consumes high energy and is more costly than other technologies which limit its industrial use [42].

1.3.4 Membrane separation

Industry, transport, residential, natural gas processing and biogas from anaerobic digestion are the primary sources of CO_2 emission. But flue gases from the coal-fired power stations and natural gas processing, have become a primary target for reduction [40]. Absorption, adsorption, and cryogenic distillation are the technologies used for CO_2 separation as discussed in earlier sections. However, research is oriented towards alternate technologies, which are energy efficient, cost-effective, having compact modular design and corrosion free. Amongst these, membrane technology is the preferred alternative for CO_2 separation because it is energy efficient, economical & easy in handling [43]. Moreover, due to the system modularity and compactness, it can be easily integrated into the industries without consuming large space [44]. Membranes are the semi-permeable barrier where a particular gas component is separated from the rest of the component in the mixture making the permeate rich in a particular gas depending upon the selective nature of the membranes [45]. The driving force for the separation process is governed by the partial pressure of components across the membrane [46]. The possible mechanisms for membrane separation are Knudson diffusion,

capillary condensation, surface diffusion, molecular sieving and solution-diffusion [45,47,48]. Membrane technology is broadly classified into ceramic membranes, mixed matrix membranes (MMMs) and supported ionic liquid membrane (SILM) and polymeric membranes. All these types of membranes have their own set of advantages and disadvantages.

Ceramic membranes are generally used where separation requires high pressure, like CO_2 separation from natural gas. Ceramic membranes are also temperature and chemical resistant. Both microporous (silica, carbon or zeolites) and dense membrane can be prepared for gas separation application [49]. However, ceramic membranes are brittle in nature and crack-free development on large scale along with good CO_2 separation performance is still a great hurdle which restricts it for industrial use [50].

Mixed matrix membranes (MMMs) are synthesized to enhance the properties of the polymeric membranes by incorporation of filler materials into the polymeric solutions [51]. The main challenge is to select a suitable filler which has a good compatibility with the polymer matrix. The low polymer-filler interaction causes agglomeration of the filler, formation of a void during membrane preparation, pore blockage and also increases the membrane rigidity, results in poor gas separation performance [52]. Various fillers like MOFs, zeolites, mesoporous silicas, carbon nanotubes and graphene oxides (GO) can give better separation performance due to their surface chemistry and pore size distribution [53]. The incorporation of fillers enhances the separation performance through changing free volume, molecular sieving effect, chain rigidity of polymer and of course polymer-filler interaction [53]. Further, the CO_2 separation performance can be enhanced by the synergetic effects of dual fillers in a polymer matrix [54]. Similarly, Bae et al. [55] synthesized a high performance mixed matrix membrane using ZIF-8 and GO. They found that ZIF-8 improves the CO_2 permeability whereas GO enhances the gas selectivity. Also, some fillers are modified with an amine to incorporate facilitated transport in MMMs for better separation performance [56]. Though some of the MMMs showed CO_2 separation above the Robeson upper bound curve, but reproducibility, scaling-up, fabrication cost and long-term stability is still a challenge [52].

Ionic liquids are thermally stable, non-inflammable organic salts which are in liquid state at room temperature. Ionic liquids are imbued into polymeric supports to form supported ionic

liquid membranes (SILMs) which allow gas transportation by either facilitated transport or solution-diffusion mechanism. Such SILMs suffer from carrier washout and degradation under pressurized or vacuum conditions that lower the membrane separation performance [57,58].

Polymeric membranes have high separation efficiency at low pressure and temperature, easy to prepare and relatively cheap [4,59]. The polymeric membranes have been used for the separation of different types of gas mixtures like H_2/O_2, H_2/N_2, He/N_2, CO_2/N_2, CO_2/CH_4, CO_2/H_2 [60,61]. Cellulose acetate is one of the polymers initially used for gas separation. Cellulose acetate (CA) had shown the CO_2 permeability of 3.23 Barrer with CO_2/CH_4 selectivity of 33.8 at a temperature of 35 °C having a feed pressure of 10.1 bar [62]. CA was also blended with poly(ethylene glycol) (PEG) having CO_2 permeability of 200 Barrer and CO_2/N_2 selectivity was 22 at 70°C [63]. Further, Puleo et al. [64] established the relation of gas permeability with the degree of acetylation and reported an increase in the gas permeability with degree of acetylation at 35 °C and ~ 1 bar pressure. Similarly, gas permeability study was done on cellulose membrane in the dry state as well as in swelling state and it was found swelling cellulose has high permeability than dry state cellulose membrane [65]. Apart from cellulose acetate membrane, other polymeric membranes including polyacetylenes [66], polyaniline [67], poly(arylene ether) [68], polyimides [69], poly(ethylene oxide) [61], polysulfone (PS) [70], etc. have been used for gas separation based on solution-diffusion mechanism. These membranes suffer from truncated CO_2/N_2 separation factor, permeance and some of these lack temperature stability. Flue gases are emitted at high temperatures and hence temperature stability is the utmost necessary criteria for membranes employed for CO_2 separation from flue gases. High gas permeance at high temperature reduces the cost of a membrane as it requires less membrane area to separate the same amount of gas while high selectivity increases the purity of the desired gas in the permeate. Membranes following solution-diffusion mechanism do not exhibit high permeance and selectivity. This can be circumvented by the facilitated transport mechanism.

During facilitated transport, the CO_2 undergoes an irreversible interaction with the molecules present in the membranes in addition to the solution-diffusion mechanism. The separation efficiency can be improved by maximizing the facilitated transport of CO_2 along with

solution-diffusion pathway [71]. The membrane following facilitated transport mechanism is preferred for CO_2 separation due to high CO_2 permeance and selectivity [72]. A carrier agent ($–NH_2$, $F^–$, $PO_4^{3–}$, $CO_3^{2–}$, $–COO^–$, etc.) is incorporated which reacts reversibly with the target gas component. The carrier with low cost, fast rate of reaction along with temperature and performance stability are the major factors for selecting a suitable carrier. Initially in facilitated transport mechanism the target gas molecule dissolves in the membrane and the facilitated through the carrier, however, the molecules (N_2) which do not react with the carrier is exclusively transported through solution-diffusion mechanism [73,74]. A schematic representation of a fixed amine based facilitated transport mechanism of CO_2 is shown in Figure 1.2.

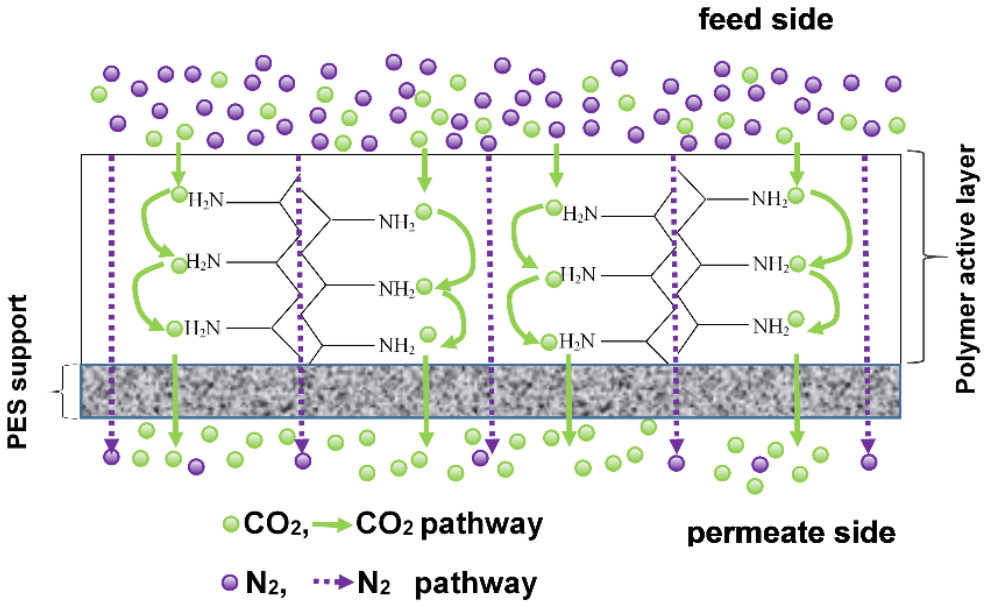

Figure 1.2 Schematic of CO_2 and N_2 transport mechanism in the membrane having fixed-site amine group.

There are mainly two types of carrier- fixed carriers and mobile carriers. Fixed carriers are chemically bonded to the solid matrix and own less mobility. Mobile carriers have free movement across the membrane. The complexes are formed by the reaction of the mobile carrier and a gas component from the feed side which moves easily across the membrane length and finally the gas molecule is detached at the downstream side. In the case of the fixed

carrier, the gas molecule from the feed is reacted with one carrier site and then moved to the next along with the applied pressure gradient [75,76]. Fixed-site-carrier (FSC) membranes are usually more stable than the membrane with mobile carriers during CO_2 separation as fixed carriers are covalently bonded with the polymer matrix [77,78]. The mobile carriers retain higher mobility and transport larger amount of CO_2, but may leach out during operation and hence long term performance can be compromised as compared to the fixed carrier. Due to these drawbacks, fixed carriers are preferred over the mobile carrier in facilitated transport membranes.

The amine carrier serves the facilitated transport mechanism by reacting with CO_2 that can be described by the following equations. CO_2 reacts with primary or secondary amines (RR′NH, where R is a functional group and R′ is a hydrogen for primary amine whereas R, R′ are functional group in case of secondary amine) to form zwitterions (Equation 1.1) as an intermediate and then the zwitterion is deprotonated by bases such as, the amine itself (Equation 1.2) and formed a protonated amine or carbamate ion and overall reaction was shown in Equation 1.3, which suggest that 2 moles of amine is required to capture one mole of CO_2 [74,79].

$$CO_2 + RR'NH \leftrightarrow RR'NH^+COO^- \quad (1.1)$$

$$RR'NH^+COO^- + RR'NH \leftrightarrow RR'NCOO^- + RR'NH_2^+ \quad (1.2)$$

$$CO_2 + 2RR'NH \leftrightarrow RR'NCOO^- + RR'NH_2^+ \quad (1.3)$$

The zwitterion then is deprotonated by bases such as H_2O to form the carbamate ion.

$$RR'NH^+COO^- + H_2O \leftrightarrow RR'NCOO^- + H_3^+O \quad (1.4)$$

If the carbamate ion of the amine carrier is not stable which is the case of satirically hindered amine then it will react with H_2O to form bicarbonate.

$$RR'NCOO^- + H_2O \leftrightarrow RR'NH + HCO_3^- \quad (1.5)$$

Similarly, for tertiary amine bicarbonate is formed following the base catalyzed mechanism [80].

$$R_3N + CO_2 + H_2O \leftrightarrow R_3N^+H + HCO_3^- \quad (1.6)$$

Water in this process is very vital as it promotes ion transfer in the hydration reaction and also enhances chain mobility of polymer matrix diminishing the gas diffusion resistance [81–83]. Presence of water augments membrane flexibility and CO_2 reacts reversibly with amines in the active layers forming carbamate and bicarbonate that diffuses rapidly across the membrane and finally dissociates in the permeate side, releasing the CO_2 [84]. Hence, membranes following facilitated transport mechanism have high CO_2 flux along with CO_2/gas selectivity. The CO_2 separation efficiency of a membrane is highly dependent on CO_2-carrier reaction kinetic. The affinity between the CO_2 molecule and amine is very strong, then they react irreversibly resulting no liberation of CO_2 at the permeate side [3]. However, if the reaction occurs very slowly and CO_2-carrier complex becomes very unstable then ideally no facilitated transport occurs as the membrane turns saturated very easily [3]. The prime requisite for facilitated transport is mild reaction rates especially at the decomposition step with moderate equilibrium constants [3]. Further, the fractional free volume (FFV) of the polymer [85], density and size of the carrier [3,79], water content [86] and pH [87] in the membrane may impact on separation processes. The large free volume of the polymer helps the CO_2 molecules to achieve reversible reaction more comfortably. More number of active sites are available in high density and small size carrier resulted in fast facilitated transport. Water is very vital for facilitated transport as water induces swelling in the membrane that creates additional free volume for the diffusing gas [3]. It was also revealed that the addition of salts in water swollen membrane can decrease the solubility of non-condensable gases like N_2, and CH_4. This is an appealing way to increase the selectivity of CO_2 over N_2 and the process is referred to as "salting out effect" [88]. However, selectivity is increased while permeability decreased after addition of salts in dry membranes popularly referred as "trade off" effect. Humidified membranes with high salt have both enhanced permeability and selectivity. The state of water (free water or bound water) which is present in the membrane affects the overall CO_2 separation performance [89]. Free water is somewhat similar to the bulk water. Bound water has two forms like freezable bound water which has low interaction with polymer whereas nonfreezable bound water makes bond (hydrogen bond) with a polymer matrix. The gas solubility is higher in bound water, whereas gas diffusivity is higher in free water [90]. It was reported that the CO_2/N_2 selectivity increases with increasing bound water [91].

1.4 Literature review

Most of the CO_2 separation membranes following facilitated transport involve the polymer poly(vinyl alcohol) (PVA) synthesis and thereof. To prepare a facilitated transport membrane, carriers are added to the PVA membrane either by blending or with crosslinking. Most of the membranes were prepared using solution casting technique.

Matsuyama et al. [92] studied the CO_2/N_2 separation using pure PVA and blend of PVA/ poly(ethylenimine) (PEI) at a temperature of 25 °C. The CO_2/N_2 selectivity of pure PVA was 70 while CO_2 and N_2 permeance trend were similar with the change of CO_2 partial pressure. They achieved CO_2 permeability of 850 Barrer (10^{-10} cm^3(STP)cm/(cm^2s.cmHg)) with the CO_2/N_2 selectivity of 160 at a CO_2 partial pressure of 0.065 bar at the same temperature. Hamouda et al. [93] prepared a membrane by blending PVA/PEG/PEI membrane for CO_2 separation and study the effect of PIE and PEF both on CO_2 separation performance at 25 °C and feed pressure of 1 bar. The CO_2 permeability was increased with PEI content due to increase in carrier content along with reduced PVA crystallinity by forming hydrogen bonding. The maximum CO_2/N_2 selectivity was found as 24 in the similar condition. However, the addition of PEG in PVA/PEI did not impact much on CO_2 separation due to its high crystallinity. Further, Deng and Hagg [94] studied the PVA/PVAm (polyvinyl amine) blend membrane and its swelling behavior which impact the CO_2 separation performance. The CO_2/N_2 selectivity was 160 at 25 °C with feed pressure little above atmospheric pressure. But the major drawback of the PVA polymers is their solubility in water at temperatures above 70 °C [82]. Hence, crosslinking is a prerequisite to enable thermal stability of PVA based polymers.

To improve the thermal stability, Ho and co-workers crosslinked the PVA polymer with formaldehyde in the solution form and blended with various mobile or fixed carriers [82,95–98]. They crosslinked 60 wt % of PVA with formaldehyde as high degree of crosslinking may form a compact network structure and observed a decrease in overall gas permeability. After crosslinking PVA, thermal stability was improved and CO_2 permeability was studied maximum up to 170 °C [82]. As a fixed carrier, poly(allylamine) (PAA) has been blended with crosslinked PVA solution along with amino acid salt and potassium hydroxide and reported CO_2 permeability of 8200 Barrer and CO_2/H_2 selectivity of 450 at 120 °C having

sweep water content of 93 mol % with a feed pressure of 2 bar [82]. The same group also modified the PAA to poly-N-isopropylallylamine, a sterically hindered amines by converting primary amine of PAA to secondary amine for CO_2/H_2 and CO_2/N_2 separation [95]. They reported the CO_2 permeability more than 6500 Barrer and CO_2/N_2 selectivity of 650 and CO_2/H_2 selectivity of 300 at feed pressure of ~ 2 bar and temperature of 110 °C. Further, they synthesized poly-N-isobutylallylamine and poly-N-tert-butylallylamine from PAA and studied the steric hindrance effect on CO_2 separation performance [96]. They found that steric hindrance PAA is better than the free PAA in terms of CO_2 separation performance. However, modification to sterically hindered amine improves the cost and makes it a tedious, time consuming, complex process compared to unmodified PAA.

Apart from PAA, various other fixed carriers like PEI [92], poly(amidoamine) (PAMAM) dendrimer [99], poly(vinylamine) (PVAm) [83], etc. have been exploited as a carrier for the facilitated transport of CO_2. Also, some alkanoamines like 2-amino-2-methyl-1-propanol (AMP), *N*-methyldiethanolamine (MDEA), monoethanolamine (MEA) and diethanolamine (DEA) were used as carrier for CO_2 separation [81]. Further, different amines in the form of amino acid salt like potassium glycinate, lithium glycinate and piperazine glycinate were used as a carrier for facilitated transport of CO_2 [100]. Similarly, arginine salt [101] and Na_2CO_3 [102] were used as mobile carriers to enhance CO_2 separation by salting out phenomenon [88,91]. Adding salts into the swelled membrane helps to reduce the solubility of non-condensable gases like N_2, CH_4 and improves the overall CO_2/gas selectivity.

Studies have also been done using blends of amine as carriers in the polymer matrix by Mondal and Mandal [103–106]. Initially, blends of 2-amino-2-hydroxymethyl-1,3-propanediol (AHPD) and poly(allylamine) (PAA) were added to crosslinked PVA and active layer was cast onto the porous support using solution casting technique [103]. They synthesized two active layers of 9 μm and 14 μm and detailed gas permeation study were performed by changing the temperature, pressure and water flow rate. Membranes with thinner active layer revealed high CO_2 flux, however, higher CO_2/N_2 selectivity was observed in the membrane with a thicker active layer. Similarly, composite membrane was also synthesized by introducing carrier in the active layer (45 μm) in the form of polyethyleneimine (PEI)/tetraethylenepentamine (TEPA) [104]. The CO_2 permeance of 29 GPU and CO_2/N_2

selectivity of 270 was achieved at a feed absolute pressure of 2.8 atm and 100 °C. The prepared membrane maintained its performance stability ~ 300 h. They also studied the effect of temperature, pressure and sweep water flow rate of the membrane having blend carrier in the form of PAA/AHPD, PAA/PEHA (pentaethylenehexamine) and PEI/PEHA for CO_2 separation [105,106].

Though crosslinking is a prerequisite to enable thermal stability of PVA based polymers, it makes the synthesis process complex and time consuming. Polymer blending for CO_2 separation, instead of synthesis of new materials can be adopted owing to its simple and cost-effective features. Chitosan (CS) is a biopolymer having amine group in its structure is thermally stable without any crosslinking, possesses good film forming ability and permits facilitated transport of CO_2 separation [107,108]. CS has one amine and one hydroxyl groups present in its ring structure (Figure A1.1a, Appendix 1). Hydroxyl and amine groups can make hydrogen bonding with absorbed moisture and introduce swelling effect on the membrane resulting in enhanced CO_2 solubility and diffusivity. Apart from that, CO_2 can react with amines reversibly in the presence of moisture which was responsible for the facilitated transport of CO_2 [3]. However, the presence of limited amine group (only one amine in the CS ring structure), does not enhance the facilitated transport.

CS membrane either blended with other polymer or amine, have been successfully used for separation of CO_2 pure gas [109], binary gas [108] and ternary gas mixture [110]. Ito et al. [108] studied the effect of dry and swell chitosan membrane for CO_2 separation. They found that the dry chitosan membrane has lower permeability than swell chitosan membrane using CO_2/N_2 and CO_2/CH_4 gas mixture. The CO_2/N_2 and CO_2/CH_4 selectivity were 70 and 28 respectively at room temperature.

Xiao et al. [111] studied the pure gas permeation of CO_2 and N_2 on chitosan membranes crosslinked with trimesoyl chloride (TMC) and reported ideal separation factor of 42 with the CO_2 permeability of 163 Barrer at room temperature. Bae et al. [109] observed high CO_2 as well as N_2 sorption in swelled chitosan membrane than dry membrane due to plasticization effect. El-Azzami et al. [107] used chitosan for facilitated transport of CO_2 from the ternary gas mixture (CO_2 10 %, H_2 10 % and N_2 80 %). They reported CO_2/H_2 and CO_2/N_2 selectivities of 43 and 250, respectively while CO_2 permeance was 7.4 GPU at 1.5 bar feed pressure and

110 °C temperature. Effect of temperature, humidity and pressure were discussed. CO_2 flux and CO_2/gas selectivity increase up to 110 °C due to the water holding capacity of the chitosan membrane and increase in facilitated transport mechanism. Also, they observed that high sweep side humidity compare to feed side showed better CO_2 separation performance. This may be due to the higher water retention capacity of the membrane when sweep side humidly was more. High water retention capacity enhances CO_2-amine reaction resulted in greater CO_2 permeance. The feed pressure played a negative role in CO_2 permeability and CO_2/gas selectivity due to carrier saturation at higher pressure. They also blended chitosan with arginine salt which has improved the CO_2 permeance to 23.4 GPU (1500 Barrer) at the same operating conditions [101]. Similarly, chitosan blend with triethanolamine (TEA) was used for pure gas separation and showed CO_2 permeation of 240 GPU having CO_2/N_2 selectivity of 63.4 with TEA content of 15 wt % at room temperature and pressure of 3 bar [112]. Further, an integrally skinned membrane based on chitosan containing imidazole group (Im-CS) mixed with PES showed CO_2 permeation 6.2 GPU and CO_2/CH_4 selectivity of 34 at 15 bar pressure with 1 % Im-CS concentration [113]. CS was blended with another polymer like Pebax® and showed a significant increase in CO_2 permeability to 2884 Barrer and a moderate separation factor of 65.3 for CO_2/N_2 at 85 °C [114]. Also, various MMMs has been synthesized by incorporating a filler in the CS matrix [110,115,116]. Coterillo et al. [115] studied the ETS-10 (Engelhard Corporation Titanosilicate)/IL/CS mixed matrix membranes and found six times higher selectivity than pure CS membrane at 50 °C and 2 bar pressure.

Further, MMMs was synthesized using a metal-organic framework (MOF)/ionic liquid/CS for CO_2/N_2 separation and reported maximum CO_2 permeability of 5413 ± 191 Barrer and CO_2/N_2 selectivity of 11.5 [116]. However, temperature effect on CO_2 performance study was absent or limited to 50 °C only as the typical flue gas contains high moisture contents in the form of vapour and temperature varies from 57-120 °C depending on the treatment of the gas like flue gas desulfurization [117,118]. Further acetate based IL (1-ethyl-3-methylimidazolium acetate) ([emim][Ac]) was incorporated in CS and CO_2 permeability of 1338 Barrer was achieved at 50 °C with a pressure difference of 0.5 bar [119]. Similarly, Shen et al. [110] synthesized a mixed matrix membrane sing polyvinyl amine (PVAm) with CS as the polymer matrix and graphene oxide (GO) grafted with hyperbranched polyethylenimine (HPEI-GO) as a nanofiller casting onto a PS support. They observed the highest CO_2 permeance of 31.3

GPU in the membrane with 3.0 wt % HPEI-GO and CO_2/N_2 selectivity of 107 at 1 bar and 25 °C. They concluded that CO_2 permeability by this MMM is mostly due to facilitated transport mechanism and also some contribution from solution-diffusion mechanism through graphene oxide. Ovarian et al. [120] also developed copolymers of CS and styrene as well as CS and acrylonitrile, doped with methylimidazolium based ionic liquids. Abdollahpour et al. [121] synthesized water soluble chitosan derivative for facilitated transport of CO_2 with reasonable CO_2 permeance and selectivity but at lower temperature region.

Developing a thermally stable (~ 150 °C) membrane by crosslinking is a complex, time consuming and costly process. CS is one of the polymer that has thermal stability, good film forming ability and presence of amine group in its structure which helps in facilitated transport of CO_2. In this study, synthetic amines were exploited as carriers in CS membranes for facilitated transport of CO_2. However, this study also embodies the use of natural amines as a carrier for the facilitated transport of CO_2. So, based on the conditions of flue gases to separate using membrane technologies following objectives have been undertaken.

1.5 Objectives of the thesis

The primary objectives of the thesis are

1. Selection and preparation of the polymeric membrane useful for CO_2 separation using facilitated transport mechanism.
2. Further improvement of the CO_2 facilitated transport by blending with synthetic or natural amines and nanoparticles.

The following research works have been undertaken on the basis of the above objectives:

I. Preparation of the CO_2 selective membrane using biopolymer that possesses high thermal stability in absence of crosslinking.
II. Development of chitosan membrane for CO_2 separation by blending with different synthetic amines.
III. Enhancement of membrane stability and CO_2 separation performance by exploring natural fixed carriers.
IV. Exploring nanomaterials to construct mixed matrix membrane to circumvent support pore filling phenomenon.

V. Optimization of the gas permeation operating conditions like temperature, pressure and moisture content along with membrane characterization and material study.

VI. Detailed performance studies (CO_2 flux, CO_2 permeance and CO_2/N_2 selectivity) under optimized membrane composition and operating conditions by the membrane using counter flow circular flat sheet membrane module.

1.6 Thesis outline

On the basis of the above discussion, thesis work has been divided into seven chapters. A brief overview of each chapter is presented below.

Chapter 1: This chapter focused on the importance of the CO_2 separation as it is one of the major greenhouse gases responsible for the global warming problem. Also, discussed various technologies available for CO_2 separation/capture and their advantages and disadvantages. Emphasis was laid on the advantages of CO_2 separation using membrane technology. Also, this chapter includes the detailed literature survey for the removal of CO_2 using thin-film polymer composite membranes and the major existing research work using chitosan polymer has been elaborated. Finally, this chapter listed its major objectives and the research work undertaken.

Chapter 2: This chapter contains detailed schematic representation and discussion of experimental setup used to complete the objectives of this thesis. This chapter focused on increasing the amine carrier in the active CS layer by blending with a synthetic amine tetraethylenepentamine (TEPA) in solution form to prepare CS-TEPA membrane and cast onto the porous support using solution casting techniques. Optimization of CS and TEPA weight ratio were carried out based on characterization involving TGA, FTIR, XRD and FESEM followed by gas permeation study. Effects of water flow rate, pressure, and temperature were concurrently studied on CS-TEPA membranes through gas permeation. The CO_2 separation performances (CO_2 flux, CO_2 permeance and CO_2/N_2 selectivity) of pure CS and CS/TEPA membrane were studied at a different sweep water flow rate, temperature and pressure.

Chapter 3: This chapter used polyamine instead of small molecule of amine as a carrier. For this purpose poly(allylamine) (PAA) has been selected as a carrier to enhance the CO_2 separation via facilitated transport. PAA consists of mainly primary amine groups which is very brittle in the dry state and inability to form stable films. CS blended with PAA membrane has been used to separate CO_2 from the CO_2/N_2 gas mixture. The composition of the PAA was optimized on the basis of characterisation techniques (TGA, FTIR, FESEM, AFM, swelling test etc.) as well as gas permeation results. The detailed study of optimized CS/PAA membrane was further performed by changing the sweep water flow rate, temperature and pressure. Also, Kaiser test was performed to check if PAA was leaching out or not during CO_2 separation.

Chapter 4: This chapter discussed a very interesting finding in the field of CO_2 separation using facilitated transport. For the first time, a natural biopolymer silk fibroin (SF) was used as a carrier instead of synthetic amines. We reasonably envision that the inherent amines in the SF can act as carriers and thereby replace the various amines processed through synthetic means. The composition of the SF was optimized on the basis of characterisation techniques (TGA, FESEM, AFM, swelling test, etc.) as well as gas permeation results. The blend membrane (CS/SF) was optimized based on the CO_2 separation performance. Its CO_2 separation performance lied above Robson upper bound which one of the criteria to judge whether the membrane is feasible for the industrial application or not. Also, the membrane maintained its CO_2 performance ability up to 30 days which was a great achievement for the facilitated transport membrane. By tailoring the properties of CS with a sensible blend of SF, the CS-SF composite will present a green route for a simple yet effective CO_2 separation. This work demonstrates our efforts of such an attempt.

Chapter 5: This chapter includes the CO_2 separation using sericin (SC) as a fixed carrier and sodium carbonate (Na_2CO_3) as a mobile carrier. The silk cocoon contains two proteins - 70-80 % SF and 20-30 % SC. During the silk degumming process, SF is extracted by dissolving in sodium carbonate (Na_2CO_3), to remove the SC. SF was used for the CO_2 separation as discussed in Chapter 4. But SC remains as a waste by-product, which contains primarily serine and glycine amino acids in its polypeptide chain that can act as fixed natural carriers to enable CO_2 facilitated transport. In this study, we investigated the CO_2 separation properties by

blending SC in the chitosan matrix in presence of Na_2CO_3 and in absence by removing Na_2CO_3 using dialysis. The detail characterization and gas permeation study of the membrane were performed. We envision that this work will invigorate a cost and time effective route of membrane preparation for CO_2 separation that will have several constructive impacts on the environment.

Chapter 6: The CO_2 separation performance by a membrane is influenced essentially by the film thickness, temperature, moisture and pressure. Pore filling of the membrane support during gas permeation study are critical factors that impede the CO_2 separation performance by changing the effective active layer thickness. This study involves the development of a novel nanocomposite membrane (CS/SF/GNP) consisting of chitosan (CS), silk fibroin (SF) and graphene nanoparticles (GNP). The CS acts as the matrix, SF contributes to the CO_2 facilitated transport by its inherent amines as carriers and GNP helped in counteracting the support pore blockage during the gas separation test.

Chapter 7: This chapter draws appropriate overall conclusions based on the investigation in the present study. This chapter also provides some useful recommendations for future research in the relevant field.

Some of the works done in this thesis have been accepted for publication in reputed international journals namely: Journal of Applied Polymer Science (Wiley), Journal of Industrial and Engineering Chemistry (Elsevier), Journal of Membrane Science (Elsevier), ACS Applied Materials & Interfaces (ACS) and one more manuscript will be communicated in the near future. The publication details of journals/conferences are included in research output section at the end.

CHAPTER 2

CO_2 Separation Performance Study by Chitosan-Tetraethylenepentamine Membrane

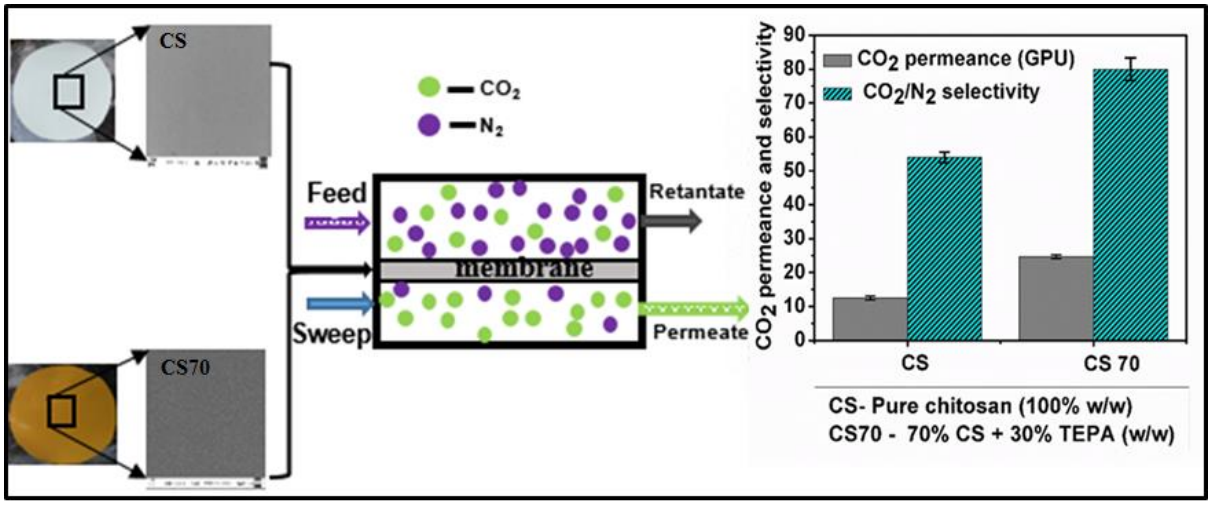

Graphical abstract of CS-TEPA blend membrane along with gas separation performance

CHAPTER 2

CO_2 Separation Performance Study by Chitosan-Tetraethylenepentamine Membrane

*Polymeric membranes for CO_2 separation using chitosan (CS) have been barely utilized. CS membrane has been prepared here and utilized for CO_2 separation. The amine carrier content in the active layer was further increased by addition of tetraethylenepentamine (TEPA) to prepare CS-TEPA membrane. This chapter discusses the CO_2 separation performances of pure CS and CS-TEPA membranes with various TEPA content. Characterization details have been furnished by various instrumental analyses. Effects of water flow rate, pressure, and temperature during gas permeation are elaborated. This work is scientifically acknowledged in "**Journal of Applied Polymer Science**".*

2.1 Introduction

CS has one amino and one hydroxyl groups present in its structure (Figure A1.1a, Appendix 1). Hydroxyl and amine groups can make hydrogen bonding with a water molecule and introduce the swelling effect on the membrane. Facilitated transport mechanism depends on the interaction of water with the amino group present in the membrane. However, the presence of limited amine group (only one amine in the CS ring structure), does not enhance the facilitated transport. TEPA has been mixed with CS in solution form to improve the amine concentration in the active layer. TEPA has two primary and three secondary amine groups present in its structure as shown in Figure A1.1b (Appendix 1). Usually, CO_2 reacts with primary and secondary amines to form a carbamic acid and then transfers a proton to an unionized amine, forming a carbamate [122]. Two moles of amine are consumed per mole of CO_2 if this pathway is followed, which is kinetically and thermodynamically favored for these kinds of amines [123].

As per our knowledge, there is no literature available on CS mixed with tetraethylenepentamine (TEPA) membrane for CO_2 separation. In the present study, a novel CS-TEPA blend membrane having different weight percent (wt %) of TEPA was synthesized following solution casting techniques onto the microporous poly(ether sulfone) support.

Different characterization techniques were used to see the effect of TEPA on film forming ability, thermal stability, and crystallinity. The CO_2 and N_2 permeation from simulated flue gas mixture were carried out on the prepared membrane at different water flow rate, pressure, and temperature.

2.2 Experimental Section

2.2.1 Material and methods

Chitosan (CS) flakes (Product Number: 419419) of high molecular weight (310000-375000 Da) and tetraethylenepentamine (TEPA) (189.3 g/mol) were procured from Sigma-Aldrich, USA and glacial acetic acid (99.99 % pure) was purchased from Merck, Germany. A microporous poly(ether sulfone) supports (thickness: ~150 μm and average pore size: 0.03 μm) were obtained from Sterlitech, USA. Feed gas mixture (20 % CO_2 and 80 % N_2), carrier gas and the sweep gas, used for the gas chromatography (GC) analysis and gas permeation tests were acquired from Vadilal Chemicals Ltd., India. Millipore® water was used during the experiment.

2.2.2 Membrane synthesis

Chitosan (1.15 g) was dissolved in 1 vol % acetic acid aqueous solution under vigorous stirring for 12 h. The solution was centrifuged at 10000 rpm for 30 min to remove undissolved particles**.** The pH of this chitosan solution was 4.35. Then, TEPA of calculated amount was added dropwise to the chitosan solution and pH recorded simultaneously. The addition of more than 50 wt % of TEPA leads to increase in pH > 6.5 of the chitosan solution and precipitation followed. Hence, 40 % TEPA was considered as the upper limit so as to keep its pH below 6.5. After addition of TEPA to the chitosan solution, it was further stirred for 4 h (hour) to achieve a homogeneous solution. The active layers of the composite membranes, having four different weight ratios of CS and TEPA (CS-TEPA) such as 100 wt% CS (CS), 85 wt % CS + 15 wt % TEPA (CS85), 70 wt % CS + 30 wt % TEPA (CS70) and 60 wt % CS + 40 wt % TEPA (CS60) were blended.

At the onset, poly(ether sulfone) support was immersed in water overnight to remove any unwanted particles. The CS-TEPA solution was then cast using a casting knife (GARDCO,

Paul N. Gardner, USA) with a gap of 30 mils, onto the poly(ether sulfone) microporous support. The membranes were kept inside the laminar air flow for 48 h and placed in an oven (Thermo Scientific™ Heratherm) thereafter. The membranes were heated at a heating rate of 1°C/min from 25 to 120 °C and held for 6 h at 120 °C. A litematic thickness gauge (Make: Mitutoyo, Model: VL-50) was used to measure the active layer thickness of the composite membranes.

2.3 Gas permeation measurements

The schematic of the gas permeation setup is shown in Figure 2.1a. The composite membrane was placed in a stainless steel counter current flat sheet module with an effective diameter of 7.78 cm as presented in Figure 2.1b. The membrane module was then inserted inside the temperature controlled hot air oven for gas permeation study. The composition of the feed mixture was 20 % CO_2 and 80 % N_2. Two mass flow controllers (Aalborg, USA) were used to control the feed gas and sweep gas (Ultrapure argon) flow rates. Two different back-pressure regulators were used to maintain the pressure inside the module. The feed pressure was varied from 2 to 6.6 bar while the permeate side was kept constant throughout the experiment at 1.21 bar. Two different saturators were used to humidify the feed and permeate gas and housed inside the oven. An appropriate amount of water was pumped to the feed and sweep side saturators using two HPLC pumps (Shimadzu, LC 20AD, Japan) to humidify the gases. Both humidifying gases flow counter-currently across the membrane inside the module and when it came out from the oven, they were dehumidified via water knockout. The flow rate of retentate and permeate coming out from module has been measured by Agilent precision gas flow meter. Varian 450 GC having thermal conductivity detector (TCD), was used to analyse the composition of permeate and retentate. Each of the membrane permeation measurements had been carried out for at least 8-10 h at a particular temperature, pressure and water flow rate, which were allowed to attain the steady state permeation. The details calculation procedures of CO_2 and N_2 flux, permeability and permeance along with CO_2/N_2 selectivity were discussed in appendix section (Appendix 2).

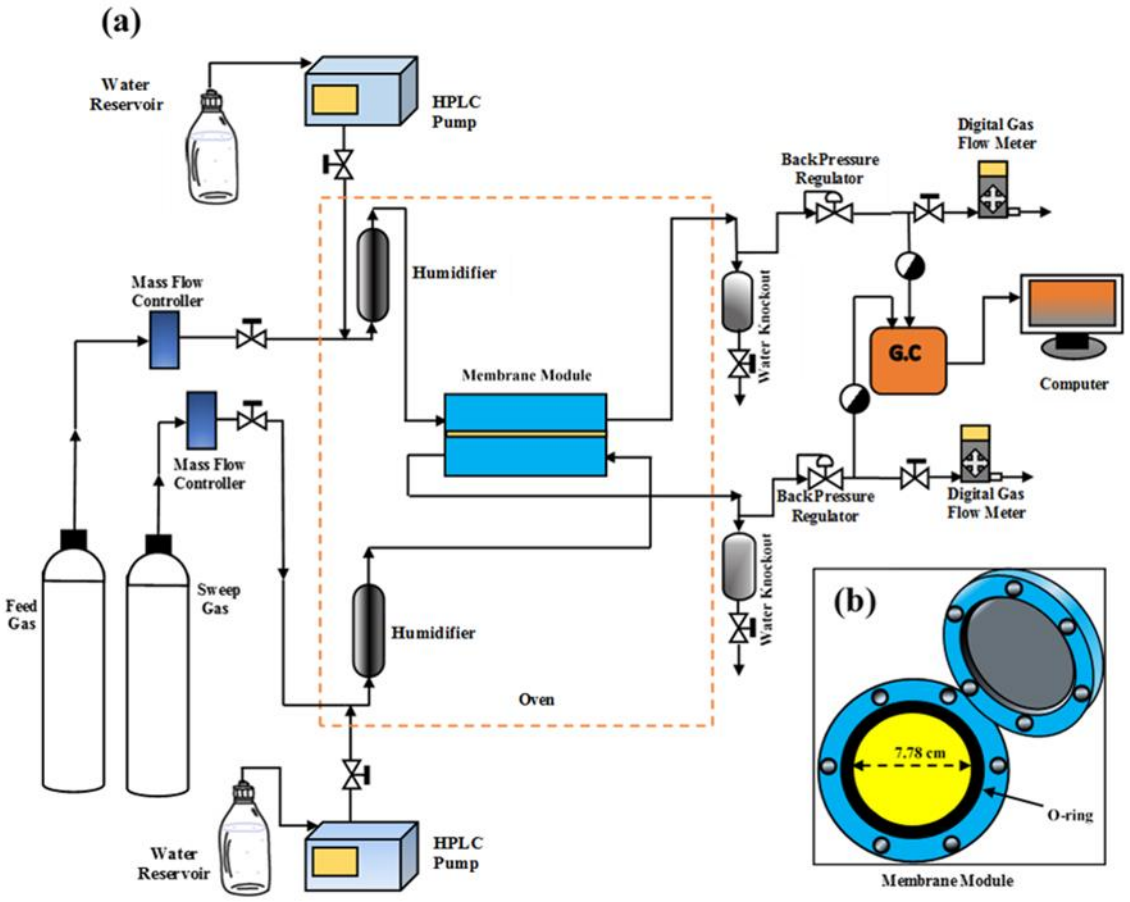

Figure 2.1 Schematic representation of (a) gas permeation apparatus and (b) membrane module

2.4 Membrane characterization

The active layers (CS-TEPA) without PES as support were characterized by thermogravimetric analysis (TGA), attenuated total reflectance-Fourier transform infrared spectroscopy (ATR-FTIR) and X-ray diffraction (XRD). TGA analysis was carried out to see the thermal stability of the film using Perkin-Elmer (Model: TL8000). ATR-FTIR (SHIMADZU, IR Affinity 1, JAPAN) analyses were carried out to resolve the functional groups present in the active layer. The peaks were analysed in the range of 4000 to 1000 cm^{-1} at an average of 20 scans per sample with a resolution of 4 cm^{-1}. The XRD analysis of the active layers was carried out using a Bruker D8-Advance diffractometer with monochromatic

$CuK_{\alpha 1}$ radiation of wavelength λ=1.54056 Å. The data was obtained at a scanning rate of 0.5° min^{-1} with a step size of 0.05°. The Crystallinity Index (*CI*) (%) was calculated using the formula $CI = \frac{A_{cryst}}{A_{total}}$, where A_{cryst} is the sum of crystalline band areas, and A_{total} is the total area under the diffractograms [124]. Field emission scanning electron microscope (FESEM, Zeiss, Germany, Model Sigma) was performed on active layers (CS-TEPA) with poly(ether sulfone) as support. FESEM was obtained at an accelerating voltage of 2-3 kV after gold sputtering.

2.5 Results and discussion

2.5.1 Thermogravimetric analysis (TGA)

TGA was carried out for pure CS and chitosan mixed with different TEPA (CS-TEPA) weight ratios. The weight loss was observed in three steps as shown in Figure 2.2a. The first step of weight loss (~11 %) for CS membrane was in the range of 30-108 °C, which was mainly due to loss of absorbed and bound moisture present in the membrane. In blend membrane, CS60 showed the maximum weight loss due to moisture in the temperature range of 30-108 °C compared to other prepared membranes. The weight loss of CS60 was 21 % while CS70 and CS85 have shown 17 % and 13 % weight loss, respectively. This indicates that the percentage weight loss due to the moisture of the membrane is dependent on the number of amines in the membrane. The amine and hydroxyl group present in the membrane can form hydrogen bonding with water and can hold more water [125]. Increased water hold-up across the membrane supports the gas permeance. The second weight loss was observed in the range of 175-297 °C and can be attributed to the de-polymerization and decomposition of polymer units [126]. Degradation of the saccharide rings and ring opening lead to the third step of weight loss around the temperature range of 297-391 °C [127]. To confirm the loss of TEPA blended with CS at a particular temperature (being a low molecular weight compound), the TGA of CS70 has been further investigated with 25 min of exposure time at temperatures (°C) of 100, 120 and 150 (Figure 2.2b). A negligible weight loss ~ 1.3 % was perceived from the isotherm at 100 °C up to 10 min which can be due to residual moisture evaporation and was constant henceforth. Almost a steady state weight loss < 0.4 % was apparent in the isotherm at 120 °C. However, the upshift in the weight loss (~ 2 %) at temperature > 120 °C (up to 150 °C and 25 min) can be ascribed to the elimination of TEPA [128]. The stability of the

membranes at a temperature < 120 °C endorses the suitability of the test membranes in CO_2 separation at temperatures below 120 °C.

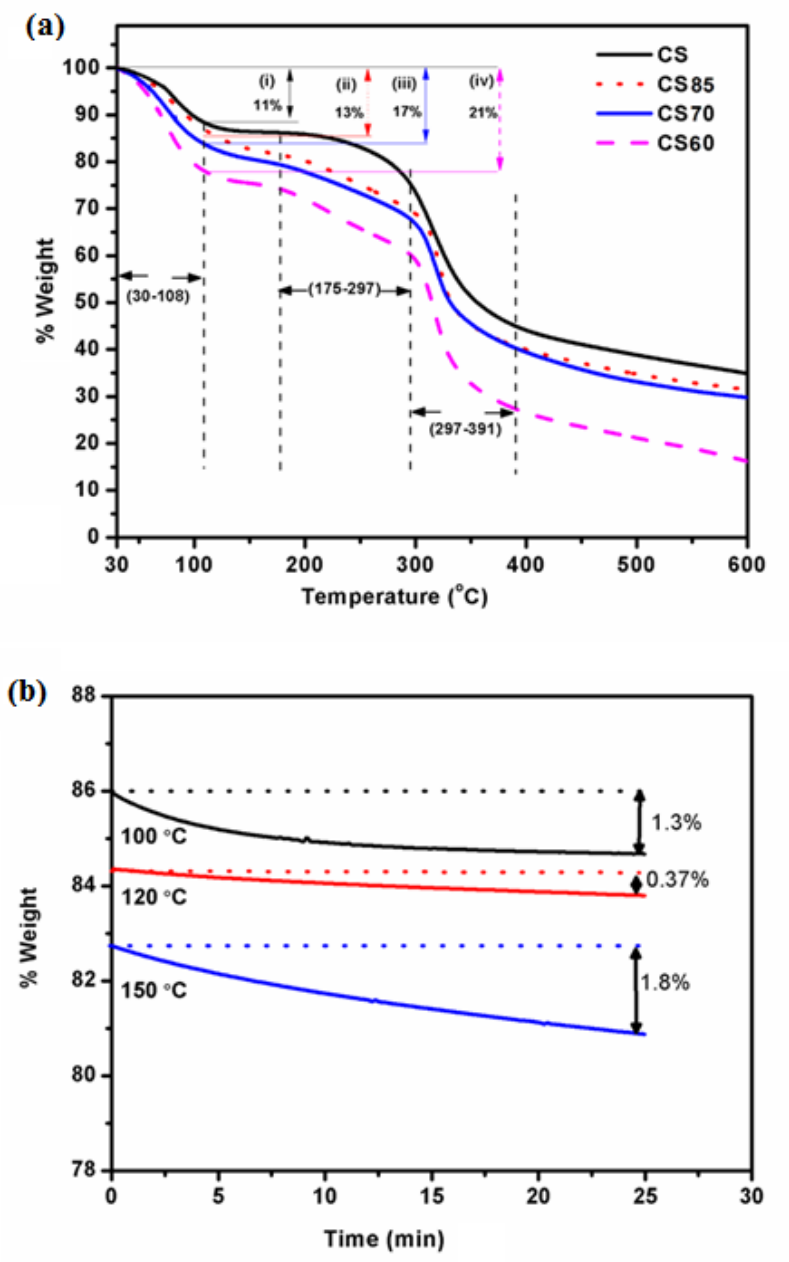

Figure 2.2 (a) TGA curve of (i) CS, (ii) CS85, (iii) CS70 and (iv) CS60 membranes, (b) TGA isotherm of CS70 at 100 °C, 120 °C and 150 °C for 25 min.

2.5.2 Characterization by FTIR spectroscopy

The FTIR peaks of CS, CS85, CS70 and CS60 membrane are shown in Figure 2.3. The FTIR spectra at around 3402 cm^{-1} was due to the cumulative effect of OH stretching, NH stretching and inter-hydrogen bond formation between OH and NH_2 groups present in the CS [129]. As compared to CS, the peak shifts from 3402 cm^{-1} to 3430 cm^{-1}, 3485 cm^{-1} and 3498 cm^{-1}

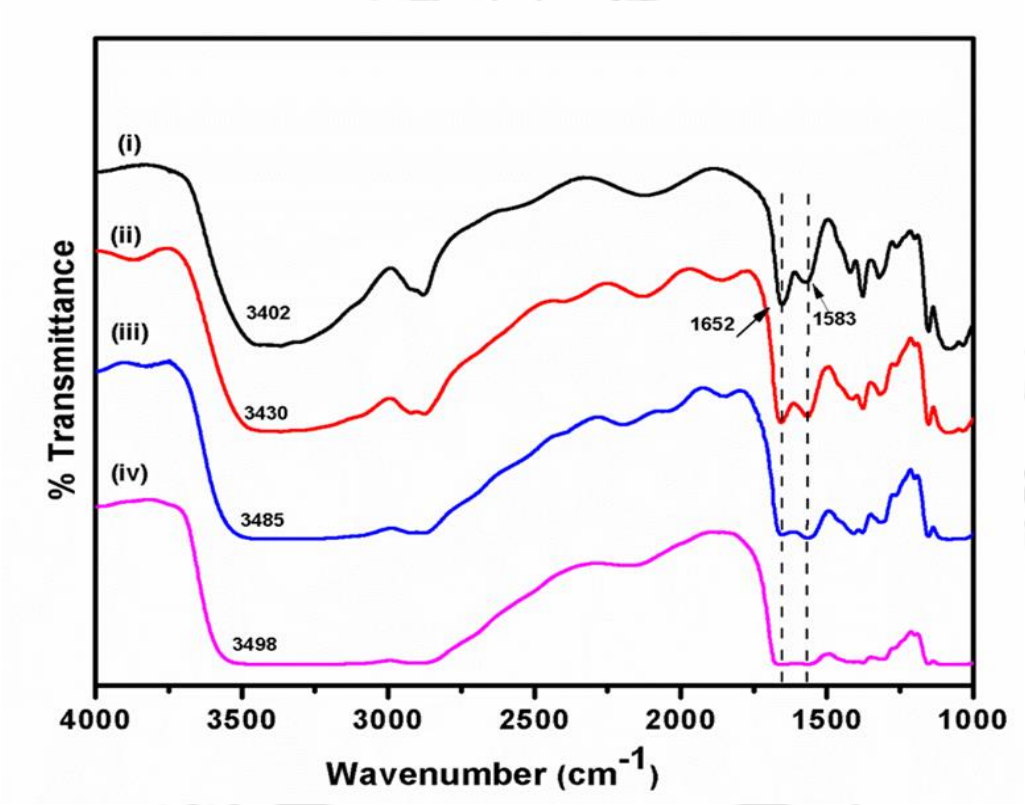

Figure 2.3 FTIR spectra of (i) CS, (ii) CS85, (iii) CS70 and (iv) CS60 membranes.

observed in membranes with increasing weight ratio of TEPA (CS85 < CS70 < CS60), respectively was due to more hydrogen bonding with water. The peaks at 2933 cm^{-1} and 2874 cm^{-1} were due to C−H stretching [126]. Further, 1652 cm^{-1} is assigned to C=O stretching of the amide group [130]. The peak at 1652 cm^{-1} has also been assigned to the imine (C=N) group, which may be formed during heating of the membrane [130,131]. The peak at 1583

cm^{-1} becomes more conspicuous with the increasing weight ratio of the amino group. This corroborates with the increasing weight ratio of TEPA in the membranes which helps in facilitated transport of CO_2 during gas separation.

2.5.3 XRD analysis

The XRD gives the idea about crystallinity of the membrane which is essential to understand the gas permeation barrier and mechanical strength. Crystallinity is inversely related to gas permeation [132,133]. Crystallinity hinders sorption of the gas molecules in their structure,

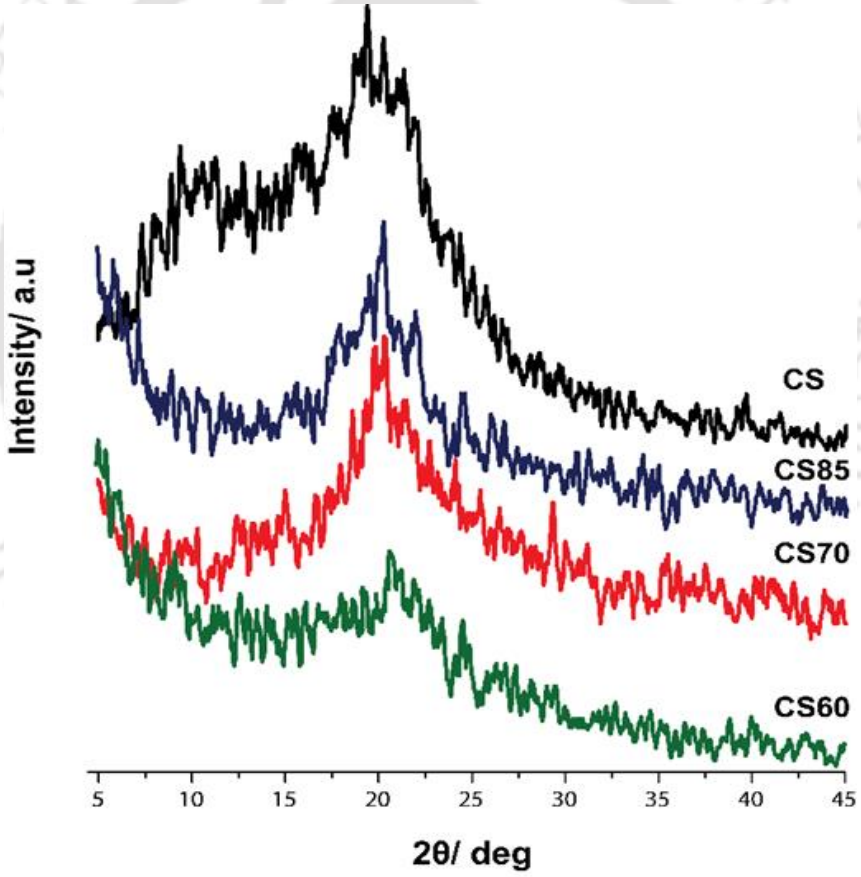

Figure 2.4 XRD spectra profile of CS, CS85, CS70 and CS60 membranes.

and diffusion takes place in the remaining amorphous phase. Wang et al. [134] demonstrated similar results in their work on thermoplastic polyurethane based membranes. The XRD study of CS membrane exhibits two peaks at 2θ = 10.3° and 20.5° (Figure 2.4), respectively which are in good agreement with the literature [126]. The peaks can be attributed to crystallinity forms I and II, respectively [126]. The peak at 2θ = 10.3° entirely disappeared when TEPA was mixed with CS and the declining intensity of the peak at 2θ = 20.5° advocates formation of reduced crystalline phase, signifying their suitable usage in gas permeation. The reason can be ascribed to chitosan's declining ability to form hydrogen bonds within the chitosan molecule after addition of amine [126]. The Crystallinity index (%, indicated in the parentheses) followed the trend CS (42.47) > CS85 (24.78) > CS70 (18.63) > CS60 (15.89) which indicates the drop in crystallinity with increasing amine content.

2.5.4 Surface morphology

The FESEM images of the top surface at 5 Kx magnification of CS, CS85, CS70 and CS60 membranes are shown in Figure 2.5. CS (Figure 2.5a) has smooth dense layer without any damage, which suggests its good membrane-forming ability. Similar smooth and dense layer was perceived from the top surface images of CS85 and CS70 (Figure 2.5b-c). CS60 (Figure 2.5d) had some patches on its surface which could be accounted due to low miscibility of TEPA at higher concentration (> 30 %). This kind of uneven surface due to low miscibility could lead to pore formation and may not be suitable for the gas separation application. The cross-sectional views of the synthesized membranes are shown in Figure 2.6. The dense top layer thicknesses of the CS and CS-TEPA membranes were in the range of 2-5 μm. It can be visualized that these membranes are well synthesized and validate their suitability for the gas separation with marginal resistance in the support layer.

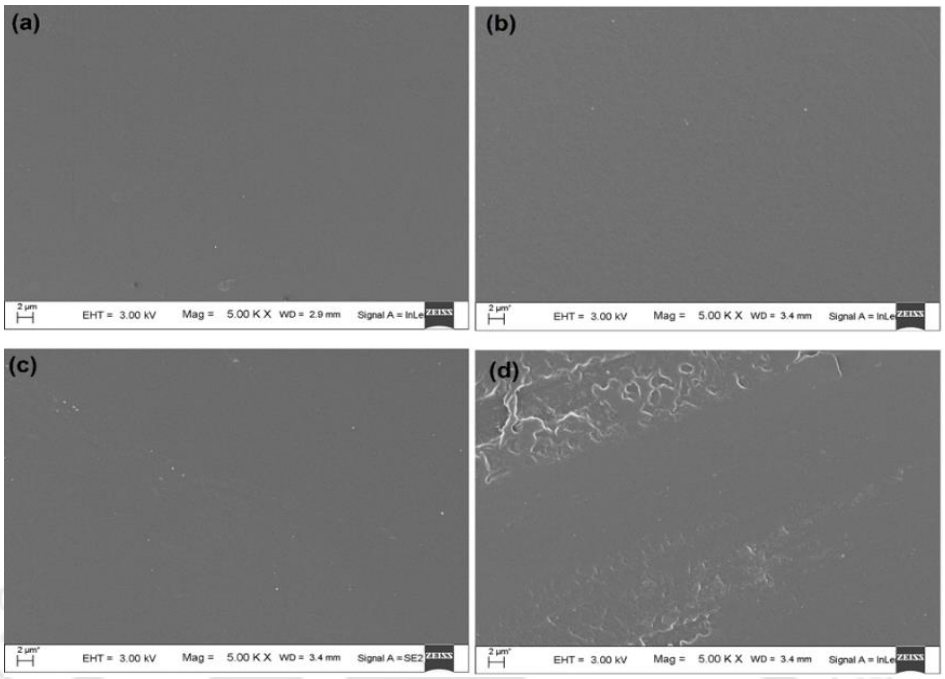

Figure 2.5 Top surface view of (a) CS, (b) CS15, (c) CS30 and (d) CS40 membranes

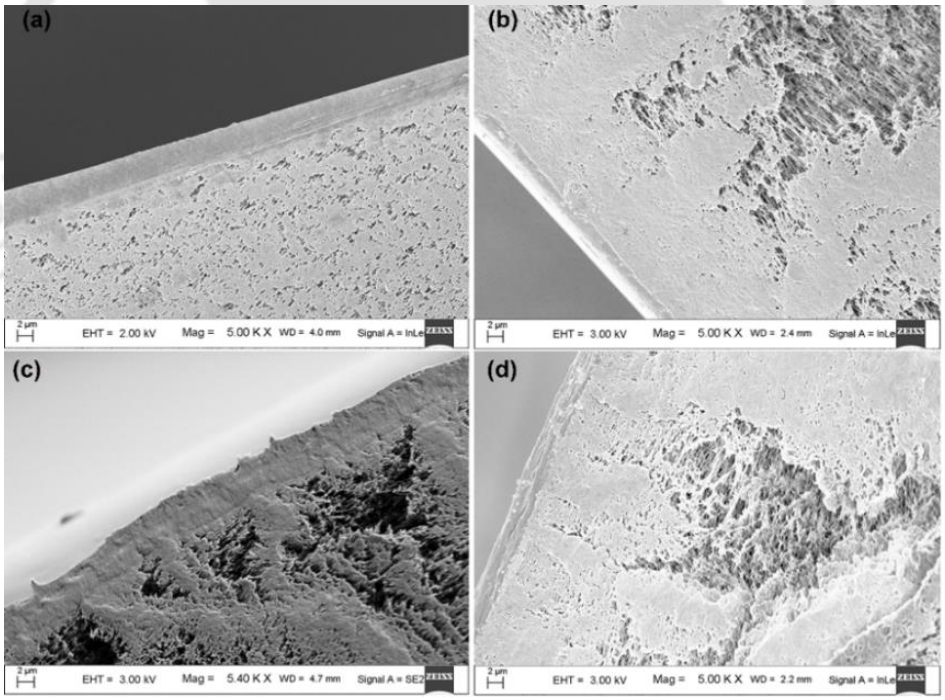

Figure 2.6 Cross-section view of (a) CS, (b) CS85, (c) CS70 and (d) CS60 membranes.

2.5.5 Gas permeation

The physical and morphological studies on CS, CS85, CS70, and CS60 membranes showed that CS70 had a balanced weight ratio of amine functional groups and miscibility with CS. The thermal stability from TGA curve (Figure 2.2b) of the blend membrane indicates its suitability for gas separation below 120 °C. The drop in crystallinity of ~ 56 % and ~ 42 % was observed in case of CS70 and CS85, respectively, as calculated from the crystallinity index. To provide an insight on the influence of TEPA content on CO_2 separation performance, the gas permeation study of CS85 and CS60 were carried out at the detected optimal temperature 90 ^oC with water flow rate = 0.03/0.05 ml/min (feed/sweep), feed absolute pressure = 2 bar and sweep absolute pressure = 1.21 bar which is provided in Table 2.1. Higher amine loading (TEPA weight ratio > 30 %) will obstruct CO_2 from reaching the CS matrix and eventually result in reduced CO_2 diffusivity and solubility [3]. This explains the drop in CO_2 permeance (~ 9 %) and CO_2/N_2 selectivity (~ 4 %) of CS60 membrane. Hence, the detailed gas permeation experiments and the effects of water flow rate, pressure and temperature were studied on CS70 with CS as a control.

Table 2.1 CO_2 permeance and CO_2/N_2 selectivity of CS, CS85, CS70 and CS60 membranes at 90 °C with water flow rate = 0.03/0.05 ml/min (feed/sweep), feed absolute pressure = 2 bar and sweep absolute pressure = 1.21 bar.

Membranes	CO_2 permeance (GPU)	CO_2/N_2 selectivity
CS	12.5 ± 0.67	54 ± 2
CS85	15.2 ± 0.85	67 ± 5
CS70	24.7 ± 0.52	80 ± 4
CS60	22.5 ± 0.74	77 ± 5

2.5.5.1 Effects of sweep side water flow rate on separation performance

The sweep side water flow rate was varied from 0.01 to 0.08 ml/min while the feed side water flow rate was kept constant at 0.03 ml/min. The feed and sweep side absolute pressure was kept constant at 2 bar and 1.21 bar, respectively and temperature was held constant at about 90 °C. The CO_2 flux, CO_2/N_2 selectivity, and CO_2 permeance increased when the sweep water flow rate exceeded the feed water flow rate (Figure 2.7). This is due to the more water hold up by the membrane which helps in the formation of more CO_2–carriers complex when sweep water flow rate is higher [107]. With the increase in the water flow rate at sweep side, the CO_2 flux initially increased linearly then became constant (Figure 2.7a). When the sweep side water flow rate varied from 0.01 to 0.08 ml/min, the CO_2 flux of CS membrane increased from 12×10^{-6} $cm^3(STP)/cm^2s$ to 221×10^{-6} $cm^3(STP)/cm^2s$ while the CO_2 flux of CS70 increased from 34×10^{-6} $cm^3(STP)/cm^2s$ to 369×10^{-6} $cm^3(STP)/cm^2s$. The maximum CO_2 flux was obtained at sweep water flow rate of 0.05 ml/min and after that the CO_2 flux becomes almost constant. The maximum CO_2 flux of CS and CS70 membranes at 0.05 ml/min water flow rate were 227×10^{-6} $cm^3(STP)/cm^2s$ and 380×10^{-6} $cm^3(STP)/cm^2s$, respectively. The N_2 flux remains constant due to solution-diffusion mechanism. However, little increase in the N_2 flux was observed above 0.05 ml/min, which might be due to more swelling of the membranes at higher water flow rate. A similar effect of sweep water flow rate was observed on CO_2 permeance (Figure 2.7b), and CO_2/N_2 selectivity (Figure 2.7c). The maximum CO_2 permeance of CS was 12.5 GPU (1 GPU = 10^{-6} $cm^3(STP)/cm^2s$ cmHg) and CO_2 permeance of CS70 was 24.7 GPU at 0.05 ml/min sweep water flow rate. The CO_2/N_2 selectivities of both the membranes in dry condition were below 10 and start increasing with water flow rate. The amine content in the CS 70 membrane was high compared to pure CS, resulted in more numbers of CO_2 molecules permeate by facilitated transport mechanism while no increase in N_2 permeation observed. This increases the CO_2/N_2 selectivity of CS70 membrane compared to CS membrane with increasing water flow rate. The slight drop in CO_2/N_2 selectivity after 0.05 ml/min water was observed due to increase of the N_2 permeation at higher swelling. The maximum CO_2/N_2 selectivities of 54 and 80 for CS and CS70 membranes were found at the same water flow rate.

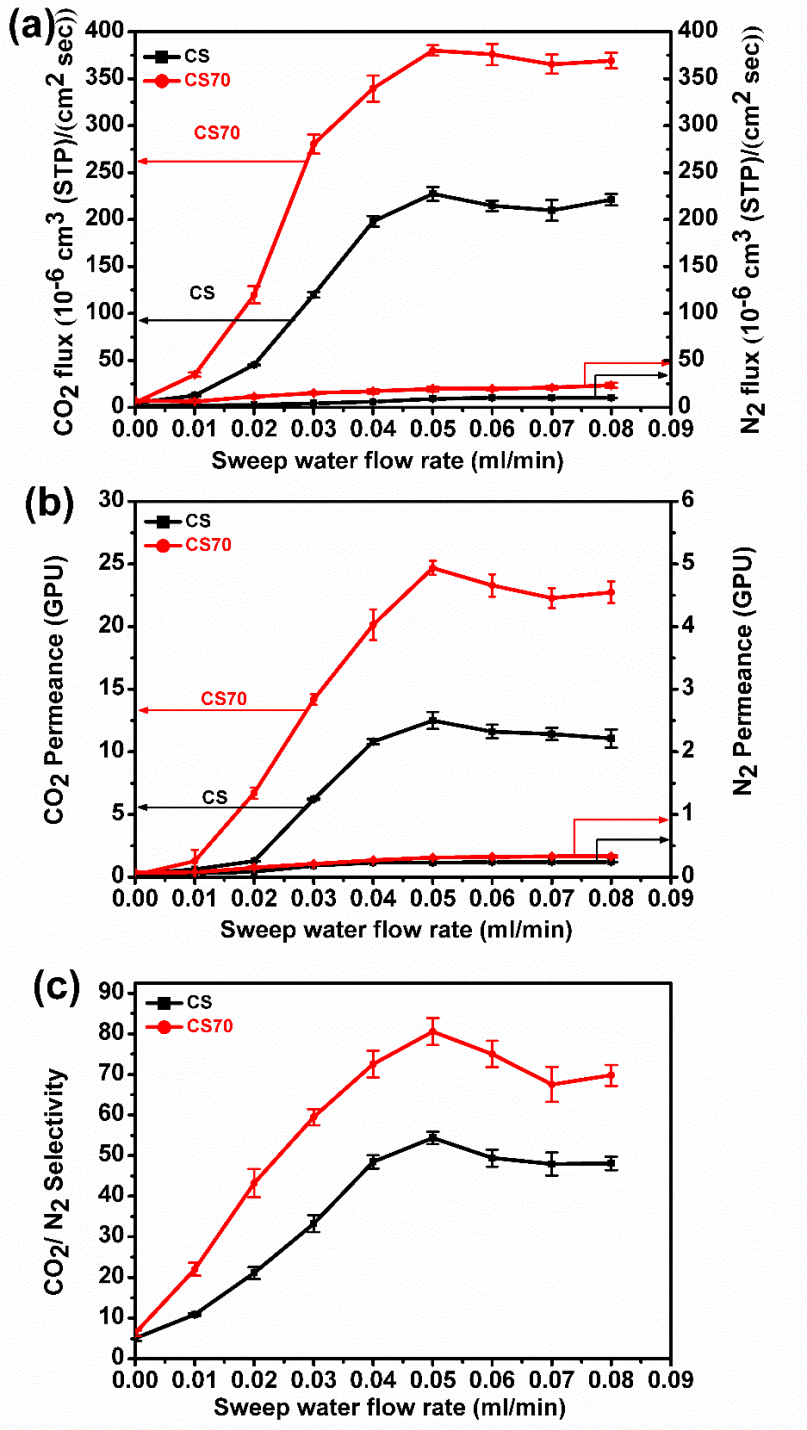

Figure 2.7 Effect of sweep water flow rate on (a) CO_2 and N_2 flux, (b) CO_2 and N_2 permeance and (c) CO_2/N_2 selectivity of CS and CS70 membranes at 90 °C with feed absolute pressure = 2 bar, sweep absolute pressure = 1.21 bar, feed water flow rate = 0.03 ml/min.

2.5.5.2 Effects of feed absolute pressure on separation performance

The effects of feed pressure on CO_2 flux, CO_2 permeance, and CO_2/N_2 selectivity were shown in Figure 2.8a-c. Feed absolute pressure was varied from 2 to 6.6 bar while sweep side absolute pressure was maintained constant at 1.21 bar. The temperature was kept constant at 90 °C while the water flow rates of feed side and sweep side were kept constant at 0.03 and 0.05 ml/min, respectively. It can be perceived from the flux vs pressure profile (Figure 2.8a), that with the increase in absolute feed pressure, the CO_2 flux increases rapidly and then maintained steady state at higher pressures (~ 5 bar). In case of CS membrane, CO_2 flux increases from 227 × 10^{-6} cm^3(STP)/cm^2s to 309 × 10^{-6} cm^3(STP)/cm^2s while for CS70, the CO_2 flux increased from 380 × 10^{-6} cm^3(STP)/cm^2s to 497 × 10^{-6} cm^3(STP)/cm^2s. This might be due to more amount of CO_2 is dissolved in the membrane through the formation of CO_2–amine complex and hence the driving force for CO_2 transport is improved. The CO_2 permeance (Figure 2.8b) of CS and CS70 at 2 bar feed absolute pressure were 12.5 GPU and 24.7 GPU, respectively. However, at a high CO_2 partial pressure when the carrier was saturated with CO_2, further enhancement of CO_2 transport ceases and CO_2 flux reaches almost a constant value. Nevertheless, N_2 flux increased linearly with feed pressure because N_2 is an inert gas whose transport is governed by solution-diffusion mechanism only. The CO_2/N_2 selectivity (Figure 2.8c) of CS and CS70 membranes were 54 and 80, respectively at 2 bar feed absolute pressure and decreased to 33 and 44 when feed absolute pressure reached to 6.6 bar. CO_2 permeance decreases with increasing pressure whereas the changes in N_2 permeance were insignificant, owing to which the downfall of CO_2/N_2 selectivity was observed, similar to that reported elsewhere in case of facilitated transport [135]. With a surge in feed pressure, CO_2 performance improved up to a certain pressure and then becomes constant due to carrier saturation and hence, facilitated transport mechanism at high CO_2 partial pressure is ineffective [136]. However, at decreased CO_2 partial pressure facilitated transport mechanism is efficient. Total flux due to the carrier is small when CO_2 partial pressure is high and CO_2 transport follows normal solution-diffusion mechanism. Thus, this membrane may be suitable for flue gas separation which has around 1 bar pressure.

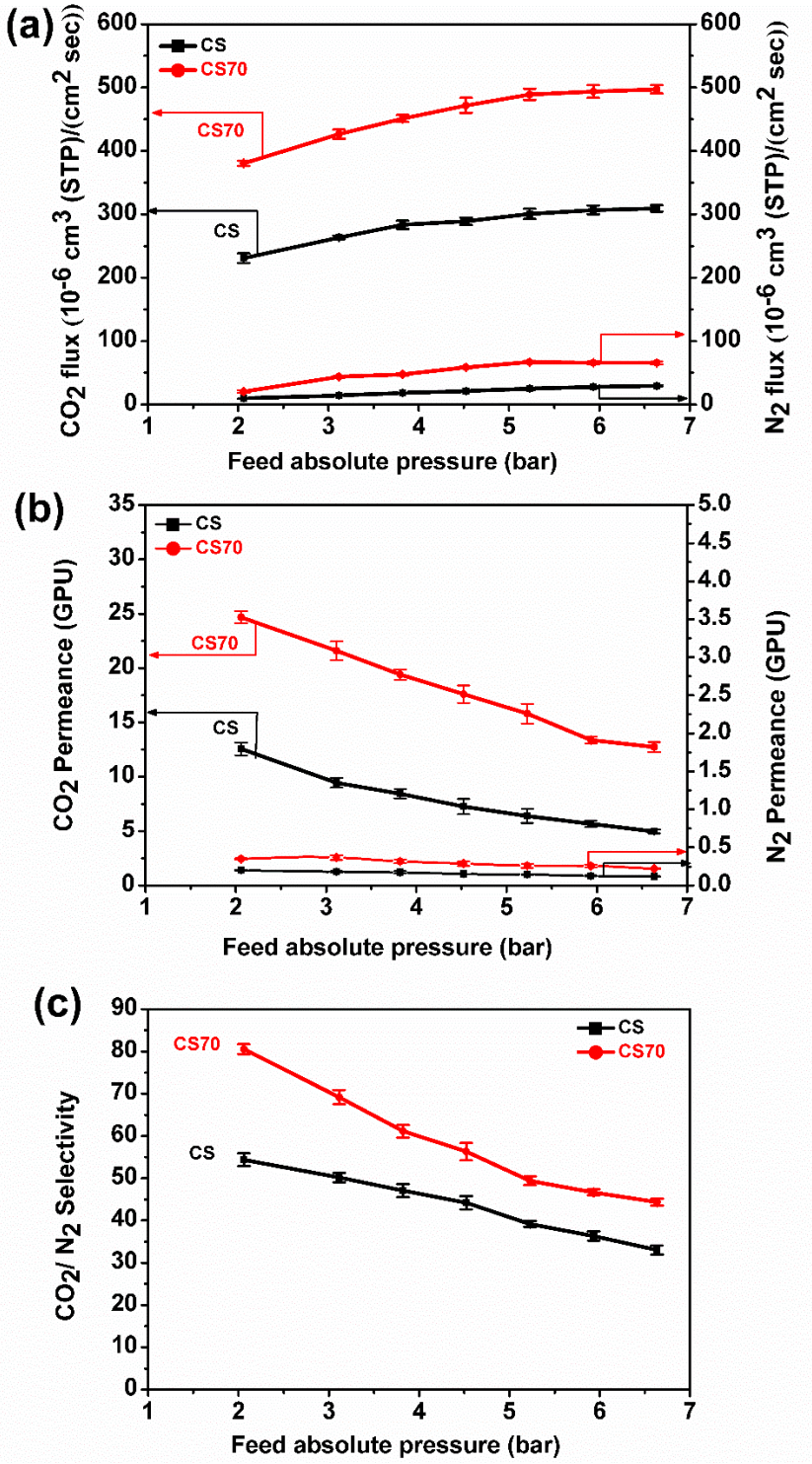

Figure 2.8 Effect of absolute feed pressure on (a) CO_2 and N_2 flux, (b) CO_2 and N_2 permeance and (c) CO_2/N_2 selectivity of CS and CS70 membranes at 90 °C with water flow rate = 0.03/0.05 ml/min (feed/sweep), sweep absolute pressure = 1.21 bar.

2.5.5.3 Effects of temperature on separation performance

The effect of temperature on CO_2 flux, CO_2 permeance and CO_2/N_2 selectivity of the membranes were investigated in the temperature range 70 to 120 °C (Figure 2.9a-c). The water flow rate of 0.03/0.05 ml/min (feed/sweep) and the absolute pressure of 2/1.21 bar (feed/sweep) were kept constant. The CO_2 separation performance was marginally improved with an upsurge in temperature from 70 to 90 °C and CO_2 separation performance drastically declined when the temperature reaches to 120 °C. The effect of temperature on pure CS and CS70 have followed the similar trend for CO_2 separation. The CO_2 flux, CO_2 permeance and CO_2/N_2 selectivity of CS membrane at 70 °C were 214 × 10^{-6} cm^3(STP)/cm^2s, 11.65 GPU, and 48, respectively, which reached to 227 × 10^{-6} cm^3(STP)/cm^2s, 54 and 12.5 GPU at 90 °C. Similarly, CO_2 flux, CO_2 permeance and CO_2/N_2 selectivity of CS70 membrane at 70 °C were 346 × 10^{-6} cm^3(STP)/cm^2s, 22.8 GPU and 69, respectively. When the temperature increased to 90 °C, the CO_2 flux, CO_2/N_2 selectivity and CO_2 permeance increased to 380 × 10^{-6} cm^3(STP)/cm^2s, 24.7 GPU and 80, respectively. This may be due to the rate of reaction between CO_2 and the carrier which enhanced as the temperature increased in the presence of water [137]. The CO_2 separation performance drops above 90 °C, owing to the reduction of moisture content in the membrane, which is responsible for the facilitated transport of CO_2. Also, the membrane flexibility is reduced with rise in temperature as less water ability of the membrane decreases. The gas molecules face more hindrance when membrane flexibility get reduced. The CO_2 flux, permeance and CO_2/N_2 selectivity of CS70 membrane were dropped to 70 × 10^{-6} cm^3(STP)/cm^2s, 3 GPU, and 17 respectively. The results suggest that water along with temperature play a very important for the facilitated transport of CO_2. The membrane temperature is suitable for high CO_2-amine reaction at which membrane can hold sufficient water inside the membrane. The CS 70 membrane is thermally stable up to 120 °C (as evident from TGA isotherm analysis). However, in terms of CO_2 separation performance, results were found better at 90 °C.

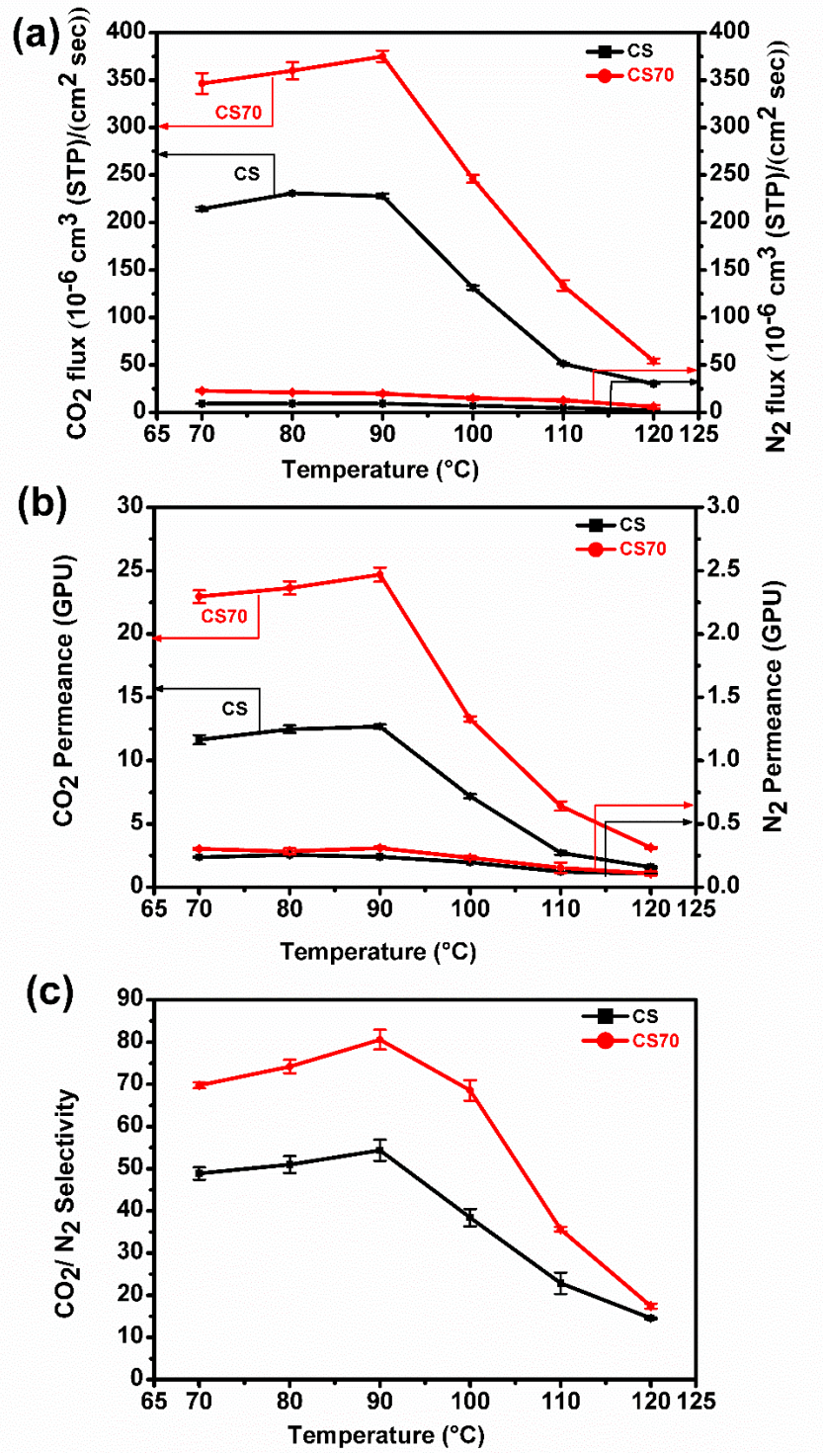

Figure 2.9 Effect of temperature on (a) CO_2 and N_2 flux, (b) CO_2 and N_2 permeance and (c) CO_2/N_2 selectivity, of CS and CS70 membranes at water flow rate = 0.03/0.05 ml/min (feed/sweep), feed absolute pressure = 2 bar and sweep absolute pressure = 1.21 bar.

2.5.6 Membrane stability performance

The stability of the membranes following facilitated transport membranes over considerable time duration is a desirable trait. The stability of CS70 membrane was checked for 300 h at 90 °C and 2 bar feed absolute pressure having water flow rate of 0.03/0.05 ml/min (feed/sweep). The membrane retained its CO_2 separation performance with little fluctuation over the period of 300 h as shown in Figure 2.10a. After completing the permeation study under different conditions, a small part of the used membrane was cut and again analysed in FESEM at 50 Kx magnification (Figure 2.10b). The top surface image showed no degradation of the active layer. Therefore, it can be concluded on the basis of FESEM analysis and permeance study that the composite membrane is suitable for the CO_2 separation.

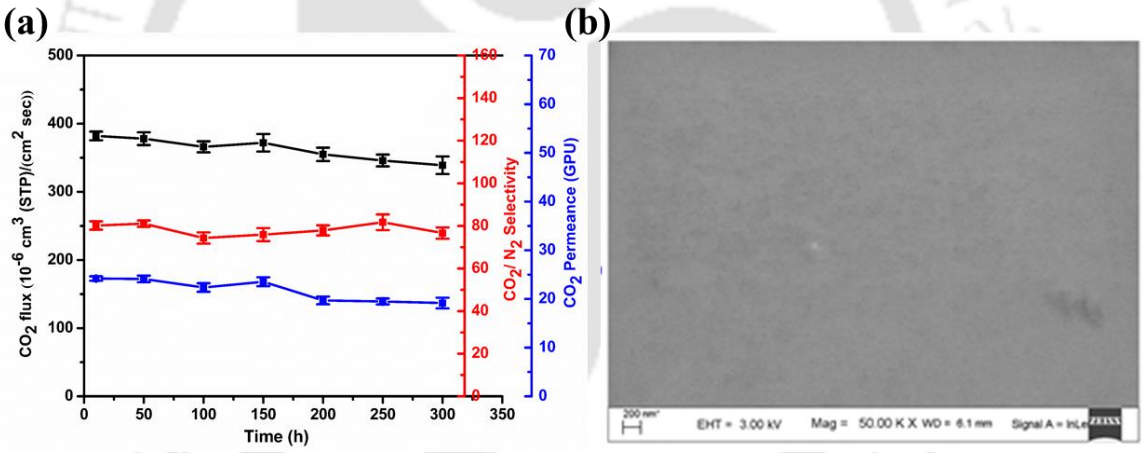

Figure 2.10 (a) Separation performance of CS70 membrane continuously run for 300 h at 90 °C with water flow rate = 0.03/0.05 ml/min (feed/sweep), feed absolute pressure = 2 bar and sweep absolute pressure = 1.21 bar, (b) FESEM image after permeation study.

2.6 Conclusions

This chapter included preparation of CS and CS-TEPA membranes with poly(ether sulfone) as support. The composition CS70 amongst the blended membranes was found to be optimum based on the characterization studies. The permeance of CS improved from 12.5 to 24.7 GPU

after addition of 30 wt % TEPA at 90 °C, having water flow rate of 0.03/0.05 ml/min (feed/sweep) and at an absolute feed pressure of 2 bar. As compared to control (CS), CS70 documented ~ 97 % and ~ 48 % higher permeance and CO_2/N_2 selectivity, respectively. The enhanced stability of the CS70 membrane has good potential for CO_2 separation.

CHAPTER 3

CO_2 Separation by Chitosan Membrane Containing Synthetic Poly(allylamine) as a Carrier

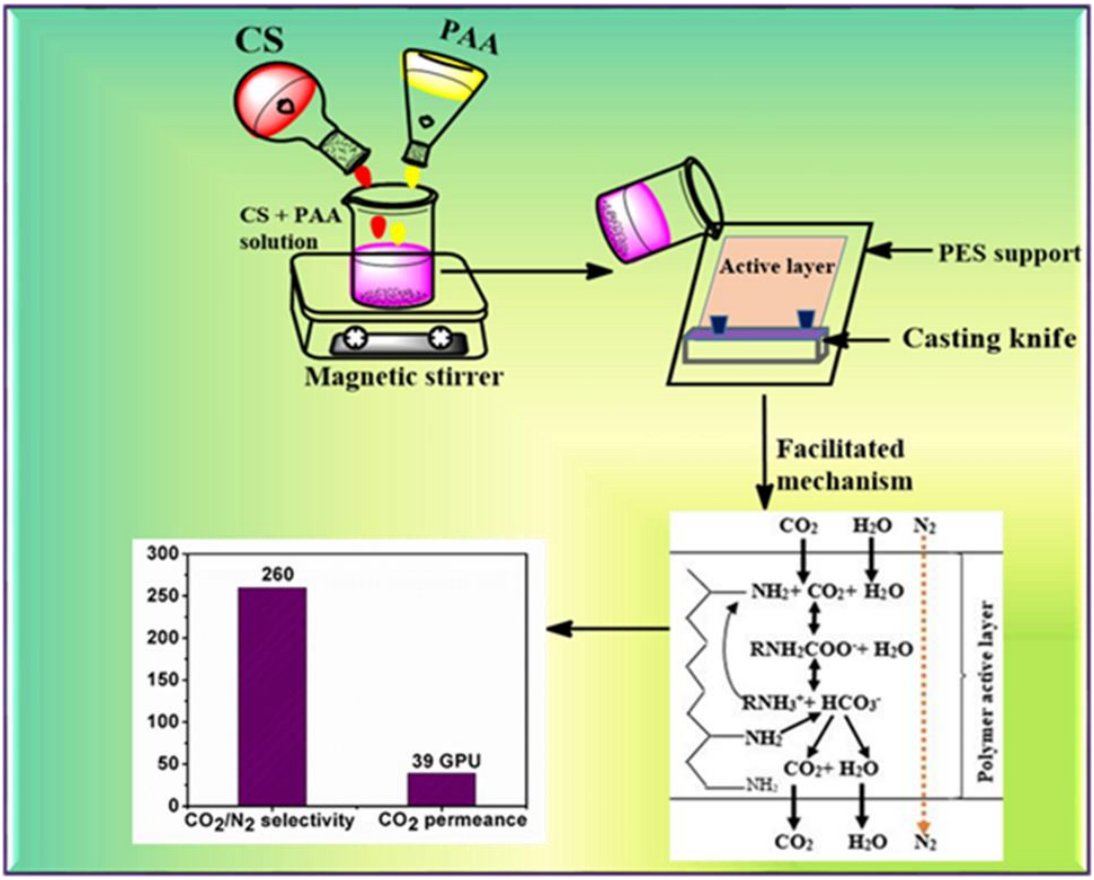

Graphical abstract of CS-PAA membrane preparation and its CO_2-amine reaction along with separation performance

CHAPTER 3

CO_2 Separation by Chitosan Membrane Containing Synthetic Poly(allylamine) as a Carrier

*Chitosan having just a single amine group per monomer unit, the total amount of amines in CS are insufficient to carry out significant facilitated transport of CO_2. The research in this chapter is oriented towards boosting the CO_2 separation performance by the addition of another synthetic poly-amine like poly(allylamine) (PAA) which is destined to be used as fixed carrier inside the CS membrane matrix, which otherwise alone is unstable film formation ability and brittle in nature. This chapter involves CS-PAA blend membrane preparation and detailed investigations of the prepared membrane including surface morphology, swelling test, thermal stability and gas permeation study at a different temperatures, pressures and water flow rates. The amalgamation of the film forming ability of CS and PAA as a fixed carrier, combined in a simple process can pave the way for a novel and efficient CO_2 gas separation. This work is scientifically acknowledged in "**Journal of Industrial and Engineering Chemistry**".*

3.1 Introduction

Facilitated transport mechanism aids in high CO_2 separation and CO_2/N_2 selectivity as compared to membranes following solution-diffusion mechanism. In the facilitated transport mechanism, mobile carriers have higher CO_2 separation capability than the fixed carriers, but lack in terms of carrier stability [138]. Poly(allylamine) (PAA) is one of the fixed carriers used for CO_2 separation in blend with other polymers, either without modification or in a sterically hindered form [82,95,96,98,103,132,139]. PAA consists of mainly primary amine groups (Figure A1.1c, Appendix 1) which is very brittle in the dry state and inability to form stable films. PAA has been extensively used in combination with crosslinked PVA for CO_2 separation [82,98,103,132] and also in mixed matrix, as a fixed site carrier [139]. The facilitated transport mechanism is boosted under temperature and moisture. Water being a solvent for PVA, might lead to degradation in CO_2 separation performance in absence of crosslinking above 70 °C [82]. In contrast, the stability of CS without any crosslinking, under

temperature and moisture conditions advocates its application for facilitated CO_2 separation. The research oriented towards the development of CS membranes for CO_2 separation has been though invigorated in literature, there is still scope for advancement by addition of PAA. The amalgamation of the film forming ability of CS and PAA as a fixed carrier, combined in a simple process can pave the way for a novel and efficient CO_2 gas separation. This study involves CS-PAA blend membrane preparation and detailed investigations of the prepared membrane including surface morphology, swelling test, thermal stability and gas permeation study at different temperature, pressure and water flow rate.

3.2 Experimental section

3.2.1 Materials

Chitosan (CS) flakes and poly(allylamine hydrochloride) were purchased from Sigma-Aldrich, USA. Pure (99.99 %) glacial acetic acid, potassium hydroxide pellets and methanol (> 99 % purity) were procured from Merck, Germany. The PES support, CO_2/N_2 gas mixtures were purchased from the suppliers as discussed in Chapter 2. Argon (Ultrapure) and Helium (99.999 % pure) were procured from Vadilal Chemicals Ltd., India. The CO_2/N_2 gas mixture and Argon were used as feed and sweep gas respectively. Helium was used as carrier gas for the gas chromatography (GC) analysis.

3.3 Membrane preparation

Chitosan flakes of 1.15 g were dissolved in 1 vol % acetic acid solution and stirred continuously for 12 h. To remove undissolved particles and bubbles, the solution was centrifuged (model: Sigma 3-30 k) for 30 min at 10000 rpm. Poly(allylamine hydrochloride) (PAA) was mixed with potassium hydroxide in methanol to get free poly(allylamine). The free PAA was added slowly to the chitosan solution under stirring for 4 h to achieve a homogenous solution. The active layers having four different weight ratio of blends of CS and PAA (CS-PAA) such as 100 wt % CS (CS), 85 wt % CS + 15 wt % PAA (PAA15), 70 wt % CS + 30 wt % PAA (PAA30) and 55 wt % CS + 45 wt % PAA (PAA45). The PES support was carefully fixed on a glass plate using tape to prevent entry of any air bubbles. The CS-PAA solution was degassed before casting onto the PES support. The thickness was controlled

using an adjustable micrometer casting knife (GARDCO, Paul N. Gardner, USA). The film formation of the cast solution took place inside the fume hood at room temperature after 48 h. Then, the membranes were cut to fit the gas module after drying in the oven (120 ºC, 6 h).

3.4 Membrane characterization

The surface topography of the membranes (active layers with PES support) were visualized using advance microscopic techniques like FESEM (ZEISS, USA) and AFM (Innova, Bruker). The samples were fixed onto carbon tape and gold sputtered before FESEM imaging of the surface and cross-sectional view at 2-3 kV. The high resolution topographical AFM images were recorded at a scan rate of 0.7 Hz in tapping mode. AFM images were further processed using flatten filter in Windows-Scanning-x-Microscope (WSxM) software [140].

Different relative humidity (RH, %) was maintained for swelling measurements, by mixing different wt % of water and glycerol. The mixture of water-glycerol at different wt % was put in a round bottom flask with three openings as shown in Figure 3.1. The humidity meter and thermometer were inserted through the side openings to measure the relative humidity and temperature, respectively. The volumes of glycerol and water for different weight ratio is calculated using the following equations [141].

$$G_v = (G_w W_r)/(100 \times 1.262) \quad (3.1)$$

Where G_v is the glycerol volume (ml), G_w is the glycerol weight in the solution, W_r is the total solution wt (g), 1.262 is the density (g/ml) of glycerol.

$$H_v = [(100- G_v) W_r]/(100 \times 1) \quad (3.2)$$

Where H_v is the water volume with density 1 g/ml.

A sample of 4 cm × 4 cm was suspended with the help of binder clip such that the sample does not touch the solution responsible for the relative humidity (RH) inside the round bottom flask. The samples were kept at a particular RH for 10-12 h to reach the saturation. The swelling (%) of the membranes were calculated as $= \frac{W_w - W_d}{W_d} \times 100$, where, W_w is the humidified weight of the membrane and W_d is the dry weight recorded after placing the membrane in the oven at 120 °C for six hours.

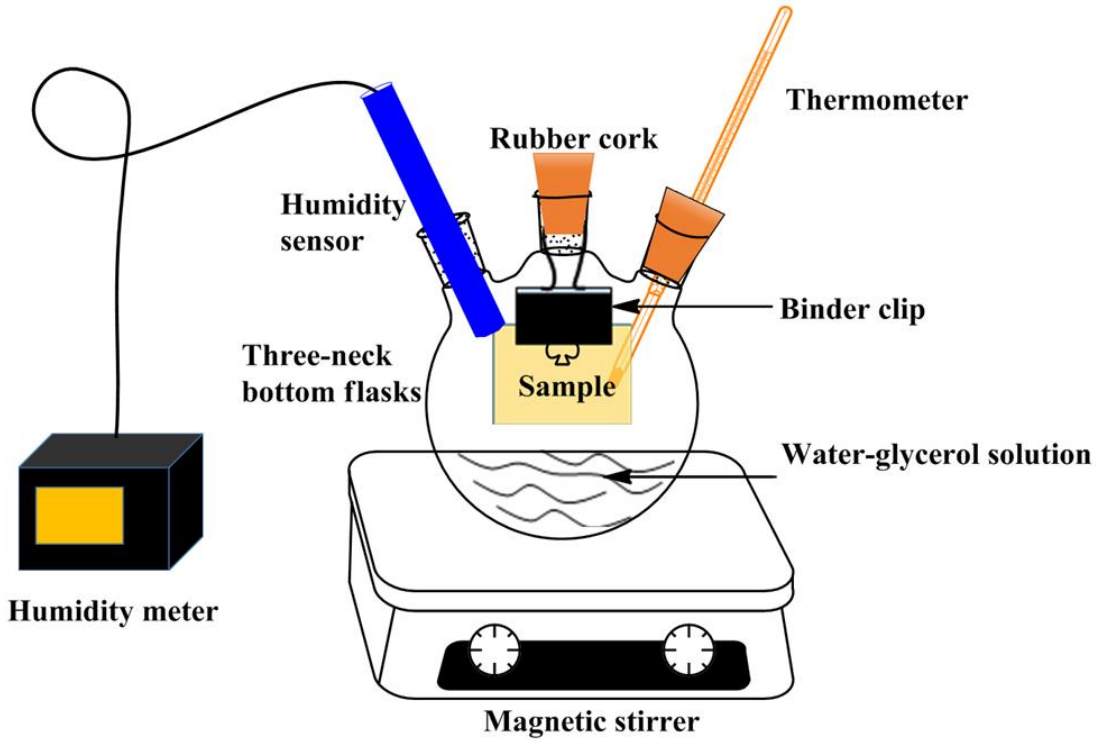

Figure 3.1 Swelling test experimental set-up.

The FTIR was recorded (SHIMADZU, IR Affinity-1, Japan) at 25 °C performing 100 scans at 4.0 cm^{-1} resolution. For thermogravimetric analysis (TGA) (TGA4000, Perkin-Elmer, USA), samples were heated from 30-450 °C at a heating rate of 10 °C /min under nitrogen environment (flow rate 20 ml/min) in order to predict the thermal stability of the prepared membranes. Further, TGA isotherm (make: NETZSCH TG 209F1, Libra) was conducted on PAA30 with waiting time of 40 min at each temperature set to 100 °C, 120 °C and 150 °C consecutively. Differential scanning calorimetry (DSC) (Mettler Toledo, STAR^{e}) of the samples were performed from 40-140 °C to obtain the moisture release temperature peaks. The physical properties of the membranes were investigated with the help of dynamic mechanical analysis (DMA) (Netzsch DMA 242E Artemis®). Membrane stiffness can be analysed from the plot of storage modulus (MPa) vs temperature (°C). The temperature was varied from 30-140 °C at a heating rate of 2.5 °C/min under N_2 environment. The instrument was operated in a tensile mode, having a frequency of 1 Hz and dynamic force of 1 N.

3.5 Results and discussion

3.5.1 Microscopic analyses

The top surface view of the porous PES support is shown in Figure 3.2a. The active dense layer of thickness ~ 4.5 μm formed on the PES support is visible in the FESEM image (Figure 3.2b). Formation of active layer confirms no leakage of solution into the pores of the support during casting. This offers minimal mass transfer resistance for passage of the gas molecules. The top surface view of the different membranes cast with varying the wt % of PAA in CS such as CS, PAA15, PAA30 and PAA45 have been shown in Figure 3.3a-d, respectively. The smooth topography of the active layer of pure CS as compared to that of the PAA blended membranes is visible in the FESEM images. The roughness increases with increase in PAA content in the membranes. Carboxylic group of acetic acid is present in the form of $-COO^-$ in aqueous solution, whereas the amine group of PAA is present in the form of NH_3^+ as PAA chains are expected to be ionized state in the pH range 5.5-6 [142]. Changes in the charge density due to the formation of $-COO^-$-NH_3^+ ionic intermolecular crosslinks can be attributed to the observed roughness factor [143]. Similar behaviour in roughness was also witnessed when PAA hydrochloride was mixed with poly(acrylic acid) [142]. As the polymers arrange themselves in loopy conformation, circular structures were visible across the CS-PAA blend membrane surfaces [142].

Hence, AFM was further performed to analyse these structures that imparted roughness. The AFM 2-D images, height profiling and 3-D images are shown in Figure 3.4. The average roughness followed the trend CS (8 nm) < PAA15 (94 nm) < PAA30 (205 nm) < PAA45 (712 nm) which corroborated with the FESEM observations. The increase in surface roughness increases the effective membrane area which improves the overall flux [144]. Hence, this increased roughness contributed positively to the gas separation performance. The height profiling of the blend membranes revealed circular patches of depth ~300 nm for PAA15 and very large ones ~ 800-900 nm for PAA30 and PAA45. This suggested that it will be challenging to synthesize a active layer with thickness < 1 μm without pores when PAA is incorporated into the CS matrix.

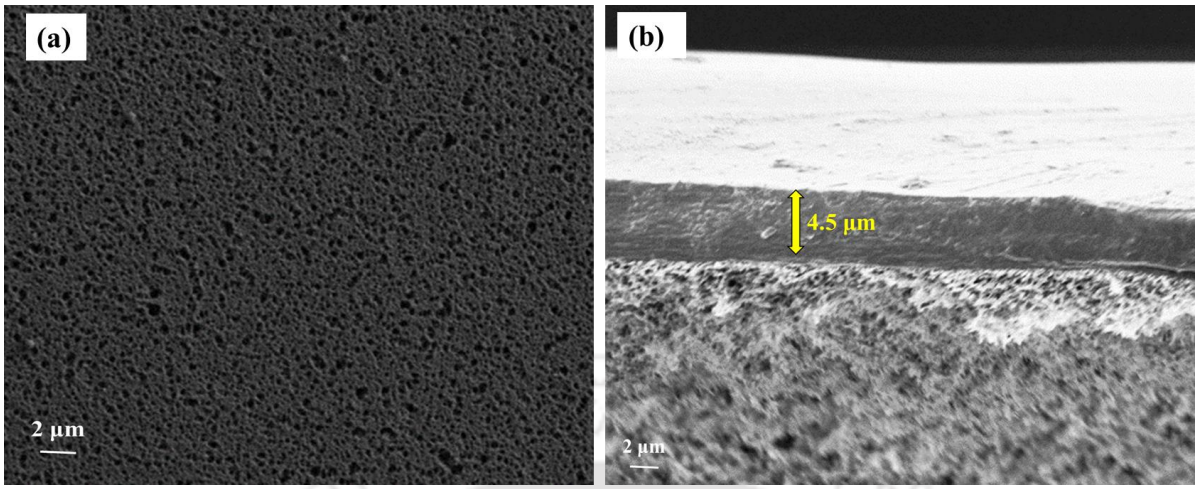

Figure 3.2 FESEM images of (a) top surface of the PES support and (b) cross-section of the active layer (PAA30) over the PES support.

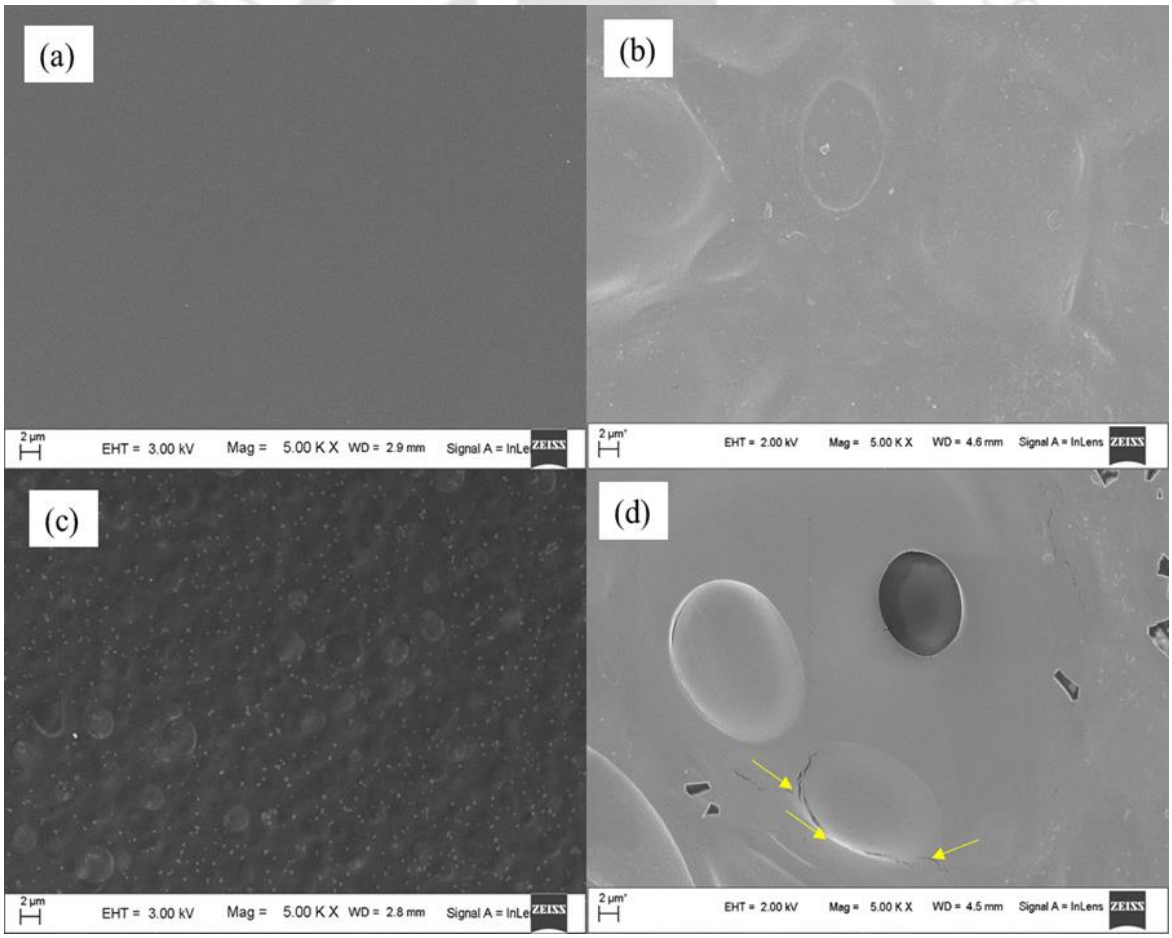

Figure 3.3 FESEM top surface view of (a) pure CS, (b) PAA15, (c) PAA30 and (d) PAA45 membranes (inset arrows indicate crack development).

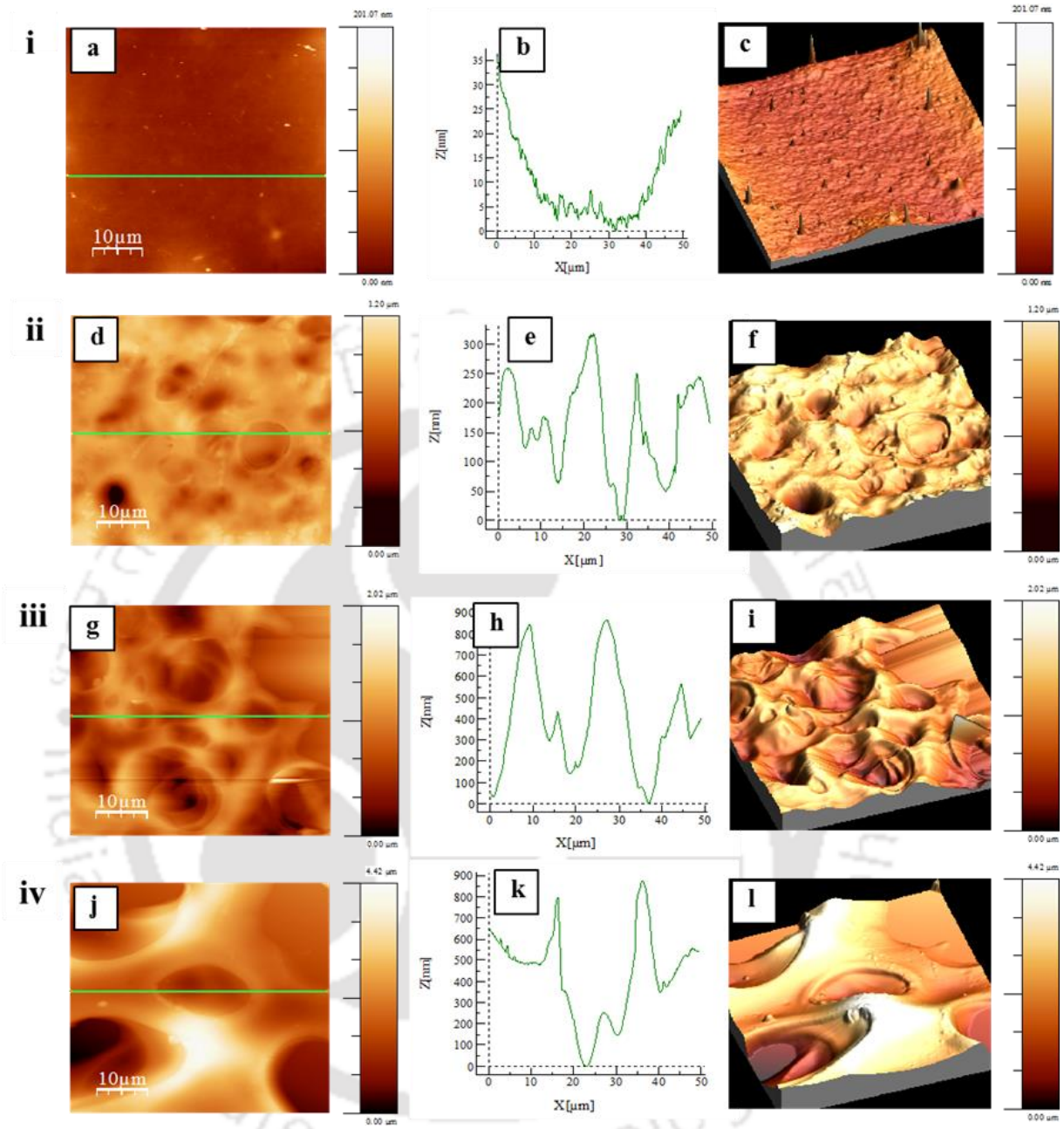

Figure 3.4 AFM topography of (i) pure CS, (ii) PAA15, (iii) PAA30 and (iv) PAA45 membranes with their respective height profiling of the 3-D images.

3.5.2 Water swelling test

From the degree of swelling of CS, PAA15, PAA30 and PAA45 at different RH (Figure 3.5), two exponential functions can be perceived. The first and the second exponential function lies

in the region of 20-80 % and > 80 % of RH, respectively. The point of RH (> 80 %) where the second phase exponential manifests, is defined as the critical RH. This kind of biphasic behavior can be related with the Flory-Huggins theory. The swelling free energy of mixing (ΔG_{mixing}) is controlled by the polymer conformation ($\Delta G_{conform}$) and contact between polymer segment and water molecules ($\Delta G_{contatct}$). This can be given by the following equations [94].

$$\Delta G_{conform} = RT\ [\ln\varphi_w + \varphi_p] \tag{3.3}$$

$$\Delta G_{contatct} = RT\chi\ \varphi^2_p \tag{3.4}$$

Where, R is the gas constant, T represents absolute temperature, ϕ is the volume fraction and χ indicates the polymer-solvent interaction parameter. The subscripts p and w indicates polymer and water, respectively.

The water holding capacity of the blend membranes in regions < 80 % RH followed the trend CS <PAA15 <PAA30 <PAA45 relative to the respective PAA concentrations. Notably, the film thickness and ionic crosslink density regulate the propagation of the water molecules across the membrane [145]. At RH regions (< 80 %), the overall swelling of the membrane is governed by $\Delta G_{conform}$ (Equation 3.3) which depends on the mixing of water and polymer chain. This induces chain relaxation and provides flexibility to the membrane that permits the gas molecules to pass through, without hindrance. Above the critical RH, the swelling is determined by the polymer affinity to water. At regions below critical RH, CS displayed the minimum swelling whereas, blending with PAA improved the water holding capability. The probable reason can be due to the high ionic crosslinking among CS and PAA in the polymer matrix [145]. The second exponential function (> 80 % RH) was due to the concerted effects of $\Delta G_{conform}$ and $\Delta G_{contatct}$ (Equation 3.4). At this region, the reduction in swelling behavior of the blend membranes can be justified by the polymer-solvent interaction parameter. Owing to the ionic crosslink, the accessible polymer for water interaction is less prospective [145]. The swelling behaviour is influenced by the internal material factors like ionic crosslinking, conformational changes, pH conditions, hydrophilic and hydrophobic behaviour of the membrane, acid-base functional groups, etc. [145]. CO_2 can pass through the matrix in the presence of moisture by solution-diffusion mechanism. The capability of the matrix to hold water is vital for CO_2 transport through the membrane and hence influences the permeance

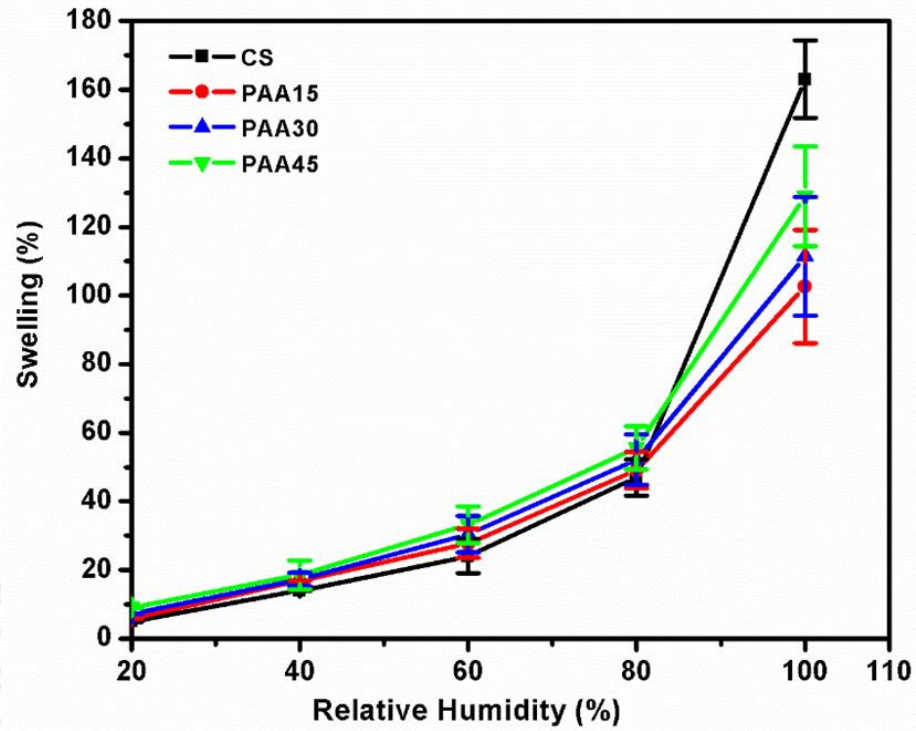

Figure 3.5 Swelling (%) vs relative humidity (%).

and selectivity. Swelling helps in the CO_2-amine reversible reaction in the membrane resulting in increase in the CO_2 flux. Further, the reasonable presence of moisture in the membrane increases the chain flexibility by plasticization effect which enhances the overall free volume and hence gas molecule face less resistance as compared to the dry membrane.

3.5.3 Characterization by FTIR spectroscopy

The FTIR peaks (Figure 3.6) detected in the range of 3000-3700 cm^{-1} for all the prepared membranes was due to N-H and O-H stretching [146]. With the addition of PAA, the spectrum in this region broadened owing to the formation of hydrogen bond with water molecules. The peak at 1652 cm^{-1} is assigned to C=O stretching of acetylated amino group [147]. The peak intensity at 1583 cm^{-1} increases with increasing concentration of PAA in the prepared membranes and can be assigned to the existence of the amine. The facilitated transport of CO_2 is aided by the presence of high amine content with PAA addition.

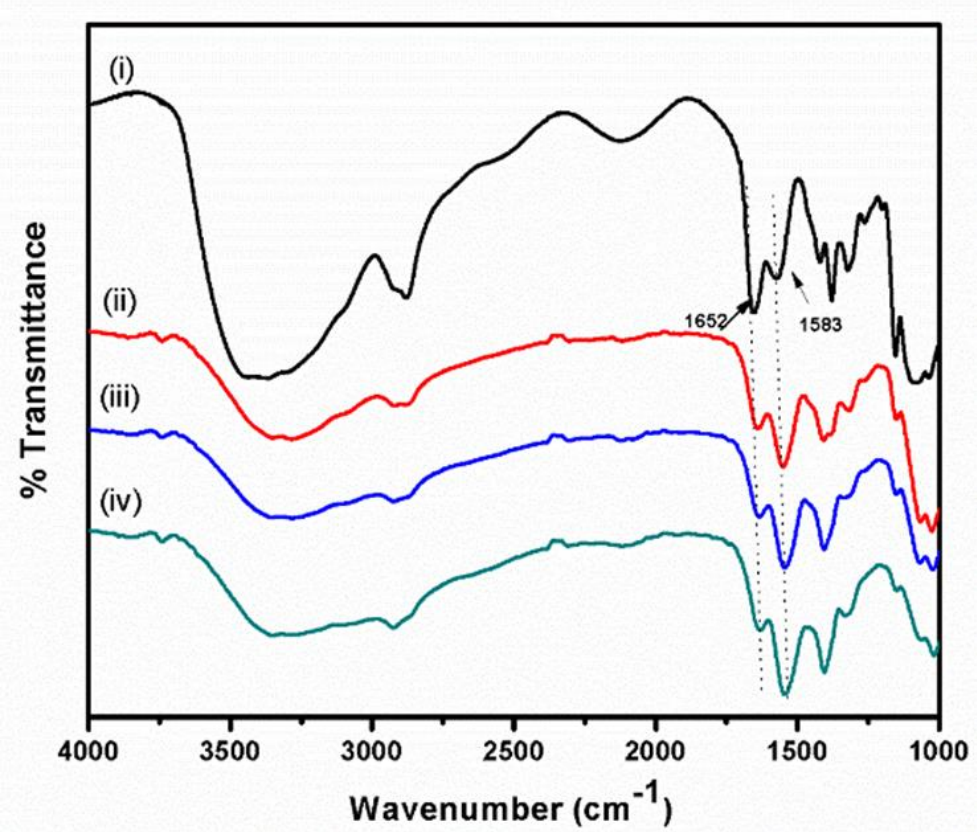

Figure 3.6 FTIR spectra of (i) CS, (ii) PAA15, (iii) PAA30 and (iv) PAA45 membranes.

3.5.4 Thermogravimetric analysis (TGA) measurements

The TGA profile of the membranes in the temperature range of 30-450 °C under study is presented in Figure 3.7. The weight loss due to moisture observed up to 120 °C for CS, PAA15, PAA30 and PAA 45 are 11 %, 14 %, 18 % and 20 %, respectively. The PAA amines in the active layer of the membranes have the potency to react with the atmospheric CO_2 in presence of moisture. Hence, the CO_2 entrapped in the membranes was released, that was perceived as weight loss during heating up to 120 °C. This also correlated to the amount of PAA content in the membranes. The unwavering stable performance of the membranes up to 175 °C as revealed by TGA, signposts the thermal stability of the membranes for CO_2 separation performance under the study range of 60-120 °C.

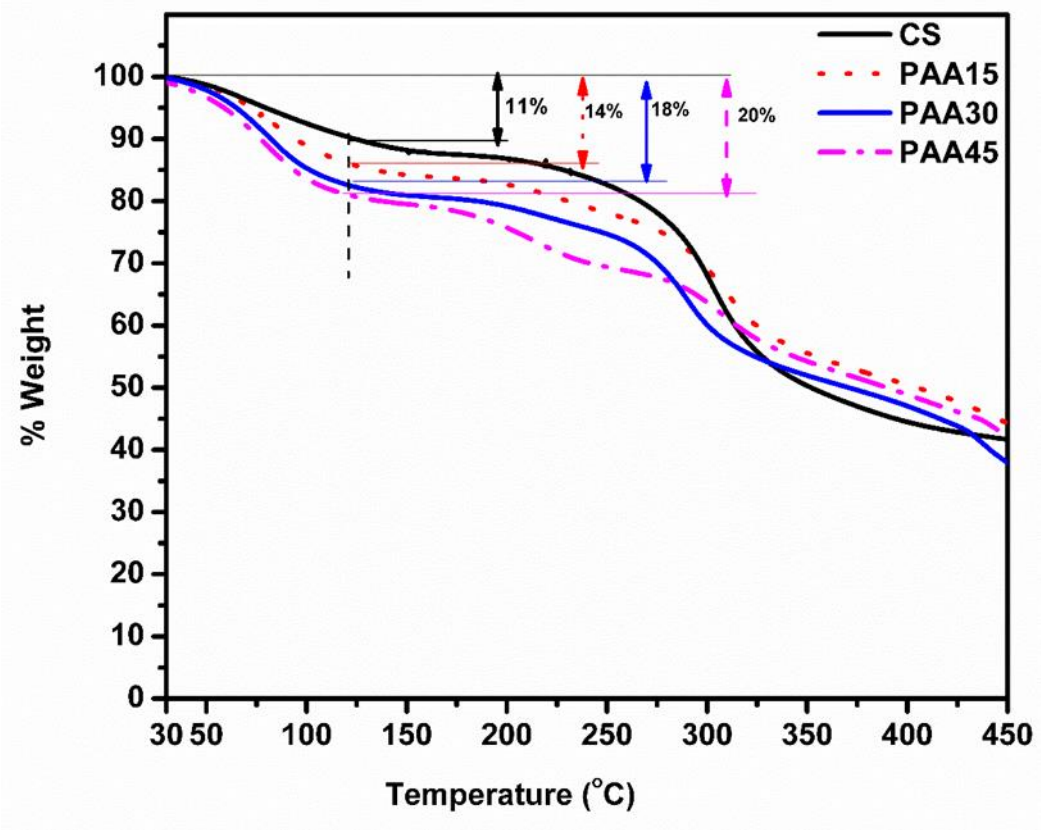

Figure 3.7 TGA curve of CS, PAA15, PAA30 and PAA45 membranes.

3.5.5 Dynamic mechanical analysis (DMA)

Dynamic mechanical analysis (DMA) is a useful tool to study the thermo-mechanical property of the membranes. The effect of variation of temperatures (30-140 °C) on the storage modulus of the prepared membranes were evaluated. The storage modulus vs temperature (Figure 3.8) furnishes substantial information on the stiffness of the membranes. The increase in storage modulus with temperature indicates the increase in stiffness of the membrane [148]. The increase in the stiffness affects the gas permeation through the membrane by increasing the mass transfer resistance. The storage modulus of CS followed an uptrend up to 140 °C. However, PAA15 and PAA30 membranes displayed escalation in the storage modulus up to 100 °C and then a deflation is observed. The initial boost of storage modulus up to 100 °C can be ascribed to the removal of water molecules that make the membrane less flexible and brittle [149][150]. Hence, PAA45 attained the stiffness peak at 85 °C itself. The collapse in the

storage modulus of all the prepared membranes except CS can be accredited to the boost in mobility of polymer at high temperature, in absence of water molecules.

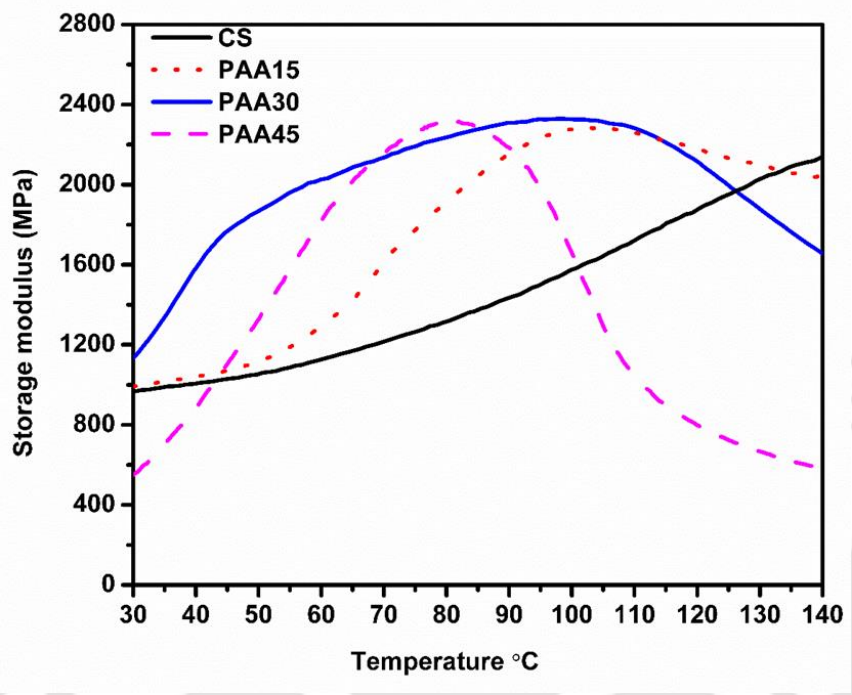

Figure 3.8 DMA curve of CS, PAA15, PAA30 and PAA45 membranes.

3.5.6 CO_2 separation performance of the prepared membranes

The prepared CS-PAA membranes were evaluated for their CO_2 separation performance ability at 90 °C, with water flow rate of 0.03/0.05 ml/min (feed/sweep) and absolute pressure of 2/1.21 bar (feed/sweep). These particular operating conditions were found to support the optimum CO_2 separation by pure CS membrane as discussed in the previous chapter. The CO_2 permeance of pure CS was 12.5 GPU while CO_2/N_2 selectivity of 54. After blending 15 wt % PAA (PAA15), the CO_2 permeance of the membrane reached to 28 GPU. Further, the addition of 30 wt % of PAA (PAA30), 39 GPU of CO_2 permeance was attained which is ~ 212 % higher as compared to that of CS. Similarly, the CO_2/N_2 selectivity of PAA15 and PAA30 were found as 175 and 260 respectively, which were ~ 224 % and ~ 381 % higher than that of CS alone. The rise in the primary amine groups in the blend membranes due to addition of

PAA are responsible for the observed enhanced facilitated transport mechanism. Additionally, the roughness factor as corroborated from FESEM and AFM study contributed to the increase in overall surface area for gas permeation [144]. However, the CO_2/N_2 selectivity decreased drastically (~ 6 fold) when PAA content reached to 45 wt % (PAA45) compared to PAA30. The roughness as well as the depth of the circular structures, as evident from the advance microscopic analysis (Figure 3.4), was excessive that deformed the membrane surface and allowed N_2 molecules to pass through. This eventually led to shrinkage of the overall selectivity. Table 3.1 indicates the best performance was displayed by PAA30. Further the effect of sweep water flow rate, temperature and feed absolute pressure were evaluated for the PAA30 membrane only.

Table 3.1 CO_2 permeance and CO_2/N_2 selectivity of CS, PAA15, PAA30 and PAA45 membranes at 90 °C with water flow rate 0.03/0.05 ml/min (feed/sweep) and absolute pressure of 2/1.21 bar (feed/sweep) (The data of pure CS has been taken from the study conducted in Chapter 2).

Membrane	CO_2 permeance (GPU)	CO_2/N_2 selectivity
CS	12.5 ± 0.67	54 ± 2
PAA15	28 ± 2.41	175 ± 7
PAA30	39 ± 1.95	260 ± 9
PAA45	44 ± 2.15	42 ± 4

3.5.6.1 Effect of sweep water flow rate on CO_2 separation performance by PAA30

The effect of varying sweep water flow rates (0.01 – 0.07 ml/min) on CO_2 flux, CO_2/N_2 selectivity and CO_2 permeance for the PAA30 membrane are represented in Figure 3.9. The feed water flow rate (0.03 ml/min), feed absolute pressure (2 bar), sweep absolute pressure (1.21 bar) and temperature (90 °C) were kept constant. The CO_2 flux, CO_2/N_2 selectivity and CO_2 permeance performances of the membrane were very inferior under dry state. As

moisture was supplied to the gas permeation system, the reversible reaction between CO_2 and amine starts immediately as the humidified gases get in contact with the active layer of the membrane. Hence, all the performance parameters gained momentum. The CO_2 flux (9/591 × 10^{-6} cm^3(STP)/cm^2s), CO_2 permeance (0.45/39), and CO_2/N_2 selectivity (8/260) improved ~ 65, ~ 86 and ~ 32 fold, respectively as the water flow rate was raised from 0.00 to 0.05 ml/min. The values in parentheses indicate the respective performance parameters at 0.00/0.05 ml/min of water flow rate. The further increase in sweep water flow rate (> 0.05 - 0.07 ml/min) do not add value to the CO_2 flux and CO_2 permeance and a saturation was

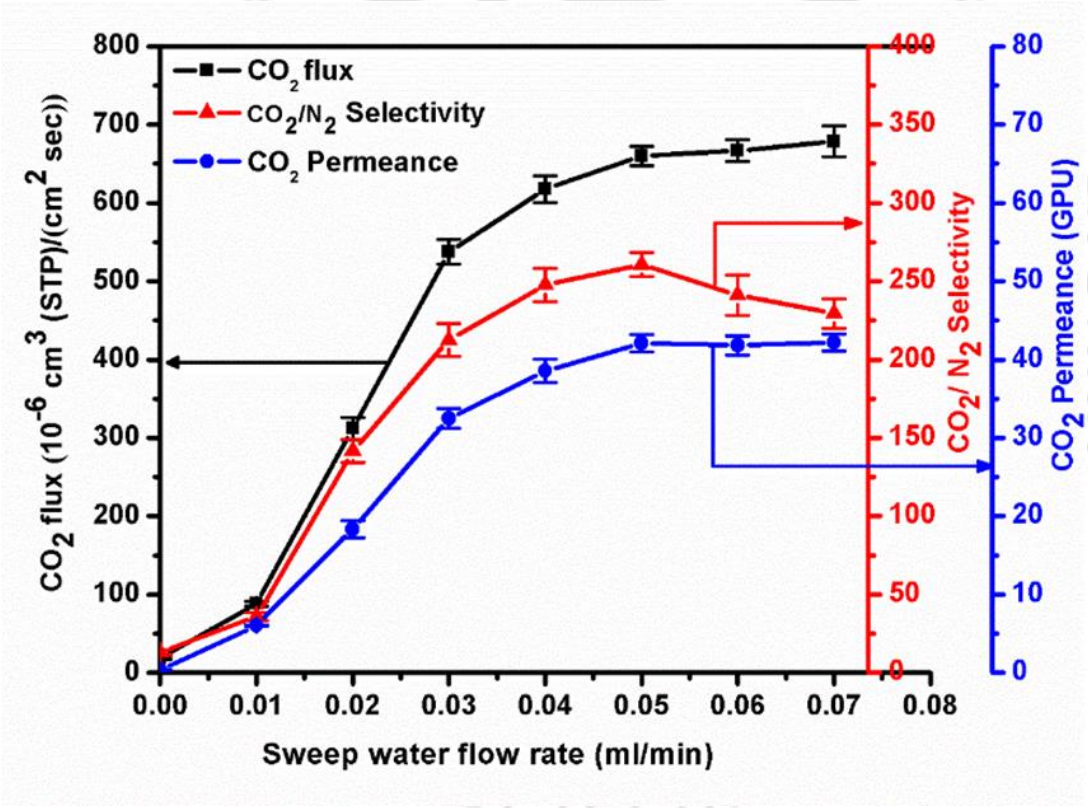

Figure 3.9 Effect of sweep water flow rate on CO_2 flux, CO_2/N_2 selectivity and CO_2 permeance of PAA30 membrane at temperature of 90 °C, feed water flow rate = 0.03 ml/min and absolute pressure = 2/1.21 bar (feed/sweep).

apparent. However, minor decrement in the CO_2/N_2 selectivity to 184 when water flow rate reached to 0.07 ml/min can be attributed to the passage of N_2 molecules through the membrane

due to high swelling. It is expected that water flow rate will provide a positive contribution to CO_2 separation when the RH does not cross the critical point. The CO_2 reacts with amines present in the active layer in the presence of moisture and transport across the membrane in the form of carbamate or bicarbonate and dissociate in sweep side to release CO_2 [151] which takes place due to the reactions between CO_2 and amine as explained in the Chapter 1, Equations (1.1) - (1.6). The diffusivity of bicarbonate is higher than the pure CO_2 resulted in high CO_2 permeance than the non-reacting gases like N_2. However, higher flow rates (> 0.05 ml/min) introduce more swelling by increasing inter-chain space of the polymer and permits a decent amount of N_2 molecules to pass [89]. Hence the overall CO_2/N_2 selectivity declined.

3.5.6.2 Effects of temperature on separation performance

The effect of temperature ranging from 60 – 120 °C of PAA30 on CO_2 separation performance is displayed in Figure 3.10. The feed and sweep side absolute pressure were kept constant at 2 bar and 1.21 bar, respectively while feed and sweep water flow rate was maintained at 0.03 ml/min and 0.05 ml/min, respectively. The positive effect of temperature on CO_2 separation performance was observed between 60 – 90 °C, where the CO_2 flux, CO_2/N_2 selectivity and CO_2 permeance had an uptrend improvement. The CO_2 flux, CO_2/N_2 selectivity and CO_2 permeance were 565 × 10^{-6} cm^3 (STP)/cm^2s, 195 and 37 GPU, respectively at 60 °C and improved to 591 × 10^{-6} cm^3 (STP)/cm^2s, 260 and 39 GPU, respectively at 90 °C temperature. In this temperature region, the retained water molecules in the membrane matrix helped to sustain the membrane flexibility and the rate of reaction between CO_2 and amine. At low temperature, flexibility and swelling of the polymer chain enables both solution-diffusion and facilitated transport mechanism to play a substantial role in CO_2 permeation. As the temperature is up surged, CO_2 permeation is backed up entirely by facilitated transport mechanism.

The DSC study (Figure 3.11) validated that most of the moisture from the membrane evaporated at temperature ≤ 100 °C. The endotherm peak of CS was realized at around 96 °C whereas, rest of the curve having an endothermic peak at below 95 °C. This can be attributed to the presence of the CS hydroxyl group that can form stronger hydrogen with water than amine molecules [125]. Beyond 90 °C, the reduced water holding capacity of the membrane diminishes the facilitated transported mechanism. High temperature also leads to membrane

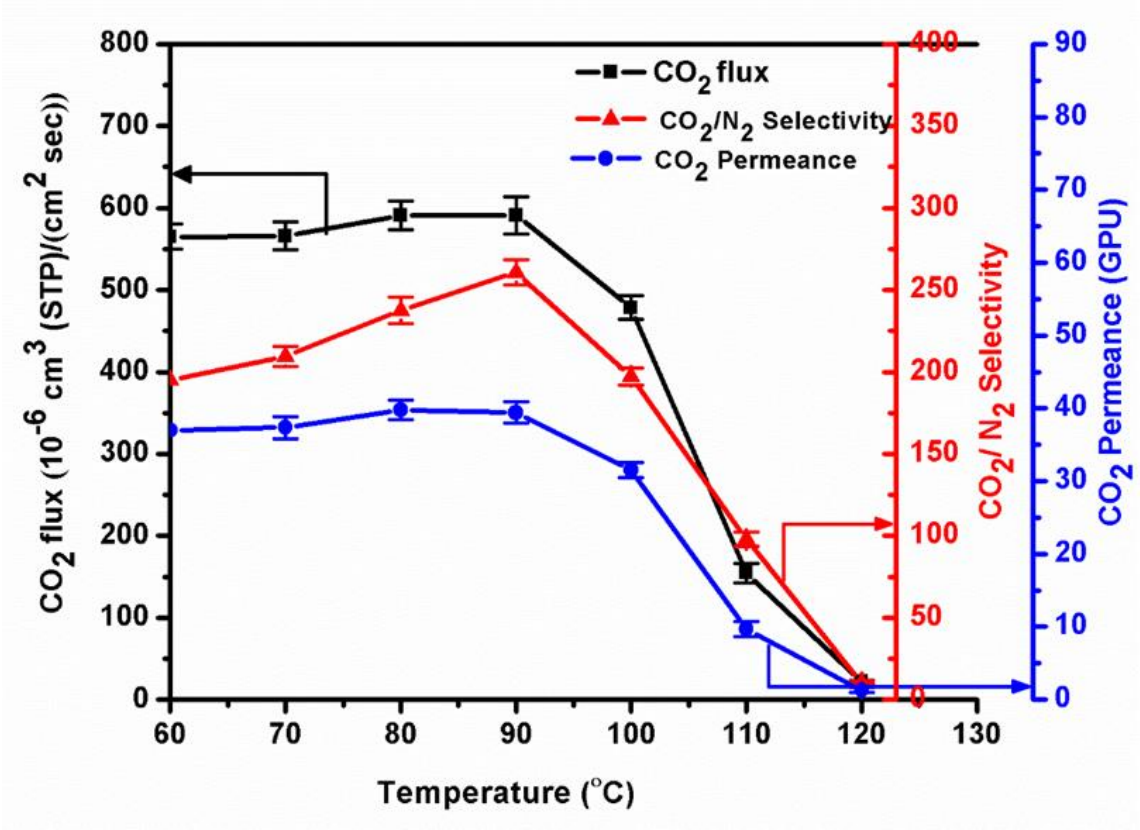

Figure 3.10 Effect of temperature on CO_2 flux, CO_2/N_2 selectivity and CO_2 permeance of PAA30 membrane at water flow rate = 0.03/0.05 ml/min (feed/sweep), feed absolute pressure = 2 bar and sweep absolute pressure = 1.21 bar.

stiffness as validated by DMA data that impedes the passage of gas molecules. The N_2 gas molecule that relies solely on solution-diffusion mechanism is not effective at high temperature. Hence, beyond 90 °C, the performance started to drop. The drastic decline in the CO_2 flux, CO_2/N_2 selectivity and CO_2 permeance at 120 °C suggested the typical facilitated transport dominated permeation of CO_2 at temperature ≤ 90 °C.

The linear TGA isotherm profile (Figure 3.12) for the extended time (40 min) at study temperatures 100 °C and 120 °C demonstrated its thermal stability and supports its application for long term operation. However, a decline of ~ 1.5 wt % was perceived for the isotherm conducted at 150 °C which can be presumed owing to PAA degradation.

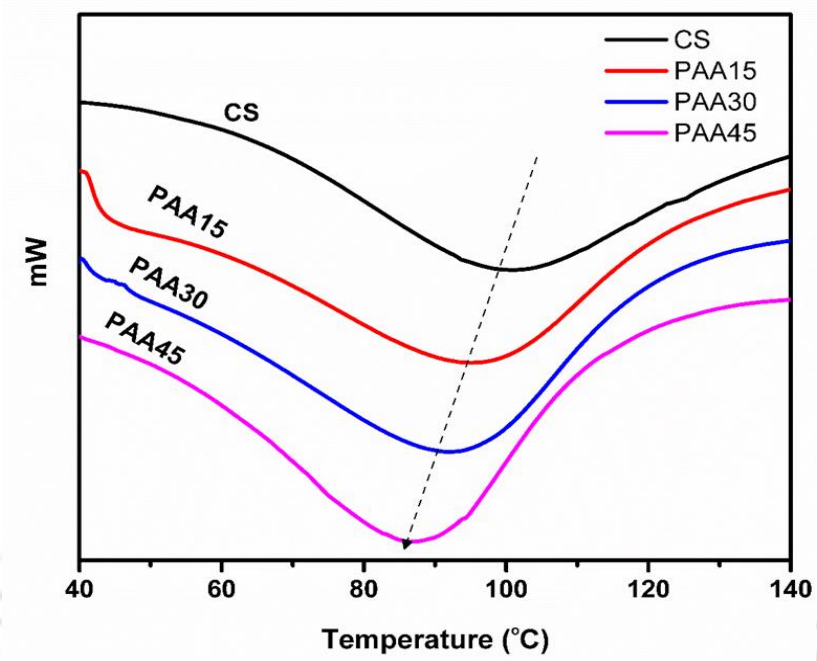

Figure 3.11 DSC (moisture peaks) of the prepared membranes.

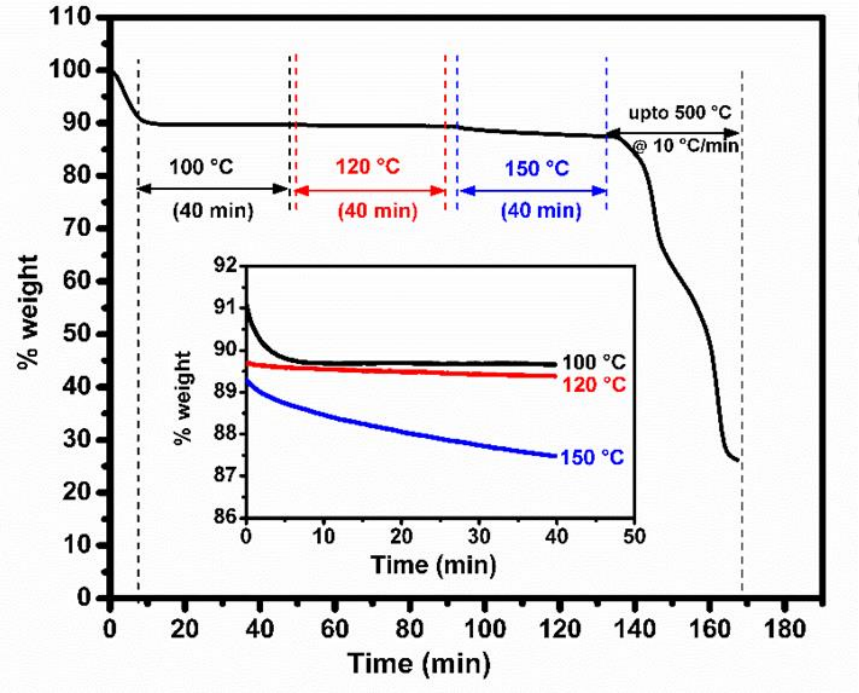

Figure 3.12 TGA profile of PAA30 at different isotherm (inset TGA isotherm at 100 °C, 120 °C, and 150 °C for 40 min).

3.5.6.3 Effects of feed absolute pressure on CO_2 separation performance

The effect of feed absolute pressure on PAA30 was studied at a constant sweep absolute pressure of 1.21 bar, temperature of 90 °C having water flow rate of 0.03/0.05 (feed/sweep) ml/min (Figure 3.13). The feed absolute pressure was varied from 2 bar to 5.91 bar. The flux at 2 bar was 591 × 10^{-6} cm^3 (STP)/cm^2s and trailed a linear boost up to 3 bar and reached to 859 × 10^{-6} cm^3 (STP)/cm^2s. The plausible reason can be the formation of the CO_2-amine complex at a high CO_2 partial pressure that drives CO_2 gas molecules. Exceeding pressure of 3 bar, the increment of CO_2 flux becomes insignificant due to carrier saturation at higher

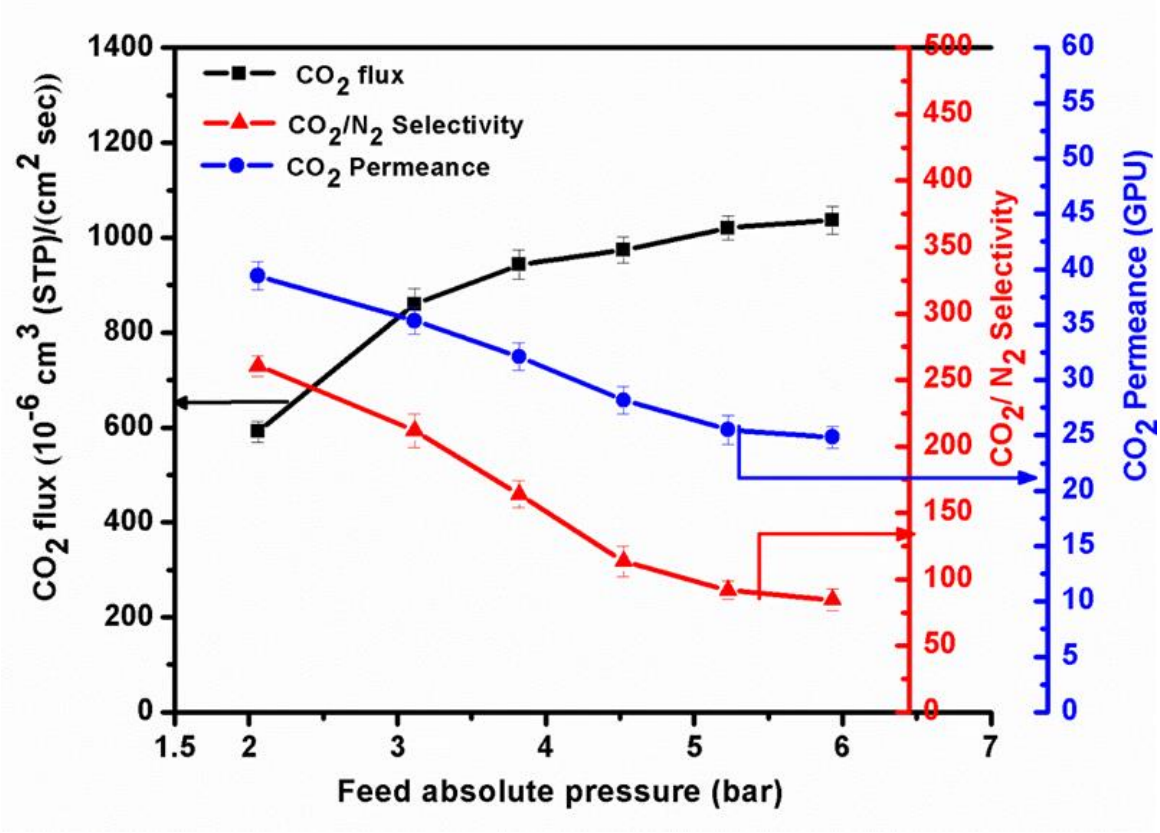

Figure 3.13 Effect of absolute feed pressure on CO_2 flux, CO_2/N_2 selectivity and CO_2 permeance of PAA30 membrane at water flow rate = 0.03/0.05 ml/min (feed/sweep), at temperature 90 °C and sweep absolute pressure = 1.21 bar.

partial pressure of CO_2. Henceforth, contribution to CO_2 flux is controlled by solution-diffusion mechanism, a characteristic trait of the membranes following facilitated transport mechanism. CO_2 facilitated transport mechanism is operational at low partial pressures until the carrier acquires saturation [152]. Incessant drop in the CO_2 permeance with increasing feed absolute pressure is evident (Figure 3.13). At 2 bar pressure, the CO_2 permeance (~ 39 GPU) declined ~ 56 % when pressure was reached to 5.91 bar (~ 25 GPU). This can be interpreted by the dependency of CO_2 permeance on pressure. As pressure is raised ~ 196 % from 2 bar to 5.91 bar, only ~ 75 % surge in CO_2 flux is observed from 591×10^{-6} $cm^3(STP)/cm^2s$ to 1036×10^{-6} $cm^3(STP)/cm^2s$. High pressure aids in passage of higher number of N_2 molecules through the membrane. Hence, although CO_2 permeance has a downtrend as pressure is raised, the constant N_2 permeance reduces the overall selectivity. The CO_2/N_2 selectivity at 2 bar was 260 and decreased 84 at 5.91 bar feed pressure. Application of high feed pressure lowers the water retention inside the membranes that turns the membrane compact and ultimately diminishes the facilitated transport mechanism.

3.5.7 Robeson upper bound

The CO_2 separation capability of a membrane can be gauged by the Robeson upper bound plot (2008) that provides the correlation between CO_2 permeability with respect to CO_2/N_2 selectivity. The Robeson upper bound plot at a different sweep water flow rate (Figure 3.14a) indicates that membrane with little sweep water flow rate (0 – 0.01 ml/min) shows poor CO_2 separation performance and hence lies below the upper bound. However, at water flow rates $\geq$ 0.03 ml/min effective CO_2 separation was observed with the maximum CO_2 permeability and CO_2/N_2 selectivity at 0.05 ml/min. From Figure 3.14b, the membrane performance in the upper bound plot for the temperature range of 60 – 100 °C supports the optimal CO_2 separation performance. The prepared PAA30 membrane delivered the best result at 90 °C.

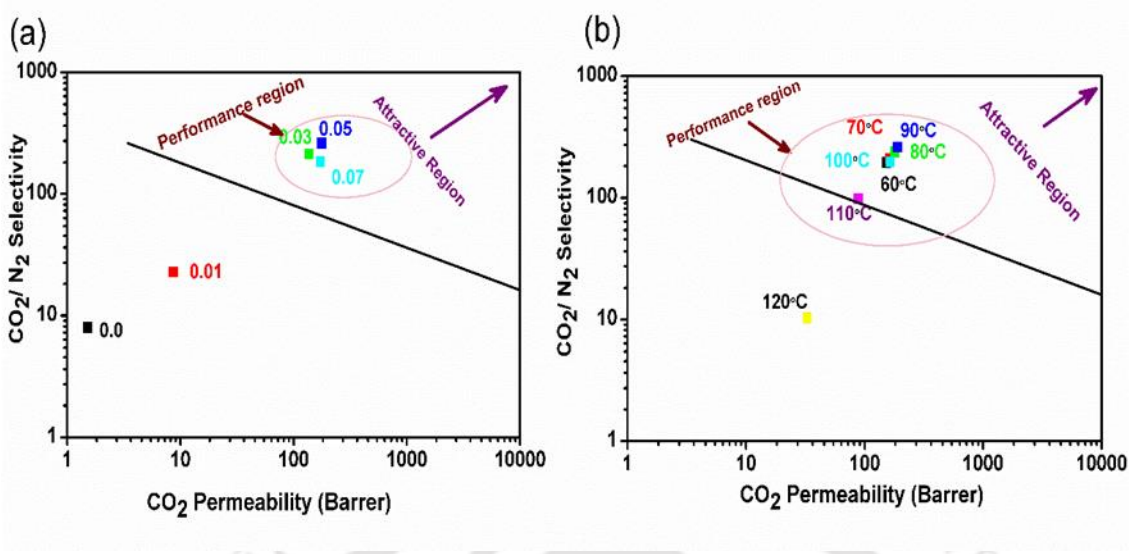

Figure 3.14 The Robeson upper bound plots for CO_2 separation from CO_2/N_2 gas mixture (a) at different sweep water flow rates (0.0, 0.01, 0.03, 0.05, 0.07 are in ml/min) and (b) at different temperatures.

3.5.8 Kaiser test

The performance is not the only criteria that indicate the membrane suitability for the gas separation application. Stability of the membranes during the CO_2 separation is a critical issue. As water is supplied to the system, membranes are prone to amine leaching. The standard Kaiser test with ninhydrin solution [153] was performed to investigate the presence of the primary amines in the dehumidified gases from feed and sweep side, condensed in their respective water knockout as shown in Figure 3.15. Pure water with PAA (1 %) was taken as the control. Ninhydrin solution of 50 µl was added to each sample and heated at 100 °C for 5 min [153]. The control developed Ruhemann's purple colour due to the reaction between ninhydrin solution and primary amine present in PAA [154]. Non-appearance of colour in the collected condensed feed and sweep water (after gas permeation tests), passed across the PAA30 membrane, established the absence of amine leaching from the membranes, which advocates the suitability of the test membranes for gas permeation under the study humidity conditions.

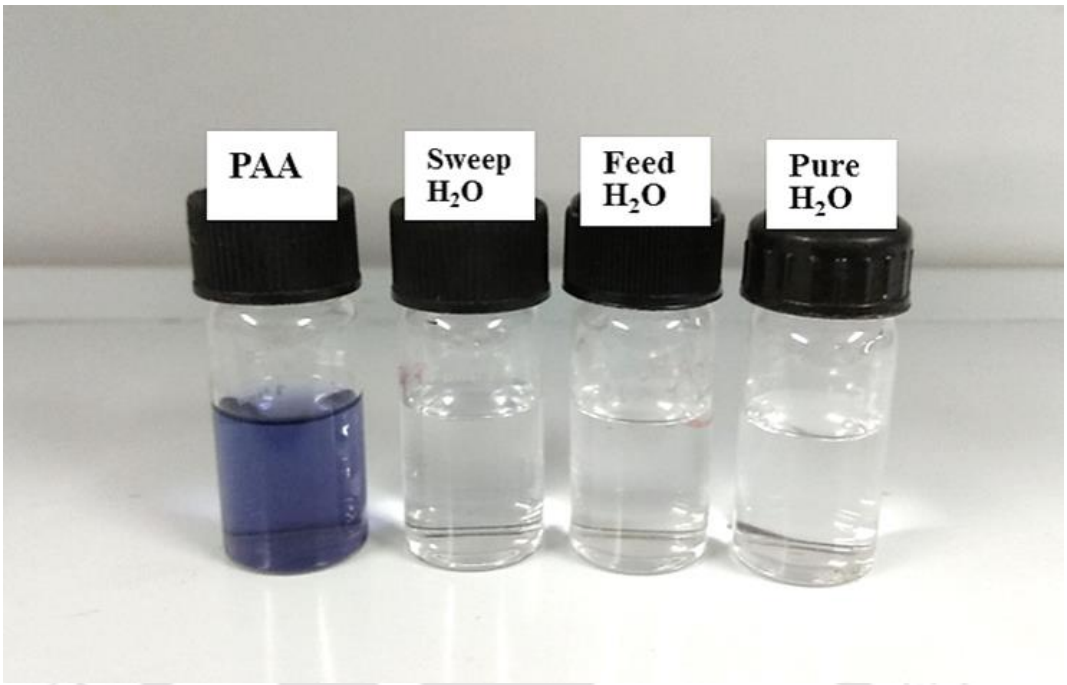

Figure 3.15 Digital images (from left) of PAA solution (control), sweep water, feed water collected from PAA30 and pure water.

3.6 Conclusions

The study in this chapter included the successful formation of CS-PAA active layers on the top of the PES support. The swelling test confirmed the water holding capacity at relative humidity < 80 % and the DMA data indicated the release of moisture and increase in stiffness up to 100 °C of the CS-PAA membranes. FTIR profile validated the incorporation of primary amines of PAA into the prepared membranes. FESEM and AFM analysis revealed the formation of the rough surface of the blended membranes that aided in increasing the surface area for reaction. However, increase in PAA content beyond 30 wt % developed some cracks in the membrane surface. The rough and cracks structures are presumed to support the passage of N_2 molecules that deterred the CO_2/N_2 selectivity. The optimized concentration of 30 wt % in chitosan matrix (PAA30) outperformed the CO_2 permeance and CO_2/N_2 selectivity of pure chitosan by ~ 3 fold and ~ 3.81 fold, respectively at 90 °C having water flow rate 0.03/0.05 (feed/sweep) ml/min and absolute pressure 2/1.21 (feed/sweep) bar when CO_2 separation from binary gas (CO_2/N_2) was conducted. The comprehensive examination of the effects of sweep

water flow rate, temperature and feed pressure on the CO_2 gas separation by PAA30 membrane indicated the optimum conditions of 0.05 ml/min of water flow rate, 90 °C, and 2 bar pressure. Further increase in the water flow rates did not improve the CO_2 flux and CO_2 permeance. Beyond 90 °C, the reduced water holding capacity of the membrane diminished the facilitated transport mechanism. At 2 bar pressure, a balance is maintained between flux and selectivity. Increase in the pressure leads to a trade-off between the flux and selectivity due to diffusion promotion of the N_2 molecules. Amines did not leach out from the PAA30 membrane during the CO_2 separation study as indicated by Kaiser test. The TGA isotherm and the performance parameters above the Robeson upper bound plot validate the prospective application of this membrane for intended industrial CO_2 separation. The study in this chapter revealed that the performance of chitosan-based membranes for CO_2 separation can be further improved by the addition of synthetic amines with proper concentration optimization and validation through gas permeation test.

CHAPTER 4

Development of CO_2-Facilitated Transport Membrane Using Natural Amine as a Green Carrier

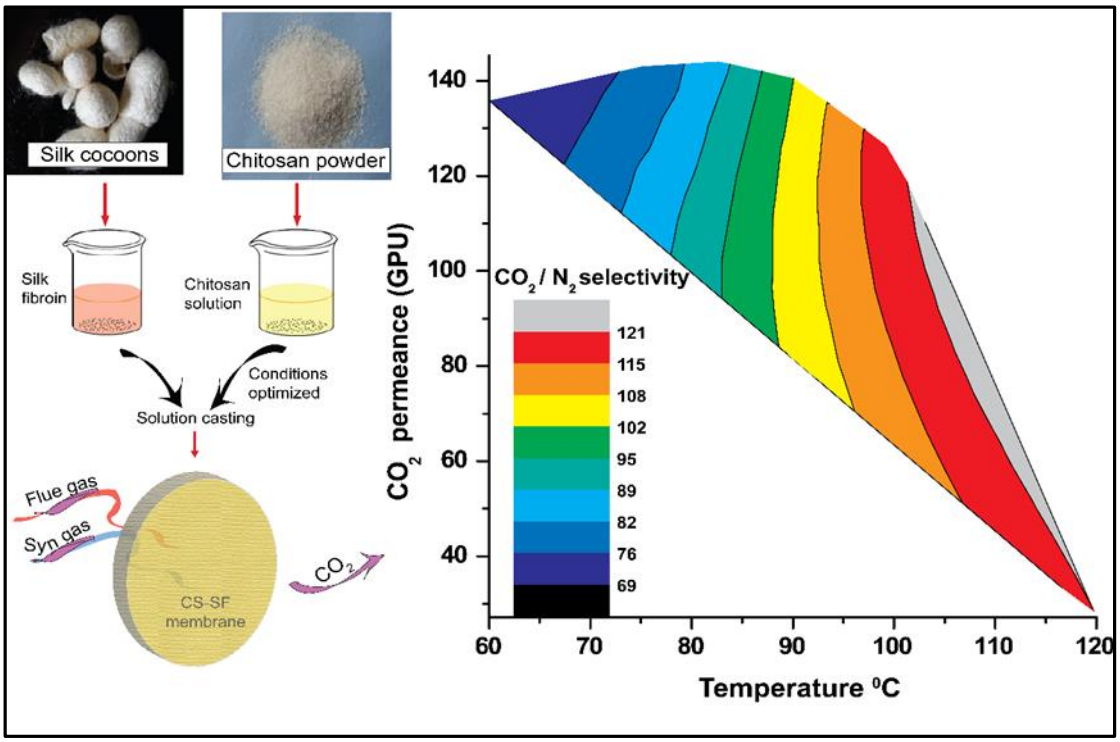

Graphical abstract of CS-SF membrane preparation and its CO_2 permeance and CO_2/N_2 selectivity at different temperatures

CHAPTER 4

Development of CO_2-Facilitated Transport Membrane Using Natural Amine as a Green Carrier

*This chapter aimed at investigating natural polymers for CO_2 separation. Silk fibroin (SF) is a biopolymer composed entirely of amines such as glycine, alanine, serine, tyrosine etc. This study was undertaken to explore these inherent natural amines as carriers for facilitated transport of CO_2. SF alone though can be cast into thin films, it is brittle. To impart mechanical stability, SF has been blended with CS to form CS-SF, which has been cast onto PES support. The detailed optimization of the concentration of SF into the CS matrix and the interesting characteristics of this novel membrane preparation have been discussed here. It is followed by the remarkable gas permeation test results. This work is scientifically published in "**Journal of Membrane Science**".*

4.1 Introduction

To employ the membranes for practical use in CO_2 separation, fabrication of membranes with long-term stability, simultaneously with high permeance through eco-friendly and cost-effective materials are of utmost concern. The separation of CO_2/N_2 is a post-combustion step, to eliminate CO_2 from flue gases and the separation of CO_2 from CO_2/H_2 is a pre-combustion processing from syngas [155]. Removal of CO_2 from syngas mixtures improves the H_2 purity that in turn enhances the fuel cell efficiency and curtails the pollution. CO_2 separation from gas mixtures also becomes indispensable during fuel cell operation, as the presence of CO_2 can lead to undesirable formation of CO via reverse water gas shift reaction that acts as a poison to platinum catalyst [107]. Additionally, during the production of carbon black by post-combustion method, tail gas is formed with the following composition in vol % : 5.3 % CO_2 , 16.4 % H_2, 60.5 % N_2 and 17.9 % CO [156]. To analyse the CO_2 separation ability of the membranes from different gas mixture, CO_2/N_2 (binary) and $CO_2/H_2/N_2$ (ternary) gas mixtures have been used as a feed stream in order to validate its suitability for varying applications as mentioned above.

Silk fibroin (SF), the natural fibrous protein (amino acid sequence motif, Figure A1.1d, Appendix 1), has achieved significant attention as biomaterial due to its distinctive mechanical and biocompatible properties. The SF extracted from *Bombyx mori* comprises of two major structural proteins-the heavy chain and the light chain associated through a disulfide bond [157]. The higher molecular weight heavy chain is dominated by the existence of β-sheet. It is characterized by the presence of 45.9 % Glycine (G), 30.3 % Alanine (A), 12.1 % Serine (S), 5.3 % Tyrosine, 1.8 % Valine and 0.25 % Tryptophan [158]. The repeating GAGAGS amino acid sequence imparts the organized crystalline β-sheet conformation to the SF polypeptide chains [159]. The proportional amount of both Silk I (α-helix and random coil) and Silk II (β-sheet) structure dictates the end properties of the SF film. However, the higher proportion of β-sheet structure in the stand-alone SF films makes them brittle [160]. Hence, other polymers are blended to enhance the properties of SF films [161]. SF can easily form a miscible polyelectrolyte complex with oppositely charged CS [162]. Formation of hydrogen bonds between the protonated CS and carboxyl groups of SF avoids the solvation of the CS-SF film in water [163], hence improving the stability and totally overcoming the leaching phenomenon. Addition of CS also contributes to the tuning of the secondary structures of the SF [164].

Chitosan-silk fibroin (CS-SF) composites have witnessed extensive application ranging from tissue engineering [165], drug delivery [166], biofilm inducer [164], to coatings of implants [158]. Noteworthy, this remarkable composite has never been explored for CO_2 separation. Different amines (blended or crosslinked with other polymers) such as poly PAA [106], PEI [92], PAMAM dendrimer [99], PVAm [83], etc. have been exploited as carrier for the facilitated transport of CO_2. We reasonably envision that the inherent amines in the SF can act as carriers and thereby replace the various amines processed through synthetic means. By tailoring the properties of CS with a sensible blend of SF, we expect that the CS-SF composite will present a green route for a simple yet effective CO_2 separation. This work demonstrates our efforts of such an attempt. The detailed findings of this interesting concept employed for CO_2 separation for binary (CO_2/N_2) and ternary gas mixtures ($CO_2/N_2/H_2$) are reported here.

4.2 Experimental section

4.2.1 Materials

Chitosan (CS) flakes (Product Number: 419419) was procured from Sigma-Aldrich, USA. Silk cocoons were acquired from a local vendor. Glacial acetic acid (99.99 % purity) and sodium carbonate (Na_2CO_3, 99.5 % purity) were purchased from Merck, Germany while Lithium bromide (LiBr, 99 % purity) was supplied by Spectrochem. Microporous poly(ether sulfone) (PES) supports (thickness: ~150 μm and average pore size: 0.03 μm) were obtained from Sterlitech, USA. Binary feed gas (CO_2/N_2) mixtures (20/80 vol %) and ternary feed gas ($CO_2/H_2/N_2$) mixtures (10/10/80 vol %) were supplied by Vadilal Chemicals Ltd., India. Helium (99.999 % pure) and Argon (Ultrapure) were acquired from the same vendor. Helium was used as carrier gas and Argon as a sweep gas for the gas chromatography (GC) analysis as well as permeation study. Millipore water (> 18 MΩ cm^{-1}, Millipore®) was used throughout the experiments.

4.2.2 Silk Extraction

Bombyx mori (*B. mori*) cocoons were used for the extraction of SF as in literature [167]. In brief, cocoons (cut into small pieces) were boiled for 30 min in 0.02 M Na_2CO_3 to remove the sericin. The SF after rinsing with water thoroughly was kept to dry overnight inside the laminar hood (LabTech®). The dried fibroin was dissolved in 9.3 M LiBr at 60 °C for 4 h. The amber colored solution hence obtained, was dialyzed against water for 72 h. The SF (yield of 6 – 7 % w/v) was stored at 4 °C until further use.

4.2.3 Membrane preparation

CS (1.15 g) was dissolved in 1 vol % acetic acid aqueous solution under vigorous stirring for 12 h followed by centrifugation (10000 rpm, 30 min, Sigma 3-30k) to get rid of undissolved particles**.** A pH ~ 5.5 was maintained by adding potassium hydroxide (KOH), to prevent irreversible gelation of SF, when added [163].

SF of the desired amount was added dropwise to the CS solution kept at 5 °C under continuous stirring to form the chitosan-silk fibroin (CS-SF) blended solution. After centrifugation

(10000 rpm, 30 min) step, the blended solution was cast onto the PES support using a casting knife (GARDCO, Paul N. Gardner, USA). The prepared membranes with different weight (wt) % of CS and SF were as follows: CS 85 % + SF 15 % (SF15), CS 70 % +SF 30 % (SF30), CS 55 % + SF 45 % (SF45) and CS 40 % + SF 60 % (SF60). The membranes were kept inside the laminar air flow for 48 h to form a dense layer and then heated at a heating rate of 1 °C /min from 25 to 120 °C and held at 120 °C for 6 h. After cooling down to room temperature, the membranes were cut into circular size to fit into the module for the gas permeation study. The membrane was placed in a stainless steel counter current flat sheet module with an effective area of 7.5 cm^2.

4.2.4 Membrane characterization and gas permeation study

The AFM (Innova, Bruker) and FESEM (ZEISS, USA) were performed on active layers of CS-SF membranes with PES as support to analyse the surface property of the membranes. The AFM images were recorded with a 0.7 Hz scan rate (tapping mode) and processed using Windows-Scanning-x-Microscope (WSxM) software [140]. The images were processed using the operation called flatten filter in WSxM. The top and cross-sectional views of the membranes were captured via FESEM (2–3 kV). The samples were fixed on a stub with a carbon tape and coated with gold sputtering prior to imaging. The contact angles analysis were done by placing uniform drops of water carefully on the active layer surface by using the instrument's in-built micrometer syringe. The water contact angles of the membranes with support were then measured using Krüss Drop Shape Analyzer-DSA25. The swelling tests were conducted as described in Chapter 3. For CO_2 separation from binary gas (CO_2/ N_2), the GC experimental set-up and conditions were as that explained in the previous Chapters 2 and 3. For ternary gas separation, a mixture of $CO_2/N_2/H_2$ was used in the same experimental set up.

DMA in tensile mode was performed using Netzsch DMA 242E Artemis® in the N_2 environment. With a frequency of 1 Hz and dynamic force of 1 N, the temperature was elevated from 30 °C to 120 °C at a heating rate of 2.5 °C/min. The TGA was performed on the active layer of SF45 without the PES support using Perkin-Elmer TGA (Model: TL8000) maintaining the heating rate of 10 °C/min and isotherm time of 40 min under N_2 environment.

Initially, the temperature was raised from 30 to 100 °C. Then the isotherms were executed at 100 °C, 120 °C and 150 °C. Finally, the temperature was elevated to 500 °C.

4.3 Results and discussion

4.3.1 Microscopic analyses

The FESEM images of the top surface of the porous support and cross-sectional view are depicted in Figure 4.1a-b. Formation of active layer (~ 3 µm thick), taking SF45 as a representative, over the porous PES support, is clearly visible in the cross-sectional view. This validates the suitability of the cast film over the support for further gas permeation analysis as the pores in the support matrix remain unfilled.

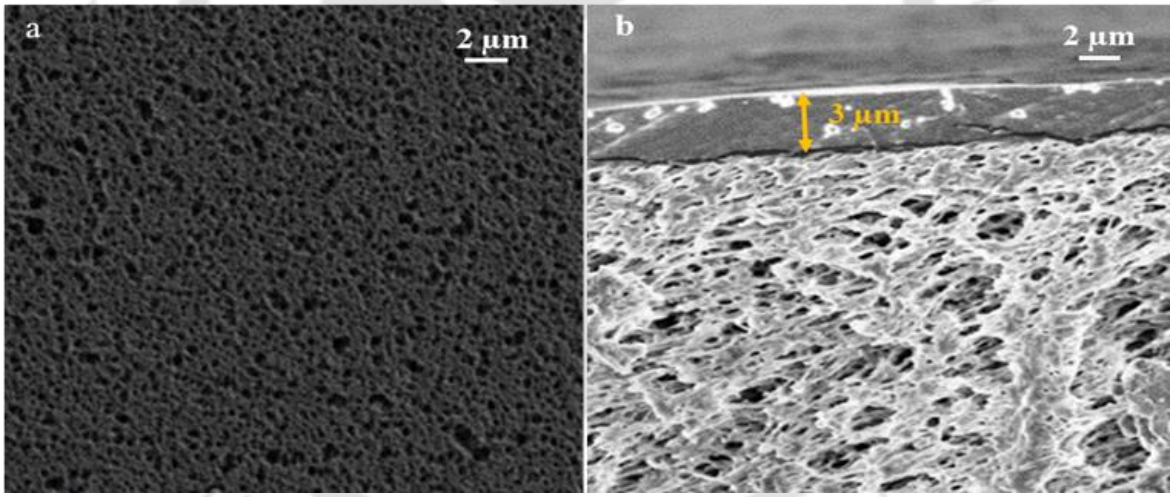

Figure 4.1 FESEM images of (a) top surface view of porous PES support and (b) cross-sectional view of active layer (SF45) and PES.

The AFM images (Figure 4.2 and Figure 4.3) suggested a smooth surface of the pristine CS membrane as compared to the blended membranes. The roughness average (nm) calculated from the AFM images follow the increasing trend CS (0.99) < SF (2.85) < SF15 (21.47) < SF30 (47.48) < SF45 (61.78) < SF60 (67.21). The results corroborated with the FESEM analysis of the prepared membranes (Figure 4.4). As the concentration of the SF content in the CS increases, the roughness of the membrane increases.

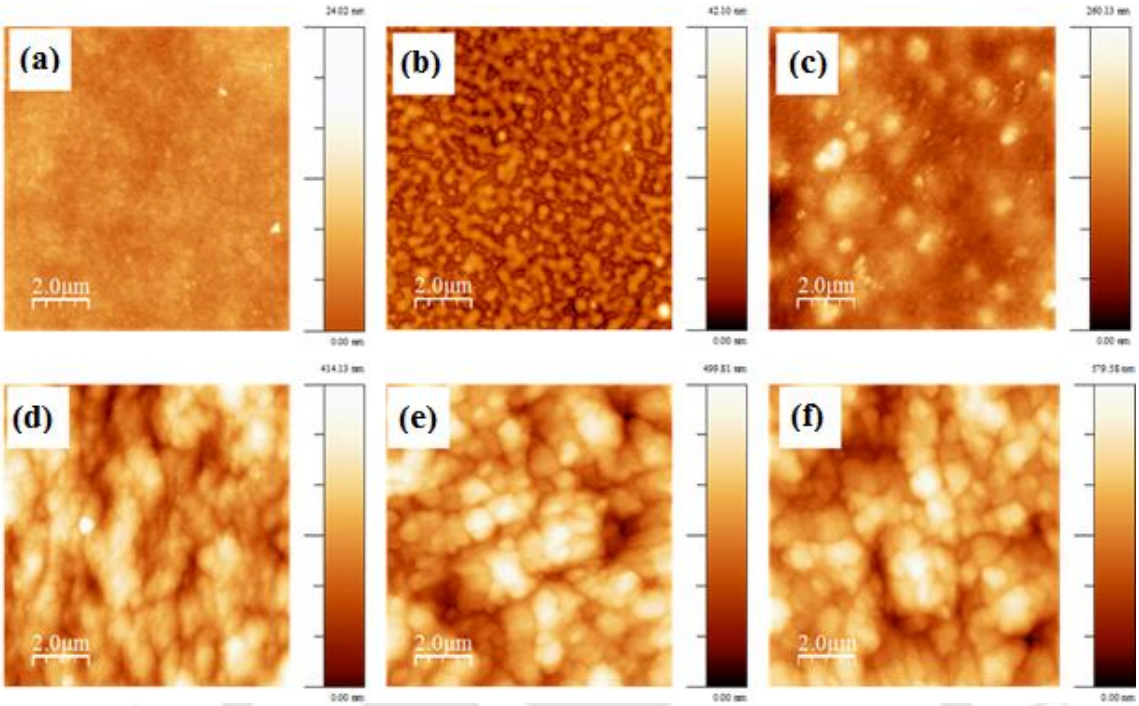

Figure 4.2 AFM images of (a) pure CS, (b) Pure SF, (c) SF15, (d) SF 30, (e) SF 45 and (f) SF 60.

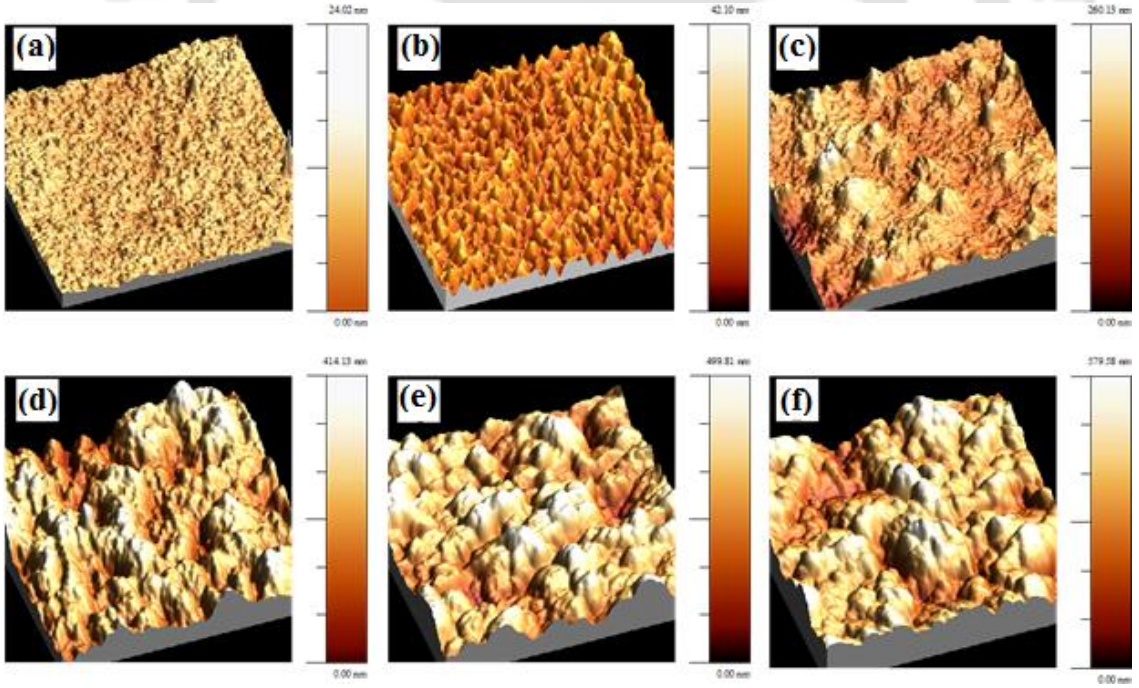

Figure 4.3 AFM images 3-D view of (a) pure CS, (b) Pure SF, (c) SF15, (d) SF 30, (e) SF 45 and (f) SF 60.

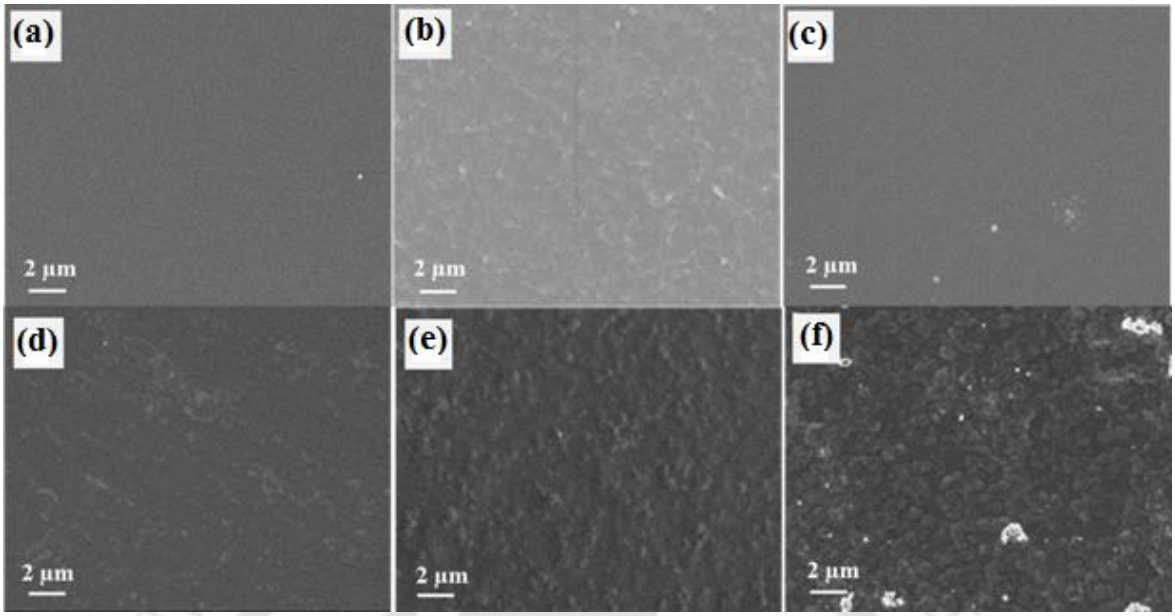

Figure 4.4 FESEM top surface view of (a) pure CS, (b) Pure SF, (c) SF15, (d) SF 30, (e) SF 45 and (f) SF 60.

4.3.2 Water swelling test

Swelling is a parameter of paramount significance in case of CO_2 separation. Water present in the membrane can enhance the CO_2 separation through dual action (i) facilitated transport by reacting reversibly with the carrier amines and (ii) can induce plasticization effect, causing flexibility of the membranes [91]. The water molecule enhances the free volume by increasing the intermolecular distance in the polymer matrix. Further, CO_2 can pass through the swelled membrane by following solution-diffusion mechanism.

Two different exponential increments of the water content were observed at 20-80 % and above 80 %, with respect to relative humidity as depicted in Figure 4.5. The relative humidity beyond which the second exponential function starts is termed as the critical relative humidity. The polymer conformation is the determining factor for the overall swelling at low relative humidity. At this stage, water molecule mixed with polymer chain initiates the chain relaxation and the degree of swelling depends on the amount of moisture present in the gas phase.

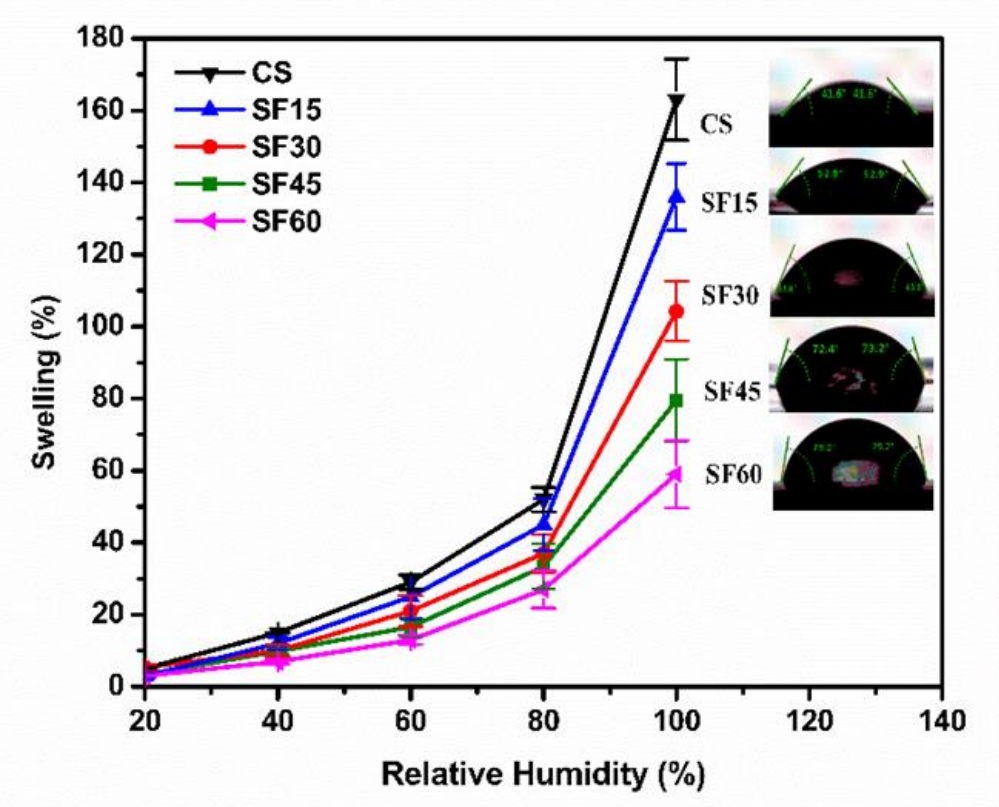

Figure 4.5 Swelling (%) vs relative humidity (%). The inset represents the water contact angles of the membranes at room temperature.

As discussed in Chapter 3, both conformation ($\Delta G_{conform}$) and contact ($\Delta G_{contact}$) plays an important role affecting the overall swelling observed during the second exponential increment. The $\Delta G_{contact}$ is governed by the affinity of water-polymer interaction. The contact angles aid to reflect the surface property of the CS and prepared membranes (Figure 4.5). The contact angle increases with the increase in the SF content following the trend CS (41.6º) > SF15 (51.9º) > SF30 (63.6º) > SF45 (72.4º) > SF60 (79.2º). The hydrophobic residues in SF (around 79 %) [168] results in high contact angle and decreased swelling. This suggests that water-polymer interaction decreases with increase in the SF content. The low contact angle of CS indicates its high hydrophilicity and suggest high water-polymer interaction ($\Delta G_{contact}$) which contributes to the maximum overall swelling. While SF60 being less hydrophilic, the overall swelling is less owing to poor water polymer interaction.

4.3.3 CO_2 separation performance study of the membranes

The CO_2 separation performance was studied for the prepared membranes at a water flow rate of 0.03/0.05 ml/min (feed/sweep) with absolute pressure of 2/1.21 bar (feed/sweep) and at temperature of 90 °C, as our previous study for pure CS membrane had shown optimum performance at these conditions. Pristine CS membrane resulted in CO_2/N_2 selectivity of 54 and CO_2 permeance of 12.5 GPU. SF15 showed substantial CO_2 permeance increment to 97 GPU and minor increment of CO_2 selectivity to 62 (Table 4.1). SF45 outperformed the rest of the membranes with ~ 11 and ~ 2 fold increments in CO_2 permeance and selectivity, respectively, as compared to CS. The increase in the effective area owing to the roughness as

Table 4.1 CO_2 permeance and CO_2/N_2 selectivity of CS, SF15, SF30, SF45 and SF60 membranes at 90 °C with water flow rate 0.03/0.05 ml/min (feed/sweep), feed absolute pressure 2 bar and sweep absolute pressure 1.21 bar. (Pure CS data has been taken from Chapter 2).

Membrane	CO_2 permeance (GPU)	CO_2/N_2 selectivity
CS	12.5 ± 0.67	54 ± 2
SF15	97 ± 2.41	62 ± 2
SF30	117 ± 2.95	78 ± 3
SF45	140 ± 2.07	103 ± 4
SF60	131 ± 1.89	98 ± 5

validated from AFM analysis, might also contribute to the gas transport [144]. The blend of CS and SF forms polyelectrolyte via ionic interaction between carboxylate present in SF and protonate amine group of CS [169]. As mentioned elsewhere [158], SF consist of six repetitive amino acids linked by peptide bonds and these amine groups perform as effective carriers that react with CO_2 reversibly in the membrane, assisting the transport of CO_2. The amino acid

rich SF enables to boost the facilitated transport of CO_2 along with CS, which also acts as a polymer matrix in the prepared membrane.

Additional SF in the CS-SF membrane increases the amount of carrier aiding in the facilitated CO_2 transport but reduces the overall swelling in the membrane, which is validated by degree of swelling. This restricts the passage of N_2 molecules, hence high CO_2/N_2 selectivity for SF45 was observed. The decline in the CO_2 separation performance of SF60 can be explained by its poor water holding capacity as observed during swelling test. So, on the basis of its optimum gas permeation performance observed under the specific conditions, a comprehensive gas permeation measurement was further investigated for SF45 membrane only.

4.3.3.1 Binary gas (CO_2 and N_2) mixtures separation

The separation of binary (CO_2/N_2) gas mixtures have been studied by varying temperature (range 60-120 °C), feed absolute pressure (range 2- 5.91 bar) and sweep water flow rate (range 0.01-0.07 ml/min) in the gas permeation setup to test the ability of SF45 membrane for CO_2 separation.

4.3.3.1.1 Effects of temperature and water flow rate on CO_2 separation by SF45 membrane

The effect of temperatures on CO_2 permeance and flux by SF45 membrane on different sweep water flow rates (0.01, 0.03, 0.05 and 0.07 ml/min) are shown in Figure 4.6a-b, respectively. The CO_2 permeance and flux increases as temperature rises from 60 to 80 °C at all the flow rates, establishing the mechanism of facilitated transport. The rate of reaction of CO_2 and amine increases with temperature in the presence of moisture [137]. The CO_2 permeance and flux are influenced by the swelling parameter, water content in the membrane and temperature. Permeance escalates as the temperature moves from 60 to 80 °C and the highest permeance at 80 °C was recorded at all water flow rates. After 80 °C, decline in the permeance was perceived for 0.01, 0.03 and 0.05 ml/min except for 0.07 ml/min. This can be attributed to the reduced membrane water retention above 80 °C, which restricts the CO_2 – amine reaction.

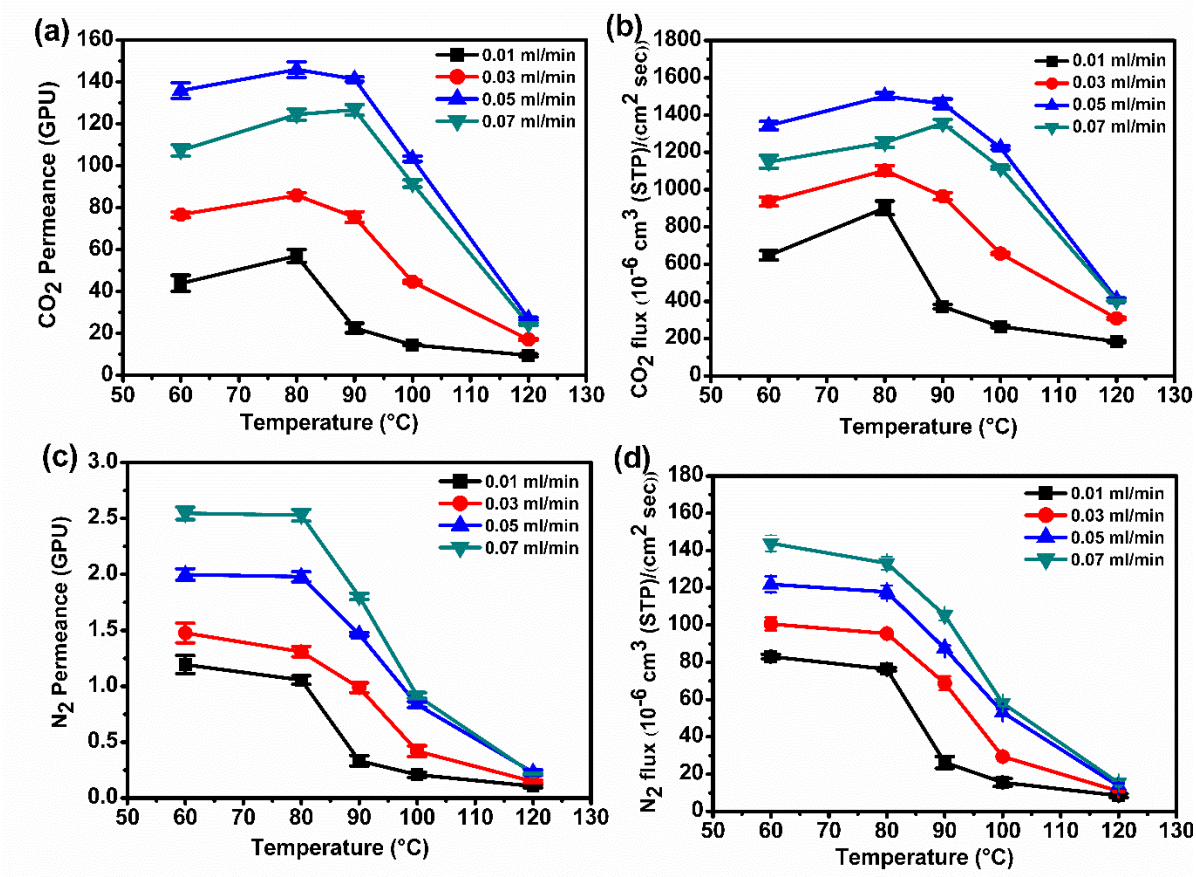

Figure 4.6 Effect of temperature on (a) CO_2 permeance, (b) CO_2 flux, (c) N_2 permeance and (d) N_2 flux with different sweep water flow rate for SF45 membrane at absolute pressure = 2/1.21 bar (feed/sweep) and feed water flow rate = 0.03 ml/min.

This reduction was more prominent when water flow rate was 0.01 ml/min. However, between 80-90 °C, at a higher water flow rate (0.07 ml/min), a marginal increase of CO_2 permeance was perceived. This is suggestive of the fact that low water flow rate cannot provide sufficient amount of moisture in the membrane at high temperature obstructing the facilitated transport mechanism.

At 120 °C, CO_2 permeance drops drastically owing to the lack of water retention. Notably, the stiffness is greater in SF films which are annealed at high temperature (owing to the higher β-sheet content) compared to the low temperature processed films [170]. The β-sheet content which imparts crystallinity in SF attains saturation after 12 h under given temperature and moisture [170]. This explains the steady state obtained after 10 – 12 h in our GC readings

during a particular temperature and water flow rate condition. Swelling of the CS-SF membrane at a controlled temperature and water flow rate improves the flexibility. The N_2 permeance (Figure 4.6c) at 60 °C is the maximum at all water flow rates and increases as the water flow rate is increased. This is indicative of the fact that the membrane has maximum flexibility at 60 °C that benefits the N_2 diffusion. Initially, water molecules interact with the amorphous region and form the hydrogen bond with SF disrupting the intramolecular amide-amide hydrogen bond. Similar chain mobility of silk at 60 °C was observed which was credited to lowering of the glass transition temperature (t_g) after absorption of moisture [171] or due to the mobility of water molecule leading to rearrangement of hydrogen bonding within the matrix [150].

The CO_2 and N_2 flux profiles (Figure 4.6b-d) follow a similar trend as was perceived for the permeance data. This is justified as the flux directly correlates to the permeance at a constant partial pressure difference. This increase in crystallinity and diminishing moisture content at high temperatures make the membrane stiffer and restricts the chain mobility and hinders the sorption of gas molecules. This is also validated by the DMA analysis of the SF45 membrane (Figure 4.7). The high storage modulus with the rise in temperature establishes the intensification of the stiffness of the membrane. This impedes the N_2 permeation and flux.

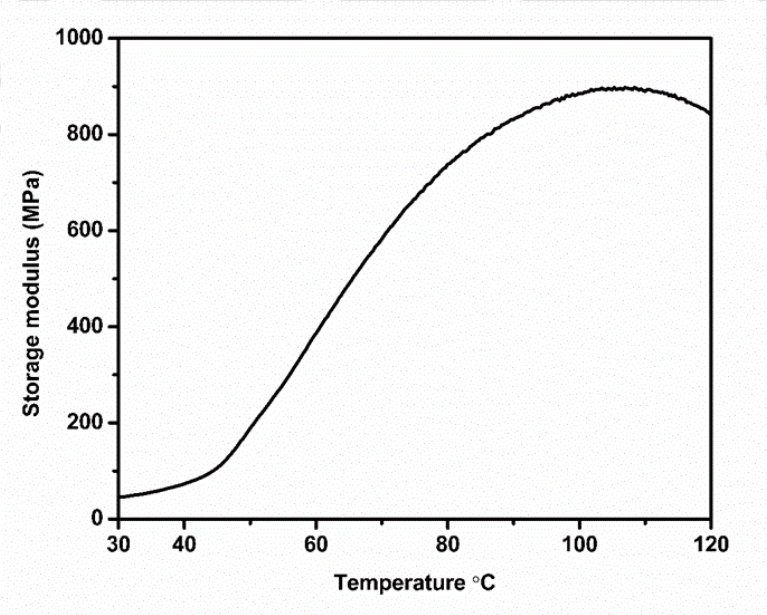

Figure 4.7 Storage modulus vs temperature of SF45 membrane by DMA analysis.

Investigation of CO_2 permeance under varying humidity conditions by providing different water flow rates further specify the role of humidity and temperature which regulates CO_2-amine reaction, membrane flexibility and gas diffusion across the membrane. The water flow rate (sweep) was varied from 0.01 to 0.07 ml/min at different temperatures (60, 80, 90, 100, and 120 °C) while the water flow rate (feed) was kept constant at 0.03 ml/min. The absolute pressure was maintained at 2/1.21 bar (feed/sweep). A slow increment of CO_2 permeance and

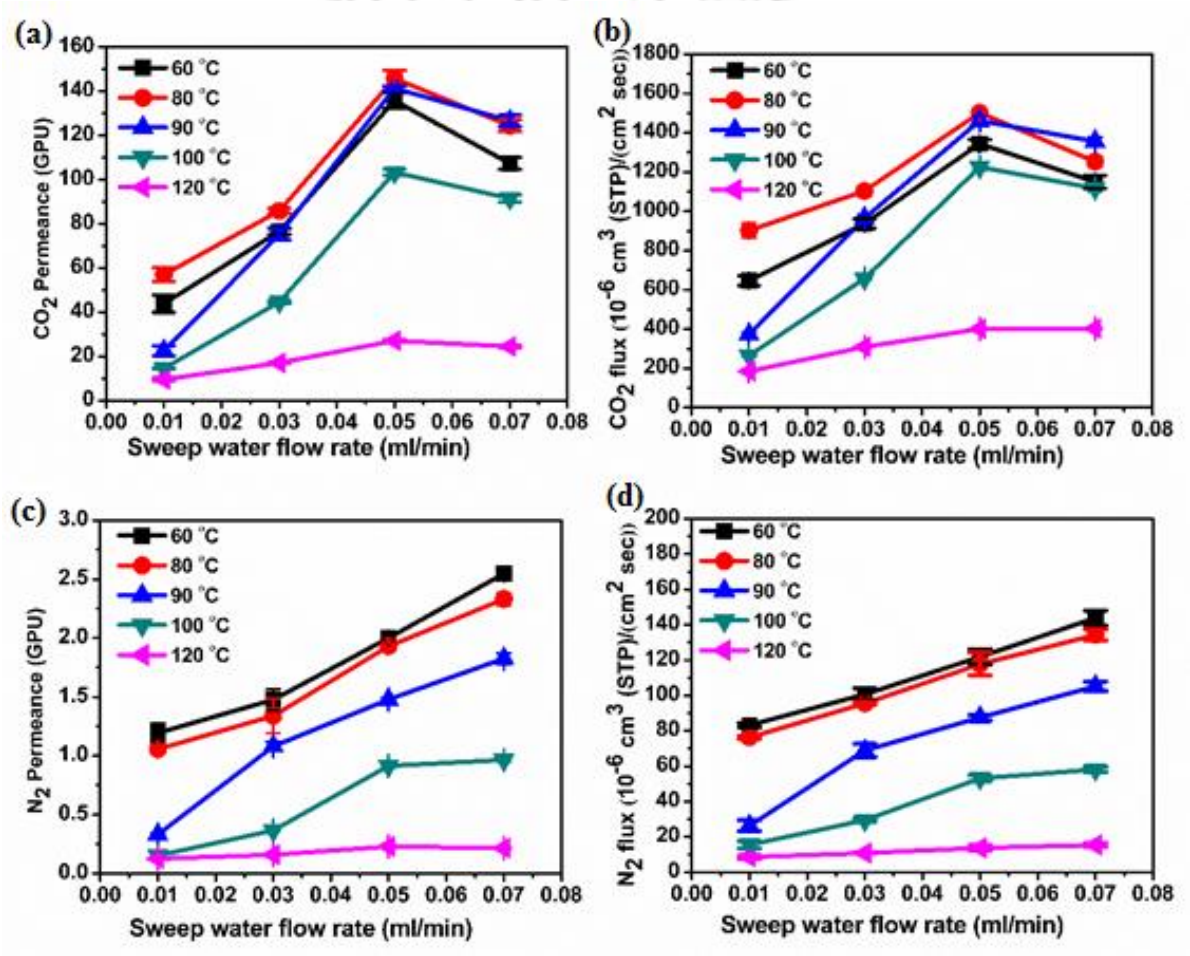

Figure 4.8 Effect of sweep water flow rate on (a) CO_2 permeance, (b) CO_2 flux, (c) N_2 permeance and (d) N_2 flux with different temperature for the SF45 membrane at absolute pressure = 2/1.21 bar (feed/sweep) and feed water flow rate = 0.03 ml/min.

flux in the range of 0.01-0.03 ml/min was detected under the studied temperatures (Figure 4.8a-b). This increase was sharp as the sweep water flow rate was changed from 0.03 to 0.05

ml/min. As the sweep side water flow rate exceeds 0.03 ml/min (surpassing that of feed water flow rate), water flux across the membrane decreases, increasing the water holding capacity of the membrane. The decline in CO_2 permeance and flux after 0.05 ml/min can be attributed to competitive sorption of CO_2 and N_2 molecule in the swelled membrane [91]. Facilitated transport is effective at that elevated temperature where membrane can hold sufficient amount of water.

At low temperature, when water retention of the membranes is high, limited facilitated transport is compensated by increase in diffusion of the gases. The N_2 permeance and flux profiles elucidate this behavior (Figure 4.8c-d). As expected, N_2 permeance at 60 °C is the highest and increases further with increase in the water flow rate. The increasing order of N_2 permeance (GPU) at 90°C for different water flow rates (ml/min) are 0.01 (0.03) < 0.03 (1.08) < 0.05 (1.47) < 0.07 (1.82). Unlike CO_2, that reacts with amine and its rate of reaction depends on water content and temperature, N_2 is a non-reacting gas that follows solution-diffusion mechanism [137]. Increase in water flow rates at all the temperatures augment N_2 permeance due to improvement in chain mobility as resistance diminishes, indicative of solution-diffusion mechanism.

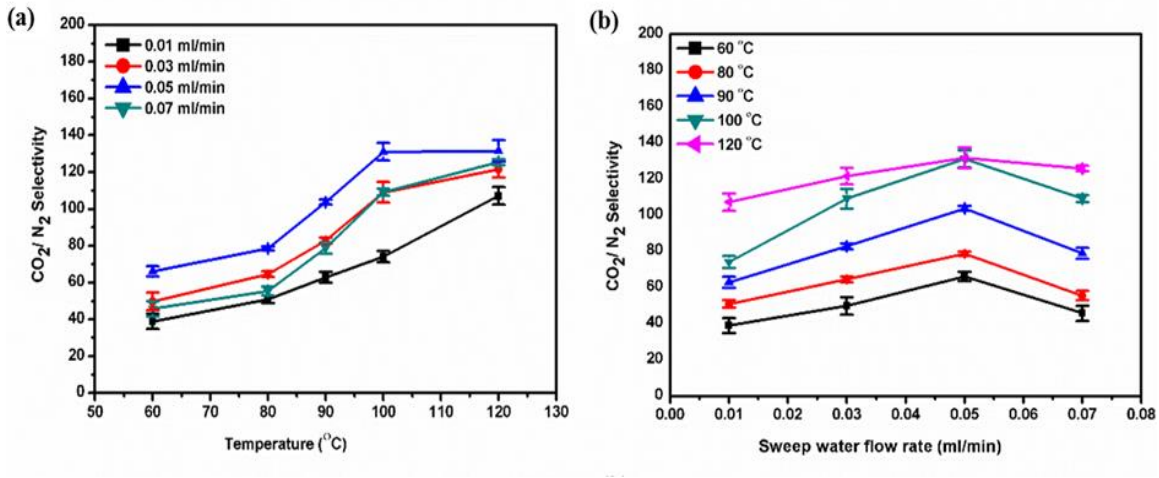

Figure 4.9 Effect of (a) temperature and (b) water flow rate on CO_2/N_2 selectivity of SF45 membrane at absolute pressure = 2/1.21 bar (feed/sweep).

As compared to CO_2 permeance (that drops after 90 °C), the CO_2/N_2 selectivity of the SF45 membrane surges up to 120 °C (Figure 4.9a). This increase in selectivity with temperature can be accredited to the negligible decline in the CO_2 permeance compared to the N_2 permeance. The CO_2/N_2 selectivity increases up to sweep water flow rate of 0.05 ml/min over the entire temperature studied. This can be attributed to the limited N_2 permeance at those water flow rates (Figure 4.9b). However, at sweep water flow rate > 0.05 ml/min, swelling occurs in the membrane which is corroborated by the swelling tests. Very high swelling of the membrane reduces the overall selectivity [89] due to adsorption of water molecule into the intrinsic active sites available for CO_2. High flow rate (0.07 ml/min) through the polymer matrix increases the inter-chain space, allowing a good amount of N_2 molecules to pass, which impedes the CO_2/N_2 selectivity [90] but augments N_2 permeance. At high temperature (120 °C), a trivial drop was realized owing to less water retention and high resistance.

The CO_2 permeance, N_2 permeance and CO_2/N_2 selectivity data for the SF45 membrane, generated at different water flow rate and temperature have been compiled to generate the gradient graphs (Figure 4.10a-c). These gradient graphs are signposts of the cumulative effects of temperature and water flow rate on CO_2 permeance, N_2 permeance and CO_2/N_2 selectivity. The optimal operating conditions required to obtain specific CO_2 permeance and/or CO_2/N_2 selectivity can be discerned from it. This allows us to tune the prepared membrane befitting the requirements. High temperature aids in maximum selectivity but not permeance for SF45 membrane. In this study, temperature in the range 90 – 100 °C and water flow rate of 0.05 ml/min have been found ideal for CO_2 separation (Figure 4.11).

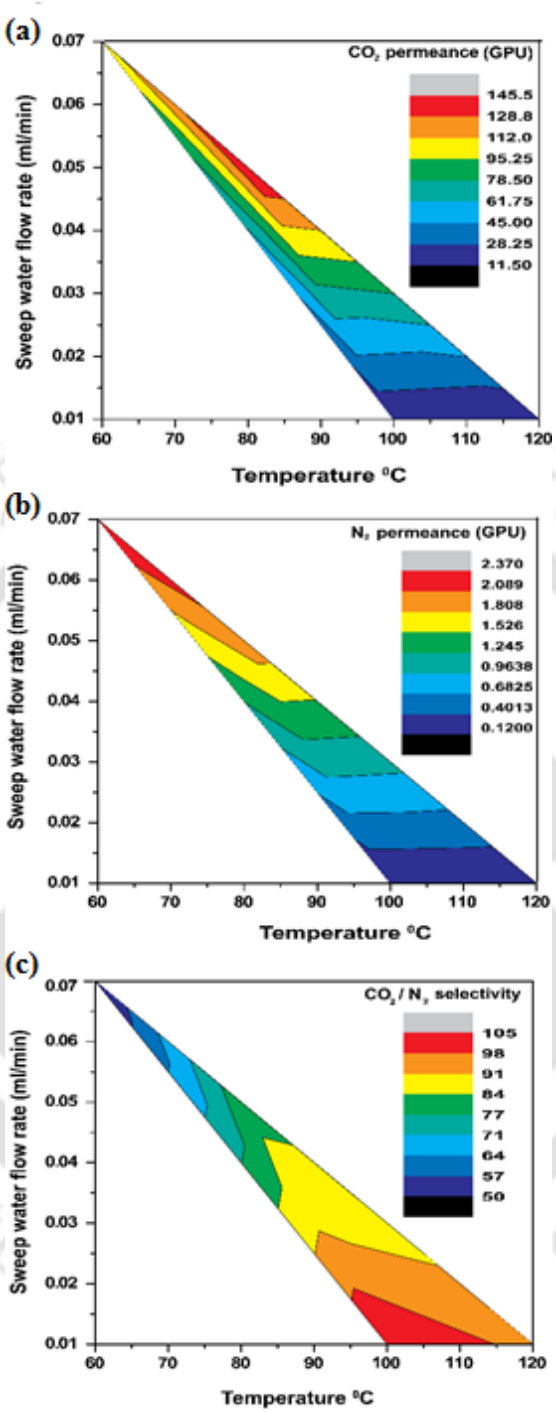

Figure 4.10 Gradient graph representing the cumulative effect of temperature and sweep water flow rate on (a) CO_2 permeance, (b) N_2 permeance and (c) CO_2 /N_2 selectivity. (Feed water flow rate = 0.03 ml/min and absolute pressure = 2/1.21 bar (feed/sweep)).

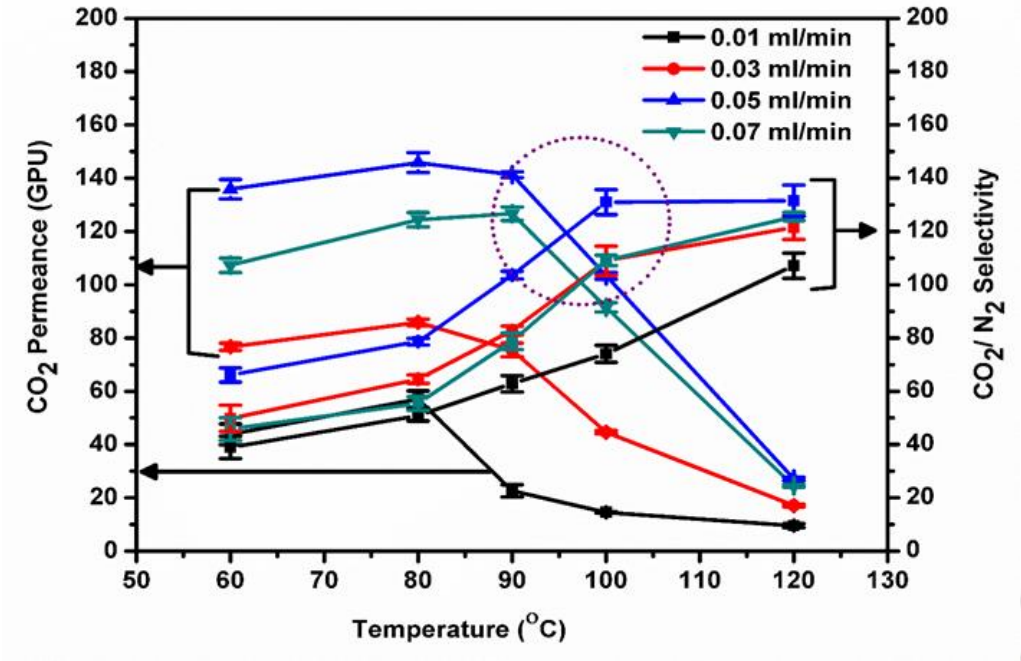

Figure 4.11 CO_2 permeance and CO_2/N_2 selectivity vs temperature at different water flow rates.

4.3.3.1.2 Effect of feed absolute pressure

The effect of feed absolute pressure has been studied in the range of 2 to 5.93 bar at 90 °C and water flow rate of 0.03/0.05 ml/min (feed/sweep) and sweep side absolute pressure at 1.21 bar. The CO_2 flux at 2 bar was 1462×10^{-6} $cm^3(STP)/cm^2s$ with a linear increase up to 3.82 bar (Figure 4.12). This can be credited to the CO_2–amine complex that prompts the CO_2 transport. Equation (1) represents the correlation between CO_2 flux, permeance and partial pressure. As the pressure is raised from 2 to 5.91 bar (~ 196 %), CO_2 permeance and CO_2/N_2 selectivity decrease ~ 48 % and ~ 32 %, respectively. This decrease can be credited to the membrane compaction due to reduced water retention and hampering facilitated transport of CO_2. At pressure > 3.82 bar, carrier saturation impedes facilitated transport and CO_2 flux reaches a stable value while N_2 flux increases linearly following solution-diffusion mechanism (Figure 4.13). This establishes the distinctive facilitated transport behavior, which is more effective at lower CO_2 partial pressure.

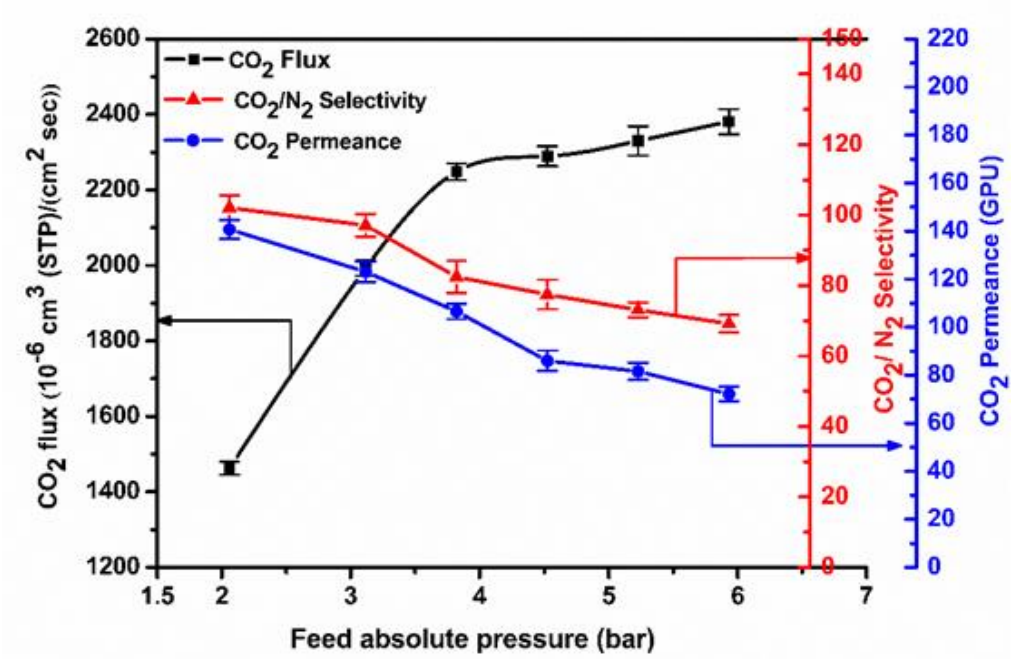

Figure 4.12 Effect of feed absolute pressure on CO_2 flux, CO_2/N_2 selectivity, and CO_2 permeance of SF45 membrane at 90 °C with water flow rate = 0.03/0.05 ml/min (feed/sweep), sweep absolute pressure = 1.21 bar.

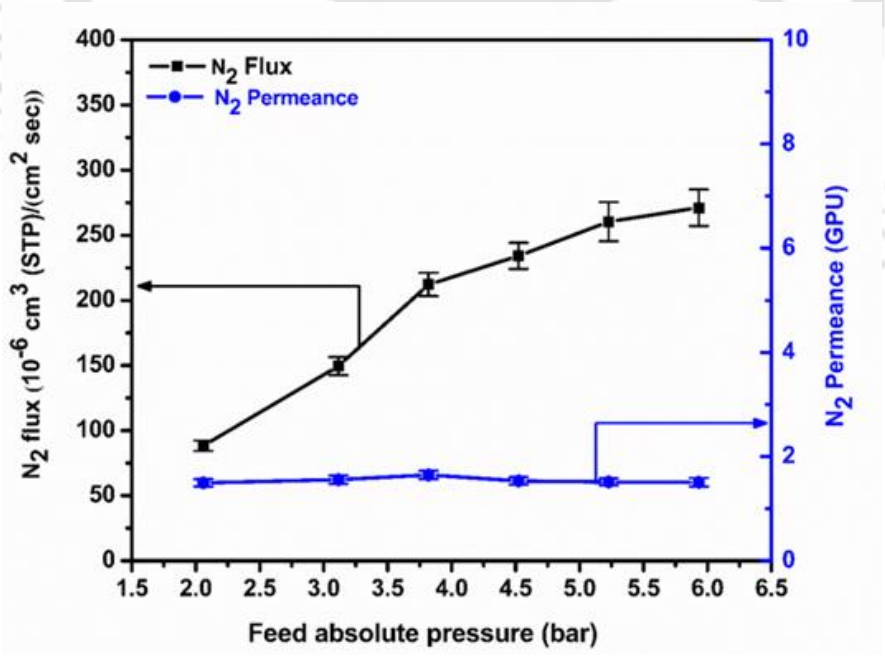

Figure 4.13 Effect of feed absolute pressure on N_2 flux and permeance (separation from binary gas) of SF45 membrane at 90 °C with water flow rate = 0.03/0.05 ml/min (feed/sweep), sweep absolute pressure = 1.21 bar.

4.3.3.2 Ternary gas (CO_2, N_2 and H_2) mixtures separation

4.3.3.2.1 Effects of temperature and pressure on CO_2 separation performance by SF45 membrane

The temperature effect (range 60 -120 °C) on separation of CO_2 from ternary gas mixtures of CO_2, N_2 and H_2 is depicted in Figure 4.14A a-b. A trend similar to binary gas mixture was observed for CO_2 flux and permeance in the range of 60 to 120 °C (Figure 4.14A a). The maximum CO_2 flux and permeance of 1332 × 10^{-6} cm^3(STP)/cm^2s and 123 GPU, respectively, were detected at 90 °C. Though the trend is similar to that of binary gas but the slight

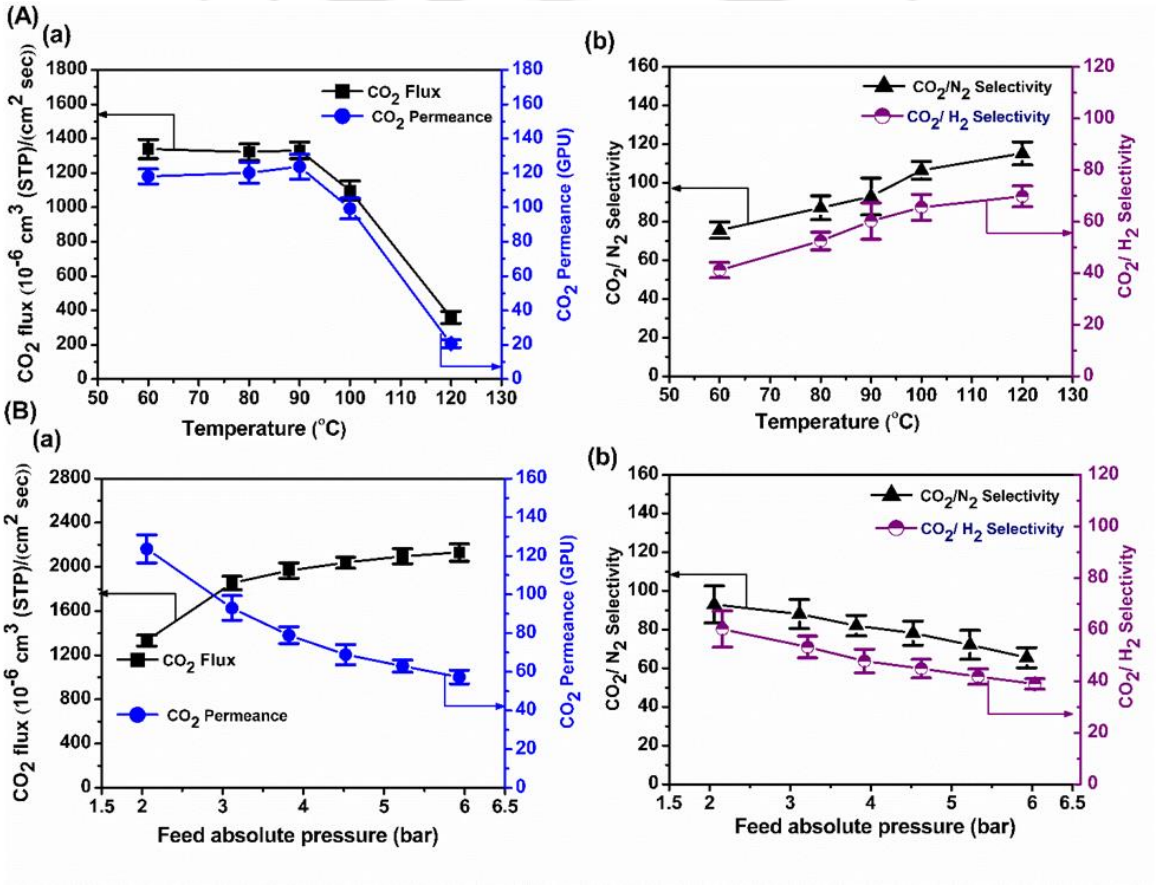

Figure 4.14 Effect on SF45 membrane (A) temperature effect (a) CO_2 flux and CO_2 permeance, (b) CO_2/N_2 and CO_2/H_2 selectivity at water flow rate = 0.03/0.05 ml/min (feed/sweep) and absolute pressure = 2/1.21 bar (feed/sweep) and (B) feed absolute pressure effect (a) CO_2 flux and CO_2 permeance, (b) CO_2/N_2 and CO_2/H_2 selectivity at 90 °C with water flow rate = 0.03/0.05 ml/min.

decrements in CO_2 flux (~ 9 %) and CO_2 permeance (~ 14 %) were recorded when ternary gas was used. The competitive sorption between CO_2, N_2 and H_2 gas molecules is believed to be the reason for the observed trend [156]. Permeation behavior is influenced by the nature of the penetrants and type of feed gas mixtures. Koros et al. [172] reported that sorption behavior of condensable gases like CO_2 and CH_4 was higher than non-condensable gases like N_2 and He, which induces plasticization effect in the polymer. The results advocate the fact that evaluation of the separation properties of ternary gas mixtures or pure gas, by analysing the permeation data of binary gas alone, might lead to inaccurate estimation.

The CO_2/N_2 and CO_2/H_2 selectivity showed an increasing trend line with increase in temperature ranging from 60 to 120 °C (Figure 4.14A b). The CO_2 flux increases with increase in the feed pressure while permeance and selectivity decreases (Figure 4.14B a-b) signifying facilitated transport. The CO_2 flux increased ~ 37% when feed absolute pressure was changed from 2 to 5.9 bar. On the other hand, CO_2 permeance, CO_2/N_2 selectivity and CO_2/H_2 selectivity decreased by 53 %, ~ 35 % and ~ 30 %, respectively.

4.3.3.3 Stability test

Maximum membranes relying on facilitated transport mechanism suffered poor CO_2 separation performance due to leaching out of the carriers or quick aging. From the stand point of commercial applications, membrane stability is of utmost importance. CO_2 separation performance for binary gas was initially checked at 90 °C and 2 bar feed absolute pressure having water flow rate of 0.03/0.05 ml/min (feed/sweep). The conditions were changed to different temperature and water flow rate for data generation. But on every fifth day, the initial conditions were provided for ten hours to attain steady state. Figure 4.15 illustrates the CO_2 separation performance for the initial conditions repeated on every fifth day. Interestingly, the membrane successfully regained its performance with negligible deflections, as was observed on the first day. This characteristic stability (up to 30 days) can be credited to the dynamic structural property of the inherent β-sheet of SF in the CS-SF blend membrane. The comprehensive effect of temperature and moisture provided, tune the annealing of the membrane and dictates its separation performance.

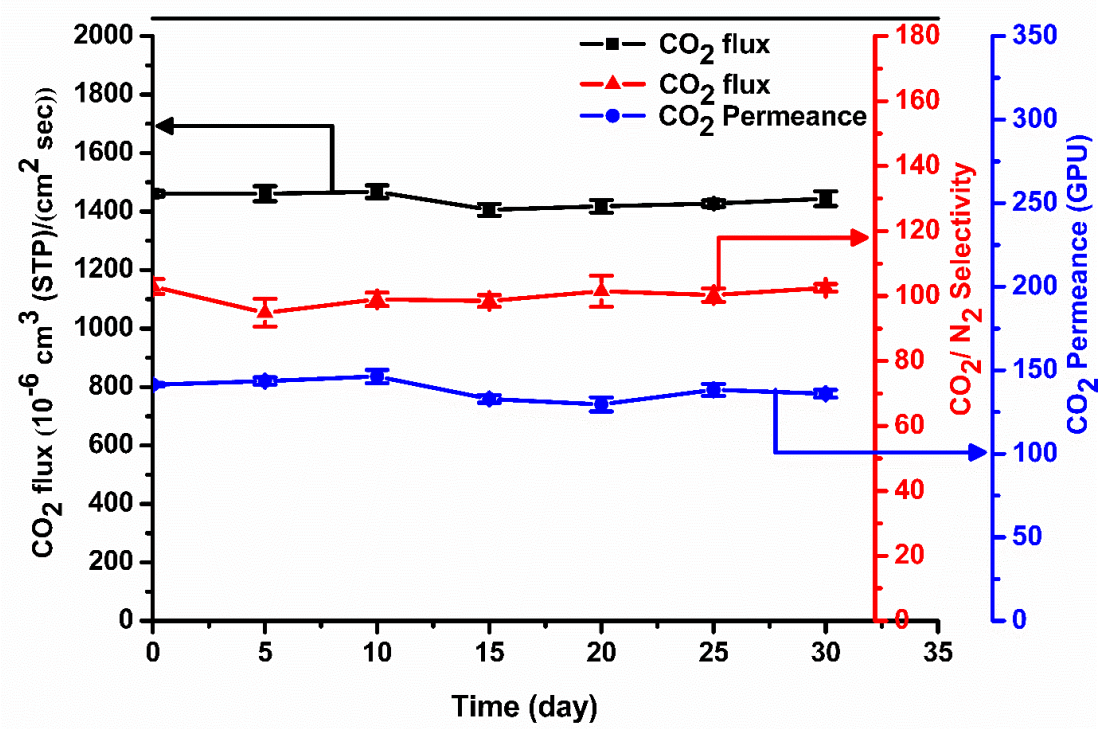

Figure 4.15 CO_2 permeance, CO_2 flux and CO_2/N_2 selectivity at 90 °C and absolute pressure = 2/1.21 bar (feed/sweep) having water flow rate of 0.03/0.05 ml/min (feed/sweep) with time.

4.3.3.4 TGA isotherm analysis

To give an insight into the thermal stability of SF45, it was exposed to isotherm at 100 °C, 120 °C and 150 °C sequentially, for 40 min each and the change in the weight loss with respect to temperature was monitored (Figure 4.16). The marginal decline (< 1 %) in weight loss during 100 °C isotherm can be ascribed to moisture removal. The weight loss (%) graph trails a straight line exhibiting trivial weight loss during 120 °C and 150 °C isotherms and subsequently a downfall after 150 °C before finally reaching 500 °C. This feature establishes the suitability of the blend membrane for flue gas separation at high temperatures.

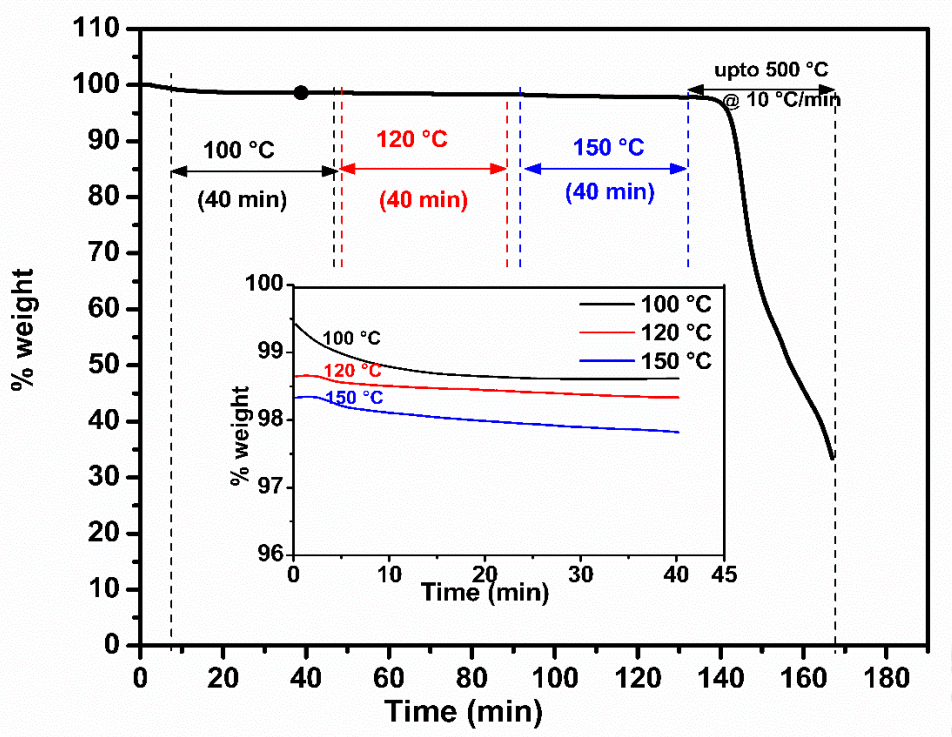

Figure 4.16 TGA profile of SF45 at different isotherm (inset TGA isotherm at 100 °C, 120 °C, and 150 °C for 40 min).

4.3.3.5 The Robeson upper bound

The Robeson upper bound (2008) plots are signposts of the performance of a membrane for gas separation [173]. Here, permeability is calculated by multiplying the permeance and thickness of the active layer and has unit - Barrer (10^{-10} cm^3(STP)cm/(cm^2s.cmHg)). The outstanding performance of SF45 membrane is demonstrated by the CO_2 permeability and CO_2/N_2 selectivity in the plot, that is pushed upper bound over the entire temperature range for both binary (Figure 4.17) and ternary gas mixtures (Figure 4.18a-b)

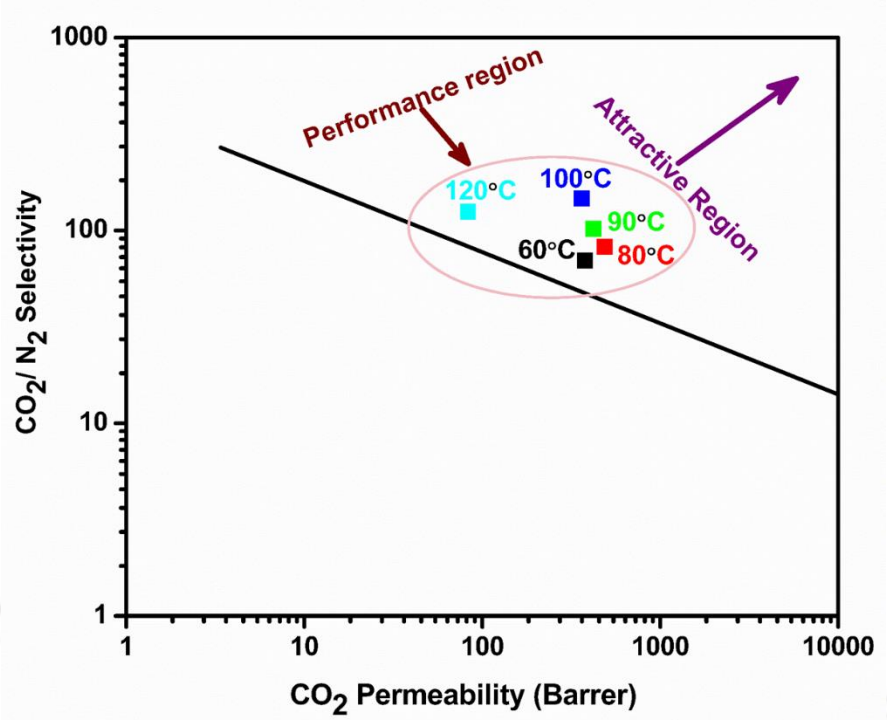

Figure 4.17 The Robeson upper bound plots for separation of CO_2/N_2 at different temperatures.

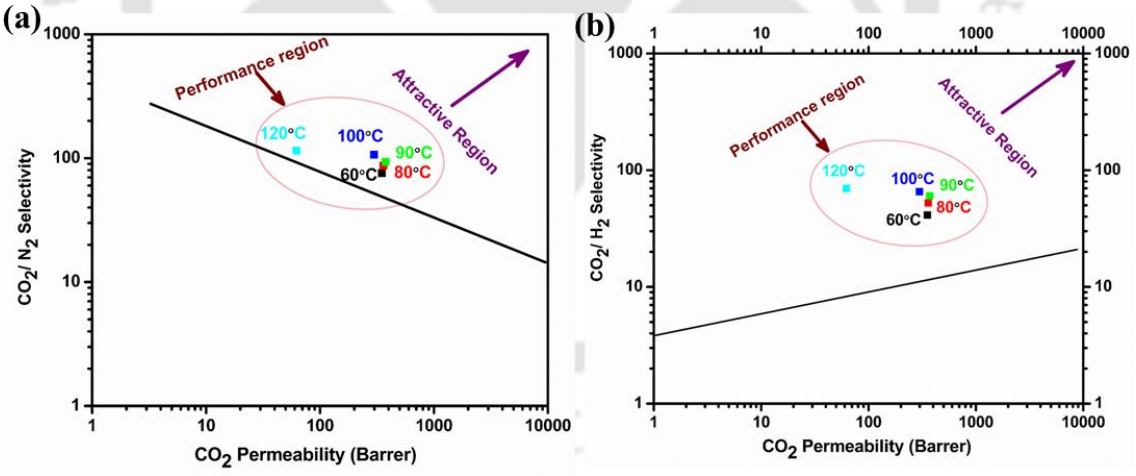

Figure 4.18 The upper bound plots for ternary gas separation (a) CO_2/N_2 and (b) CO_2/H_2 for SF45 membrane at different temperature with absolute pressure 2/1.21 bar (feed/sweep). The CO_2/H_2 upper bound is from ref. [174].

4.4 Conclusions

The study undertaken in this chapter consisted of two versatile biopolymers CS and SF, which were blended in varying concentrations to form CS-SF membranes. AFM and FESEM showed an increase in roughness with SF addition to CS - a positive trait for enhancing the available effective area. The swelling test and contact angles indicated favourable moisture holding properties. SF45 displayed optimum performance for CO_2 separation at 90 °C under water flow rate of 0.03/0.05 ml/min (feed/sweep) and absolute pressure of 2/1.21 bar (feed/sweep) with remarkable ~ 11 and ~ 2 fold increments in CO_2 permeance and selectivity, respectively as compared to CS membrane void of SF. The maximum CO_2 flux and permeance of 1332 × 10^{-6} cm^3(STP)/cm^2s and 123 GPU, respectively, were achieved at 90 °C when ternary gas mixtures were used. The SF45 membrane revealed significant CO_2/N_2 (93) and CO_2/H_2 (60) selectivities at 90 °C. The inherent natural amino acids in SF act as carriers in the matrix thereby augmenting facilitated transport. The β-sheet which imparts crystallinity to the SF, can be modulated to the presence of temperature and moisture. This opens up scope to tune the membrane performance by changing temperature and water flow rate. SF45 displayed regulated swelling constraining the passage of N_2. Temperature in the range 90-100 °C, sweep water flow rate of 0.05 ml/min and pressure of 2/1.21 bar (feed/sweep) have been found ideal for CO_2 separation from binary gas. The outstanding performance of SF45 membrane was also observed for CO_2 separation from ternary gas. This presents an unprecedented platform to use the natural SF amines as carriers as leaching can be circumvented. The exceptional CO_2 separation performance stability up to 30 days and thermal stability confer the suitability of SF45 for CO_2 separation from flue gas and syngas.

CHAPTER 5

Tailored Blend of Natural Fixed Carrier and Synthetic Mobile Carriers in Chitosan Membrane for Enhanced CO_2 Separation

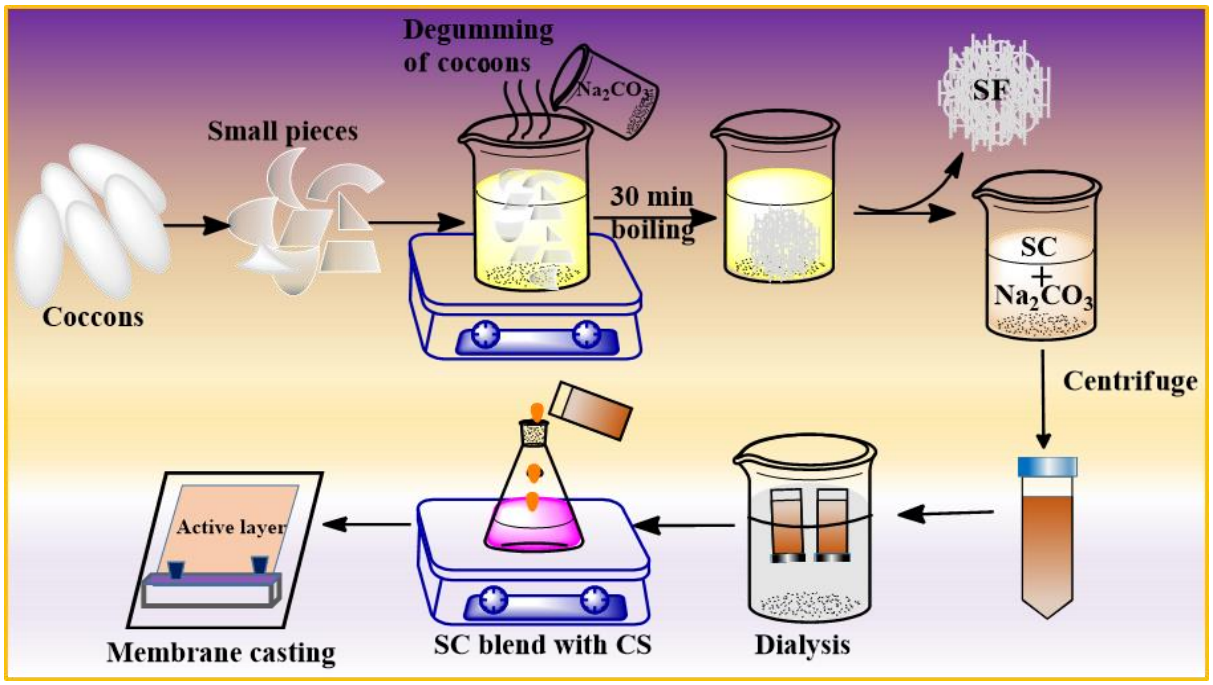

Graphical abstract of SC extraction from silk cocoon and preparation of CS-SC membrane for CO_2 separation

CHAPTER 5

Tailored Blend of Natural Fixed Carrier and Synthetic Mobile Carriers in Chitosan Membrane for Enhanced CO_2 Separation

This chapter includes the CO_2 separation using sericin (SC) as a fixed carrier and sodium carbonate (Na_2CO_3) as a mobile carrier. The silk cocoons contain two proteins- 65-85 % silk fibroin (SF) and 15-30 % sericin. During the silk degumming process, SF is extracted by dissolving in sodium carbonate (Na_2CO_3), to remove the SC. SF is used for CO_2 separation in Chapter 4. But SC remains as a waste by-product, which contains primarily serine and glycine in its polypeptide chain that can act as fixed natural carriers to enable CO_2 facilitated transport. In this study, we investigated the CO_2 separation properties by blending SC in the chitosan matrix in presence of Na_2CO_3 and in absence by removing Na_2CO_3 by dialysis. Detailed material characterizations were performed by XPS and advance microscopic techniques to reveal the layer formations in the membrane active layer. We envision that this work will invigorate a cost and time effective route of membrane preparation for CO_2 separation that will have several constructive impacts on the environment.

5.1 Introduction

Fossil fuel usage is indispensable to human growth and economy. Hence, the greenhouse gas emission resulting from it has become a worldwide concern. Interests in research followed by advances have spawned in membrane technology owing to the state-of-the-art developments in membrane for CO_2 separation and/or capture. Petrochemical-based polymers are although well established for a wide range of applications from dialysis, water purification to gas separation, but do not support green technology. Hence, bio-based/natural polymers have research appeals owing to its reduced liability on economy and environment. The silk from silkworm has two proteinaceous polymeric compounds: the silk fibroin (SF) and sericin (SC). The former contributes to the fibrous structural integrity and the latter as an adhesive of the fibres [175]. In the silk cocoon, the SF accounts for 65-85 % and SC contributes to ~ 15-30

% depending on the species used for extraction [176]. SC can be separated during degumming of SF. During the silk degumming process, SF is dissolved in sodium carbonate (Na_2CO_3) to remove SC. Dialysis is further required to remove Na_2CO_3 to obtain pure SC solution. The molecular weight of the extracted SC varies from 24-400 kDa [177]. SC has been widely used for functional coatings, cosmetic formulations, cell culture, drug delivery, antioxidant and as an antimicrobial agent [178].

In Chapter 4, SF was explored for CO_2 separation application as a potential green carrier in substitution to various other synthetic amine carriers. The inherent amines (largely glycine, alanine and serine) present in the SF structure boosted the CO_2 permeation by facilitated transport mechanism. SC also contains primarily serine (29.63 %), aspartic acid (17.77 %) and glycine (16.21 %) amino residues in its polypeptide chain [177,179]. The secondary structure of SC has β-sheet (35%) and random coil (63 %) that can be modulated in the presence of moisture and temperature [177,180]. Using this waste to a valuable product will reduce the cost for commercial purpose and also, provides an environment friendly approached to prepare a facilitated transport membrane.

Although, it has amine groups in its polypeptide chain, the stable film forming ability and mechanical property of the pure SC is a great concern. These properties can be improved by crosslinking of sericin or blending with another polymer having good film forming ability and mechanical strength [181]. The CS-SC blend was prepared by various method for different application. The CS/SC/PVA biodegradable membrane was prepared by elctro-spinning method and effect on morphology in the presence of silver nitrate, changing volume ration of CS and SC and spinning distance was studied. [182]. Nayak et al. [183] chosen SC/alginate/CS composition to prepare microcapsule for the improvement of cellular function. Similarly, Du et al [184] used CS/SC blend for the adsorption of bovine serum albumin. Further, S. Kim [185] prepared SC/PVA membrane crosslinked with glutaraldehyde having an active layer thickness of ~ 23-30 µm and used for gas separation at 25 °C. CO_2 permeability of ~ 126 Barrer and CO_2/N_2 selectivity of ~ 54 were found at same temperature with 6.6 wt % SC content. It was also reported that the maximum SC content in the membrane suitable for gas separation should be below 31 wt %.

An interesting yet simple way to tackle the selectivity-permeability trade-off is to blend polymers possessing different characteristics. SC remains as a waste by-product, when SF is used in most of the applications. In this study, a unique resolution was undertaken to make use of this waste by-product by blending the extracted SC solution with CS matrix in the absence and presence of Na_2CO_3. The pure SC was achieved by removing Na_2CO_3 using dialysis. Our main objective here is to use SC-Na_2CO_3 solution as it helps in reducing cost and time. Further, Na_2CO_3 add advantages like its low cost and easy accessibility [26].

Na_2CO_3 itself can promote facilitated transport mechanism. The reaction mechanism involved between CO_2 and Na_2CO_3 in the presence of moisture is given below [186]

$$Na_2CO_3 + CO_2 + H_2O \longleftrightarrow 2NaHCO_3 \quad (5.1)$$

$$Na_2CO_3 + 0.6\ CO_2 + 0.6\ H_2O \longleftrightarrow 0.4\ [Na_2CO_3.\ 3NaHCO_3] \quad (5.2)$$

The first reaction (Equation 5.1) produces sodium bicarbonate ($NaHCO_3$) and second reaction (Equation 5.2) forms a double salt commonly known as Wegscheider's salt [186]. The reaction depends on the temperature which affects the kinetics and thermodynamics of the reaction. $NaHCO_3$ is formed below 70 °C and the Wegscheider's salt is produced above 70 °C [186]. From Equation 5.1, one mole of Na_2CO_3 resulted in production of two moles of $NaHCO_3$ which reveals high amine loading capacity as compared to amine facilitated transport mechanism [187]. Moreover, Na_2CO_3 is non-corrosive with limited evaporation loss due to its negligible vapor pressure [187].

Detailed material characterizations were performed by XPS (depth analysis) and advance microscopic techniques to reveal the proper active layer formation. We envision that this work will invigorate a cost and time effective route of membrane preparation for CO_2 separation that will have several constructive impacts on the environment.

5.2 Experimental section

5.2.1 Materials

Chitosan (CS) flakes (Product Number: 419419) were procured from Sigma-Aldrich, USA. Silk cocoons were acquired from a local vendor. Glacial acetic acid (99.99 % purity) and sodium carbonate (Na_2CO_3, 99.5 % purity) were purchased from Merck, Germany. Mini

dialysis kit (GE, 1 kDa) was procured from Sigma. Argon, Helium, binary gas mixture and ternary mixture compositions and purity were same as discussed in Chapter 4. Millipore water (>18 MΩ cm^{-1}, Millipore®) was used throughout the experiments.

5.2.2 Sericin Extraction

Bombyx mori (*B. mori*) cocoons were used for the extraction of SC as in literature [167]. In brief, cocoons (cut into small pieces) were boiled for 30 min in 0.02 M Na_2CO_3 to remove the sericin. The SF was extracted and washed thoroughly and dried overnight inside the laminar hood (LabTech®). The SC-Na_2CO_3 solution was heated to concentrate the solution. This solution was centrifuged to remove some undissolved particle or small fraction of SF left during extraction. The centrifuged solution was dialyzed using GE dialysis kit against Millipore water for 72 hours. During dialysis Na_2CO_3 comes out to the water and pure SC was obtained and stored at 4 °C for further use.

5.2.3 Membrane preparation, characterization and gas permeation test

1.15 % (wt/vol) of CS solution was prepared in 1 vol % acetic acid solution. The SC solution was added drop-wise to the CS solution kept at 5 °C under continuous stirring to form the chitosan-sericin (CS-SC) blended solution. A total of 1 ml of acetic acid was added in 99 ml of SC solution to get a proper viscous solution. CS of 1.15 g was dissolved in acidic SC solution. The solution was continuously stirred for 12 h to get a homogenous blend solution. In order to understand the effect of Na_2CO_3 in gas separation phenomenon, a membrane was prepared with Na_2CO_3 impregnated in CS matrix. For this, a calculated amount of Na_2CO_3 was dissolved in water and added to pure CS solution under continuous stirring for 2 h. The prepared blend solution was cast onto the PES support using a casting knife (GARDCO, Paul N. Gardner, USA). The prepared membranes with different weight (wt) % of CS, SC and Na_2CO_3 were as follows: 70 wt % CS + 30 wt % SC (M1), 70 wt % CS + 30 wt % Na_2CO_3 (M2), and 70 wt % CS + 15 wt % SC + 15 wt % Na_2CO_3 (M3). The membranes were kept inside the laminar air flow for 48 h to form a dense layer and then heated at a heating rate of 1 °C /min from 25 to 120 °C and held at 120 °C for 6 h. After cooling down to room temperature, the membranes were cut into circular size to fit into the module for the gas permeation study. The membrane area used here is 7.5 cm^2. The sample preparation and

operating conditions of all the charcterization techniques and the related software used in this chapter are described in Chapter 4. Gas permeation test was carried out in gas chromatography (GC) set under the conditions similar to the work as elaborated in Chapter 4. Further, the membranes (sample size 1 cm × 0.5 cm) were exposed to X-ray Photoelectron Spectroscopy (XPS), using Thermo Scientific Escalab Xi^+ XPS spectrometer. The X-ray source used was mono-chromated Al k-alpha having pot size of 400 μm. A vacuum pressure of 7×10^{-8} mbar was maintained during cluster etching. The ion beam energy of 8 keV having cluster size of 150 atoms and beam current of 35 nA were used.

5.3 Results and discussion

5.3.1 Microscopics analyses

Dense surface void of pores were visible in the FESEM top surface view of the prepared membranes (Figure 5.1). This indicated good miscibility of SC and Na_2CO_3 with CS in the solution form with variation in roughness. To better analyse the surface roughness AFM was

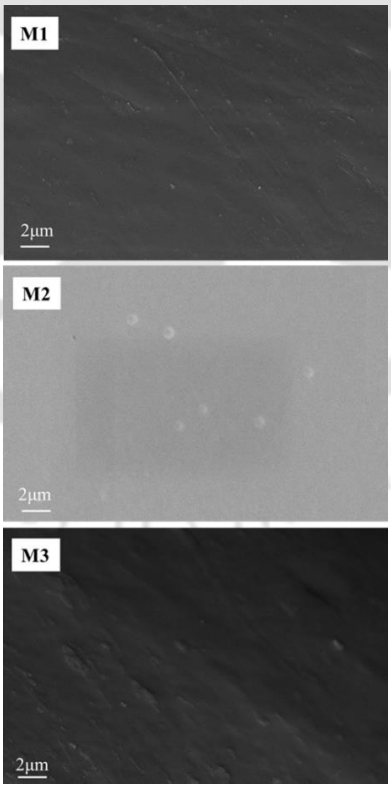

Figure 5.1 FESEM top surface view of the prepared membranes.

further performed. The AFM with 2-D images, height profiling and 3-D images of all the membrane are shown in Figure 5.2 respectively. The average roughness of the M1 membrane (with SC) was 24.59 nm whereas M2 (with Na_2CO_3) and M3 (with both SC and Na_2CO_3) were 17 nm and 23.5 nm, respectively. The average roughness of the pure CS was 0.99 nm at similar condition as discussed in Chapter 4. The increased roughness compared to pure CS may enhance the CO_2 separation by increasing the overall effective area of the membrane [144].

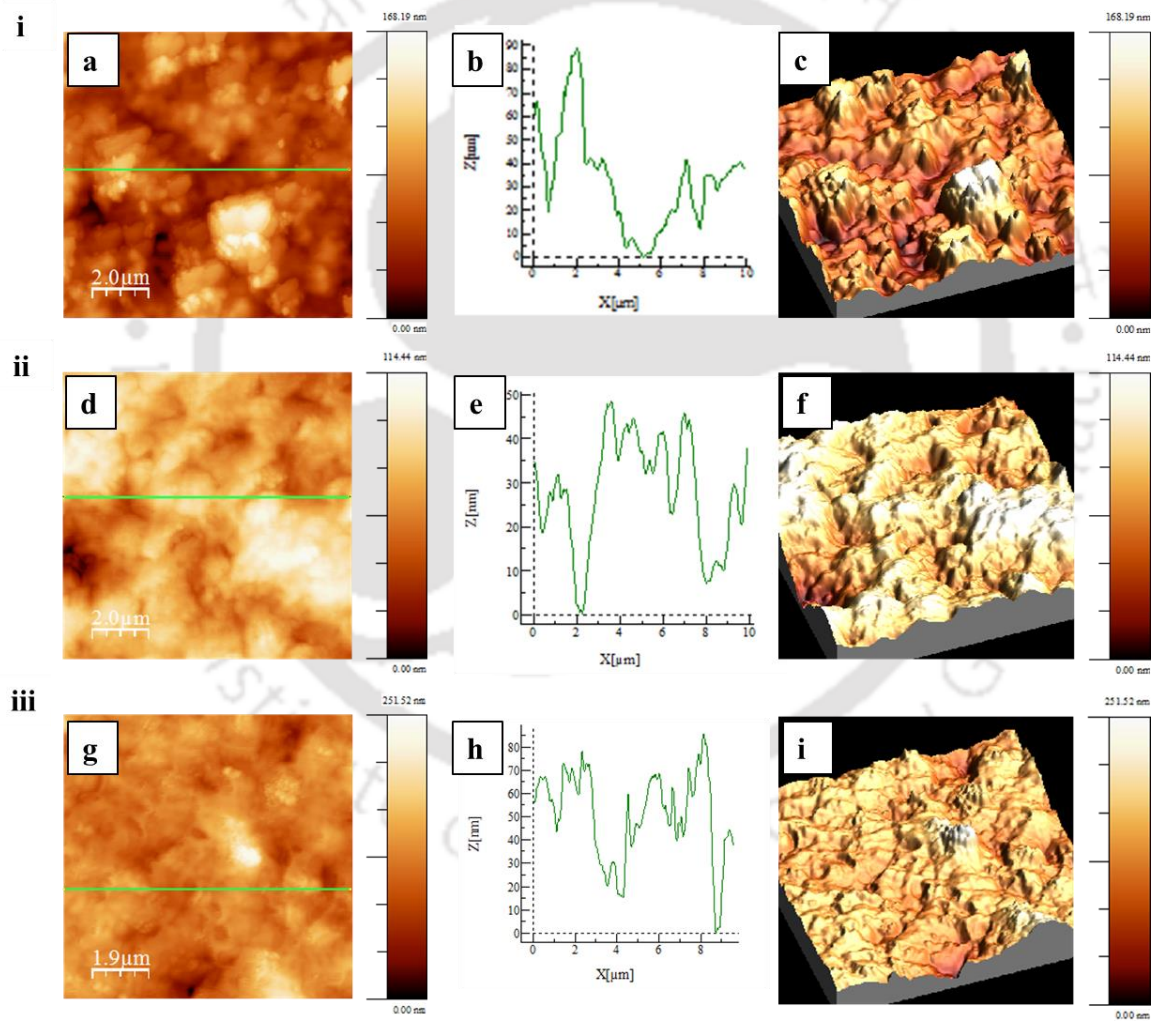

Figure 5.2 AFM topography of (i) M1, (ii) M2, and (iii) M3 membranes with their respective 2-D images (a,d,g), height profiling (b,e,h) and 3-D images (c,f,i).

5.3.2 Swelling test

The relative humidity vs swelling has been performed and compared with CS membrane (Figure 5.3). It was observed that the swelling of all the membranes (M1, M2, M3) were higher than the pure CS membrane (the study for the CS membrane has been extended from the work in Chapter 4). SC has 18 amino acids sequence and these amino acid contains hydrophilic groups of amino, hydroxyl and carboxyl [178] residues in its structure which has contributed to the high degree of swelling. Similarly, Na_2CO_3 is hygroscopic in nature due to strong hydrogen bonding with water molecule [188]. The water holding capacity followed the trend CS < M1 < M3 < M2. The degree of swelling exhibited two exponential functions: first one was up to 80 RH % and second one was after 80 RH % [94]. Due to high degree of swelling, enhanced flexibility is anticipated with reduced resistance to mass transfer of the gas molecules during permeation study. Further, it will enhance the CO_2-carrier reaction at a specific temperature.

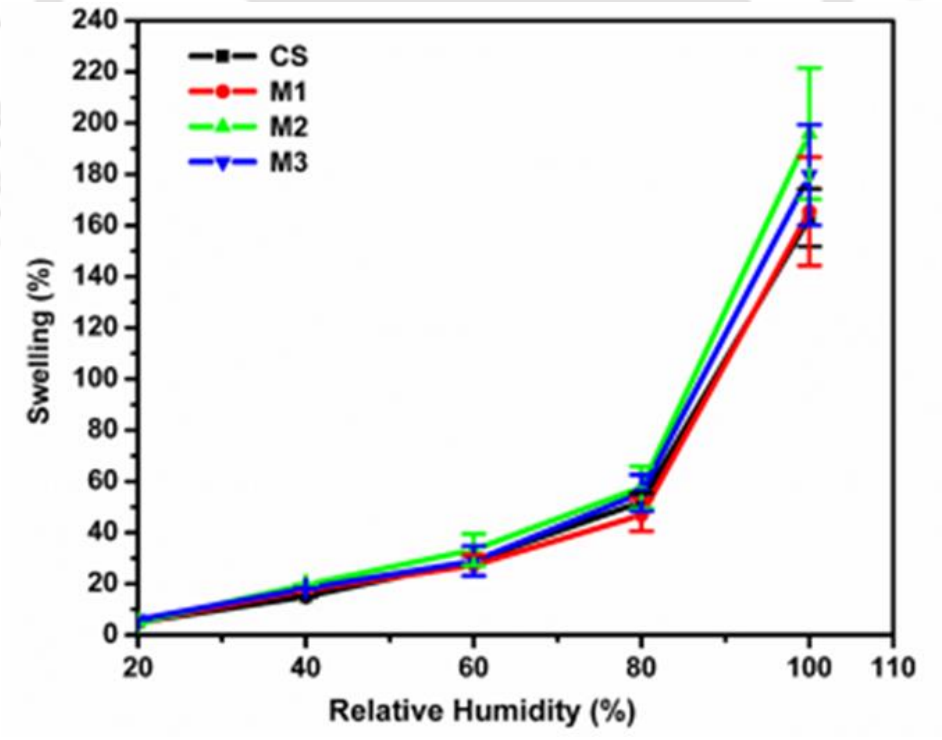

Figure 5.3 Swelling (%) vs relative humidity (%) of CS, M1, M2 and M3 membranes.

5.3.3 Dynamic mechanical analysis

The DMA analysis was done in the temperature range of 30-140 °C (Figure 5.4), a useful analysis to understand the temperature effect on the membrane. The upswing in storage modulus of all the membranes was witnessed with rise in temperature. The storage modulus is directly proportional to the membrane stiffness but indirectly proportional to the membrane flexibility. However, the increase in the stiffness of the membrane will hinder the passage of gas molecules through the active layer.

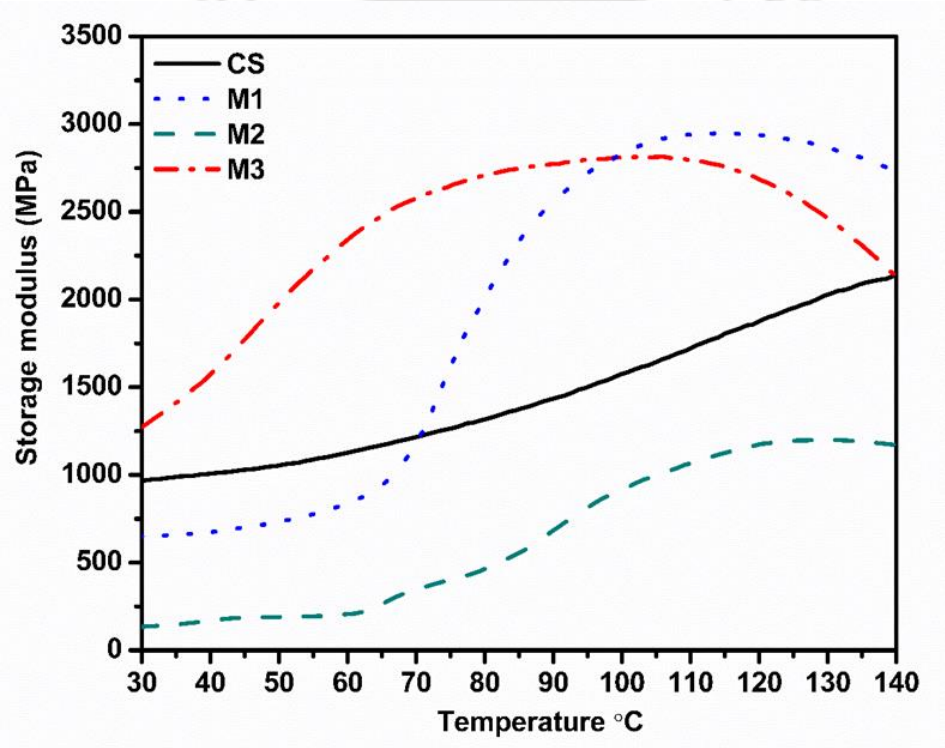

Figure 5.4 DMA analysis of CS, M1, M2 and M3 membranes.

5.3.4 Gas permeation study using binary gas mixture

5.3.4.1 Effect of sweep water flow rate

The effect of sweep water flow rate was studied by keeping feed water flow rate constant at 0.03 ml/min with temperature 90 °C and absolute pressure 2/1.21 (feed/sweep) bar. The CO_2 separation performances of M1, M2 and M3 membranes are depicted in Figure 5.5. The CO_2 flux, CO_2 permeance and CO_2/N_2 selectivity of all the membranes were minimum at 0.01

ml/min sweep water flow rate and then followed an increasing trend up to 0.05 ml/min before reaching saturation. The CO_2 flux of M1, M2 and M3 membranes were 442, 712 and 521 ($\times 10^{-6}$ $cm^3(STP)/cm^2s$) and reached to 1490 (~ 237 %), 2599 (~ 265 %) and 1842 (~ 253 %) $\times 10^{-6}$ $cm^3(STP)/cm^2s$, respectively at sweep water flow rate of 0.05 ml/min. The % increase in CO_2 flux is indicated in the parentheses. Similarly, CO_2 permeance of the M1, M2 and M3 membranes were increased ~ 264 %, ~ 446 % and ~ 273 %, when sweep water flow rate increases from 0.01 ml/min to 0.05 ml/min. The CO_2 permeance of M1, M2 and M3 membranes were 91, 164 and 112 GPU, respectively at 0.05 ml/min. The results suggest water play a positive role in CO_2 separation performance by helping in formation of CO_2-carrier complex. The bicarbonate (HCO_3^-) is formed during CO_2-carrier reaction in the high pressure region (feed side) and dissociate in the low pressure region (permeate side) by releasing CO_2 and water [79]. The diffusivity of the HCO_3^- complex is much higher than the CO_2 alone. Thus, the facilitated transport mechanism improves the CO_2 flux or permeance as compared to the non-reacting gases like N_2. Apart from facilitated transport mechanism, water induces swelling of the membrane as the water molecules are held inside the matrix. This swelling increases the free volume of the membrane which aids the gas molecules to pass through the active layer effortlessly. Water molecule acts as a plasticizing agent and induced chain relaxation of the membrane and increases the flexibility of the membrane which ultimately reduces the mass transfer resistance to the gas molecules. At low water flow rate, the carbonate fraction increases in the membrane (M2 and M3), and acts as a barrier to the gas solubility [102]. CO_2 can also pass through the water molecule present inside the matrix. The CO_2/N_2 selectivities of all the membranes were increased in the similar trend up to sweep water flow rate of 0.05 ml/min. The CO/N_2 selectivities of M1, M2 and M3 membranes were 67, 52 and 73, respectively. Both the CO_2 flux and permeance of the M2 membrane is higher than the M1 and M3 membranes as M1 contains 30 % Na_2CO_3 as carrier. The $NaCO_3$ acts as mobile carriers while SC acts as a fixed carrier in the matrix. The mobile carriers can move easily from one position to another while fixed carrier can move about its equilibrium position. However, in M3 membrane both mobile and fixed carriers work in conjunction to facilitate the transport of CO_2 and its CO_2 flux and CO_2 permeance lies in between M1 and M2.

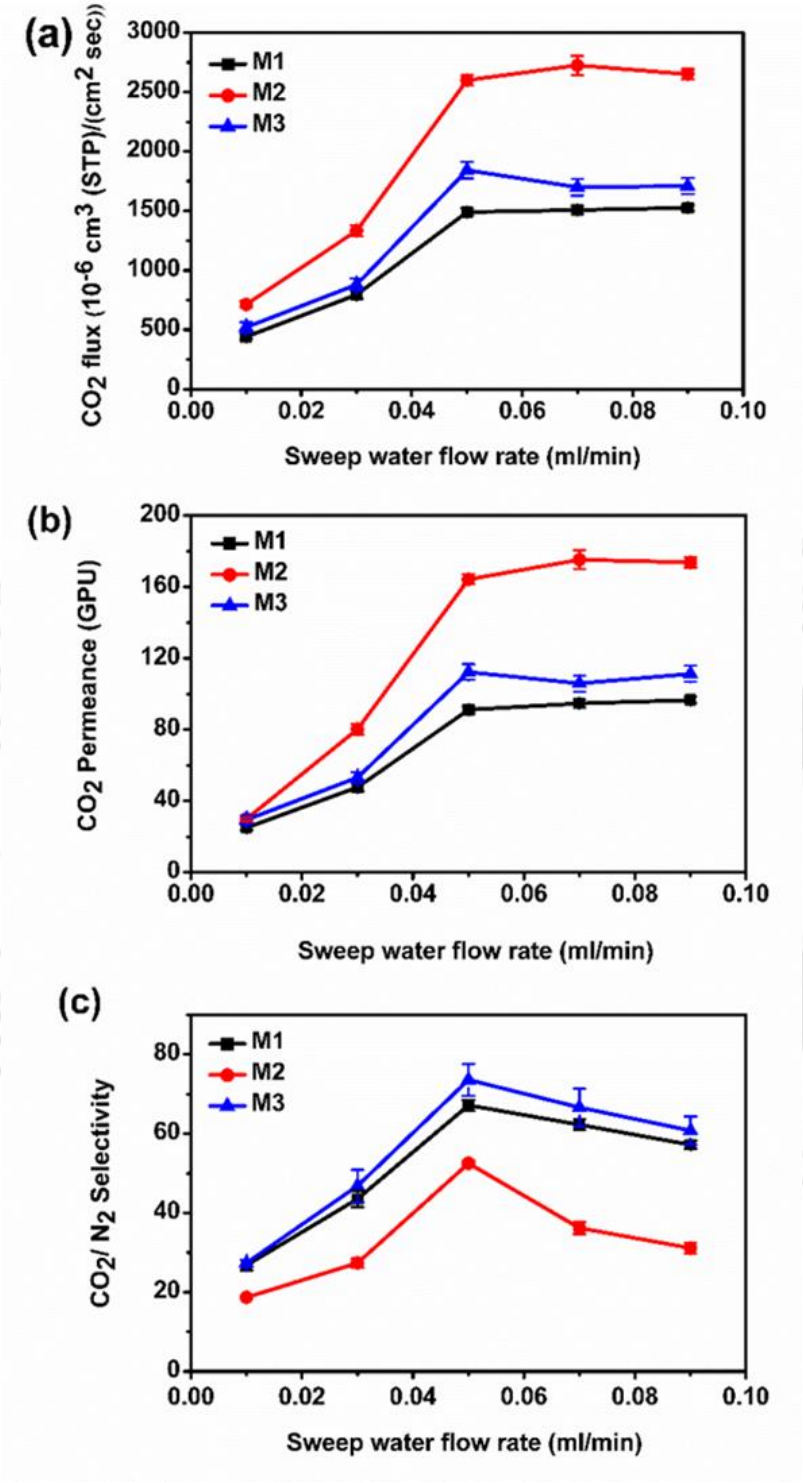

Figure 5.5 Effect of sweep water flow rate on (a) CO_2 flux, (b) CO_2 permeance and (c) CO_2/N_2 selectivity of M1, M2 and M3 membranes at temperature of 90 °C, feed water flow rate = 0.03 ml/min and absolute pressure = 2/1.21 bar (feed/sweep).

Further improvement in the CO_2 flux and CO_2 permeance after 0.05 ml/min are not perceptible due to carrier saturation. Moreover, the CO_2/N_2 selectivity of all the membranes showed a marginal decline in the trend line after 0.05 ml/min. This may be due to the fact that high water flow rate causes higher swelling of the membrane due to which membrane flexibility increases and allow N_2 molecules to pass. This resulted in a decrease in overall selectivity of all the membranes. The drop in selectivity was more for the M2 membrane due to very high water holding capacity suggested by the swelling test (Figure 5.3). The membranes displayed positive contribution below critical relative humidity.

5.3.4.2 Effect of temperature on CO_2 separation

The temperature effect was studied in the temperature range of 60-120 °C with absolute pressure of 2/1.21 (feed/sweep) bar and water flow rate of 0.03/0.05 (feed/sweep) ml/min. The CO_2 flux and CO_2 permeance of M1, M2 and M3 membranes at 60 °C were 1511, 2154 and 1605 × 10^{-6} cm^3(STP)/cm^2s, respectively and reached to 1490, 2599 and 1842 (× 10^{-6} cm^3 (STP)/cm^2s) (Figure 5.6a-b). The membrane containing SC as a carrier (M1) showed an increase in the CO_2 flux and permeance up to 80 °C and then negligible decrease in the performance was apparent when temperature reached to 90 °C. This can be alluded to the fact that desorption rate is faster than the absorption rate due presence of SC [179,185]. Further, a slight decrease after 80 °C may be due to the increase in the β-sheet of the silk SC with increasing temperature in the presence of moisture [180], which leads to membrane stiffness. On the other hand, increase in membrane crystallinity due to presence of SC obstructs the transport of gas molecules through the active layer. The interplay of crystallinity and reaction rate at a particular temperature decides the CO_2 separation performance with the dominant one playing the upper hand. The membrane M2 containing only Na_2CO_3 as carrier indicates increase in the CO_2 flux and permeance as temperature reached from 60 to 90 °C. It may be noted that the rate of reaction between CO_2 and carrier increases with temperature in the presence of moisture which results in increase in CO_2 flux and CO_2 permeance with increase in temperature. The water holding capacity of the membrane containing Na_2CO_3 is higher than the blend M1 containing SC, due to stronger hydrogen bonding between Na_2CO_3 and water

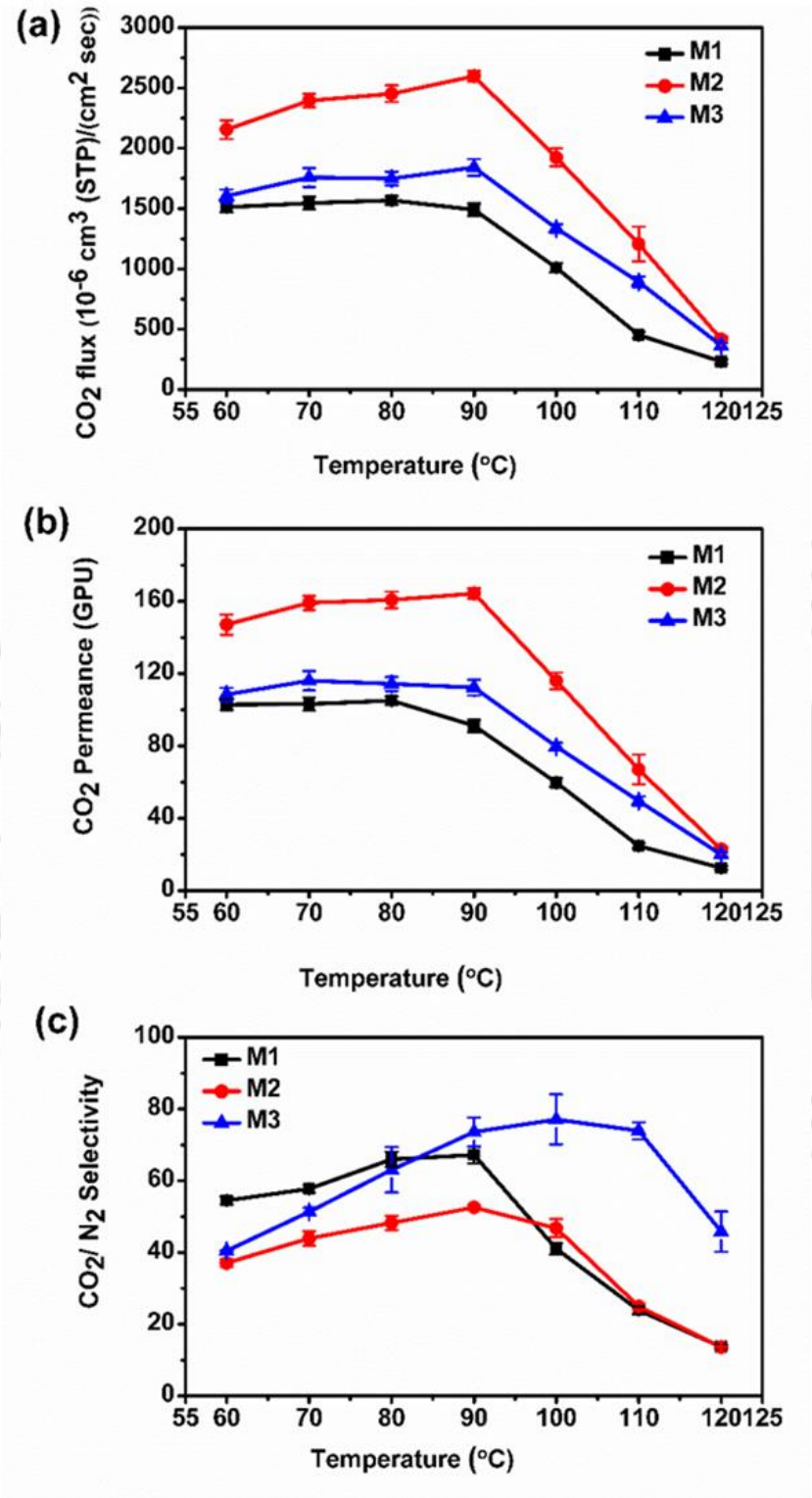

Figure 5.6 Effect of temperature on (a) CO_2 flux, (b) CO_2 permeance, and (c) CO_2/N_2 selectivity of M1, M2 and M3 membrane at water flow rate = 0.03/0.05 ml/min (feed/sweep), feed absolute pressure = 2 bar and sweep absolute pressure = 1.21 bar.

molecule [188]. However, when temperature of M2 membrane reached to 100-120 °C the water content in the membrane decreases and $NaHCO_3$ gets converted to Na_2CO_3 [186].

The CO_2 permeance of M1, M2 and M3 membrane at 90 °C were 91, 164 and 112 GPU, respectively and abrupt drop was detected after 90 °C which resulted in CO_2 permeance of 12, 23 and 20 GPU respectively. The sudden drop in CO_2 separation performance after 90 °C can be attributed to the loss of water holding capability of the membrane at that temperature. The temperature at which the membrane can hold sufficient amount of water is suitable for better CO_2 separation performance. Additionally, loss of water at high temperature reduces the membrane flexibility as suggested by DMA analysis and increases the mass transfer resistance to the gas molecules to pass through the active layer, which diminishes the CO_2 flux and permeance. Similarly, CO_2/N_2 selectivity (Figure 5.6) of M1, M2 and M3 membranes were 54, 37 and 40, respectively and upsurges to 67 (~ 24 %), 52 (~ 40 %) and 73 (~ 82 %) respectively. The % fold increase is specified in the parentheses. The CO_2/N_2 selectivity of M1 membrane showed a drastic drop in selectivity due to rise in β-sheet and stiffness of the membrane with temperature. However, for the M2 and M3 membranes, CO_2/N_2 selectivity was stable up to 100 °C which can be explained by temperature dependent formation of bicarbonate using K_2CO_3 and of salting out phenomena [88,189].

5.3.4.3 Effect of feed absolute pressure

The effect of feed absolute pressure was studied for all the three membranes with water flow rate of 0.03/0.05 ml/min (feed/sweep) at 90 °C (Figure 5.7). As expected the CO_2 flux of all the membranes increased with increase in feed pressure. The CO_2 flux of M1, M2 and M3 membranes were 1490, 2599 and 1842 ($\times 10^{-6}$ cm^3(STP)/cm^2s) at 2 bar feed absolute pressure. The flux increases up to 3.81 bar and reached to 2172 (~ 45 %), 3359 (~ 29 %) and 2600 (~ 41 %) $\times 10^{-6}$ cm^3(STP)/cm^2s. The % fold increase is specified in the parentheses. The reason behind increase is due to high partial pressure of CO_2 and resulting in more amount of CO_2 dissolved in the active layer due to pressure difference across the membrane. After 3.81 bar feed absolute pressure, the increase in the CO_2 flux is limited due to carrier saturation which restricts the further formation of CO_2-carrier complex. After carrier saturation, the CO_2 flux in governed by solution-diffusion mechanism. The maximum CO_2 flux of all the membranes

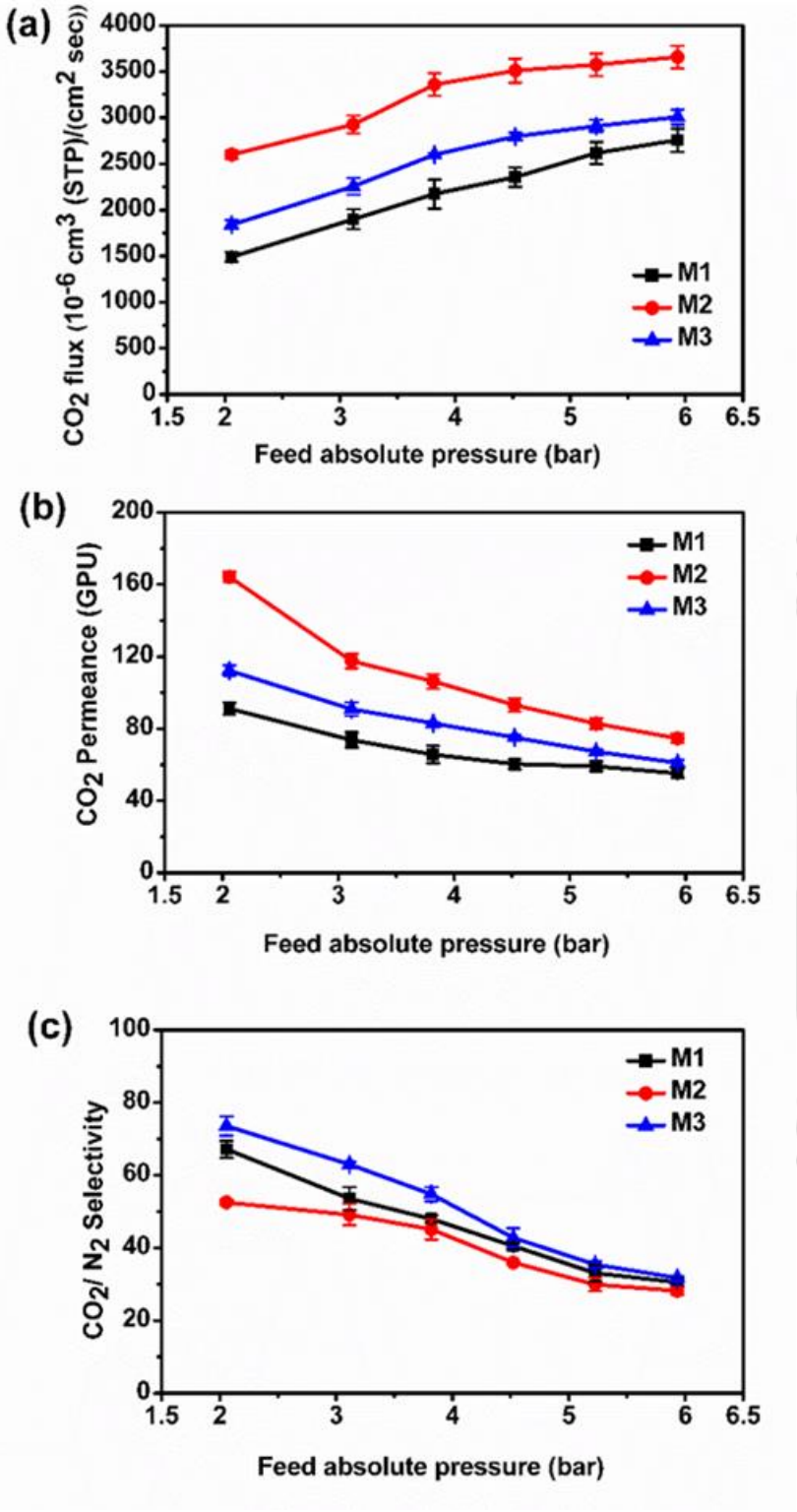

Figure 5.7 Effect of absolute feed pressure on (a) CO_2 flux, (b) CO_2 permeance and (c) CO_2/N_2 selectivity of M1, M2 and M3 membranes, at water flow rate = 0.03/0.05 ml/min (feed/sweep), at temperature 90 °C and sweep absolute pressure = 1.21 bar.

at 5.91 bar were 2756 (M1), 3655 (M2), and 3006 (M3) ($\times 10^{-6}$ cm^3 (STP)/cm^2s). High pressure forces out the water molecules from the membrane and leads to membrane compaction. As a result, the gas molecules encounter resistance to cross through the membrane. However, the CO_2 permeance as well as CO_2/N_2 selectivity followed the opposite trend as compared to CO_2 flux. The CO_2 permeance is inversely related to the partial pressure difference and directly related to the CO_2 flux. The proportion at which CO_2 partial pressure was increased, at the same rate the CO_2 flux was not increasing and resulted overall drop in CO_2 permeance was observed. This suggested that facilitated transport mechanism is feasible at lower partial pressure. This is a typical behavior of the membranes following facilitated transport mechanism. At 2 bar of feed pressure, the CO_2 permeance detected for the membranes were 91 (M1), 164 (M2) and 112 (M3) GPU and then declined to 55 (~ 40 %), 74 (~ 54 %) and 60 (~ 46 %) GPU at 5.91 bar. The % fold increase is indicated in the parentheses. Similarly, the CO_2/N_2 selectivity of M1, M2 and M3 membranes were 67, 52 and 73 at 2 bar and reached to 30, 38 and 32, respectively at 5.91 bar. The decrease in CO_2/N_2 selectivity with an increase in feed pressure can be explained by the solubility of more amount N_2 at high N_2 partial pressure which creates the concentration difference of N_2 across the membrane.

5.3.5 Gas permeation study using ternary gas mixture

Nature of the penetrants and feed gas mixture plays a vital effect on the permeation behaviour. Pure gas permeation behaviour varies from mixed gas permeation through the same membrane due to competitive sorption among the molecules to be separated. Ternary gas mixture ($CO_2/N_2/H_2$) separation performance of the prepared membranes were evaluated. The CO_2 separation from N_2 is generally used for post-combustion process while CO_2 separation in presence of H_2 can be used for pre-combustion process of syngas.

5.3.5.1 Effects of temperature and pressure on CO_2 separation performance by M3 membrane

Using ternary gas mixture, the temperature (in the range 60 to 120 °C) and pressure effects (in the range of 2 bar to 5.91 bar) on M3 membrane were examined (Figure 5.8 i-ii). The effect of temperature on CO_2 flux and CO_2 permeance follow the similar trend as observed for binary gas. The CO_2 flux and CO_2 permeance at 90 °C were 1918 $\times 10^{-6}$ cm^3 (STP)/cm^2s and 120 GPU respectively which were ~ 4 % and ~ 7 % higher when binary gas was used. The marginal

higher value of CO_2 flux and permeance may be due to the lower partial pressure of CO_2 at 2 bar feed absolute pressure as 10 % of CO_2 is present in the ternary gas mixture instead of 20 % of CO_2 available in case of binary gas mixture. Membrane following facilitated transport is effective at low partial pressure. The CO_2/N_2 selectivity was found to decline by ~ 41 % to 43 as compared to binary gas mixture at similar conditions. The drop in selectivity can be explained by the increase in N_2 permeance due to competitive sorption of the gas molecules. Another possible reason may be that membrane stability of the membrane with passes time is decreasing as the same membrane was also used for binary gas mixture.

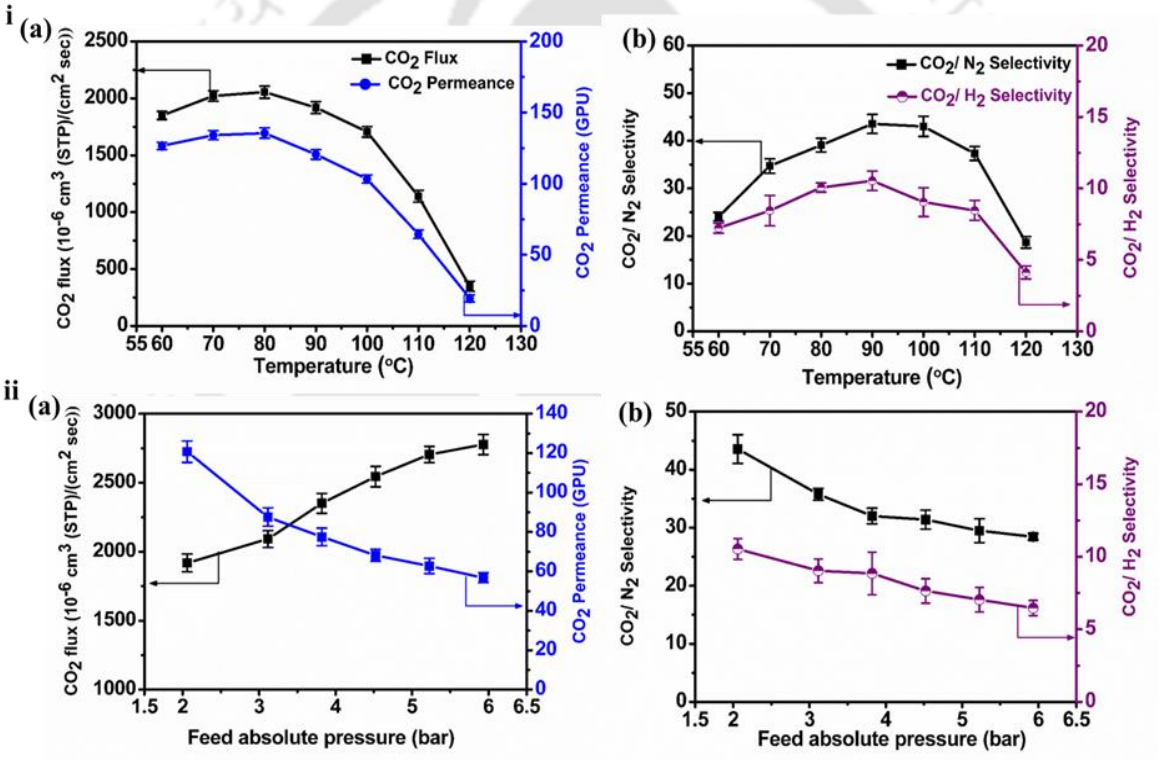

Figure 5.8 Effect on M3 membrane (i) temperature effect (a) CO_2 flux and CO_2 permeance, (b) CO_2/N_2 and CO_2/H_2 selectivity at water flow rate = 0.03/0.05 ml/min (feed/sweep) and absolute pressure = 2/1.21 bar (feed/sweep) and (ii) feed absolute pressure effect (a) CO_2 flux and CO_2 permeance, (b) CO_2/N_2 and CO_2/H_2 selectivity at 90 °C with water flow rate = 0.03/0.05 ml/min.

The CO_2/H_2 selectivity of the M3 membrane was 10 and lower selectivity of CO_2/H_2 compared to CO_2/N_2 can be explained by the difference in kinetic diameter of H_2 (2.8 Å) and

N_2 (3.64 Å) [190]. Similarly, David et al. [156] found CO_2/H_2 selectivity of 4.7 for the pure gas permeation of H_2 and CO_2 while CO_2/H_2 selectivity decreased to 2.7 when a mixture of H_2 and CO_2 was used. This can be alluded to the competitive sorption of CO_2, H_2, and N_2 in the swelled membrane. Thus, assessment of the separation properties of the membrane solely on the basis of permeation data using pure gas may lead to erroneous valuation [191,192]. Similarly, pressure effect was also studied in the pressure range of 2 bar to 5.91 bar (Figure 5.8 ii). The CO_2 flux reached to 2777×10^{-6} $cm^3(STP)/cm^2s$ when feed absolute pressure was raised to 5.91 bar. On the other hand, CO_2 permeance decreased from 120 to 56 GPU with change in pressure from 2 to 5.91 bar (Figure 5.8 ii-a), whereas the CO/N_2 and CO_2/H_2 selectivity (Figure 5.8 ii-b) were 43 and 10 at 2 bar and decreased to 28 and 6, respectively at 5.91 bar.

5.3.6 XPS analysis of M3 membrane

5.3.6.1 Depth profiling

XPS is a high-end sensitive equipment used for surface analysis of the materials. In addition, depth profiling analysis was also performed by combining etching source which eliminates the layers of the materials without causing harm to the next layer material [193]. However, layer damaging depends upon either single atom of cluster ion being used as a source of sputtering [193]. Depth profiling using cluster beam provide advantages over source like high sputter yield, minimal damage to the layer, better quality of data and low penetration depth [194]. Since our ultimate motivation was to utilize the waste by-product from SF extraction i.e. (SC dissolved in Na_2CO_3 solution), XPS depth profiling was carried out only for M3 membrane The depth profile experiment of M3 membrane (Figure 5.9) was conducted by upholding the temperature at 90 °C, which enabled the study of the stability of the elemental composition at 90 °C. During the etch phases, the sample was exposed to a beam of 8 keV, Ar^+_{150} ions. XPS survey and high resolution spectra were acquired at each level of the depth profile. This continued until the relative concentrations of the elements present in the sample had reached an equilibrium. In the first 100 s of the depth profiling, there is a region of variation in relative atomic composition. This is a common feature encountered in-depth profiling and is a result of the removal of surface contamination. The variation in relative

atomic % has reached equilibrium at around etch time of 300 seconds and remains unchanged with etching time.

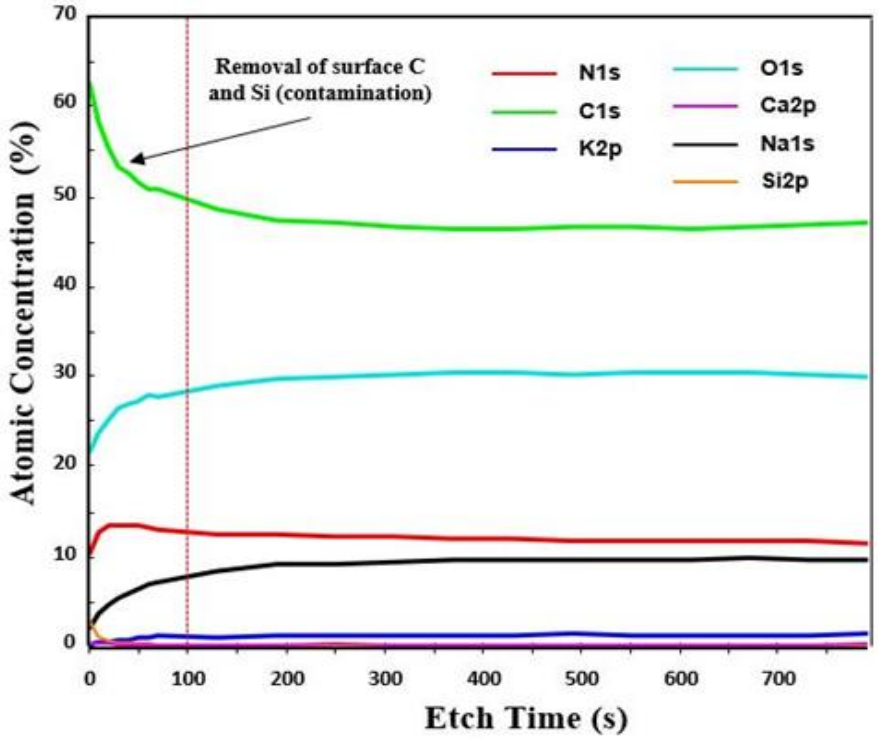

Figure 5.9 XPS depth profiling of M3 membrane active layer at 90 °C.

The results suggest that the elemental composition of the M3 membrane was evenly distributed across the depth of the membrane and clustering of any specific atom was absent. This means that SC, Na_2CO_3 in blend with CS formed a homogeneous layer. This indicated well prepared blend membranes suitable for gas separation.

5.3.6.2 Survey scan, narrow scan and elemental composition analysis using XPS

From the practical application standpoint, the membranes should endure high temperature stability as the output flue gas or syngas from industries are at high temperatures. We further engaged ourselves to investigate the stability of M3 membrane as this membrane is intended for practical applications employing the discarded waste from SF extraction. In order to investigate the membrane stability with temperature for a prolonged period, XPS survey scan

was performed for the M3 membrane at temperatures of 24, 30, 60, 90 and 120 °C. From the survey scan of the M3 membrane (Figure 5.10 i-a), the significant spectra perceived were C 1s, N 1s, O 1s and Na 1s. These peaks arise from CS and SC that possess C, N and O in its structure whereas the contribution of Na along with C and O was due to the presence of Na_2CO_3. The same survey scan when performed at different temperatures (Figure 5.10 i-b), no shift/change in the respective peaks were discerned. Additionally, the absence of peak shift in the high resolution spectra of the individual C 1s, N 1s and O 1s (Figure 5.10 ii-a,b,c) confirms the temperature stability of the membrane up to 120 °C. The C 1s region was further deconvoluted to get the different carbon states at different binding energy (Figure 5.10 ii-d).

The elemental composition of the membrane M3 at various temperatures is represented in Table 5.1. The elements present in M3 membrane at 24 °C were C (~ 63.43 %), O (~ 24.2 %), N (~ 9.57 %) and Na (~ 2.56 %) which persisted with trivial variation up to 120 °C. This trivial change in composition percentage can be attributed to loss of water molecules and CO_2 adsorbed from the surrounding atmosphere at room temperature. This composition analysis with the variation of temperature suggests that the membrane is thermally stable up to 120 °C and is suitable for CO_2 separation in this temperature range.

Table 5.1 Surface elemental concentration (%) analysis of M3 membrane at temperatures (°C) 24, 30, 60, 90 and 120.

Element	24 °C	30 °C	60 °C	90 °C	120 °C
C	63.43	63.46	63.51	64.02	64.23
O	24.2	23.91	23.58	23.02	22.51
N	9.57	9.7	9.83	9.87	10.04
Na	2.56	2.57	2.73	2.81	2.86
Ca	0.09	0.17	0.17	0.15	0.18
S	0.15	0.19	0.18	0.16	0.18

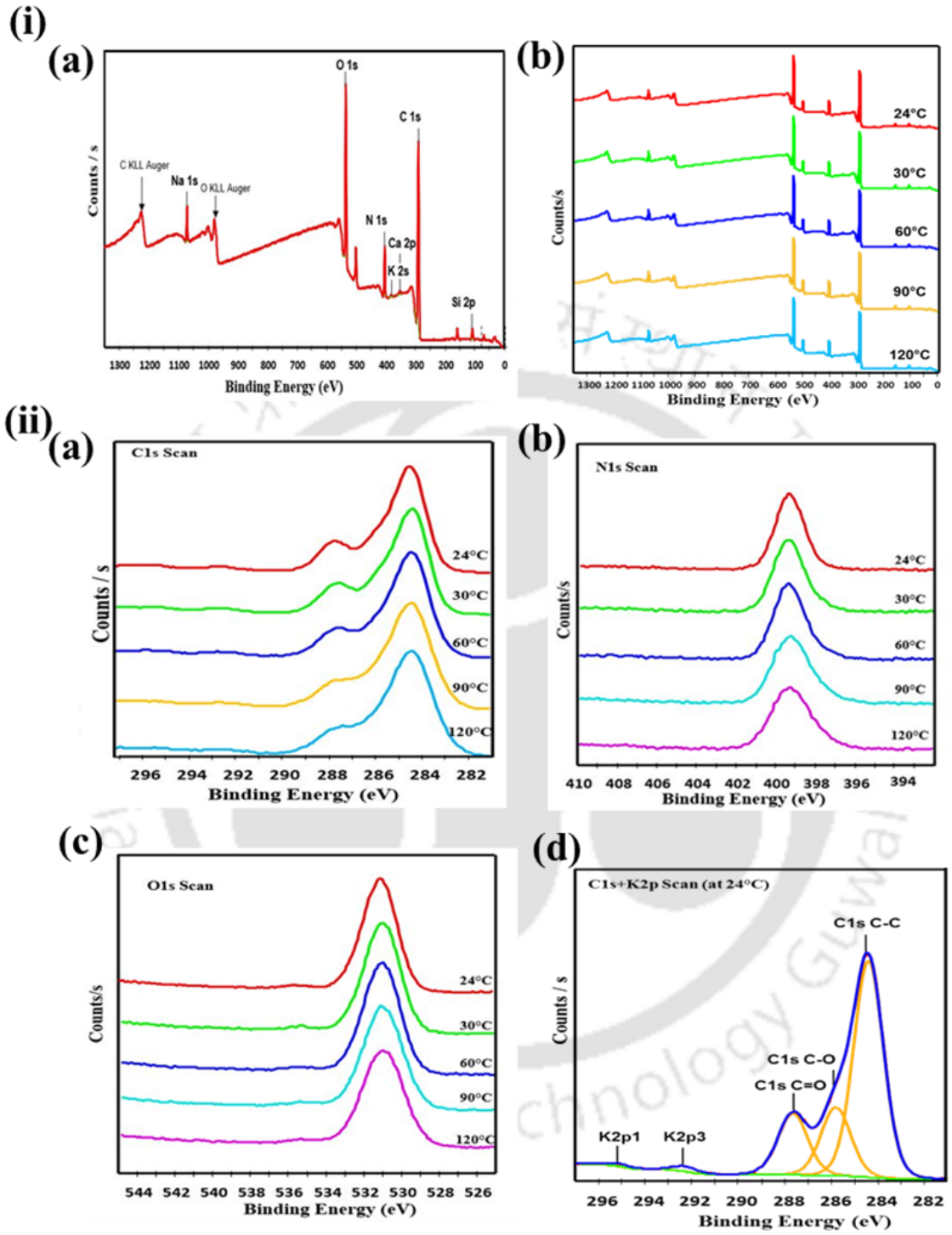

Figure 5.10 The XPS data profile of the M3 membrane (i) survey scan (a) at 24 °C and (b) at different temperatures; (ii) narrow scan range for (a) C 1s, (b) N 1s, (c) O 1s at different temperatures and (d) deconvoluted peak C 1s, at 24 °C.

5.4 Conclusions

Towards the end of this chapter, we initiated a full proof concept of utilizing the whole of raw silk from the cocoons for applicability in gas separation. In this novel approach, the discarded sericin solution (SC polymer dissolved in Na_2CO_3 solution) after SF extraction was incorporated inside the CS matrix that led to the formation of a uniform textured membrane (M3) with dense active layer and desired roughness, as evident from the advance microscopic analysis. For having a better insight into the CO_2 separation phenomenon, two other membranes were prepared. M1 membrane with dialyzed SC solution blended with CS and another M2 membrane, where Na_2CO_3 has been deliberately added to the CS matrix. The uniformly disseminated elemental composition was confirmed from XPS depth profiling for the M3 membrane. Intermediate swelling and stiffness were indicated through the swelling test and DMA study, respectively. The CO_2 selectivity and permeance for binary gas, though lie in the intermediate region as compared to M1 and M2, at 0.05 ml/min of sweep water flow rate, 90 °C and 2 bar feed pressure, the CO_2/N_2 selectivity was found to be the optimum for the M3 membrane at all the conditions. In case of ternary gas mixture, CO_2/N_2 and CO_2/H_2 selectivities were 43 and 10 respectively. XPS survey scan at different temperature failed to detect any peak shift in the elemental composition which established the temperature stability of the membrane. We can conclude that the prepared sericin-chitosan based membrane will have major implications for CO_2 separation when employed for industrial flue gas separation.

CHAPTER 6

Biopolymer-Graphene Nanoparticle Based Mixed Matrix Membrane to Counteract the Support Pore Filling Phenomenon during CO_2 Separation

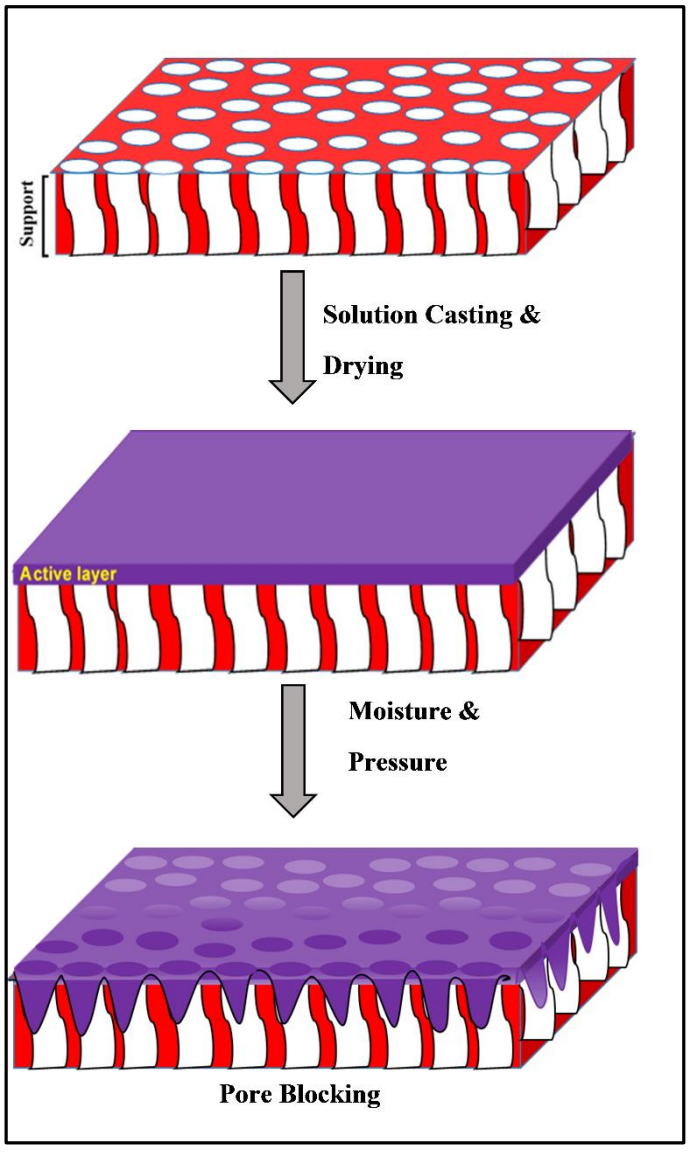

Scheme of the support pore filling by the active layer during gas permeation in the presence of moisture and pressure

CHAPTER 6

Biopolymer-Graphene Nanoparticle Based Mixed Matrix Membrane to Counteract the Support Pore Filling Phenomenon during CO_2 Separation

*This chapter encompasses the preparation of mixed matrix membrane (MMM) by incorporation of graphene nanoparticles (GNP) into the CS/SF matrix which is highly robust mechanically and thermally. In Chapter 4, we have already discussed the novelty and stability improvement of the CS/SF membranes for CO_2 separation. To further improve the membrane properties, in this study, a novel MMM has been developed by incorporating GNP into the CS/SF to bestow the membrane with unique properties. This study also entails an insight into the CO_2 separation mechanism by the nanocomposite matrix with an effort towards mitigating/controlling the challenges of pore blockage of the support membrane. This work is scientifically acknowledged in "**ACS Applied Materials and Interfaces**".*

6.1 Introduction

Various mixed matrix membranes (MMMs) have also been synthesized by incorporating organic filler in the CS matrix [110,115,116,195,196]. The gas separation performance ability of MMMs is governed by both inorganic filler and the polymer matrix [197]. The MMMs were synthesized by adding different inorganic fillers such as silica gel, zeolites, activated carbons, carbon nanotubes, metal organic frameworks (MOFs) and even non-porous solid fillers [55,198–200]. These MMMs have their own set of disadvantages like low dispersion and selectivity [55,200–202]. However, graphene-based MMMs overcome these disadvantages due to good dispersion and are widely used for CO_2 separation application [55]. Ying et al. [202] reported nano-confinement of ionic liquid (IL) by graphene, whereas Dong et al. [54] reported dual-inorganic composite membranes with molecular sieving effect. Further improvement in the gas transfer passage was achieved with MOF and graphene [55,200]. Similarly, Abtin et al. [198] proposed a new concept of guest-host nanocomposite membrane for gas separation. The separation mechanism by these membranes are based on solution-diffusion or Knudsen diffusion mechanism [203]. Although Zhou et al. [204] used

piperazine along with graphene for facilitated CO_2 transport, the mechanism of membrane preparation is quite cumbersome and tedious. Moreover, the complex membrane preparation procedures reported deter their commercial application.

Graphene is a versatile material which is highly robust mechanically and thermally, and possess high aspect ratio that bestows it with the capability of forming thin films [205]. Graphene blends well with polymers and such graphene-based membranes for CO_2 separation have been investigated as discussed above [56]. However, the gas separation mechanism by graphene oxide (GO) remains unclear. The CO_2 separation by GO has been ascertained to 2D capillaries formed by closely spaced graphene sheets [206], edge-to-edge openings [207] or selective structural defects [208]. Recently, inter-sheet and inner-sheet defect pathway models were proposed by Ibrahim et al. [208]. In the first case, the gas molecule can pass through the inter-sheet nanoscale wrinkles and inter-galleries between stacked GO sheets and the second pathway suggests the passage of a gas molecule through the inner-sheet defect pathway, which provides straight channels for gas molecules.

Silk fibroin (SF) is a unique biopolymer with applications in different fields owing to its good mechanical robustness and biocompatibility [209]. The inherent amines present in SF primarily consists of glycine (Gly) (43 %) and alanine (Ala) (30 %) [210]. In our previous chapter, we undertook a unique approach to exploit these inherent amines present naturally in SF as carriers amines for CO_2 separation. The CS/SF blend membrane displayed sustained high CO_2 separation performance with enhanced performance stability as the leaching of amines was mitigated. The dominant crystalline β-sheet structure of SF that governs the eventual membrane properties, can be regulated by varying temperature and moisture conditions, which imparts the desired performance characteristics to the membrane. However, SF alone is known to be brittle with inadequate mechanical strength [211].

6.2 Experimental section

6.2.1 Materials

Chitosan (CS) flakes (Mw~ 310000-375000 Da) were supplied by Sigma-Aldrich, USA while silk cocoons (*Bombyx mori*) were procured from a local vendor. Sodium carbonate (Na_2CO_3,

99.5 % purity) and glacial acetic acid (99.99 % purity) were purchased from Merck, Germany. Lithium bromide (LiBr, 99 % purity) was supplied by Spectrochem. GNP was acquired from Graphene Laboratories Inc., New York. The poly(ether sulfone) (PES) supports (thickness: ~150 μm and average pore size: 0.03 μm) were kindly supplied by Sterlitech, USA. Binary feed gas (CO_2/N_2) mixtures (20/80 vol %) and ternary feed gas ($CO_2/H_2/N_2$) mixtures (10/10/80 vol %) were obtained from Vadilal Chemicals Ltd., India. Helium (99.999 % pure) and Argon (Ultrapure) were acquired from the same vendor. Helium was used as carrier gas for GC and Argon as a sweep gas for the permeation study. Millipore water (>18 MΩ cm^{-1}, Millipore®) was used throughout the experiments.

6.2.2 Silk extraction

Silk fibroin (SF) was extracted following the protocols as discussed in Chapter 4. Briefly, silk cocoons were cut into small pieces to dispose worms. The cocoons were boiled for 30 min in 0.02 M Na_2CO_3 to remove the sericin. Then, the degummed silk was rinsed thrice in water for 20 min each and dried overnight inside the laminar hood (LabTech®). Then it was dissolved in 9.3 M LiBr at 60 °C for 4 h and the solution was transferred into a dialysis tube (1 kDa MWCO, GE) to dialyze against water for 72 h to elute the LiBr. Finally, the obtained amber coloured SF solution was centrifuged (Sigma 3-30k) at 10000 rpm for 20 min. The SF (yield of 6-7 % w/v) was stored at 4 °C until further use.

6.2.3 Membrane preparation

The graphene nanoparticles (GNP) (0.5 g) were sonicated in 100 ml acetic acid solution (1 vol %) for 20 min. Then, 1.15 g of CS was added to the solution and left under vigorous stirring for 12 h. Finally, chitosan and graphene nanoparticles (CS/GNP) solution was centrifuged at 10000 rpm, for 30 min to remove the undissolved particle. In order to avert SF gelation, potassium hydroxide (KOH) was added to preserve the pH at ~ 5.5 [163]. Before adding the calculated amount of SF in the CS/GNP solution, the temperature was maintained at ~ 5 °C by placing the entire solution in ice bath and stirring again for 15 min. After centrifugation (10000 rpm, 30 min, 5 °C), the CS/SF/GNP solution was cast onto the PES support using casting knife (Digital II Microm, GARDCO, USA). The membranes were prepared with dry wt % as 99.5 % CS + 0.5 % GNP (CS/GNP) and CS 54.5 % + SF 45 % +

0.5 % GNP (CS/SF/GNP). A dense layer was formed when the membranes were dried as in our work in Chapter 4. Circular membrane, to fit the size of the module, was cut from the cooled membranes for gas permeation analysis.

6.2.4 Membrane characterization and gas permeation study

Gas permeation data was obtained using the experimental GC set up as explained elaborately in Chapter 2 and the details of the composition for CO_2 separation from binary and ternary gas have been provided in Chapter 4.

The active layers of the membranes with PES support have been used to analyse the surface topography by using AFM, Innova, Bruker and FESEM, ZEISS, USA. The AFM was performed in tapping mode with scanning rate of 0.7 Hz. The recorded AFM images were further processed using Windows-Scanning-x-Microscope (WSxM) software [140]. For FESEM imaging, the samples were fixed on a stub with a carbon tape and gold sputtered. Rest of the analytical studies were conducted on the active layers without support. Swelling test was done by maintaining a different relative humidity as mentioned in the earlier chapter. DMA for the prepared samples were performed (Netzsch DMA 242E Artemis®) under nitrogen environment at temperatures ranging from 30 to 140 °C with a heating rate of 2.5 °C/min. The analyses were conducted in the tensile mode having dynamic force of 1 N and frequency of 1 Hz.

The TGA isotherms were conducted at temperatures (°C) 100, 120 and 150 successively, to check the thermal stability of the prepared membranes. Further, the membranes (sample size 1 cm × 0.5 cm) were exposed to X-ray Photoelectron Spectroscopy (XPS), recorded at different temperatures (24 °C, 30 °C, 60 °C, 90 °C and 120 °C) using Thermo Scientific Escalab Xi^+ XPS spectrometer, for the quantitative and qualitative analysis of surface chemical state. Samples were mounted on the Escalab Xi^+ sample holder. A thermocouple in contact with the sample surface was used to measure the sample temperature during the data acquisition. The X-ray source used was mono-chromated Al k-alpha having pot size of 400 μm. A vacuum pressure of 7×10^{-8} mbar was maintained during cluster etching. The ion beam energy of 8 keV having cluster size of 150 atoms and beam current of 35 nA were used. The analysis of the recorded XPS data was conducted using Avantage v5.984 software.

6.3 Results and discussion

6.3.1 CO_2 permeance performance of the membranes with time

The pore development on the membrane and support pore clogging phenomenon during membrane preparation for gas separation study is a critical issue of concern. The blockage of pores of the support membrane can alter the effective thickness of the membrane which might be different from actual thickness. The active layer thickness significantly affects the CO_2 permeability as CO_2 flux is inversely related to the thickness of the active layer [212]. This is visible at two stages (i) blockage of PES support pores owing to leaching of low viscous solution during casting and (ii) penetration of the active layer into the pores of the support in the presence of moisture and feed pressure during gas permeation study. The low viscosity polymer solution can easily penetrate across the pores of the PES support and eventually create high mass transfer resistance for passage of gas molecules. A low viscosity polymer solution (~ 600 cp) will percolate through the pores of the support, as visualized in the FESEM cross-section image during membrane formation (Figure 6.1). For the formation of a uniform

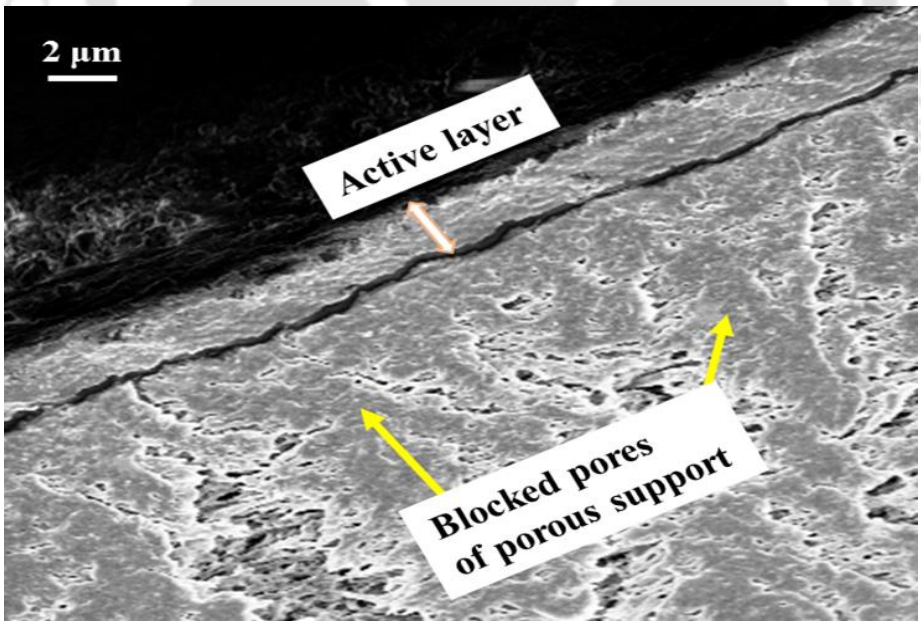

Figure 6.1 Support pore blockage due to casting of low viscous solution (FESEM cross-sectional view of CS/SF/GNP).

layer onto the PES support without any pore blockage, high solution viscosity (~ 1400-1500 cp) is a requisite. Another phenomenon that might contribute to the overall effective thickness is the penetration of the swelled active layer into the support membrane in the presence of feed pressure during gas permeation study (Figure 6.2-i). When moisture is supplied at a given temperature and pressure, the active layer of the membrane gets swelled that improves its flexibility. Further, when pressure is applied, it penetrates the support pores and results in the pore clogging. As swelling increases, the penetration intensifies into the PES support as shown in the schematic (Figure 6.2-i). However, there is only negligible swelling effect on the PES support in presence of moisture. Due to poor hydrophilic nature of the PES support, water molecules are not retained in their pores and can be obtained as permeate knockout. Pores filled with water also provide mass transfer resistance to the gas molecule resulting in reduced flux [213].

A decay in the CO_2 permeance performance by the test membranes was observed initially which finally gained a saturation phase after 12 h (Figure 6.2-ii). This initial sink in the CO_2 permeance observed by Okabe et al. [214] was attributed to the increased membrane thickness due to moisture absorbance from feed gas. The observed drop in CO_2 permeance was meagre 7 % in case of CS/SF/GNP membrane as compared to 13 %, and 34 % in case of CS/GNP and CS, respectively. This implied that the proposed concept of the increased active layer thickness due to swelling, prohibits the initial transit of gas molecules as evident in case of CS membrane. Nanomaterials such as graphene, when incorporated in the polymer matrix, can efficiently control swelling effect [215]. Owing to the regulated swelling and support pore filling under application of moisture and pressure, substantial improvement during the initial 12 h was observed in the membranes with GNP. The additional enhancement in the CO_2 permeance by CS/SF/GNP can be attributed to the tuneable properties of silk fibroin as discussed in our previous work [215].

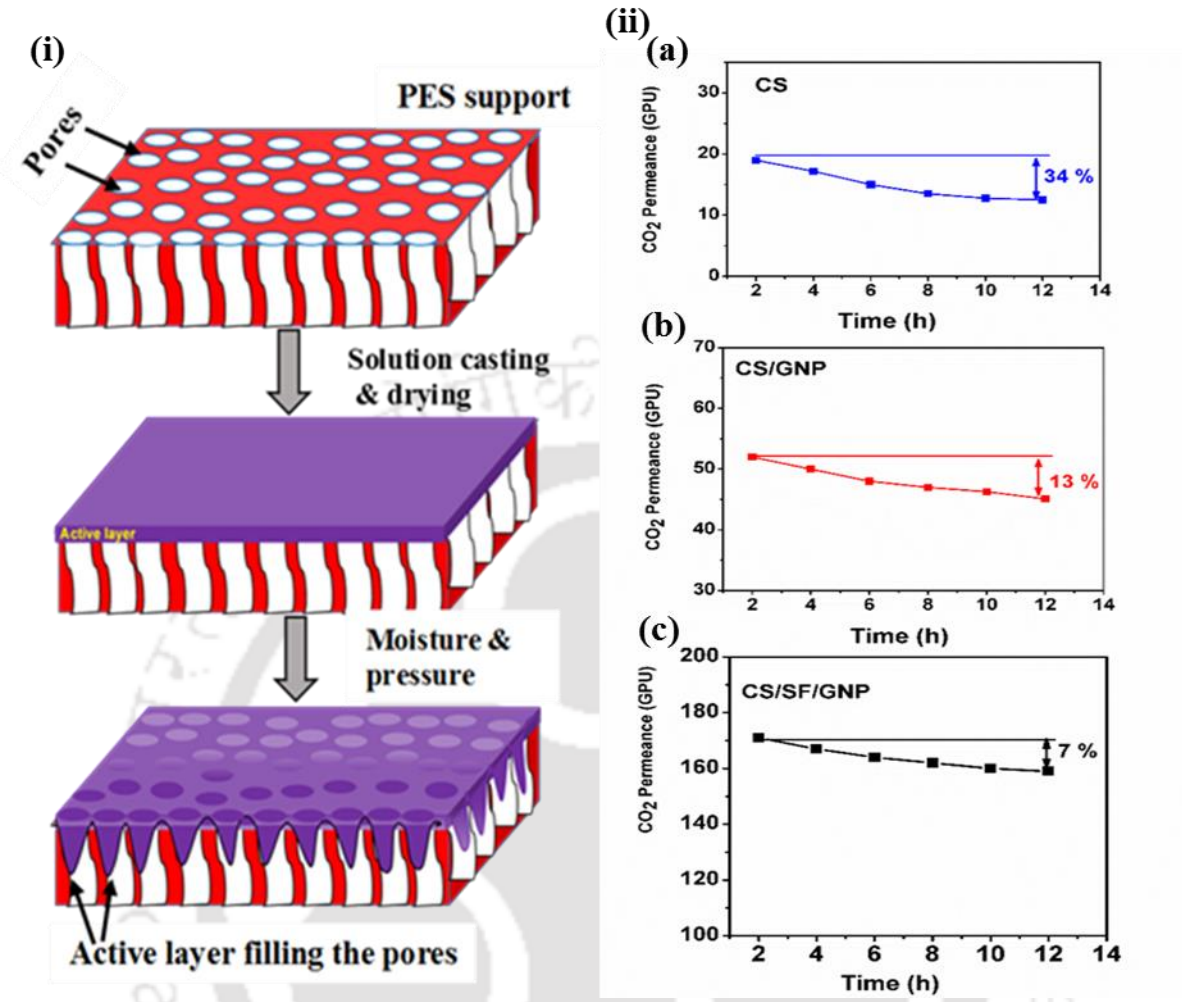

Figure 6.2 (i) Scheme of pore filling during gas permeation in the presence of moisture and pressure and (ii) CO_2 permeation results of the membranes (a) CS, (b) CS/GNP and (c) CS/SF/GNP at temperature of 90 °C, water flow rate = 0.03/0.05 (feed/sweep) ml/min and absolute pressure = 2/1.21 bar (feed/sweep).

6.3.2 Topography analyses using microscopic techniques

The proper dispersion of nanofillers in the polymer matrix is a prerequisite for the preparation of desired membrane. Lower dispersion of the nanofillers leads to agglomeration of the fillers which ultimately reduce the mechanical strength of the membrane by minimizing the maximum load transfer [216]. Also, a minimal amount of filler is required for the desired application when dispersion is excellent. The smooth surface of CS/GNP and CS/SF/GNP as perceived in FESEM images (Figure 6.3a-b) suggested proper dispersion of GNP with CS

(CS/GNP) and CS/SF (CS/SF/GNP) matrix. The cross-sectional images of FESEM (Figure 6.3c-d) suggest the formation of dense layers onto the PES support. The cross-sectional images clearly indicate that there is no pore filling into the pores of PES support and the desired active layer is formed onto the support.

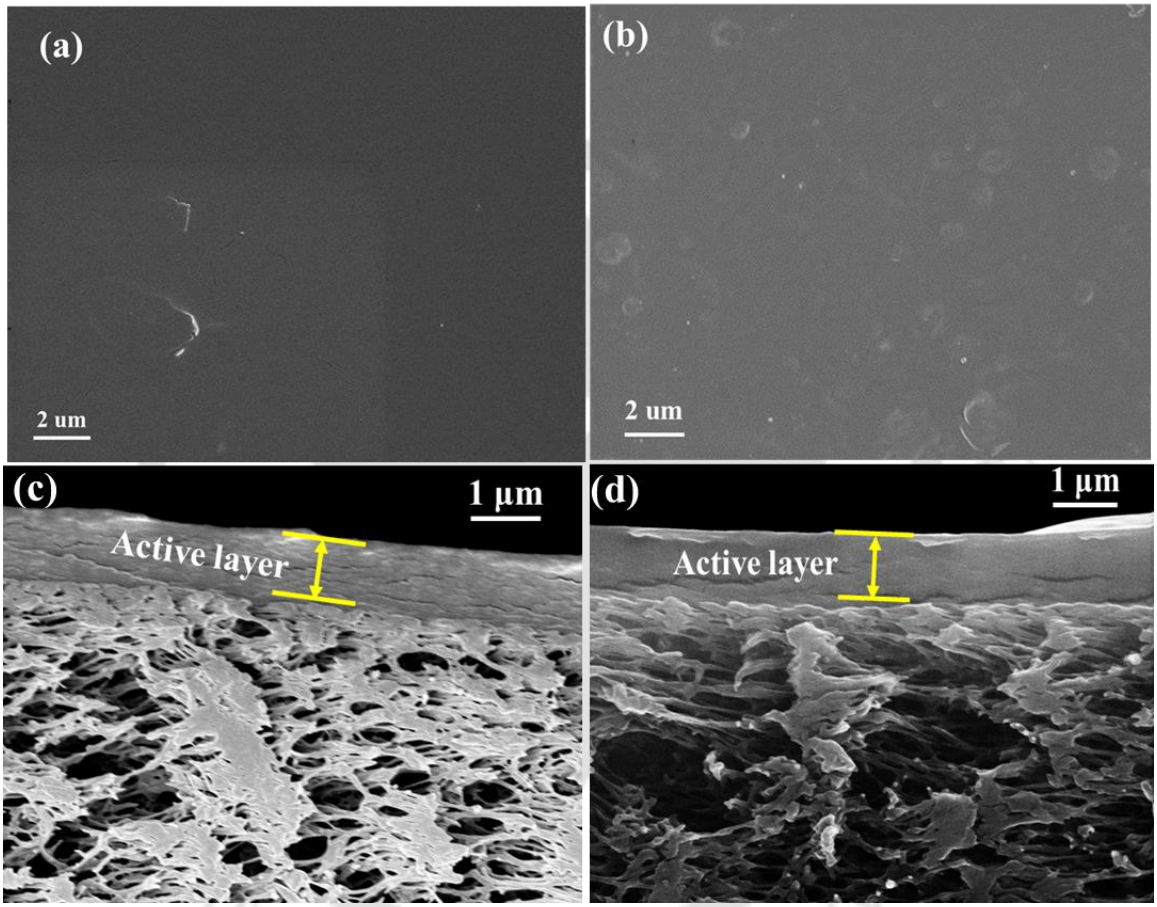

Figure 6.3 FESEM top surface view of the membranes with PES support (a) CS/GNP, (b) CS/SF/GNP and cross-sectional view (c) CS/GNP, and (d) CS/SF/GNP.

Similarly, AFM images (Figure 6.4) suggested the formation of complete mixing of GNP with the matrix for dense active layer of the membranes. However, the surface roughness calculated from AFM images indicated increased roughness of CS/SF/GNP (7.03 nm) membrane than the CS/GNP (2.8 nm) membrane compared to pure CS (0.99 nm).

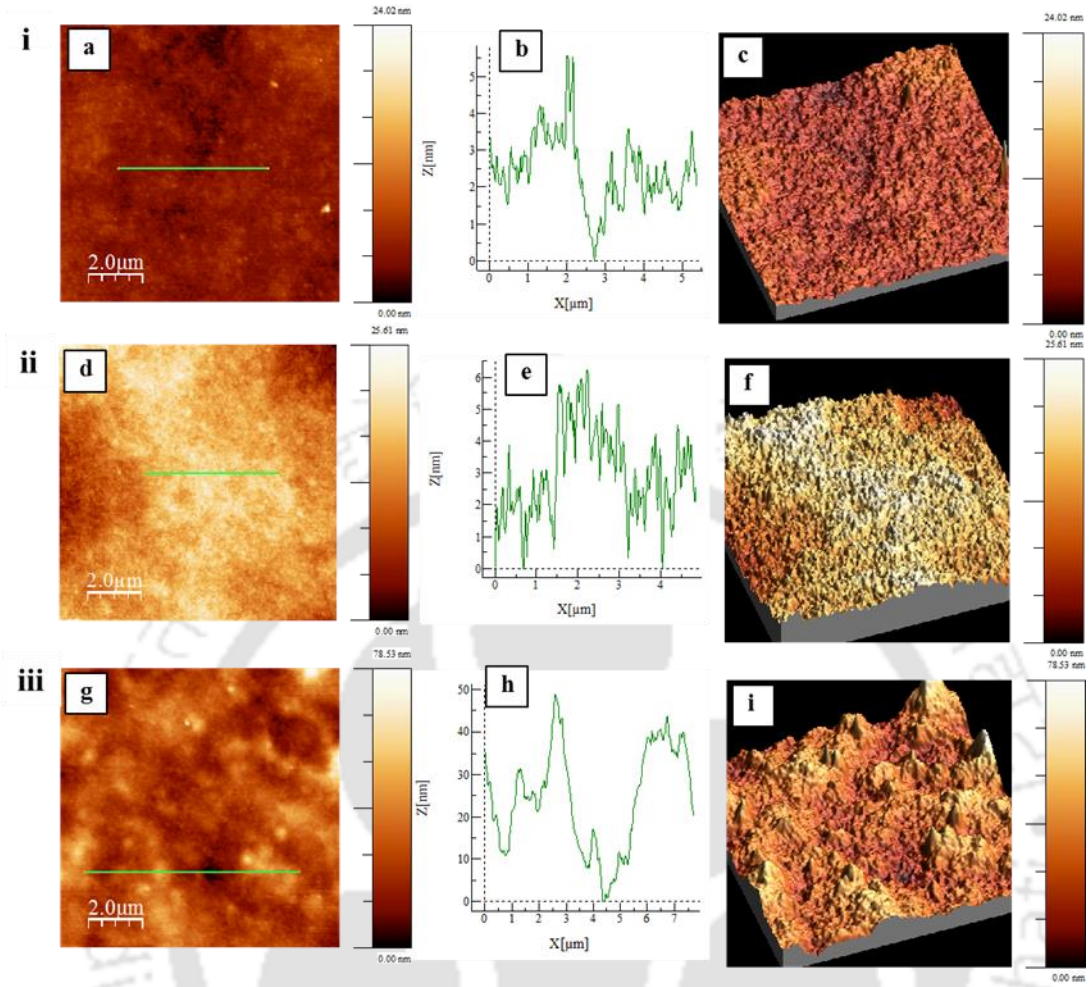

Figure 6.4 AFM topography of (i) pure CS, (ii) CS/GNP, and (iii) CS/SF/GNP membranes with their respective 2-D images (a,d,g), height profiling (b,e,h) and 3-D images (c,f,i).

6.3.3 DMA analysis

The storage modulus with respect to temperature of the prepared membranes are revealed in Figure 6.5. The increase in storage modulus of CS and CS/GNP with temperature followed a linear trend indicating increase in stiffness of the membrane with ascending temperature. However, the (CS/SF/GNP) membrane displayed exponential increment of the storage modulus up to 110 °C and then a decline due to thermal chain mobility [150]. With the inclusion of the SF biopolymer, the mechanical strength and stiffness of the prepared membrane increase owing to the robustness of the natural biopolymer. However, with increase

in temperature, the reaction rate is enhanced and enriched due to the inherent amines existing in SF.

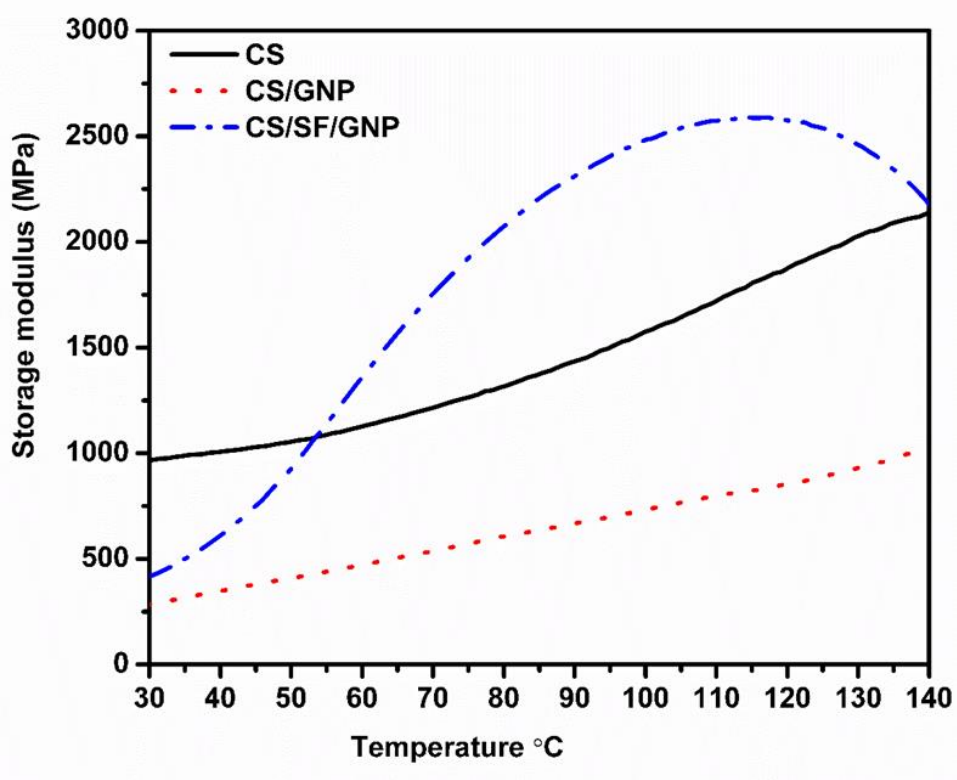

Figure 6.5 DMA analysis of CS, CS/GNP and CS/SF/GNP membranes.

6.3.4 Water swelling test

Water molecules present in the swelled polymer matrix, supports the flexibility of the membrane by plasticization effect that counteracts the overall mass transfer resistance. This, however encourages the channeling of inert gas molecules (N_2, H_2) and degrades the CO_2/gas selectivity. The swelling vs relative humidity (RH) profile (Figure 6.6) of all the membranes depicted two exponential phases as explained in Chapter 3. The first exponential swelling that occurred up to 80 % RH, is associated with the water and polymer chain mixing and induces chain relaxation [94]. The second exponential swelling that trailed at RH (> 80 %), is termed as critical RH and depends on water-polymer affinity. Membranes are to be operated below

critical RH (< 80 %), as above critical RH, escalated polymer free volume allow inert gas molecules to pass that decreases the selectivity. The high swelling of CS (Figure 6.6) is owing to the hydrophilic nature of CS due to presence of OH and NH_2 groups in its structure. The comparatively decreased swelling behaviour of CS/GNP and CS/SF/GNP can be attributed to the reduced support pore clogging in the presence of GNP as well as hydrophobic nature of SF [168]. The swelling (%) of the membranes at 100 % humidity followed the trend CS (163 %) > CS/GNP (71 %) > CS/SF/GNP (61 %).

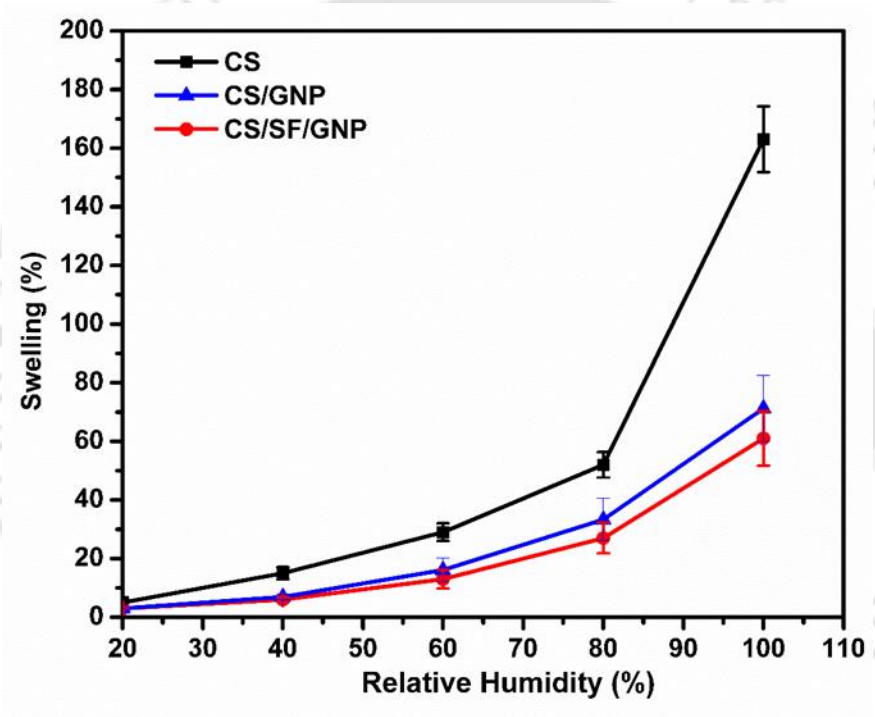

Figure 6.6 Swelling (%) vs relative humidity (%) of the CS, CS/GNP and CS/SF/GNP.

6.3.5 Effects of water flow rate on CO_2 separation

The effect of sweep water flow rate on the CO_2 flux, CO_2 permeance and CO_2/N_2 selectivity were studied in the range of 0.01-0.07 ml/min at temperature of 90 °C and feed absolute pressure of 2 bar (Figure 6.7). The conditions were adopted following our previous gas permeation study conducted using pristine chitosan (CS) membrane as discussed in previous

Chapter 2. Initially at 0.01 ml/min, the CO_2 flux of CS/GNP and CS/SF/GNP membrane was 300 × 10^{-6} cm^3(STP)/cm^2s and 1109 × 10^{-6} cm^3(STP)/cm^2s, respectively (Figure 6.7a-b).

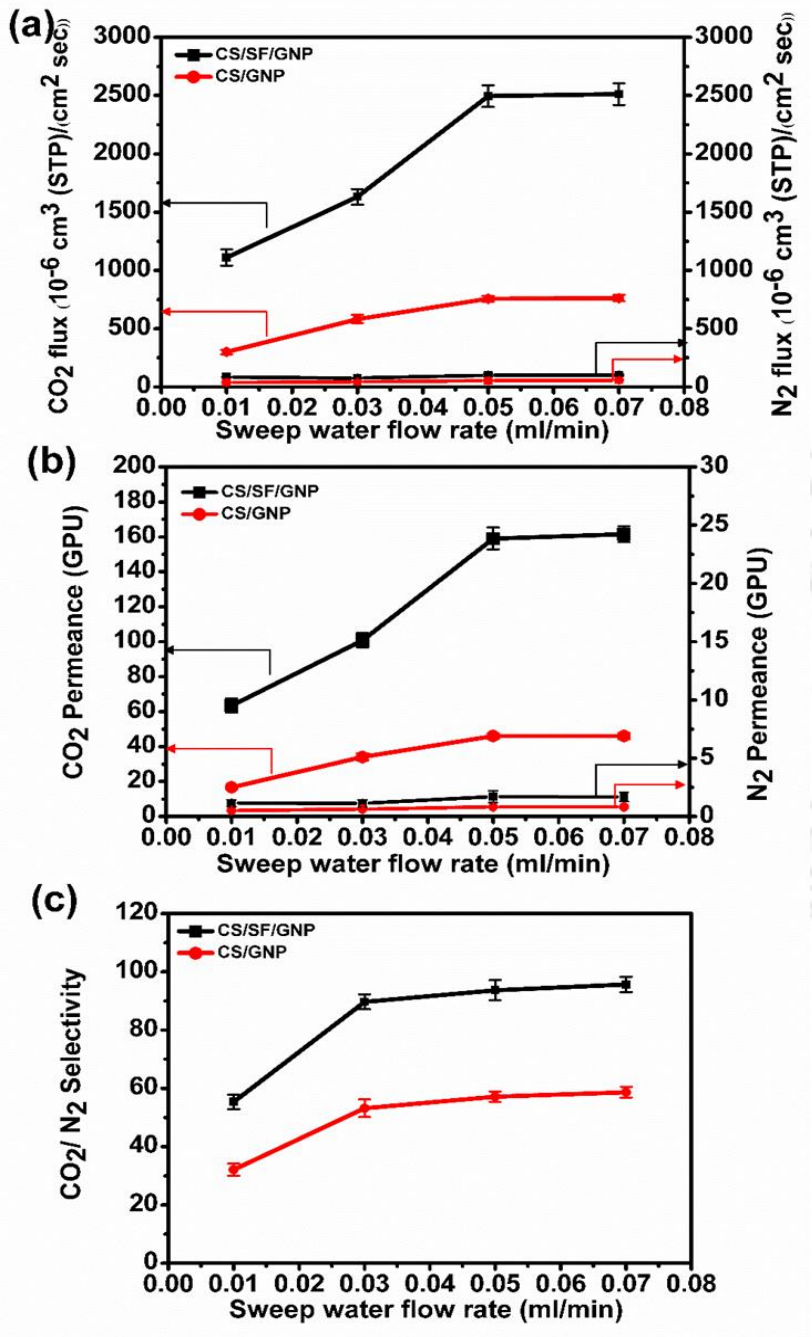

Figure 6.7 Effect of sweep water flow rate on (a) CO_2 flux, (b) CO_2 permeance and (c) CO_2/N_2 selectivity of CS/GNP and CS/SF/GNP membranes at temperature of 90 °C, feed water flow rate = 0.03 ml/min and absolute pressure = 2/1.21 bar (feed/sweep).

This was amplified ~ 152 % and ~ 125 % to 757 and 2495 [× 10^{-6} cm^3(STP)/cm^2s], respectively at 0.05 ml/min sweep water flow rate. The CO_2 permeance and CO_2/N_2 selectivity (Figure 6.7c) improved and saturated around 0.05 ml/min sweep water flow rate for both CS/GNP and CS/SF/GNP membranes. This is a signature behavior of membranes following facilitated transport mechanism. All the separation performance parameters (flux, selectivity and permeance) amplified when the sweep water flow rate exceeded the feed water flow rate. This can be attributed to the water retention capability of the membranes that aids in the formation of extra CO_2–carrier complex when the sweep water flow rate is higher. High swelling increases the free volume by enhancing the inter-chain space of the polymer. Water inside the membrane can be present in different states such as free water, freezable bound water and non-freezable bound water [107]. Gas solubility and diffusivity properties in free water are similar to that in bulk water. But freezable bound water interacts poorly with polymers. In the third case, non-freezable bound water forms hydrogen bonding with polymer matrix which augments better gas solubility as compared to the free water [217]. At 0.05 ml/min, CS/SF/GNP displayed exceptionally fine CO_2 flux of 2495 × 10^{-6} cm^3(STP)/cm^2s and CO_2 permeance of 159 GPU as compared to CS [227 × 10^{-6} cm^3(STP)/cm^2s and 12.5 GPU] in the work included in Chapter 2 and CS/SF [1462 × 10^{-6} cm^3(STP)/cm^2s and 140 GPU)] from the study conducted in Chapter 4. Presence of water augments membrane flexibility and CO_2 reacts reversibly with amines in the active layers forming HCO_3^- that diffuses rapidly across membrane and finally dissociates in the permeate side, releasing the CO_2. The carrier amines existed in much higher concentration in the CS/SF/GNP membrane owing to the properties of silk. Additionally, the CO_2 solubility in water being higher than N_2 or H_2 gases, CO_2 permeation can take place by following the relaxed solution-diffusion mechanism [90]. Moreover, nanoparticles have high surface to volume ratio. Graphene has a large specific surface area [209]. Incorporation of graphene might alter the free volume inside the polymer chains ensuing in increased surface area that boosts the diffusivity of gases [56].

6.3.6 Effects of temperature on CO_2 separation

The CO_2 separation performance in the temperature range from 60 to 120 °C has been studied for both the membranes at water flow rate 0.03/0.05 (feed/sweep) and feed absolute pressure of 2 bar as shown in Figure 6.8. The CS/GNP and CS/SF/GNP membranes exhibited optimum

CO_2 flux and CO_2 permeance at temperatures < 90 °C. In the presence of moisture, as the temperature (60-90 °C) was increased, the rate of reaction between amine and CO_2 is accelerated that promotes CO_2 flux and permeance. The CO_2 flux and permeance are dominated by solution-diffusion mechanism which is predominant at low temperature whereas facilitated transport mechanism principally is prevalent at high temperature. The CS/GNP and CS/SF/GNP membranes demonstrated improved CO_2 flux (Figure 6.8a) of 757 $\times 10^{-6}$ cm^3 (STP)/cm^2s and 2495 $\times 10^{-6}$ cm^3(STP)/cm^2s which are ~ 173 % and ~ 800 % higher as compared to that of CS at 90 °C. However, superior performance of CO_2 flux and permeance (Figure 6.8b) of ~ 229 % and ~ 245 % by CS/SF/GNP as compared to CS/GNP can be attributed to the presence of high amine carriers in silk fibroin as compared to just single amine group per CS unit that facilitates CO_2 transport. Beyond 90 °C, both CO_2 flux and permeance of the membranes declined drastically and reached the minimum as temperature touched 120 °C. The CO_2/N_2 selectivity (Figure 6.8c) revealed an uptrend from 60 °C up to 110 °C for the CS/SF/GNP membrane and up to 90 °C for CS/GNP. This difference in behaviour can be ascribed to the characteristic silk β- sheet and inherent amines that displays tailored performance with interplay of temperature and moisture application [170]. The CO_2/N_2 selectivity of CS/GNP and CS/SF/GNP at 90 °C were 57 and 93, respectively. At high temperature > 90 °C, the depletion of moisture content restricts the membrane flexibility and transition of gas molecules. The stiffness of the membrane at high temperature was also evident from the DMA study (Figure 6.5) as discussed above as well as from the degrading behaviour in N_2 permeance and flux. The descent in the N_2 flux and permeance with a rise in temperature can be attributed to the non-reactive nature of the N_2 molecule that follows only solution-diffusion mechanism. The substantial decline in N_2 permeance as compared to CO_2 permeance enhanced the selectivity factor for CS/SF/GNP. This performance behaviour of CO_2 permeation suggested that the impact of temperature on CO_2 facilitated transport mechanism is greater as compared to that of CO_2 concentration and pressure.

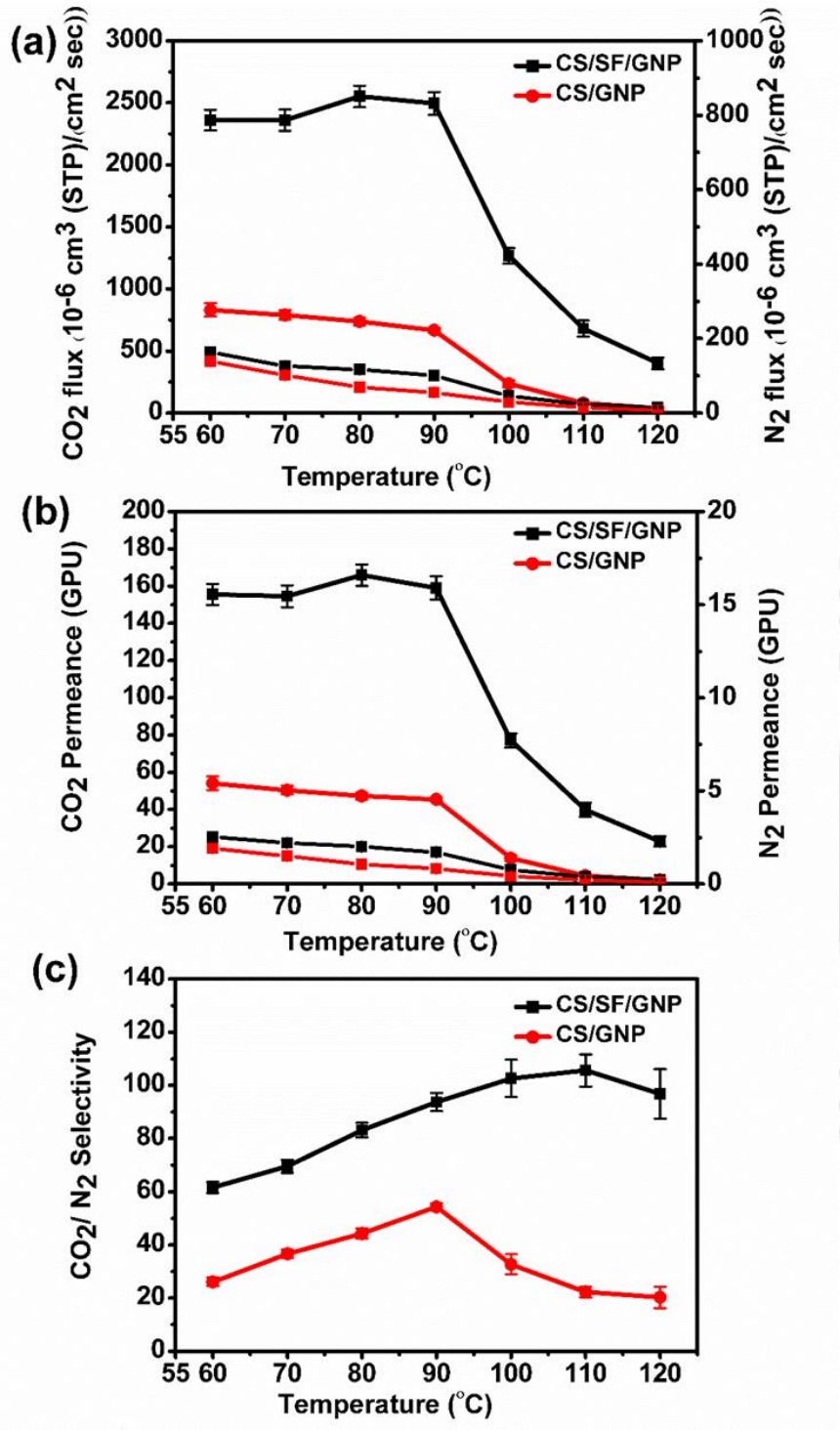

Figure 6.8 Effect of temperature on (a) CO_2 flux, (b) CO_2 permeance, and (c) CO_2/N_2 selectivity of CS/GNP and CS/SF/GNP membranes at water flow rate = 0.03/0.05 ml/min (feed/sweep), feed absolute pressure = 2 bar and sweep absolute pressure = 1.21 bar.

6.3.7 Effects of pressure on CO_2 separation

With increase in feed pressure from 2 to 5.91 bar, the CO_2 flux of CS/GNP and CS/SF/GNP membranes surged from 757 × 10^{-6} cm^3(STP)/cm^2s to 1341 × 10^{-6} cm^3(STP)/cm^2s and 2495 × 10^{-6} cm^3(STP)/cm^2s to 3652 × 10^{-6} cm^3(STP)/cm^2s, respectively (Figure 6.9a). After 3.7 bar, the changes in CO_2 flux were trivial in both the membranes due to carrier saturation at high CO_2 partial pressure. This trait at high pressure is a characteristic of membranes with carriers. However, the maximum CO_2 flux was perceived at 5.91 bar with CS/SF/GNP demonstrating ~ 172 % and ~ 53 % higher than that of CS/GNP and CS/SF, respectively. At high CO_2 partial pressure, when facilitated transport becomes limited due to carrier saturation, solution-diffusion mechanism contributes to the surge in flux. This suggests the ineffectiveness of facilitated transport mechanism at high CO_2 partial pressure. The CO_2 permeance of CS/GNP and CS/SF/GNP at 2 bar were ~ 45 GPU and ~ 159 GPU and decreased to ~ 26 and ~ 71 GPU, respectively when the pressure reached to 5.91 bar (Figure 6.9b). Though the inherent carrier amines served in high facilitated transport and an elevated CO_2 permeance for the CS/SF/GNP membrane, the downslope in CO_2 permeance was steep at high pressure. But for CS/GNP membrane the CO_2 permeance decay was trivial as the limited amount of amines in CS made the membrane rely on solution-diffusion mechanism. Additionally, high pressure leads to membrane compression that diminishes the water holding capacity of the membranes and has a negative effect on gas permeation. Both the above phenomena confines the polymer chain mobility and free volume space. Similarly, the overall selectivity (Figure 6.9c) of CS/GNP and CS/SF/GNP decreased to ~ 53 % (57 to 26) and ~ 42 % (93 to 54), respectively as pressure reached from 2 bar to 5.91 bar.

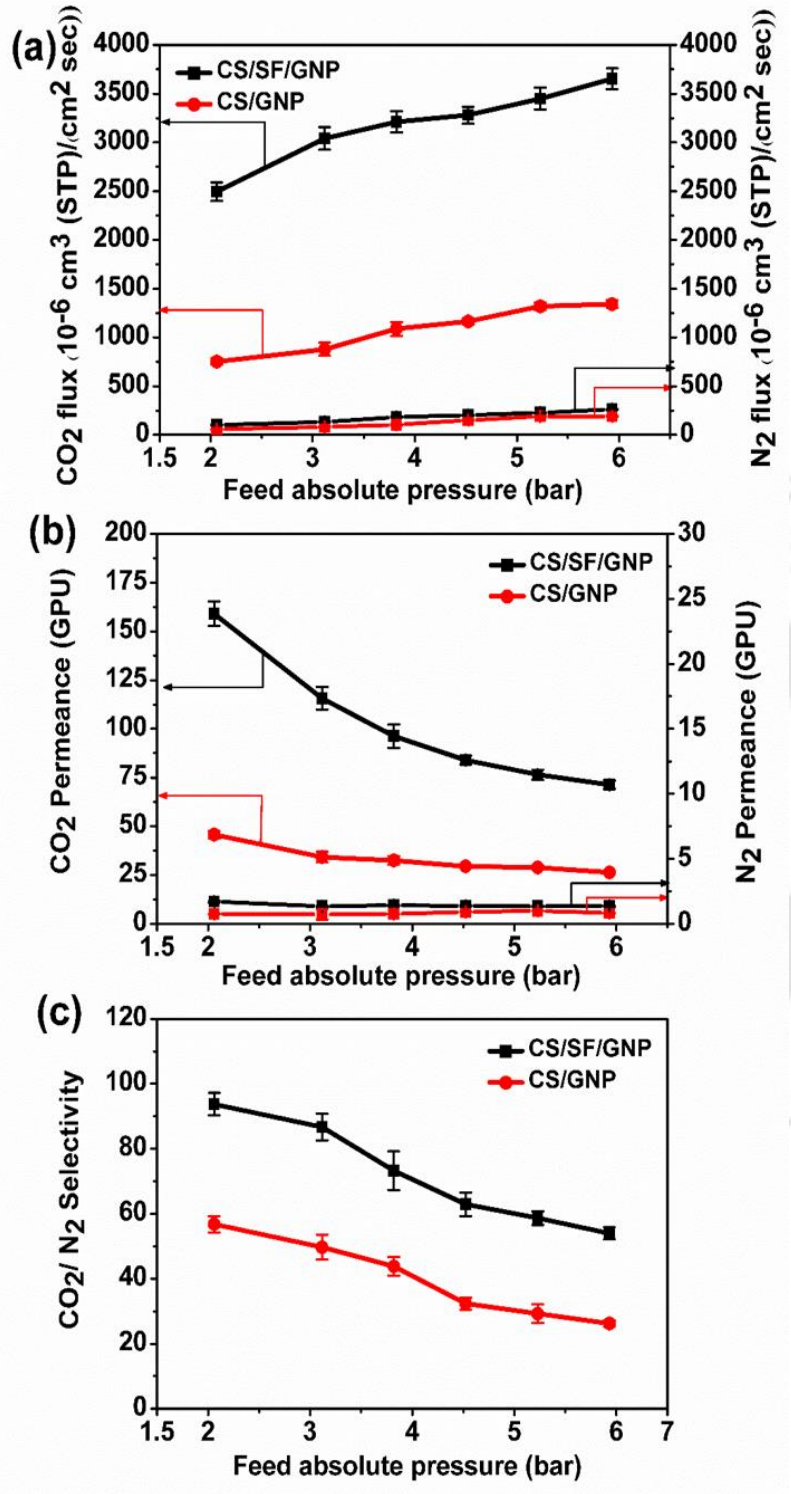

Figure 6.9 Effect of absolute feed pressure on (a) CO_2 flux, (b) CO_2 permeance and (c) CO_2/N_2 selectivity of CS/GNP and CS/SF/GNP membranes, at water flow rate = 0.03/0.05 ml/min (feed/sweep), at temperature 90 °C and sweep absolute pressure = 1.21 bar.

6.3.8 Ternary gas (CO_2, N_2 and H_2) mixture separation

6.3.8.1 Effects of temperature and pressure on CO_2 separation performance by membrane

The gas permeation study using a ternary gas mixture (CO_2, N_2 and H_2) was further carried out using CS/SF/GNP membrane, considering its superior performance than CS/GNP in the temperature range from 60-120 °C [Figure 6.10(i) a-b]. The CO_2 flux and permeance trends were similar to that as observed in case of binary gas. However, the CO_2 flux and permeance were marginally inferior to that of the binary gas, owing to the competitive sorption among the gas molecules. The CO_2 flux and CO_2 permeance of CS/SF/GNP using ternary gas mixture were found as 1861×10^{-6} cm^3 (STP)/cm^2s and 126 GPU, respectively. Initially at 60 °C, the CO_2 permeance was 112 GPU and reached to 126 GPU at 90 °C and finally, the performance retarded reaching 19 GPU at 120 °C.

The CO_2/N_2 and CO_2/H_2 selectivity [Figure 6.10(i)-b] enhanced with increase in the temperature. The CO_2/N_2 and CO_2/H_2 selectivity at 60 °C were 76 and 35 and reached to 52 and 104 at 90 °C, respectively. The selectivity for CO_2/H_2 is ~ 50 % inferior than that for CO_2/N_2. This can be justified by their kinetic diameter [H_2 (2.8 Å) and N_2 (3.64 Å)] variation [190]. Although, the CO_2/H_2 selectivity is lower than CO_2/N_2 selectivity, the membrane showed decent CO_2/H_2 selectivity which could be used for hydrogen purification for fuel cell application.

The CO_2 flux increased constantly up to ~ 5.91 bar feed absolute pressure and obtained a steady value as carrier saturated whereas CO_2 permeance followed an opposite trend [Figure 6.10(ii)-a]. This can be explained by the fact that the increase in CO_2 flux and the feed absolute pressure are not proportional. When the feed absolute pressure was changed from 2 to 5.91 bar (~ 196 %), the CO_2 flux improved merely 34 % [1891 to 2535×10^{-6} cm^3(STP)/cm^2s]. The overall CO_2 permeance dropped with rise in pressure. The CO_2/N_2 selectivity reduced ~ 51 %, while CO_2/H_2 selectivity [Figure 6.10(ii)-b] declined from 52 to 24 as pressure was increased from 2 to 5.91 bar. The observed downtrend can be assigned to the diminishing facilitated transport at high pressure and transport of N_2 and H_2 molecules across the membrane.

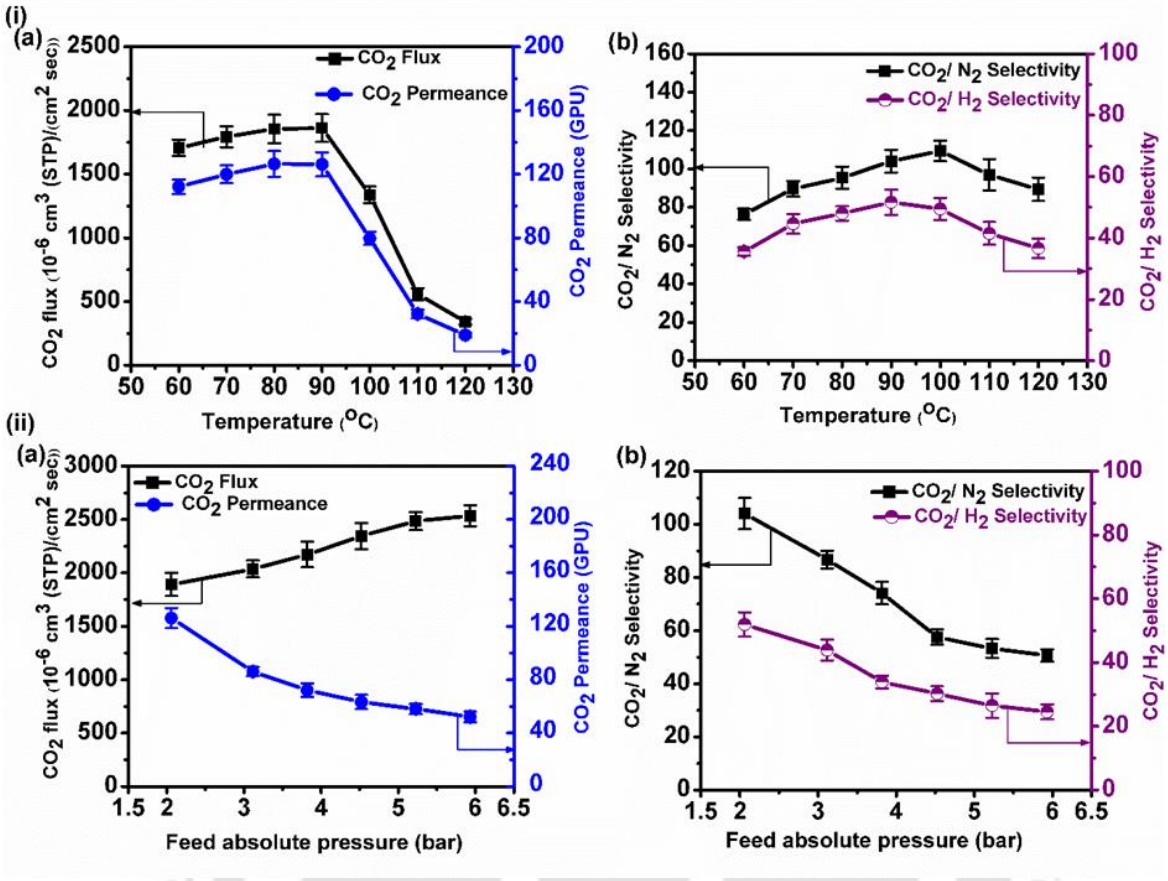

Figure 6.10 Effect on CS/SF/GNP membrane (i) temperature effect (a) CO_2 flux and CO_2 permeance, (b) CO_2/N_2 and CO_2/H_2 selectivity at water flow rate = 0.03/0.05 ml/min (feed/sweep) and absolute pressure = 2/1.21 bar (feed/sweep) and (ii) feed absolute pressure effect (a) CO_2 flux and CO_2 permeance, (b) CO_2/N_2 and CO_2/H_2 selectivity at 90 °C with water flow rate = 0.03/0.05 ml/min.

6.3.9 TGA isotherm

The TGA isotherm at temperatures (°C) 100, 120 and 150 of the CS/SF/GNP membrane (Figure 6.11) specified its thermal stability up to 150 °C even in absence of any crosslinking within the membrane. The 40 min linear isotherms at 100, 120 and 150 °C indicated negligible weight loss during that period.

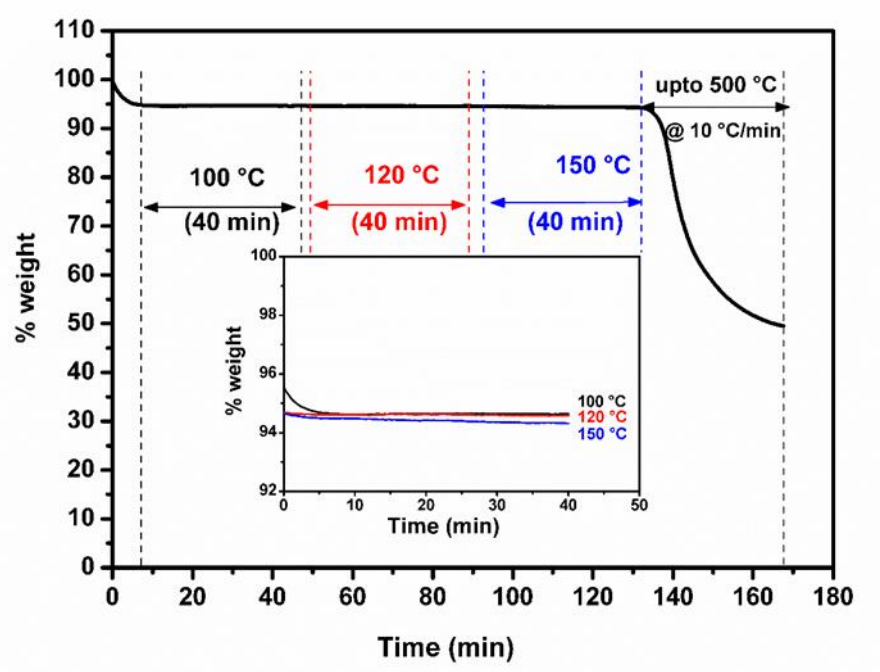

Figure 6.11 TGA profile of CS/SF/GNP at different isotherm (inset TGA isotherm at 100 °C, 120 °C, and 150 °C for 40 min).

6.3.10 XPS analysis

The XPS analysis of the CS/SF/GNP membrane was performed at temperatures (°C) 24, 30, 60, 90 and 120 to validate the quantitative and qualitative nature of the chemical state of the membrane surface. The peak observed at 284.7 eV represents the carbon-carbon (C-C) or carbon- hydrogen (C-H) bonds [218]. The peak detected at 286.6 eV can be assigned to hydroxyl groups (C-OH) and carbon bound to nitrogen (C-N) whereas the peak witnessed at 287.7 eV can be attributed to the bonds carboxylate (O=C-OH) and amide carbon (N-C=O) existing in chitosan. The amide and/or amines present in CS and SF resulted in the major N 1s peak at ~ 400 eV observed at all the temperatures whereas, the oxygen in the polymer backbone contributed to the major O 1s peak at ~ 533 eV.

No shift in the peak spectrum was evident in the XPS data profile (Figure 6.12) of the CS/SF/GNP membrane (i) survey scan (a) at 24 °C and (b) at different temperatures; (ii) narrow scan range for (a) C 1s, (b) N 1s, (c) O 1s at different temperatures, and (d) de-convoluted peak C 1s, at 24 °C. This demonstrated the absence of any chemical state change

of the polymer during heating, which denoted the potential of the CS/SF/GNP membrane for gas separation even at high temperature ~120 °C.

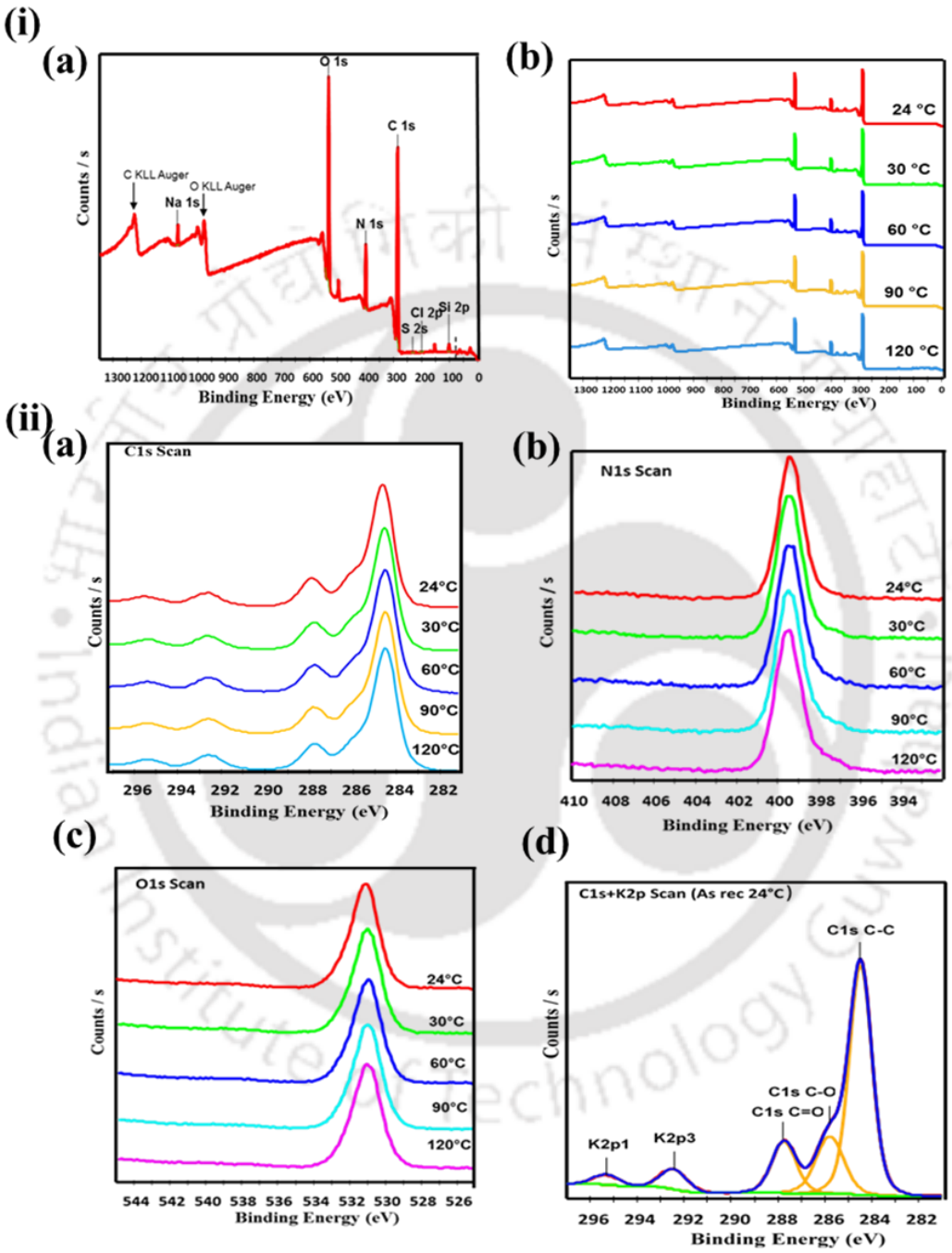

Figure 6.12 The XPS data profile of the CS/SF/GNP membrane (i) survey scan (a) at 24 °C and (b) at different temperatures; (ii) narrow scan range for (a) C 1s, (b) N 1s, (c) O 1s at different temperatures, and (d) de-convoluted peak C 1s, at 24 °C.

However, quantifying the relative concentrations of the elements (Table 6.1) present in the samples at the different study temperatures revealed minor variation at the atomic level. The atomic concentration variation of C, N and O at 24 °C as compared to that at 120 °C, can be ascertained to the loss of water at 120 °C. The addition of KOH during membrane preparation contributed to the element K. The negligible contamination during handling might be accounted for the insignificant Si and Ca content [219]. The acquired data suggested that the surface chemistry of CS/SF/GNP membrane remained consistent at all temperatures.

Table 6.1 Surface elemental concentration (%) analysis of CS/SF/GNP membrane at temperatures (°C) 24, 30, 60, 90 and 120.

Element	24 °C	30 °C	60 °C	90 °C	120 °C
C	69.64	69.30	69.38	69.45	69.43
O	17.68	17.54	17.31	17.16	17.13
N	9.73	9.93	9.94	10.05	10.09
K	1.59	1.82	1.87	1.80	1.89
Si	0.76	0.77	0.80	0.82	0.76
Ca	0.61	0.63	0.69	0.72	0.70

The data obtained in this study has been comprehensively compared with the high quality-recent researches in MMMs for gas separation and presented in

Table **6.2**. Taking into account both CO_2 permeance and selectivity, CS/SF/GNP membrane has outperformed the rest with ~ 1 μm thickness and at 90 °C. With the simplicity of membrane preparation and outstanding performance, the developed membrane can be scaled up for commercial applications.

Table 6.2 Comparative account on the performance of various mixed matrix membranes.

Membrane	**Thickness (µm)**	**T (°C)**	**CO_2 permeance (GPU)**	**Selectivity (CO_2/N_2)**	**Ref.**
GO-[BMIM][BF4] ionic liquid	1.05	20	68.5	382	[202]
Cobalt (Co)- zeolite Y - Matrimid®	0.38	35	18.96	111 (CO_2/CH_4)	[198]
Porous rGO-mHNTs Pebex1657	54	-	2.3	118	[54]
GO-ZIF 8-polyimide	-	25	146 (Barrer)	41 (CO_2/CH_4)	[55]
GO-PZ hollow fiber membranes	0.02	80	1020	680	[204]
PVAm-CS- HPEI-GO.	2.25	25	36	107	[110]
EC/ZIF-8@GO	50	25	4.1	33	[200]
CS/SF/GNP	1	90	159	93	Present work

6.3.11 Robeson upper bound

Robeson upper bound (2008) that relates the permeability with selectivity can serve as the yardstick for membrane performance evaluation. The CO_2 separation performance of the CS/SF/GNP in the temperature range 60-120 °C lied inline, or above the Robeson upper bound for the binary gas mixture (Figure 6.13). Similar suitable performance was also observed when the ternary gas mixture was used as depicted in Figure 6.14(a)-(b).

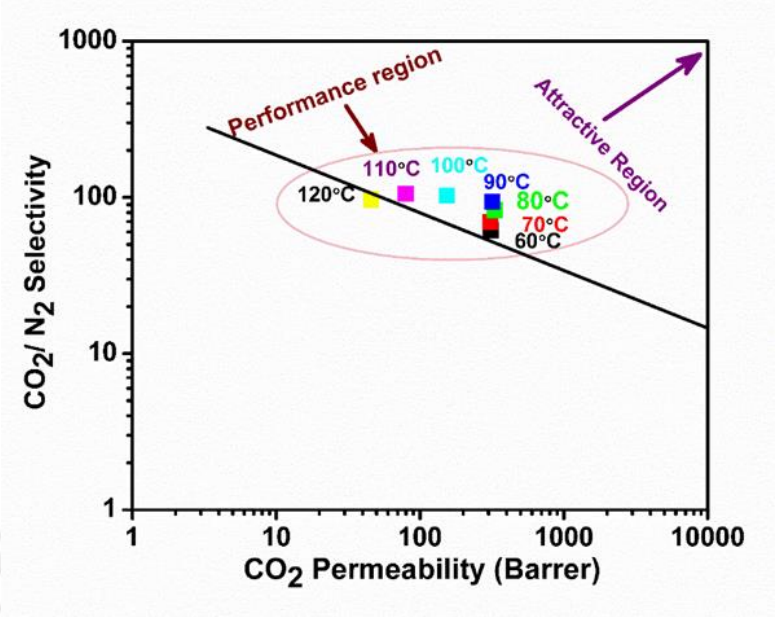

Figure 6.13 Robeson upper bound plot of CS/SF/GNP membrane at different temperature for the binary gas mixture.

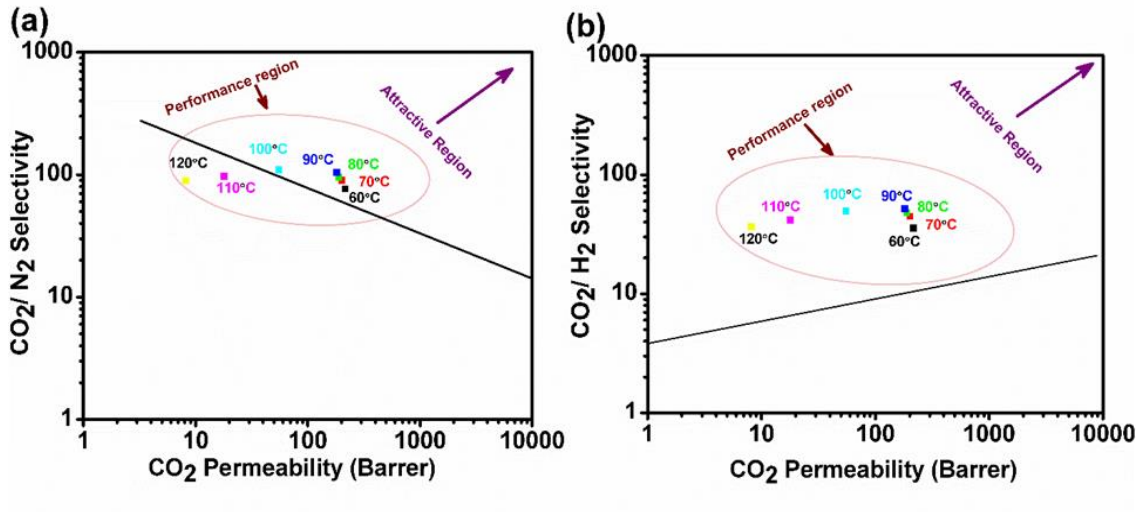

Figure 6.14 The upper bound plots for ternary gas separation (a) CO_2/N_2 and (b) CO_2/H_2 at different temperatures, for CS/SF/GNP membrane with absolute pressure 2/1.21 bar (feed/sweep).

6.4 Conclusions

This study reports the development of a novel mixed matrix membrane CS/SF/GNP with chitosan, silk and graphene nanoparticles and its application for CO_2 separation. The work also demonstrated an unprecedented mechanism of counteracting the support pore blockage during gas separation application under humid condition by incorporation of graphene nanoparticles (GNP). The membrane preparation is quite simple and can be scaled up for commercial applications. A balanced swelling needs to be poised to attain the optimal CO_2 permeance with selectivity. The inclusion of GNP drastically improved the CO_2 permeance performance in the initial 12 h. This provided an exceptional approach to enhance CO_2 separation performance by regulating the active layer swelling and support pore filling phenomenon, frequently observed during moisture and pressure application in gas permeation studies. The increased roughness of the membrane provided a high surface area for gas infusion. The collective effect of the carrier amines from SF that aided in facilitated transport and the assistance of GNP in solution-diffusion mechanism, enriched the performance factors of CS/SF/GNP matrix. The CO_2 flux of CS/SF/GNP membrane was ~ 800 % greater than that of CS membrane at 90 °C (in case of binary gas), and also established the superior effect of temperature on membrane separation performance. The improved CO_2 flux and CO_2 permeance of CS/SF/GNP using ternary gas mixture suggested that CS/SF/GNP membrane can be utilized to separate CO_2 from CO_2/H_2 gas mixture which can be used in fuel cell application. The thermal and chemical stability based on TGA and XPS analyses along with its superior gas permeation properties suggest that the prepared membranes can be used for flue gas as well as syngas purification.

CHAPTER 7

Overall Conclusions and Recommendations for Future Work

CHAPTER 7

Overall Conclusions and Recommendation for Future Work

This chapter draws appropriate conclusions based on the investigations carried out in the present study. This chapter also provides some useful recommendations for future research in the relevant field.

7.1 Major conclusions

The major conclusions of the thesis are summarized below

- The detailed gas permeation study of pure CS was performed at different temperatures, pressures and sweep water flow rates and operating conditions were optimized based on CO_2 separation performance. TEPA was blended with CS and composition of 30 wt % TEPA was found to be optimum based on gas permeation and the characterization studies using TGA, AFM, FTIR, XRD, and FESEM. The permeance of CS improved from 12.5 to 24.7 GPU after addition of 30 wt % TEPA at 90 °C, having water flow rate of 0.03/0.05 ml/min (feed/sweep) and at an absolute feed pressure of 2 bar. As compared CS, CS70 documented ~ 97 % and ~ 48 % higher permeance and CO_2/N_2 selectivity, respectively.

- The CS-PAA active layers were formed successfully on the top of the PES support. FESEM and AFM analysis revealed the formation of the rough surface of the blended membranes that aided in increasing the surface area for reaction. The optimized concentration of 30 wt % in chitosan matrix (PAA30) outperformed the CO_2 permeance and CO_2/N_2 selectivity of pure chitosan by ~ 3 fold and ~ 3.81 fold, respectively at 90 °C. Amines did not leach out from the PAA30 membrane during the CO_2 separation study as indicated by Kaiser test.

- Two versatile biopolymers CS and SF were blended in varying concentrations to form CS-SF membranes. SF45 (45 wt % SF) displayed optimum performance with remarkable ~ 11 and ~ 2 fold increments in CO_2 permeance and selectivity, respectively as compared to

CS membrane for binary gas mixture. The SF45 membrane was also used for ternary gas mixture ($CO_2/N_2/H_2$) and revealed significant CO_2/N_2 (93) and CO_2/H_2 (60) selectivity at 90 °C. The β-sheet which imparts crystallinity to the SF, can be modulated to the presence of temperature and moisture. This opens up scope to tune the membrane performance by changing temperature and water flow rates. The exceptional CO_2 separation performance stability up to 30 days and thermal stability confer the suitability of SF45 for CO_2 separation.

- The CS-SC (M1), CS-Na_2CO_3 (M2) and CS-SC-Na_2CO_3 (M3) membranes were prepared and CO_2 separation performance study at different temperatures, pressures and water flow rates were studied using binary and ternary gas mixture. The DMA analysis indicated the membrane stiffness with rise in temperature for all the membranes. The XPS depth profiling of the M3 membrane showed a homogeneous distribution of the elements (C, O, and N) along the various layers. The thermal stability and surface elemental analyses were done using XPS analysis at temperatures (°C) 24, 30, 60, 90 and 120 revealed that the membrane is stable under the study temperatures. Since Na_2CO_3 acts as a mobile carrier and SC as a fixed carrier, the CO_2 permeance of M2 is higher than the M1 and M3 membranes but M3 outperformed the M1 and M2 membranes in terms of CO_2/N_2 selectivity.

- A novel mixed matrix membrane CS/SF/GNP with chitosan, silk and graphene nanoparticles was developed. The inclusion of GNP drastically improved the CO_2 permeance performance in the initial 12 h. This provided an unprecedented approach to enhance CO_2 separation performance by regulating the active layer swelling and support pore filling phenomenon, frequently observed during moisture and pressure application in gas permeation studies. The CS/SF/GNP membrane was used for CO_2 separation using binary as well as ternary gas mixtures.

- This study was undertaken to improve the CO_2 separation performance using chitosan membrane by employing facilitated transport mechanism. To achieve this, we undertook two approaches. The first approach was using synthetic amines such as TEPA and PAA

Table 7.1 A comparative account on the CO_2 separation performance by the membranes conducted under this research study at 90 °C and absolute pressure = 2/1.21 bar (feed/sweep) having water flow rate of 0.03/0.05 ml/min (feed/sweep)**.**

Membrane Composition (wt %)	Membrane code	CO_2 permeance (GPU)	CO_2/N_2 selectivity
100 % CS	CS	12.5 ± 0.67	54 ± 2
70 % CS + 30 % TEPA	CS70	24.7 ± 0.52	80 ± 4
70 % CS + 30 % PAA	PAA30	39.0 ± 1.95	260 ± 9
55 % CS + 45 % SF	SF45	140.0 ± 2.07	103 ± 4
70 % CS + 15 % SC+ 15 % Na_2CO_3	M3	112.3 ± 2.85	73 ± 3
CS 54.5 % + SF 45 % + 0.5 % GNP	CS/SF/GNP	159.1 ± 6.24	93 ± 4

and the latter by engaging the fixed amines existent in natural biopolymers of silk fibroin and sericin. TEPA and PAA addition increased the carrier amines that facilitated transport of CO_2 and reasonable performance was obtained as observed in Table 7.1. However, after blending of silk fibroin, the prepared novel CS/SF membrane outperformed the rest in collective terms of selectivity, permeance and carrier stability, amongst all the membranes under study. An apt balance was a strike between the permeance and selectivity performance. This was achieved owing to the moisture and temperature responsive properties of the versatile silk fibroin biopolymer. The stability of the membrane was enhanced owing to the non-leaching behavior of the natural amines and mechanical stability of the silk fibroin. Incorporation of graphene nanoparticles enabled the newly fabricated nanocomposite membrane to curtail the support pore blocking phenomenon during gas permeation test. Additionally, we embarked on to explore sericin (a waste by product of silk fibroin extraction) for gas permeation test. The performance was quite encouraging. SC solution mixed with Na_2CO_3 was utilized in order to adopt an easy and less time consuming process. This will enable utilization of the total raw material (silk cocoons) and also Na_2CO_3 used during silk fibroin extraction. Overall, it can be concluded that the work undertaken here forwards an innovative route for utilization of the

test biopolymers for CO_2 separation with an effort to convert waste to wealth along with positive impact on energy and environment.

7.2 Recommendations for future research

- In the present investigation, the gas permeation study for the test membranes was performed using either binary or ternary gas mixture. Apart from CO_2, N_2, and H_2, the industrial flue gas also contains SOx and NOx as impurities. The performance of the prepared membranes can be further evaluated with SOx and NOx in the feed gas.
- Economic cost assessment of the prepared membranes can be appraised to endorse their applications for commercial usages in industries.
- The PAA may be replaced with polyvinylamine (PVAm) as it has the highest amino content among all the polyamines.
- Preparation of thinner membranes (< 3 μm) may be considered to achieve a high CO_2 permeance of more than 800 GPU as it is needed for CO_2 capture from flue gas for reducing the capture cost.
- The incorporation of graphene nanoparticles curtailed the support pore blockage phenomenon during gas permeation test leading to improvement in the overall CO_2 permeation. However, there are further scope of improvement and reformation in this regard by exploring other nanomaterials and fillers.
- CS-SF membrane exhibited unprecedented stability of 30 days when verified for CO_2 permeance. However, the study of the effect of O_2 on the membrane will provide additional information as most of the amines are oxidized in the presence of O_2.
- Ionic liquid has been extensively explored for their suitable application in membrane preparation. Addition of ionic liquid to the test membranes can open up new avenues for boosting up the membrane performance.
- Furthermore, the chitosan itself can be functionally modified to increase its solubility in neutral to basic pH to simplify the process of blending.

References

[1] R. Carapellucci, A. Milazzo, Membrane systems for CO_2 capture and their integration with gas turbine plants, Proc. Inst. Mech. Eng. Part A J. Power Energy. 217 (2003) 505–517.

[2] H. Yang, Z. Xu, M. Fan, R. Gupta, R.B. Slimane, A.E. Bland, I. Wright, Progress in carbon dioxide separation and capture: A review, J. Environ. Sci. 20 (2008) 14–27.

[3] S. Wang, X. Li, H. Wu, Z. Tian, Q. Xin, G. He, D. Peng, S. Chen, Y. Yin, Z. Jiang, M.D. Guiver, Advances in high permeability polymer-based membrane materials for CO_2 separations, Energy Environ. Sci. 9 (2016) 1863–1890.

[4] C.E. Powell, G.G. Qiao, Polymeric CO_2/N_2 gas separation membranes for the capture of carbon dioxide from power plant flue gases, J. Memb. Sci. 279 (2006) 1–49.

[5] P. Shao, M.M. Dal-Cin, M.D. Guiver, A. Kumar, Simulation of membrane-based CO_2 capture in a coal-fired power plant, J. Memb. Sci. 427 (2013) 451–459.

[6] J.K. Adewole, A.L. Ahmad, S. Ismail, C.P. Leo, Current challenges in membrane separation of CO_2 from natural gas: A review, Int. J. Greenh. Gas Control. 17 (2013) 46–65.

[7] A. Arneth, S.P. Harrison, S. Zaehle, K. Tsigaridis, S. Menon, P.J. Bartlein, J. Feichter, A. Korhola, M. Kulmala, D. O'Donnell, G. Schurgers, S. Sorvari, T. Vesala, Terrestrial biogeochemical feedbacks in the climate system, Nat. Geosci. 3 (2010) 525.

[8] F.A. Rahman, M.M.A. Aziz, R. Saidur, W.A.W.A. Bakar, M.. Hainin, R. Putrajaya, N.A. Hassan, Pollution to solution: capture and sequestration of carbon dioxide (CO_2) and its utilization as a renewable energy source for a sustainable future, Renew. Sustain. Energy Rev. 71 (2017) 112–126.

[9] R. Steeneveldt, B. Berger, T.A. Torp, CO_2 capture and storage, Chem. Eng. Res. Des. 84 (2006) 739–763.

[10] S. Mccoy, E. Rubin, An engineering-economic model of pipeline transport of CO_2 with

application to carbon capture and storage, Int. J. Greenh. Gas Control. 2 (2008) 219–229.

[11] C. Stewart, M. A. Hessami, A study of methods of carbon dioxide capture and sequestration-The sustainability of a photosynthetic bioreactor approach, Energy Convers. Manag. 46 (2005) 403–420.

[12] J.D. Figueroa, T. Fout, S. Plasynski, H. McIlvried, R.D. Srivastava, Advances in CO_2 capture technology-The U.S. Department of Energy's Carbon Sequestration Program, Int. J. Greenh. Gas Control. 2 (2008) 9–20.

[13] R.S. Haszeldine, Carbon capture and storage: how green can black be?, Science (80-.). 325 (2009) 1647–1652.

[14] D.Y.C. Leung, G. Caramanna, M.M. Maroto-Valer, An overview of current status of carbon dioxide capture and storage technologies, Renew. Sustain. Energy Rev. 39 (2014) 426–443.

[15] D. Jansen, M. Gazzani, G. Manzolini, E. van Dijk, M. Carbo, Pre-combustion CO_2 capture, Int. J. Greenh. Gas Control. 40 (2015) 167–187.

[16] M. Kanniche, R. Gros-Bonnivard, P. Jaud, J. Valle-Marcos, J.-M. Amann, C. Bouallou, Pre-combustion, post-combustion and oxy-combustion in thermal power plant for CO_2 capture, Appl. Therm. Eng. 30 (2010) 53–62.

[17] J. Li, H. Zhang, Z. Gao, J. Fu, W. Ao, J. Dai, CO_2 Capture with Chemical Looping Combustion of Gaseous Fuels: An Overview, Energy & Fuels. 31 (2017) 3475–3524.

[18] M. Ryden, A. Lyngfelt, Using steam reforming to produce hydrogen with carbon dioxide capture by chemical-looping combustion, Int. J. Hydrogen Energy. 31 (2006) 1271–1283.

[19] H. Fang, L. Haibin, Z. Zengli, Advancements in development of chemical-looping combustion: A review, Int. J. Chem. Eng. 2009 (2009) 1–16.

[20] J.C.M. Pires, F.G. Martins, M.C.M. Alvim-Ferraz, M. Simões, Recent developments on carbon capture and storage: An overview, Chem. Eng. Res. Des. 89 (2011) 1446–

1460.

[21] A.S. Bhown, B.C. Freeman, Analysis and status of post-combustion carbon dioxide capture technologies, Environ. Sci. Technol. 45 (2011) 8624–8632.

[22] A. Yamasaki, An overview of CO_2 mitigation options for global warming-emphasizing CO_2 sequestration options, J. Chem. Eng. Japan. 36 (2003) 361–375.

[23] V. Darde, K. Thomsen, W.J.M. van Well, E.H. Stenby, Chilled ammonia process for CO_2 capture, Int. J. Greenh. Gas Control. 4 (2010) 131–136.

[24] S. Lu, Y. Ma, C. Zhu, S. Shen, The enhancement of CO_2 chemical absorption by K_2CO_3 aqueous solution in the presence of activated carbon particles, Chinese J. Chem. Eng. 15 (2007) 842–846.

[25] Y.E. Kim, J.H. Choi, S.C. Nam, Y. Il Yoon, CO_2 absorption characteristics in aqueous K_2CO_3/piperazine solution by NMR spectroscopy, Ind. Eng. Chem. Res. 50 (2011) 9306–9313.

[26] W. Dong, X. Chen, F. Yu, Y. Wu, $Na_2CO_3/MgO/Al_2O_3$ solid sorbents for low-temperature CO_2 capture, Energy & Fuels. 29 (2015) 968–973.

[27] M.E. Majchrowicz, D.W.F. (Wim) Brilman, M.J. Groeneveld, Precipitation regime for selected amino acid salts for CO_2 capture from flue gases, Energy Procedia. 1 (2009) 979–984.

[28] J.N. Knudsen, J.N. Jensen, P.-J. Vilhelmsen, O. Biede, Experience with CO_2 capture from coal flue gas in pilot-scale: Testing of different amine solvents, Energy Procedia. 1 (2009) 783–790.

[29] T.C. Drage, K.M. Smith, C. Pevida, A. Arenillas, C.E. Snape, Development of adsorbent technologies for post-combustion CO_2 capture, Energy Procedia. 1 (2009) 881–884.

[30] S. Choi, J.H. Drese, C.W. Jones, Adsorbent Materials for carbon dioxide capture from large anthropogenic point sources, ChemSusChem. 2 (2009) 796–854.

[31] M.T. Ho, G.W. Allinson, D.E. Wiley, Reducing the cost of CO_2 capture from flue gases

using membrane technology, Ind. Eng. Chem. Res. 47 (2008) 1562–1568.

[32] C.-H. Yu, A Review of CO_2 capture by absorption and adsorption, Aerosol Air Qual. Res. (2012).

[33] M.G. Plaza, S. García, F. Rubiera, J.J. Pis, C. Pevida, Post-combustion CO_2 capture with a commercial activated carbon: Comparison of different regeneration strategies, Chem. Eng. J. 163 (2010) 41–47.

[34] Q. Wang, J. Luo, Z. Zhong, A. Borgna, CO_2 capture by solid adsorbents and their applications: current status and new trends, Energy Environ. Sci. 4 (2011) 42–55.

[35] X. Liu, J. Li, L. Zhou, D. Huang, Y. Zhou, Adsorption of CO_2, CH_4 and N_2 on ordered mesoporous silica molecular sieve, Chem. Phys. Lett. 415 (2005) 198–201.

[36] T.-L. Chew, A.L. Ahmad, S. Bhatia, Ordered mesoporous silica (OMS) as an adsorbent and membrane for separation of carbon dioxide (CO_2), Adv. Colloid Interface Sci. 153 (2010) 43–57.

[37] R. Banerjee, H. Furukawa, D. Britt, C. Knobler, M. O'Keeffe, O.M. Yaghi, Control of pore size and functionality in isoreticular zeolitic imidazolate frameworks and their carbon dioxide selective capture properties, J. Am. Chem. Soc. 131 (2009) 3875–3877.

[38] R.J. Kuppler, D.J. Timmons, Q.-R. Fang, J.-R. Li, T.A. Makal, M.D. Young, D. Yuan, D. Zhao, W. Zhuang, H.-C. Zhou, Potential applications of metal-organic frameworks, Coord. Chem. Rev. 253 (2009) 3042–3066.

[39] I. Pfaff, A. Kather, Comparative thermodynamic analysis and integration issues of CCS steam power plants based on oxy-combustion with cryogenic or membrane based air separation, Energy Procedia. 1 (2009) 495–502.

[40] A. Hart, N. Gnanendran, Cryogenic CO_2 capture in natural gas, Energy Procedia. 1 (2009) 697–706.

[41] R.P. Lively, W.J. Koros, J.R. Johnson, Enhanced cryogenic CO_2 capture using dynamically operated low-cost fiber beds, Chem. Eng. Sci. 71 (2012) 97–103.

[42] T. Burdyny, H. Struchtrup, Hybrid membrane/cryogenic separation of oxygen from air

for use in the oxy-fuel process, Energy. 35 (2010) 1884–1897.

[43] M.M. Moftakhari Sharifzadeh, A. Ebadi Amooghin, M. Zamani Pedram, M. Omidkhah, Time-dependent mathematical modeling of binary gas mixture in facilitated transport membranes (FTMs): A real condition for single-reaction mechanism, J. Ind. Eng. Chem. 39 (2016) 48–65.

[44] K.C. Wong, P.S. Goh, A.F. Ismail, Thin film nanocomposite: the next generation selective membrane for CO_2 removal, J. Mater. Chem. A. 4 (2016) 15726–15748.

[45] S. Kentish, C. Scholes, G. Stevens, Carbon dioxide separation through polymeric membrane systems for flue gas applications, Recent Patents Chem. Eng. 1 (2008) 52–66.

[46] M. Wang, A. Lawal, P. Stephenson, J. Sidders, C. Ramshaw, Post-combustion CO_2 capture with chemical absorption: A state-of-the-art review, Chem. Eng. Res. Des. 89 (2011) 1609–1624.

[47] A.A. Olajire, CO_2 capture and separation technologies for end-of-pipe applications - A review, Energy. 35 (2010) 2610–2628.

[48] D. Luebke, C. Myers, H. Pennline, Hybrid membranes for selective carbon dioxide separation from fuel gas, Energy & Fuels. 20 (2006) 1906–1913.

[49] B. Shimekit, H. Mukhtar, F. Ahmad, S. Maitra, Ceramic membranes for the separation of carbon dioxide - A review, Trans. Indian Ceram. Soc. 68 (2009) 115–138.

[50] A.F. Ismail, P.S. Goh, S.M. Sanip, M. Aziz, Transport and separation properties of carbon nanotube-mixed matrix membrane, Sep. Purif. Technol. 70 (2009) 12–26.

[51] H.R. Amedi, M. Aghajani, Aminosilane-functionalized ZIF-8/PEBA mixed matrix membrane for gas separation application, Microporous Mesoporous Mater. 247 (2017) 124–135.

[52] H. Vinh-Thang, S. Kaliaguine, Predictive models for mixed-matrix membrane performance: A review, Chem. Rev. 113 (2013) 4980–5028.

[53] M. Vinoba, M. Bhagiyalakshmi, Y. Alqaheem, A.A. Alomair, A. Pérez, M.S. Rana,

Recent progress of fillers in mixed matrix membranes for CO_2 separation: A review, Sep. Purif. Technol. 188 (2017) 431–450.

[54] G. Dong, X. Zhang, Y. Zhang, T. Tsuru, Enhanced permeation through CO_2-stable dual-inorganic composite membranes with tunable nano-architectured channels, ACS Sustain. Chem. Eng. 6 (2018) 8515–8524.

[55] W. Li, S.A.S.C. Samarasinghe, T.H. Bae, Enhancing CO_2/CH_4 separation performance and mechanical strength of mixed-matrix membrane via combined use of graphene oxide and ZIF-8, J. Ind. Eng. Chem. (2018) 4–11.

[56] Q. Xin, Z. Li, C. Li, S. Wang, Z. Jiang, H. Wu, Y. Zhang, J. Yang, X. Cao, Enhancing the CO_2 separation performance of composite membranes by the incorporation of amino acid-functionalized graphene oxide, J. Mater. Chem. A. 3 (2015) 6629–6641.

[57] O.H. LeBlanc, W.J. Ward, S.L. Matson, S.G. Kimura, Facilitated transport in ion-exchange membranes, J. Memb. Sci. 6 (1980) 339–343.

[58] J.D. Way, R.D. Noble, D.L. Reed, G.M. Ginley, L.A. Jarr, Facilitated transport of CO_2 in ion exchange membranes, AIChE J. 33 (1987) 480–487.

[59] C.A. Scholes, S.E. Kentish, G.W. Stevens, The effect of condensable minor components on the gas separation performance of polymeric membranes for carbon dioxide capture, Energy Procedia. 1 (2009) 311–317.

[60] R.W. Baker, Membrane Technology and Applications, 2004.

[61] H. Lin, B.D. Freeman, Gas solubility, diffusivity and permeability in poly(ethylene oxide), J. Memb. Sci. 239 (2004) 105–117.

[62] A.Y. Houde, B. Krishnakumar, S.G. Charati, S.A. Stern, Permeability of dense (homogeneous) cellulose acetate membranes to methane, carbon dioxide, and their mixtures at elevated pressures, J. Appl. Polym. Sci. 62 (1996) 2181–2192.

[63] J. Li, K. Nagai, T. Nakagawa, S. Wang, Preparation of polyethyleneglycol (PEG) and cellulose acetate (CA) blend membranes and their gas permeabilities, J. Appl. Polym. Sci. 58 (1995) 1455–1463.

[64] A.C. Puleo, D.R. Paul, S.S. Kelley, The effect of degree of acetylation on gas sorption and transport behavior in cellulose acetate, J. Memb. Sci. 47 (1989) 301–332.

[65] J. Wu, Q. Yuan, Gas permeability of a novel cellulose membrane, J. Memb. Sci. 204 (2002) 185–194.

[66] K. Takada, H. Matsuya, T. Masuda, T. Higashimura, Gas permeability of polyacetylenes carrying substituents, J. Appl. Polym. Sci. 30 (1985) 1605–1616.

[67] L. Rebattet, M. Escoubes, E. Genies, M. Pineri, Effect of doping treatment on gas transport properties and on separation factors of polyaniline memebranes, J. Appl. Polym. Sci. 57 (1995) 1595–1604.

[68] Z. Xu, C. Dannenberg, J. Springer, S. Banerjee, G. Maier, Novel poly(arylene ether) as membranes for gas separation, J. Memb. Sci. 205 (2002) 23–31.

[69] M. Al-Masri, H.R. Kricheldorf, D. Fritsch, New Polyimides for gas separation. 1. polyimides derived from substituted terphenylenes and 4,4‘-(Hexafluoroisopropylidene) diphthalic anhydride, Macromolecules. 32 (1999) 7853–7858.

[70] H. Abdul Mannan, H. Mukhtar, M. Shima Shaharun, M. Roslee Othman, T. Murugesan, Polysulfone/poly(ether sulfone) blended membranes for CO_2 separation, J. Appl. Polym. Sci. 133 (2016) 42946.

[71] R. Quinn, J.B. Appleby, G.P. Pez, New facilitated transport membranes for the separation of carbon dioxide from hydrogen and methane, J. Memb. Sci. 104 (1995) 139–146.

[72] J. Shen, L. Wu, D. Wang, C. Gao, Sorption behavior and separation performance of novel facilitated transport membranes for CO_2/CH_4 mixtures, Desalination. 223 (2008) 425–437.

[73] W.S.W. Ho, K.K. Sirkar, eds., Membrane Handbook, Springer US, Boston, MA, 1992.

[74] J. Huang, J. Zou, W.S.W. Ho, Carbon dioxide capture using a CO_2-selective facilitated transport membrane, Ind. Eng. Chem. Res. 47 (2008) 1261–1267.

[75] A. Bhown, E.L. Cussler, Mechanism for selective ammonia transport through poly(vinylammonium thiocyanate) membranes, J. Am. Chem. Soc. 113 (1991) 742–749.

[76] E.L. Cussler, R. Aris, A. Bhown, On the limits of facilitated diffusion, J. Memb. Sci. 43 (1989) 149–164.

[77] M. Yoshikawa, T. Ezaki, K. Sanui, N. Ogata, Selective permeation of carbon dioxide through synthetic polymer membranes having pyridine moiety as a fixed carrier, J. Appl. Polym. Sci. 35 (1988) 145–154.

[78] M. Yoshikawa, K. Fujimoto, H. Kinugawa, T. Kitao, Y. Kamiya, N. Ogata, Specialty polymeric membranes. V. Selective permeation of carbon dioxide through synthetic polymeric membranes having 2-(N,N-dimethyl)aminoethoxycarbonyl moiety, J. Appl. Polym. Sci. 58 (1995) 1771–1778.

[79] Z. Tong, W.S.W. Ho, Facilitated transport membranes for CO_2 separation and capture, Sep. Sci. Technol. 52 (2017) 156–167.

[80] Z. Idris, D.A. Eimer, Representation of CO_2 absorption in sterically hindered amines, Energy Procedia. 51 (2013) 247–252.

[81] G.J. Francisco, A. Chakma, X. Feng, Membranes comprising of alkanolamines incorporated into poly(vinyl alcohol) matrix for CO_2/N_2 separation, J. Memb. Sci. 303 (2007) 54–63.

[82] J. Zou, W.S.W. Ho, CO_2-selective polymeric membranes containing amines in crosslinked poly(vinyl alcohol), J. Memb. Sci. 286 (2006) 310–321.

[83] T.-J. Kim, B. Li, M.-B. Hägg, Novel fixed-site-carrier polyvinylamine membrane for carbon dioxide capture, J. Polym. Sci. Part B Polym. Phys. 42 (2004) 4326–4336.

[84] H. Matsuyama, M. Teramoto, H. Sakakura, Selective permeation of CO_2 through poly 2-(N,N-dimethyl)aminoethyl methacrylate membrane prepared by plasma-graft polymerization technique, J. Memb. Sci. 114 (1996) 193–200.

[85] C. Nagel, K. Günther-Schade, D. Fritsch, T. Strunskus, F. Faupel, Free volume and

transport properties in highly selective polymer membranes, Macromolecules. 35 (2002) 2071–2077.

[86] L. Deng, T.J. Kim, M.-B. Hägg, Facilitated transport of CO_2 in novel PVAm/PVA blend membrane, J. Memb. Sci. 340 (2009) 154–163.

[87] T.J. Kim, H. Vrålstad, M. Sandru, M.B. Hägg, Separation performance of PVAm composite membrane for CO_2 capture at various pH levels, J. Memb. Sci. 428 (2013) 218–224.

[88] L. Zhang, R. Wang, Salting-out effect on facilitated transport membranes for CO_2 separation: From fluoride salt to polyoxometalates, RSC Adv. 2 (2012) 9551.

[89] Y. Li, Q. Xin, H. Wu, R. Guo, Z. Tian, Y. Liu, S. Wang, G. He, F. Pan, Z. Jiang, Efficient CO_2 capture by humidified polymer electrolyte membranes with tunable water state, Energy Environ. Sci. 7 (2014) 1489.

[90] L. Liu, A. Chakma, X. Feng, Gas permeation through water-swollen hydrogel membranes, J. Memb. Sci. 310 (2008) 66–75.

[91] J. Wang, S. Wang, Q. Xin, Y. Li, Perspectives on water-facilitated CO_2 capture materials, J. Mater. Chem. A. 5 (2017) 6794–6816.

[92] H. Matsuyama, A. Terada, T. Nakagawara, Y. Kitamura, M. Teramoto, Facilitated transport of CO_2 through polyethylenimine/poly(vinyl alcohol) blend membrane, J. Memb. Sci. 163 (1999) 221–227.

[93] S. Ben Hamouda, Q.T. Nguyen, D. Langevin, S. Roudesli, Poly(vinylalcohol)/poly(ethyleneglycol)/poly(ethyleneimine) blend membranes - structure and CO_2 facilitated transport, Comptes Rendus Chim. 13 (2010) 372–379.

[94] L. Deng, M.B. Hägg, Swelling behavior and gas permeation performance of PVAm/PVA blend FSC membrane, J. Memb. Sci. 363 (2010) 295–301.

[95] Y. Zhao, W.S.W. Ho, CO_2-selective membranes containing sterically hindered amines for CO_2/H_2 separation, Ind. Eng. Chem. Res. 52 (2013) 8774–8782.

[96] Y. Zhao, W.S. Winston Ho, Steric hindrance effect on amine demonstrated in solid

polymer membranes for CO_2 transport, J. Memb. Sci. 415–416 (2012) 132–138.

[97] W. Salim, V. Vakharia, K.K. Chen, M. Gasda, W.S.W. Ho, Oxidatively stable borate-containing membranes for H_2 purification for fuel cells, J. Memb. Sci. 562 (2018) 9–17.

[98] Y. Zhao, B.T. Jung, L. Ansaloni, W.S.W. Ho, Multiwalled carbon nanotube mixed matrix membranes containing amines for high pressure CO_2/H_2 separation, J. Memb. Sci. 459 (2014) 233–243.

[99] T. Kouketsu, S. Duan, T. Kai, S. Kazama, K. Yamada, PAMAM dendrimer composite membrane for CO_2 separation: Formation of a chitosan gutter layer, J. Memb. Sci. 287 (2007) 51–59.

[100] Y. Chen, L. Zhao, B. Wang, P. Dutta, W.S. Winston Ho, Amine-containing polymer/zeolite Y composite membranes for CO_2/N_2 separation, J. Memb. Sci. 497 (2016) 21–28.

[101] L.A. El-Azzami, E.A. Grulke, Carbon dioxide separation from hydrogen and nitrogen facilitated transport in arginine salt-chitosan membranes, J. Memb. Sci. 328 (2009) 15–22.

[102] H. Chen, A.S. Kovvali, K.K. Sirkar, Selective CO_2 separation from CO_2-N_2 mixtures by immobilized glycine-Na-glycerol membranes, Ind. Eng. Chem. Res. 39 (2000) 2447–2458.

[103] A. Mondal, B. Mandal, Synthesis and characterization of crosslinked poly(vinyl alcohol)/poly(allylamine)/2-amino-2-hydroxymethyl-1,3-propanediol/polysulfone composite membrane for CO_2/N_2 separation, J. Memb. Sci. 446 (2013) 383–394.

[104] A. Mondal, B. Mandal, CO_2 separation using thermally stable crosslinked poly(vinyl alcohol) membrane blended with polyvinylpyrrolidone/polyethyleneimine/ tetraethylenepentamine, J. Memb. Sci. 460 (2014) 126–138.

[105] A. Mondal, B. Mandal, Novel CO_2-selective cross-linked poly(vinyl alcohol)/polyvinylpyrrolidone blend membrane containing amine carrier for CO_2 –N_2 separation: synthesis, characterization, and gas permeation study, Ind. Eng. Chem. Res.

53 (2014) 19736–19746.

[106] A. Mondal, M. Barooah, B. Mandal, Effect of single and blended amine carriers on CO_2 separation from CO_2/N_2 mixtures using crosslinked thin-film poly(vinyl alcohol) composite membrane, Int. J. Greenh. Gas Control. 39 (2015) 27–38.

[107] L.A. El-Azzami, E.A. Grulke, Carbon dioxide separation from hydrogen and nitrogen by fixed facilitated transport in swollen chitosan membranes, J. Memb. Sci. 323 (2008) 225–234.

[108] A. Ito, M. Sato, T. Anma, Permeability of CO_2 through chitosan membrane swollen by water vapor in feed gas, Angew. Makromol. Chemie. 248 (1997) 85–94.

[109] S.Y. Bae, K.H. Lee, S.C. Yi, H.T. Kim, Y.H. Kim, H. Kumazawa, CO_2, N_2 gas sorption and permeation behavior of chitosan membrane, Korean J. Chem. Eng. 15 (1998) 223–226.

[110] Y. Shen, H. Wang, J. Liu, Y. Zhang, Enhanced performance of a novel polyvinyl amine/chitosan/graphene oxide mixed matrix membrane for CO_2 Capture, ACS Sustain. Chem. Eng. 3 (2015) 1819–1829.

[111] S. Xiao, X. Feng, R.Y.M. Huang, Trimesoyl chloride crosslinked chitosan membranes for CO_2/N_2 separation and pervaporation dehydration of isopropanol, J. Memb. Sci. 306 (2007) 36–46.

[112] M. Yu, Y. Dai, K. Yang, H. Li, H. Guo, G. He, TEA incorporated CS blend composite membrane for high CO_2 separation performance, RSC Adv. 6 (2016) 27016–27019.

[113] S. Saedi, B. Nikravesh, F. Seidi, L. Moradi, A. Arabi Shamsabadi, M. Babaei Salarabadi, H. Salimi, Facilitated transport of CO_2 through novel imidazole-containing chitosan derivative/PES membranes, RSC Adv. 5 (2015) 67299–67307.

[114] Y. Liu, S. Yu, H. Wu, Y. Li, S. Wang, Z. Tian, Z. Jiang, High permeability hydrogel membranes of chitosan/poly ether-block-amide blends for CO_2 separation, J. Memb. Sci. 469 (2014) 198–208.

[115] C. Casado-Coterillo, M. Del Mar López-Guerrero, A. Irabien, Synthesis and

Characterisation of ETS-10/Acetate-based Ionic Liquid/Chitosan Mixed Matrix Membranes for CO_2/N_2 Permeation., Membranes (Basel). 4 (2014) 287–301.

[116] C. Casado-Coterillo, A. Fernández-Barquín, B. Zornoza, C. Téllez, J. Coronas, Á. Irabien, Synthesis and characterisation of MOF/ionic liquid/chitosan mixed matrix membranes for CO_2/N_2 separation, RSC Adv. 5 (2015) 102350–102361.

[117] Y. Chen, W.S.W. Ho, High-molecular-weight polyvinylamine/piperazine glycinate membranes for CO_2 capture from flue gas, J. Memb. Sci. 514 (2016) 376–384.

[118] J.P. Roy, M.K. Mishra, A. Misra, Parametric optimization and performance analysis of a waste heat recovery system using organic rankine cycle, Energy. 35 (2010) 5049–5062.

[119] E. Santos, E. Rodríguez-Fernández, C. Casado-Coterillo, Á. Irabien, Hybrid ionic liquid-chitosan membranes for CO_2 separation: mechanical and thermal behavior, Int. J. Chem. React. Eng. 14 (2016).

[120] K. V. Otvagina, A.E. Mochalova, T.S. Sazanova, A.N. Petukhov, A.A. Moskvichev, A. V. Vorotyntsev, C.A.M. Afonso, I. V. Vorotyntsev, Preparation and characterization of facilitated transport membranes composed of chitosan-styrene and chitosan-acrylonitrile copolymers modified by methylimidazolium based ionic liquids for CO_2 separation from CH_4 and N_2, Membranes (Basel). 6 (2016).

[121] I. Abdollahpour, F. Seidi, S. Saedi, Preparation and characterization of a novel water soluble amino chitosan (amino-CS) derivative for facilitated transport of CO_2, Polym. Sci. Ser. B. 59 (2017) 173–182.

[122] M.S.A. Rahaman, L. Zhang, L.H. Cheng, X.-H. Xu, H.-L. Chen, Capturing carbon dioxide from air using a fixed carrier facilitated transport membrane, RSC Adv. 2 (2012) 9165.

[123] G. Puxty, R. Rowland, A. Allport, Q. Yang, M. Bown, R. Burns, M. Maeder, M. Attalla, Carbon dioxide postcombustion capture: A novel screening study of the carbon dioxide absorption performance of 76 amines, Environ. Sci. Technol. 43 (2009) 6427–6433.

[124] A.K. Pal, V. Katiyar, Nanoamphiphilic chitosan dispersed poly(lactic acid)

bionanocomposite films with improved thermal, mechanical, and gas barrier properties, Biomacromolecules, 17 (2016) 2603–2618.

[125] C.G.T. Neto, J.A. Giacometti, A.E. Job, F.C. Ferreira, J.L.C. Fonseca, M.R. Pereira, Thermal analysis of chitosan based networks, Carbohydr. Polym. 62 (2005) 97–103.

[126] X.Y. Huang, X.Y. Mao, H.T. Bu, X.Y. Yu, G.B. Jiang, M.H. Zeng, Chemical modification of chitosan by tetraethylenepentamine and adsorption study for anionic dye removal, Carbohydr. Res. 346 (2011) 1232–1240.

[127] S. Rivero, M.A. García, A. Pinotti, Physical and chemical treatments on chitosan matrix to modify film properties and kinetics of biodegradation, J. Mater. Phys. Chem. 1 (2013) 51–57.

[128] M. Fan, A.G. Russell, Modified nanosepiolite as an inexpensive support of tetraethylenepentamine for CO_2 sorption, Nano Energy. 11 (2014) 235–246.

[129] J. Nunthanid, S. Wanchana, P. Sriamornsak, S. Limmatavapirat, M. Luangtana-anan, S. Puttipipatkhachorn, Effect of heat on characteristics of chitosan film coated on theophylline tablets., Drug Dev. Ind. Pharm. 28 (2002) 919–30.

[130] P. Fernandez-Saiz, J.M. Lagarón, M.J. Ocio, Optimization of the film-forming and storage conditions of chitosan as an antimicrobial agent, J. Agric. Food Chem. 57 (2009) 3298–3307.

[131] J.M. Urreaga, M.U. de la Orden, Chemical interactions and yellowing in chitosan-treated cellulose, Eur. Polym. J. 42 (2006) 2606–2616.

[132] Y. Cai, Z. Wang, C. Yi, Y. Bai, J. Wang, S. Wang, Gas transport property of polyallylamine-poly(vinyl alcohol)/polysulfone composite membranes, J. Memb. Sci. 310 (2008) 184–196.

[133] J. Liu, X. Lu, C. Wu, Effect of preparation methods on crystallization behavior and tensile strength of poly(vinylidene fluoride) membranes, Membranes (Basel). 3 (2013) 389–405.

[134] Y. Wang, M. Gupta, D.A. Schiraldi, Oxygen permeability in thermoplastic

polyurethanes, J. Polym. Sci. Part B Polym. Phys. 50 (2012) 681–693.

[135] Y. Zhang, Z. Wang, S. Wang, Novel fixed-carrier membranes for CO_2 separation, J. Appl. Polym. Sci. 86 (2002) 2222–2226.

[136] D.E. Gottschlich, D.L. Roberts, J.D. Way, A theoretical comparison of facilitated transport and solution-diffusion membrane modules for gas separation, Gas Sep. Purif. 2 (1988) 65–71.

[137] R. Yegani, H. Hirozawa, M. Teramoto, H. Himei, O. Okada, T. Takigawa, N. Ohmura, N. Matsumiya, H. Matsuyama, Selective separation of CO_2 by using novel facilitated transport membrane at elevated temperatures and pressures, J. Memb. Sci. 291 (2007) 157–164.

[138] J. Sun, Z. Yi, X. Zhao, Y. Zhou, C. Gao, CO_2 separation membranes with high permeability and CO_2/N_2 selectivity prepared by electrostatic self-assembly of polyethylenimine on reverse osmosis membranes, RSC Adv. 7 (2017) 14678–14687.

[139] R. Xing, W.S.W. Ho, Crosslinked polyvinylalcohol-polysiloxane/fumed silica mixed matrix membranes containing amines for CO_2/H_2 separation, J. Memb. Sci. 367 (2011) 91–102.

[140] I. Horcas, R. Fernández, J.M. Gómez-Rodríguez, J. Colchero, J. Gómez-Herrero, A.M. Baro, WSXM: A software for scanning probe microscopy and a tool for nanotechnology, Rev. Sci. Instrum. 78 (2007) 013705.

[141] C.F. Forney, D.G. Brandl, Control of humidity in small controlled-environment chambers using glycerol-water solutions, Hort Technol. 2 (1992) 52–54.

[142] S.S. Shiratori, M.F. Rubner, pH-dependent thickness behavior of sequentially adsorbed layers of weak polyelectrolytes, Macromolecules. 33 (2000) 4213–4219.

[143] J.D. Mendelsohn, C.J. Barrett, V. V. Chan, A.J. Pal, A.M. Mayes, M.F. Rubner, Fabrication of microporous thin films from polyelectrolyte multilayers, Langmuir. 16 (2000) 5017–5023.

[144] A.A. Akhmetshina, I.M. Davletbaeva, E.S. Grebenschikova, T.S. Sazanova, A.N.

Petukhov, A.A. Atlaskin, E.N. Razov, I.I. Zaripov, C.F. Martins, L.A. Neves, I. V. Vorotyntsev, The effect of microporous polymeric support modification on surface and gas transport properties of supported ionic liquid membranes, Membranes (Basel). 6 (2015) 1–18.

[145] S.E. Burke, C.J. Barrett, Swelling behavior of hyaluronic acid/polyallylamine hydrochloride multilayer films, Biomacromolecules. 6 (2005) 1419–1428.

[146] G.P. Lim, M.S. Ahmad, Development of Ca-alginate-chitosan microcapsules for encapsulation and controlled release of imidacloprid to control dengue outbreaks, J. Ind. Eng. Chem. 56 (2017) 382–393.

[147] E. Bagheripour, A.R. Moghadassi, S.M. Hosseini, B. Van der Bruggen, F. Parvizian, Novel composite graphene oxide/chitosan nanoplates incorporated into PES based nanofiltration membrane: Chromium removal and antifouling enhancement, J. Ind. Eng. Chem. (2018) 1–10.

[148] M.J. Cho, B.D. Park, Tensile and thermal properties of nanocellulose-reinforced poly(vinyl alcohol) nanocomposites, J. Ind. Eng. Chem. 17 (2011) 36–40.

[149] P.M. Cunniff, S.A. Fossey, M.A. Auerbach, J.W. Song, D.L. Kaplan, W.W. Adams, R.K. Eby, D. Mahoney, D.L. Vezie, Mechanical and thermal properties of dragline silk from the spider Nephila clavipes, Polym. Adv. Technol. 5 (1994) 401–410.

[150] J. Guan, D. Porter, F. Vollrath, Thermally induced changes in dynamic mechanical properties of native silks, Biomacromolecules. 14 (2013) 930–937.

[151] S. Rafiq, L. Deng, M.-B. Hägg, Role of Facilitated transport membranes and composite membranes for efficient CO_2 capture - A review, ChemBioEng Rev. 3 (2016) 68–85.

[152] A. Santaniello, G. Golemme, Interfacial control in perfluoropolymer mixed matrix membranes for natural gas sweetening, J. Ind. Eng. Chem. 60 (2018) 169–176.

[153] E. Kaiser, R.L. Colescott, C.D. Bossinger, P.I. Cook, Color test for detection of free terminal amino groups in the solid-phase synthesis of peptides, Anal. Biochem. 34 (1970) 595–598.

[154] M. Friedman, Applications of the ninhydrin reaction for analysis of amino acids, peptides, and proteins to agricultural and biomedical sciences, J. Agric. Food Chem. 52 (2004) 385–406.

[155] H. Wang, D. Cao, Diffusion and separation of H_2, CH_4, CO_2, and N_2 in diamond-like frameworks, J. Phys. Chem. C. 119 (2015) 6324–6330.

[156] O.C. David, D. Gorri, A. Urtiaga, I. Ortiz, Mixed gas separation study for the hydrogen recovery from H_2/CO/N_2/CO_2 post combustion mixtures using a Matrimid membrane, J. Memb. Sci. 378 (2011) 359–368.

[157] D.L. Ma, Y. Ma, Z.W. Chen, A.M. Hu, A silk fabric derived carbon fibre net for transparent capacitive touch pads and all-solid supercapacitors, J. Mater. Chem. A. 5 (2017) 20608–20614.

[158] Y. Yang, Z. Shao, X. Chen, P. Zhou, Optical spectroscopy to investigate the structure of regenerated bombyx mori silk fibroin in solution, Biomacromolecules. 5 (2004) 773–779.

[159] X. Liu, K.-Q. Zhang, Silk Fiber - molecular formation mechanism, structure- property relationship and advanced applications, Oligomerization Chem. Biol. Compd., InTech, 2014.

[160] C. Zhang, D. Song, Q. Lu, X. Hu, D.L. Kaplan, H. Zhu, Flexibility regeneration of silk fibroin in vitro, Biomacromolecules. 13 (2012) 2148–2153.

[161] L. Wang, C. Lu, B. Zhang, B. Zhao, F. Wu, S. Guan, Fabrication and characterization of flexible silk fibroin films reinforced with graphene oxide for biomedical applications, RSC Adv. 4 (2014) 40312–40320.

[162] Z. Zhang, T. Jiang, K. Ma, X. Cai, Y. Zhou, Y. Wang, Low temperature electrophoretic deposition of porous chitosan/silk fibroin composite coating for titanium biofunctionalization, J. Mater. Chem. 21 (2011) 7705.

[163] M.A. de Moraes, G.M. Nogueira, R.F. Weska, M.M. Beppu, Preparation and characterization of insoluble silk fibroin/chitosan blend films, Polymers (Basel). 2 (2010) 719–727.

[164] S. Kaushik, M.K. Sarma, P. Dema, M. Santhosh, P. Goswami, Thin films of silk fibroin and its blend with chitosan strongly promote biofilm growth of *Synechococcus sp* . *BDU 140432*, J. Colloid Interface Sci. 479 (2016) 251–259.

[165] S.S. Silva, T.C. Santos, M.T. Cerqueira, A.P. Marques, L.L. Reys, T.H. Silva, S.G. Caridade, J.F. Mano, R.L. Reis, The use of ionic liquids in the processing of chitosan/silk hydrogels for biomedical applications, Green Chem. 14 (2012) 1463.

[166] R. Rujiravanit, S. Kruaykitanon, A.M. Jamieson, S. Tokura, Preparation of crosslinked chitosan/silk fibroin blend films for drug delivery system, Macromol. Biosci. 3 (2003) 604–611.

[167] D.N. Rockwood, R.C. Preda, T. Yücel, X. Wang, M.L. Lovett, D.L. Kaplan, Materials fabrication from Bombyx mori silk fibroin, Nat. Protoc. 6 (2011) 1612–1631.

[168] U.J. Kim, J. Park, H. Joo Kim, M. Wada, D.L. Kaplan, Three-dimensional aqueous-derived biomaterial scaffolds from silk fibroin, Biomaterials. 26 (2005) 2775–2785.

[169] N. Bhardwaj, S.C. Kundu, Silk fibroin protein and chitosan polyelectrolyte complex porous scaffolds for tissue engineering applications, Carbohydr. Polym. 85 (2011) 325–333.

[170] X. Hu, K. Shmelev, L. Sun, E.-S. Gil, S.-H. Park, P. Cebe, D.L. Kaplan, Regulation of silk material structure by temperature-controlled water vapor annealing, Biomacromolecules. 12 (2011) 1686–1696.

[171] X. Hu, D. Kaplan, P. Cebe, Effect of water on the thermal properties of silk fibroin, Thermochim. Acta. 461 (2007) 137–144.

[172] W.J. Koros, A.H. Chan, D.R. Paul, Sorption and transport of various gases in polycarbonate, J. Memb. Sci. 2 (1977) 165–190.

[173] L.M. Robeson, The upper bound revisited, J. Memb. Sci. 320 (2008) 390–400.

[174] E. V. Lin, H. Wagner, Plasticization-enhanced hydrogen purification using polymeric membranes, Science. 311 (2006) 639–642.

[175] E. Wenk, H.P. Merkle, L. Meinel, Silk fibroin as a vehicle for drug delivery

applications, J. Control. Release. 150 (2011) 128–141.

[176] T.T. Cao, Y.Q. Zhang, Processing and characterization of silk sericin from Bombyx mori and its application in biomaterials and biomedicines, Mater. Sci. Eng. C. 61 (2016) 940–952.

[177] S.C. Kundu, B.C. Dash, R. Dash, D.L. Kaplan, Natural protective glue protein, sericin bioengineered by silkworms: Potential for biomedical and biotechnological applications, Prog. Polym. Sci. 33 (2008) 998–1012.

[178] M.L. Gimenes, L. Liu, X. Feng, Sericin/poly(vinyl alcohol) blend membranes for pervaporation separation of ethanol/water mixtures, J. Memb. Sci. 295 (2007) 71–79.

[179] W. Tao, M. Li, R. Xie, Preparation and structure of porous silk sericin materials, macromol. Mater. Eng. 290 (2005) 188–194.

[180] H. Teramoto, M. Miyazawa, Molecular orientation behavior of silk sericin film as revealed by atr infrared spectroscopy, Biomacromolecules. 6 (2005) 2049–2057.

[181] Q. Zhang, L. Cui, P. Wang, C. Deng, Q. Wang, X. Fan, Improving properties of silk sericin membranes via enzymatic oxidation with laccase and TEMPO, Biotechnol. Appl. Biochem. 65 (2018) 372–380.

[182] E. Hadipour-Goudarzi, M. Montazer, M. Latifi, A.A.G. Aghaji, Electrospinning of chitosan/sericin/PVA nanofibers incorporated with in situ synthesis of nano silver, Carbohydr. Polym. 113 (2014) 231–239.

[183] S. Nayak, S. Dey, S.C. Kundu, Silk sericin-alginate-chitosan microcapsules: Hepatocytes encapsulation for enhanced cellular functions, Int. J. Biol. Macromol. 65 (2014) 258–266.

[184] J.R. Du, X. Su, X. Feng, Chitosan/sericin blend membranes for adsorption of bovine serum albumin, Can. J. Chem. Eng. 95 (2017) 954–960.

[185] S.J. Kim, Gas permeation through water-swollen sericin / PVA membranes, UWSpace, 2007.

[186] Y. Liang, D.P. Harrison, R.P. Gupta, D.A. Green, W.J. McMichael, Carbon dioxide

capture using dry sodium-based sorbents, Energy and Fuels. 18 (2004) 569–575.

[187] B. Dutcher, M. Fan, B. Leonard, M.D. Dyar, J. Tang, E.A. Speicher, P. Liu, Y. Zhang, Use of nanoporous FeOOH as a catalytic support for $NaHCO_3$ decomposition aimed at reduction of energy requirement of $Na_2CO_3/NaHCO_3$ based CO_2 separation technology, J. Phys. Chem. C. 115 (2011) 15532–15544.

[188] P.K. Verma, A. Kundu, M.S. Puretz, C. Dhoonmoon, O.S. Chegwidden, C.H. Londergan, M. Cho, The bend+libration combination band is an intrinsic, collective, and strongly solute-dependent reporter on the hydrogen bonding network of liquid water, J. Phys. Chem. B. 122 (2018) 2587–2599.

[189] H. Chioyama, H. Luo, T. Ohba, H. Kanoh, Temperature-dependent double-step CO_2 occlusion of K_2CO_3 under moist conditions, Adsorpt. Sci. Technol. 33 (2015) 243–250.

[190] Z. Kang, M. Xue, L. Fan, L. Huang, L. Guo, G. Wei, B. Chen, S. Qiu, Highly selective sieving of small gas molecules by using an ultra-microporous metal–organic framework membrane, Energy Environ. Sci. 7 (2014) 4053–4060.

[191] S.S. Dhingra, E. Marand, Mixed gas transport study through polymeric membranes, J. Memb. Sci. 141 (1998) 45–63.

[192] F. Wu, L. Li, Z. Xu, S. Tan, Z. Zhang, Transport study of pure and mixed gases through PDMS membrane, Chem. Eng. J. 117 (2006) 51–59.

[193] J.B. Gilbert, M.F. Rubner, R.E. Cohen, Depth-profiling X-ray photoelectron spectroscopy (XPS) analysis of interlayer diffusion in polyelectrolyte multilayers, Proc. Natl. Acad. Sci. 110 (2013) 6651–6656.

[194] R. Simpson, R.G. White, J.F. Watts, M.A. Baker, XPS investigation of monatomic and cluster argon ion sputtering of tantalum pentoxide, Appl. Surf. Sci. 405 (2017) 79–87.

[195] A. Fernández-Barquín, C. Casado-Coterillo, Á. Irabien, Separation of CO_2-N_2 gas mixtures: Membrane combination and temperature influence, Sep. Purif. Technol. 188 (2017) 197–205.

[196] A. Fernández-Barquín, C. Casado-Coterillo, M. Etxeberria-Benavides, J. Zuñiga, A.

Irabien, Comparison of flat and hollow-fiber mixed-matrix composite membranes for CO_2 separation with temperature, Chem. Eng. Technol. 40 (2017) 997–1007.

[197] Y. Zhang, J. Sunarso, S. Liu, R. Wang, Current status and development of membranes for CO_2/CH_4 separation : A review, Int. J. Greenh. Gas Control. 12 (2013) 84–107.

[198] A. Ebadi Amooghin, H. Sanaeepur, M. Omidkhah, A. Kargari, "Ship-in-a-bottle", a new synthesis strategy for preparing novel hybrid host–guest nanocomposites for highly selective membrane gas separation, J. Mater. Chem. A. 6 (2018) 1751–1771.

[199] B. Seoane, J. Coronas, I. Gascon, M.E. Benavides, O. Karvan, J. Caro, F. Kapteijn, J. Gascon, Metal-organic framework based mixed matrix membranes: a solution for highly efficient CO_2 capture?, Chem. Soc. Rev. 44 (2015) 2421–2454.

[200] K. Yang, Y. Dai, W. Zheng, X. Ruan, H. Li, G. He, ZIFs-modified GO plates for enhanced CO_2 separation performance of ethyl cellulose based mixed matrix membranesf, Sep. Purif. Technol. (2018).

[201] A. Ebadi, M. Omidkhah, A. Kargari, The effects of aminosilane grafting on NaY zeolite – Matrimid s 5218 mixed matrix membranes for CO_2/CH_4 separation, J. Memb. Sci. 490 (2015) 364–379.

[202] W. Ying, J. Cai, K. Zhou, D. Chen, Y. Ying, Y. Guo, X. Kong, Z. Xu, X. Peng, Ionic liquid selectively facilitates CO_2 transport through graphene oxide membrane, ACS Nano. 12 (2018) 5385–5393.

[203] M. Rezakazemi, A. Ebadi, Progress in polymer science state-of-the-art membrane based CO_2 separation using mixed matrix membranes (MMMs): An overview on current status and future directions, Prog. Polym. Sci. 39 (2014) 817–861.

[204] F. Zhou, H.N. Tien, W.L. Xu, J.T. Chen, Q. Liu, E. Hicks, M. Fathizadeh, S. Li, M. Yu, Ultrathin graphene oxide-based hollow fiber membranes with brush-like CO_2-philic agent for highly efficient CO2capture, Nat. Commun. 8 (2017).

[205] X. Li, Y. Cheng, H. Zhang, S. Wang, Z. Jiang, R. Guo, H. Wu, Efficient CO_2 capture by functionalized graphene oxide nanosheets as fillers to fabricate multi-permselective mixed matrix membranes, ACS Appl. Mater. Interfaces. 7 (2015) 5528–5537.

[206] R.R. Nair, H.A. Wu, P.N. Jayaram, I. V. Grigorieva, A.K. Geim, Unimpeded permeation of water through helium-leak-tight graphene-based membranes, Science. 335 (2012) 442–444.

[207] H.W. Kim, H.W. Yoon, S.-M. Yoon, B.M. Yoo, B.K. Ahn, Y.H. Cho, H.J. Shin, H. Yang, U. Paik, S. Kwon, J.-Y. Choi, H.B. Park, Selective gas transport through few-layered graphene and graphene oxide membranes, Science. 342 (2013) 91–95.

[208] H. Li, Z. Song, X. Zhang, Y. Huang, S. Li, Y. Mao, H.J. Ploehn, Y. Bao, M. Yu, Ultrathin, Molecular-sieving graphene oxide membranes for selective hydrogen separation, Science. 342 (2013) 95–98.

[209] S. Kaushik, M.K. Sarma, P. Goswami, FRET-guided surging of cyanobacterial photosystems improves and stabilizes current in photosynthetic microbial fuel cell, J. Mater. Chem. A. 5 (2017) 7885–7895.

[210] C. Vepari, D.L. Kaplan, Silk as a biomaterial, Prog. Polym. Sci. 32 (2007) 991–1007.

[211] Z. Zhu, S. Ling, J. Yeo, S. Zhao, L. Tozzi, M.J. Buehler, F. Omenetto, C. Li, D.L. Kaplan, High-strength, durable all-silk fibroin hydrogels with versatile processability toward multifunctional applications, Adv. Funct. Mater. 1704757 (2018) 1704757.

[212] M.S. Eikeland, M.-B. Hägg, M.A. Brook, M. Ottøy, A. Lindbråthen, Durability of poly(dimethylsiloxane) when exposed to chlorine gas, J. Appl. Polym. Sci. 85 (2002) 2458–2470.

[213] H. Kreulen, C.A. Smolders, G.F. Versteeg, W.P.M. Van Swaaij, Determination of mass transfer rates in wetted and non-wetted microporous membranes, Chem. Eng. Sci. 48 (1993) 2093–2102.

[214] K. Okabe, N. Matsumiya, H. Mano, Stability of gel-supported facilitated transport membrane for carbon dioxide separation from model flue gas, Sep. Purif. Technol. 57 (2007) 242–249.

[215] J.H. Ding, H.R. Zhao, H. Bin Yu, A water-based green approach to large-scale production of aqueous compatible graphene nanoplatelets, Sci. Rep. 8 (2018) 1–8.

[216] X. Yang, Y. Tu, L. Li, S. Shang, X.M. Tao, Well-dispersed chitosan/graphene oxide nanocomposites, ACS Appl. Mater. Interfaces. 2 (2010) 1707–1713.

[217] A. Higuchi, M. Abe, J. Komiyama, T. Iijima, Gas permeation through hydrogels I. Gel cellophane membranes, J. Memb. Sci. 21 (1984) 113–121.

[218] Y.-C. Wang, C.O. Mohan, J. Guan, C.N. Ravishankar, S. Gunasekaran, Chitosan and gold nanoparticles-based thermal history indicators and frozen indicators for perishable and temperature-sensitive products, Food Control. 85 (2018) 186–193.

[219] H. Maachou, M.J. Genet, D. Aliouche, C.C. Dupont-Gillain, P.G. Rouxhet, XPS analysis of chitosan-hydroxyapatite biomaterials: From elements to compounds, Surf. Interface Anal. 45 (2013) 1088–1097.

Appendix 1

Structure of various polymers and amines used in this study

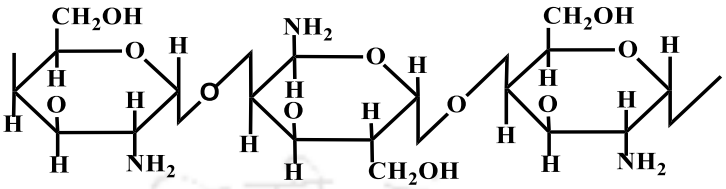

(a) Chitosan (CS)

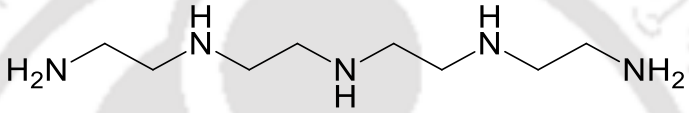

(b) Tetraethylenepentamine (TEPA)

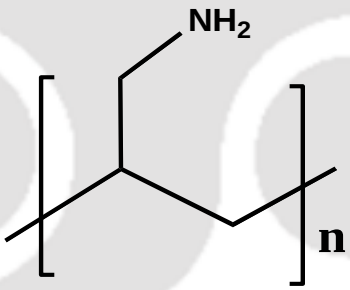

(c) Poly(allylamine) (PAA)

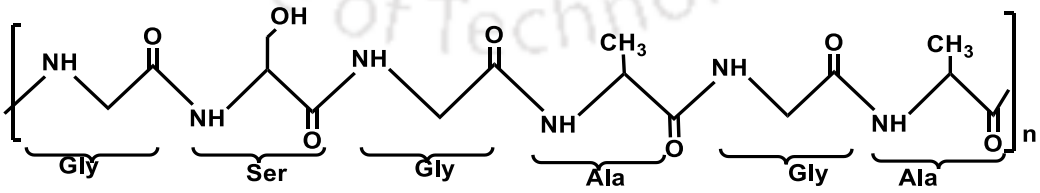

(d) Silk Fibroin (SF)

Figure A1.1 Chemical structure of (a) CS, (b) TEPA, (c) PAA and (d) SF.

Appendix 2

A2.1 Gas Transport Parameters Calculation and Gas Chromatography Data

Gas transport parameters (CO_2 and N_2 fluxes, CO_2 and N_2 permeability, CO_2/N_2 selectivity) calculation (The calculation procedure adapted here was originally taken from PhD thesis of Arijit Mondal, reference given at the end of the Appendix**)**

η_R (mol/min) = retentate molar flow rate = $\frac{PV}{RT}$

Where,

P (atmospheric pressure at which the retentate gas is emitting) = 1 atm.

V (volumetric flow rate of mixed gas at retentate side) = 45 cc/min = 45 $\times 10^{-6}$ m^3/min.

T (room temperature at °K) = 298.15 °K.

R (universal gas constant) = 8.205746 × 10^{-5} m^3 atm /°K mol.

$$\boldsymbol{\eta_R}\ \textbf{(Mole/min)} = \frac{1 \times 45 \times 10^{-6}}{8.205746 \times 10^{-5} \times 298.15} = \textbf{1.84} \times \textbf{10}^{-3}\ \textbf{mole /min.}$$

η_{Ar} (Mole/min) = argon (carrier gas) molar flow rate = $\frac{PV}{RT}$

P (atmospheric pressure at which the carrier gas is emitting) = 1 atm

V (volumetric flow rate of carrier gas at permeate side) = 43 cc/min = 43 × 10^{-6} m^3/min.

T (room temperature at °K) = 298.15 °K.

R (universal gas constant) = 8.205746 × 10^{-5} m^3 atm /°K mol.

$$\boldsymbol{\eta_{Ar}}\ \textbf{(mol/min)} = \frac{\mathbf{1 \times 43 \times 10^{-6}}}{\mathbf{8.205746 \times 10^{-5} \times 298.15}} = \textbf{1.75} \times \textbf{10}^{-3}\ \textbf{mol /min.}$$

η_P (mol/min) = permeate molar flow rate =

$$[(CO_2 \text{ mole fraction} \times \frac{CO_2}{CO_2}\frac{(P)_{G.C}}{(F)_{G.C}} + (N_2 \text{ mole fraction} \times \frac{N_2}{N_2}\frac{(P)_{G.C}}{(F)_{G.C}})]$$

$$\times \frac{Ar\ molar\ flow\ rate\ (mol/min)}{[1-(CO_2 \text{ mole fraction} \times \frac{CO_2(P)_{G.C}}{CO_2(F)_{G.C}} - (N_2 \text{ mole fraction} \times \frac{N_2(P)_{G.C}}{N_2(F)_{G.C}})]}$$

Where.

$CO_2(P)_{G.C}$ = CO_2 mole fraction at permeate side from G.C analysis (**Figure A2.1**)

$CO_2(F)_{G.C}$ = CO_2 mole fraction at feed side from G.C analysis (**Figure A2.1**)

$N_2(P)_{G.C}$ = N_2 mole fraction at permeate side from G.C analysis (**Figure A2.1**)

$N_2(F)_{G.C}$ = N_2 mole fraction at feed side from G.C analysis (**Figure A2.1**)

CO_2 mole fraction = 0.2

N_2 mole fraction = 0.8

Ar molar flow rate = 1.75×10^{-3} mol /min.

η_P (mol/min) = permeate molar flow rate = 7.65×10^{-5} mol/min.

p_{CO_2} (R,psi) = CO_2 partial pressure at retentate side =

$$[BP_F \text{ (psig)} + P_{ambient} \text{ (kPa)} \times \frac{14.7}{101.325}] \times$$

$$\frac{[\eta_R - 0.5 \times \eta_P]\ (mol/min) \times CO_2\ mole\ fraction \times [0.5 + 0.5 \times \frac{CO_2(R)_{G.C}}{CO_2(F)_{G.C}}]}{[\eta_R - 0.5 \times \eta_P]\ (mol/min) + \frac{[(0.5 \times H_2O_F) + (0.5 \times H_2O_{distribution} \times (H_2O_F + H_2O_S))]\ (ml/min)}{18\ (ml/mol)}}$$

Where,

BP_F =Back pressure (psig) at feed side of the membrane = 14.7 psig.

$P_{ambient}$ = Ambient pressure (kPa) =101.6 kPa

$CO_2(R)_{G.C}$ = CO_2 mole fraction at retentate side from G.C analysis (**Figure A2.1**)

$CO_2(F)_{G.C}$ = CO_2 mole fraction at feed side from G.C analysis (**Figure A2.1**)

H_2O_F = Feed side water flow rate (ml/min) = 0.03 ml /min

H_2O_S = Sweep side water flow rate (ml/min) = 0.05 ml/min

$H_2O_{distribution}$ = Total water distribution =

$$\frac{\text{Retentate } side\ water\ knockout\ volume}{\text{Retentate } side\ water\ knockout\ volume + Sweep\ side\ water\ knockout\ volume} = 0.24$$

η_R = 1.84×10^{-3} mole /min

η_P = 7.65×10^{-5} mol/min

CO_2 mole fraction = 0.2

p_{CO_2} (R,psi) = CO_2 partial pressure at retentate side = 3.04 psi

p_{CO_2} (P, psi) = CO_2 partial pressure at permeate side =

$$[BP_S\,(\text{psig}) + P_{ambient}\,(\text{kPa}) \times \frac{14.7}{101.325}] \times \frac{[(\eta_{Ar} + 0.5 \times \eta_P)(mol/min) \times CO_2\ mole\ fraction \times 0.5 \times \frac{CO_2(P)_{G.C}}{CO_2(F)_{G.C}}]}{[\eta_{Ar} + 0.5 \times \eta_P](mol/min) + \frac{[(0.5 \times H_2O_S) + (0.5 \times (1 - H_2O_{distribution}) \times (H_2O_F + H_2O_S))]\,(ml/min)}{18\,(ml/mol)}}$$

BP_S = Back pressure at Sweep side of the membrane module = 4 psig.

$P_{ambient}$ = Ambient pressure (kPa) =101.6 k Pa

$CO_2(P)_{G.C}$ = CO_2 mole fraction at permeate side from G.C analysis (**Figure A2.1**)

$CO_2(R)_{G.C}$ = CO_2 mole fraction at feed side from G.C analysis (**Figure A2.1**)

H_2O_F = Feed side water flow rate (ml/min) = 0.03 ml /min

H_2O_S = Sweep side water flow rate (ml/min) = 0.05 ml/min

$H_2O_{distribution}$ = Total water distribution = 0.24

η_{Ar} = 1.75×10^{-3} mole /min

η_P = 7.65×10^{-5} mol/min

CO_2 mole fraction = 0.2

p_{CO_2} (P,psi) = CO_2 partial pressure at permeate side = 0.14 psi

p_{N_2}(R,psi) = N_2 partial pressure at retentate side =

$$[BP_F\,(\text{psig}) + P_{ambient}\,(\text{kPa}) \times \frac{14.7}{101.325}\,] \times$$

$$\times \frac{[\eta_R - 0.5 \times \eta_P]\,(mol/min) \times N_2\ mole\ fraction \times [0.5 + 0.5 \times \frac{N_2(R)_{G.C}}{N_2(F)_{G.C}}]}{[\eta_R - 0.5 \times \eta_P]\,(mol/min) + \frac{[(0.5 \times H_2O_F) + (0.5 \times H_2O_{distribution} \times (H_2O_F + H_2O_S))]\,(ml/min)}{18\,(ml/mol)}}$$

Where,

BP_F = Back pressure (psig) at feed side of the membrane module = 14.7 psig

$P_{ambient}$ = Ambient pressure (kPa) =101.6kPa

$N_2(R)_{G.C}$ = N_2 mole fraction at retentate side from G.C analysis (**Figure A2.1**)

$N_2(F)_{G.C}$= N_2 mole fraction at feed side from G.C analysis (**Figure A2.1**)

H_2O_F = Feed side water flow rate (ml/min) = 0.03 ml/min

H_2O_S = Sweep side water flow rate (ml/min) = 0.05 ml/min

$H_2O_{distribution}$= Total water distribution = 0.24

Molecular weight of water = 18 g/mol = 18 ml/min (if density of water is 1)

η_{Ar} = 1.75 × 10^{-3} mole /min

η_P = 7.65 × 10^{-5} mol/min

N_2 mole fraction = 0.8

p_{N_2}(R,psi) = N_2 partial pressure at retentate side = 13.6 psi

p_{N_2}(P,psi) = N_2 partial pressure at permeate side =

$$[BP_S\,(\text{psig}) + P_{ambient}\,(\text{kPa}) \times \frac{14.7}{101.325}] \times \frac{[\eta_{Ar} + 0.5 \times \eta_P](mol/min) \times N_2\ mole\ fraction \times 0.5 \times \frac{N_2(P)_{G.C}}{N_2(F)_{G.C}}]}{[\eta_{Ar} + 0.5 \times \eta_P](mol/min) + \frac{[(0.5 \times H_2O_S) + (0.5 \times (1 - H_2O_{distribution}) \times (H_2O_F + H_2O_S))]\,(ml/min)}{18\,(ml/mol)}}$$

Where,

BP_S = Back pressure (psig) at sweep side of the membrane module = 4 psig

$P_{ambient}$ = Ambient pressure (kPa) =101.6kPa

$N_2(P)_{G.C}$ = N_2 mole fraction at permeate side from G.C analysis (**Figure A2.1**)

$N_2(F)_{G.C}$ = N_2 mole fraction at feed side from G.C analysis (**Figure A2.1**)

H_2O_F = Feed side water flow rate (ml/min) = 0.03 ml/min

H_2O_S = Sweep side water flow rate (ml/min) = 0.05 ml/min

$H_2O_{distribution}$ = Total water distribution = 0.24

η_{Ar} = 1.75 × 10^{-3} mol /min

η_P = 7.65 × 10^{-5} mol/min

N_2 mole fraction = 0.8

p_{N_2}(P,psi)= **N_2 partial pressure at permeate side = 0.0027 psi**

Volumetric flow rates calculations:

V_{CO_2}(cm^3/sec) = permeate side volumetric flow rate of CO_2 at STP =

$$\frac{\eta_{Ar} \times CO_2(P)_{G.C} \times CO_2\ mole\ fraction \times 8.314 \times 273.15 \times 1000000}{CO_2(F)_{G.C} \times 101325 \times 60 \times [1 - (CO_2\ mol\ fraction \times \frac{CO_2(P)_{G.C}}{CO_2(F)_{G.C}}) - (N_2\ mol\ fraction \times \frac{N_2(P)_{G.C}}{N_2(F)_{G.C}})]}$$

$V_{CO_2}(cm^3/sec)$ = permeate volumetric gas flow rate of CO_2 = 2.80 × $10^{-02}$$cm^3$/sec

$V_{N_2}(cm^3/sec)$ = permeate volumetric gas flow rate of N_2=

$$\frac{\eta_{Ar} \times N_2(P)_{G.C} \times N_2\ mole\ fraction \times 8.314 \times 273.15 \times 1000000}{N_2(F)_{G.C} \times 101325 \times 60 \times [1 - (CO_2\ mol\ fraction \times \frac{CO_2(P)_{G.C}}{CO_2(F)_{G.C}}) - (N_2\ mol\ fraction \times \frac{N_2(P)_{G.C}}{N_2(F)_{G.C}})]}$$

V_{N_2}(cm^3/sec) = permeate volumetric gas flow rate of N_2= 5.48 ×$10^{-04}$$cm^3$/sec

CO_2 Flux (10^{-6} cm^3(STP)/cm^2sec), CO_2 Permeability (Barrer), CO_2 Permeance (GPU) and CO_2/NO_2 Selectivity

$(\Delta p)_{CO_2}$ at psi = partial pressure difference at psi = p_{CO_2}(R, psi) - p_{CO_2} (P, psi)

$(\Delta p)_{CO_2}$ at psi = 2.90 psi

$(\Delta p)_{CO_2}$ at cmHg = partial pressure difference at cm Hg = $\frac{(\Delta p)_{CO_2}\ \text{at psi}}{14.7} \times 76$

$(\Delta p)_{CO_2}$ = 15.01 cm Hg

CO_2 flux = $\frac{V_{CO_2}\ cm^3/sec}{\text{area of membrane } (cm^2)}$

Where,

V_{CO_2} (cm^3/sec) = **2.80×10^{-02}** (cm^3/sec)

Area of membrane = 47.5 cm^2

CO_2 flux = 590 × 10^{-6} cm^3 (STP)/cm^2s

CO_2 permeability = $\frac{V_{CO_2}\ (cm^3/sec) \times \text{thickness(cm)}}{\text{area of membrane } (cm^2) \times (\Delta p)_{CO_2}\ \text{at cm Hg}}$

Where,

V_{CO_2} (cm^3/sec) **= 2.80 × 10^{-2}** cm^3/sec

Area of membrane = 47.5cm^2

Thickness = 0.00045 cm = 4.5 micron

$(\Delta p)_{CO_2}$ at cm Hg = 15.01 cm Hg

CO_2 Permeability = ~177 × 10^{-10} cm^3 (STP) cm/cm^2s cmHg = 177 Barrer

CO_2 permeance = $\frac{CO_2\ \text{Permeability}}{thickness}$ = $\frac{177\ (Barrer)}{4.5}$ = ~ 39 GPU

1 GPU = 10^{-6} cm^3 (STP)/cm^2s cmHg

$\frac{CO_2}{N_2}$ Selectivity = $\frac{\frac{CO_2\ (P)_{G.C.}}{N_2\ (P)_{G.C.}}}{\frac{CO_2\ (R)_{G.C.}}{N_2\ (R)_{G.C.}}} = \frac{\frac{0.0409}{0.0008}}{\frac{0.1637}{0.8345}} = 260$

N_2 Flux (10^{-6} cm^3 (STP)/cm^2sec), N_2 Permeability (Barrer), and N_2 Permeance (GPU).

$(\Delta p)_{N_2}$ (psi) = partial pressure difference at psi = p_{N_2}(R, psi) - p_{N_2} (P, psi)

$(\Delta p)_{CO_2}$ (psi) = 13.67 psi

$(\Delta p)_{N_2}$ (cm Hg) = partial pressure difference at cm Hg = $\frac{(\Delta p)_{N_2} \text{at psi}}{14.7} \times 76$

$(\Delta p)_{N_2}$ = 70.71 cm Hg

N_2 flux = $\frac{V_{N_2}\ (cm^3/\text{sec})}{area\ of\ membrane\ (cm^2)}$

V_{N_2} (cm^3/sec) = 5.48 ×10^{-04} (cm^3/sec)

Area of membrane = 47.5 cm^2

N_2 flux = ~ 11 × 10^{-6} cm^3(STP)/cm^2s

N_2 permeability = $\frac{V_{N_2}\ (\text{cm}^3/\text{sec}) \times \text{thickness(cm)}}{\text{area of membrane } (\text{cm}^2) \times (\Delta p)_{N_2} \text{ at cm Hg}}$

Where

V_{N_2} (cm^3/sec) = 5.48 × 10^{-04} (cm^3/sec)

Area of membrane = 47.5 cm^2

Thickness = 0.00045cm = 4.5 micron

$(\Delta p)_{N_2}$ at cm Hg = 70.71 cm Hg

N_2 Permeability = 0.7 × 10^{-10} cm^3 (STP) cm/cm^2s cmHg = 0.7 Barrer

N_2 permeance = $\frac{N_2 \text{ Permeability}}{\text{thickness}}$ = $\frac{0.7}{4.5}$ = **0.16 GPU**

1 GPU = 10^{-6} cm^3(STP)/cm^2s cmHg

Similarly, the same calculation procedures were followed for ternary gas mixture (CO_2/N_2/H_2).

A2.2 Gas Chromatography Operating Protocol

Here, we have used Varian-450 G.C for all the permeation experiments. The detail G.C operating protocols are mentioned below:

Injector programing: Heater (ON) at 120 °C

Tine (min)	Split state	Split ratio
Initial	ON	1
0.00	ON	1
1.00	ON	1

Oven programing:

Column oven (ON) and Rear oven (ON) at 100 °C

Rate (°C /**min)**	**Temperature** (°C**)**	**Time (min)**	**Total time (min)**
Initial	40	2.00	2.00
10	70	5.00	10.00
			Total time 10.00

Column pneumatics: (pressure program)

Rate (psi/min)	Pressure (psi)	Time (min)	Total time (min)
Initial	15	10.00	10.00
			Total time 10.00

Detector (TCD) programing:

Heater (ON) at 95 °C

Electronics (ON)

Filament temperature at 235 °C

Filament temperature limit at 390 °C

TCD event table

Time (min)	Range	Auto zero	Polarity
Initial	0.05	YES	Negative

Gas sampling valve (GSV) programing:

Time (min)	Gas sampling valve
Initial	Fill
0.02	Inject

A2.3 Detail Purity Percentage of all Calibration Gases

Name	Purity compositions
4 % CO_2 + 4 % N_2, balance Argon	CO_2 (99.999 %), N_2 (99.999 %), Ar (99.999 %), H_2O (< 2 ppm) and CO (< 0.5 ppm)
8 % CO_2 + 8 % N_2, balance Argon	CO_2 (99.999 %), N_2 (99.999 %), Ar (99.999 %), H_2O (< 2 ppm) and CO (< 0.5 ppm)
12 % CO_2 + 12 % N_2, balance Argon	CO_2 (99.999 %), N_2 (99.999), Ar (99.999 %), H_2O (< 2 ppm) and CO (< 0.5 ppm)
20 % CO_2, balance N_2	CO_2 (99.999 %), N_2 (99.999 %), H_2O (< 2 ppm) and CO (< 0.5 ppm)
40 % CO_2, balance N_2	CO_2 (99.999 %), N_2 (99.999 %), H_2O (< 2 ppm) and CO (< 0.5 ppm)
Pure CO_2	CO_2 (99.999 %)
Pure N_2	N_2 (99.999 %)
Pure H_2	H_2 (99.999 %)

Feed side

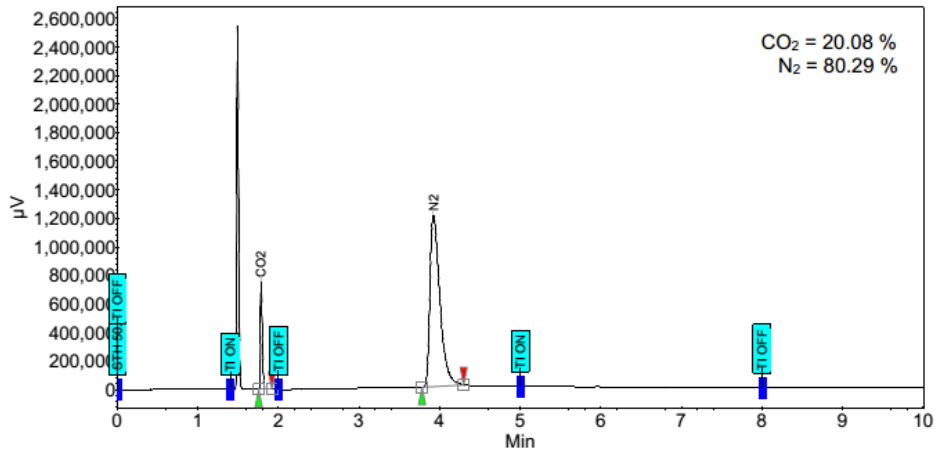

Retentate side

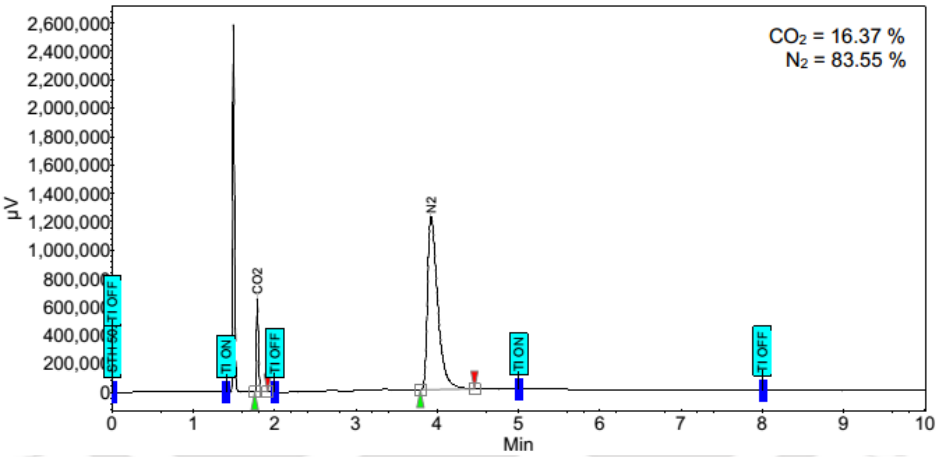

Permeate side

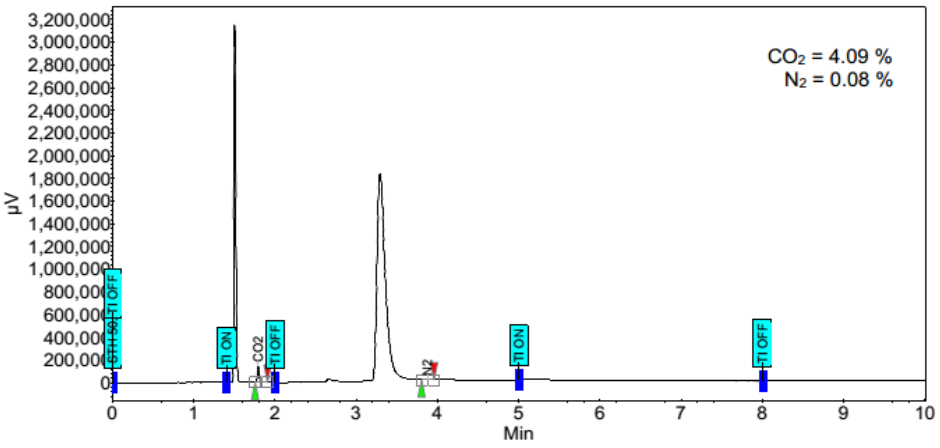

Figure A2.1 GC peaks of PAA 30 membrane at 90 °C and absolute pressure = 2/1.21 bar (feed/sweep) having water flow rate of 0.03/0.05 ml/min (feed/sweep).

Reference (Appendix 2)

Mondal, A. CO_2-Selective Thin-Film Polymer Composite Membranes: Improvement of Thermal Stability and Role of Amine Carriers. PhD dissertation, Indian Institute of Technology, Guwahati, 2014.

Research Output

Journal publications

1. **B. Prasad**, B. Mandal. "CO_2 separation performance by chitosan / tetraethylenepentamine / poly (ether sulfone) composite membrane", *Journal of Applied Polymer Science***,** 134 (2017) 45206. **(Wiley, Impact Factor 1.90)**.

2. **B. Prasad**, B. Mandal. "Preparation and characterization of CO_2-selective facilitated transport membrane composed of chitosan and poly(allylamine) blend for CO_2/N_2 separation", *Journal of Industrial and Engineering Chemistry***,** *66 (2018) 419-429*. **(Elsevier, Impact Factor 4.84)**.

3. **B. Prasad**, B. Mandal. "Moisture responsive and CO_2 selective biopolymer membrane containing silk fibroin as a green carrier for facilitated transport of CO_2", *Journal of Membrane Science,* 550 (2018) 416–426. **(Elsevier, Impact Factor 6.58)**.

4. **B. Prasad**, B. Mandal. "Graphene incorporated bio-polymeric mixed matrix membrane for enhanced CO_2 separation by regulating the support pore filling," *ACS Applied Materials and Interfaces, 10, (2018) 27810-27820***. (ACS, Impact Factor 8.01)**.

5. **B. Prasad**, B. Mandal. "Enhanced CO_2 separation by membrane prepared from fixed natural carriers of sericin and Na_2CO_3". (**To be communicated**).

Research Output

National and International Conference:

1. **B. Prasad**, B. Mandal, (2018). "Facilitated transport of CO_2 in novel biopolymer bend membrane". *Advances in Sustainable Polymers (ASP 17)*, Jan. 8-11, IIT Guwahati, Assam, India.

2. **B. Prasad**, B. Mandal, (2017). "CO_2 selective mixed matrix membrane for the application of flue gas separation". *International Conference on Advanced Nanomaterials and Nanotechnology 2017 (ICANN-2017),* Dec. 18-21, IIT Guwahati, Assam, India.

3. **B. Prasad**, B. Mandal, (2017). "CO_2 separation study using polymeric composite membrane from CO_2/N_2 gas mixture". *International Conference on Sophisticated Instruments in Modern Research (ICSIMR 2017),* Jun. 30- Jul.1, CIF, IIT Guwahati, Assam, India.

4. **B. Prasad**, R. Borgohain, B. Mridusmita, B. Mandal, (2016). "Chitosan/amine blend /poly(ether sulfone) composite membrane for CO_2 separation from CO_2/N_2 mixture gas at higher temperature". *The Indian Chemical Engineering Congress (CHEMCON 2016),* Dec. 27-30, Chennai, India.

5. **B. Prasad**, R. Borgohain, B. Mridusmita, B. Mandal, (2016). "Novel amine/chitosan thin-film composite membrane for CO_2 separation from flue gas". *Advances in Sustainable Polymers 2016 (ASP 16)*, Aug. 4-6, Kyoto Institute of Technology (KIT), Japan.

6. **B. Prasad**, H. Kalita, B. Mandal, (2015). "Synthesis and characterization of thermally stable bio-polymer membrane for CO_2 separation**".** *The Indian Chemical Engineering Congress (CHEMCON 2015)*, Dec. 27-30, IIT Guwahati, India.

Awards and Achievements

1. **Best poster award,** *International Conference on Sophisticated Instruments in Modern Research* (*ICSIMR 2017*), Jun. 30- Jul.1, 2017, CIF, IIT Guwahati, Assam, India.

2. **Best poster awards (3rd position**), *The Indian Chemical Engineering Congress (CHEMCON 2016)*, Dec. 27-30, 2016, Chennai, India.

3. **Best oral presentation award,** *Research Conclave* (RC'18), 8-11th March, 2018, IIT Guwahati, Assam, India.

Front Page of the Papers Published in Various Reputed International Journals

JOURNAL OF Applied Polymer SCIENCE

CO_2 separation performance by chitosan/tetraethylenepentamine/poly(ether sulfone) composite membrane

Babul Prasad, Bishnupada Mandal
Department of Chemical Engineering, Indian Institute of Technology Guwahati, Guwahati Assam 781039, India
Correspondence to: B. Mandal (E-mail: bpmandal@iitg.ernet.in)

ABSTRACT: CO_2 separation from CO_2/N_2 (20:80) gas mixture has been demonstrated by tetraethylenepentamine blended with chitosan (CS-TEPA) membrane. Optimization of CS and TEPA weight ratio were carried out based on characterization details involving thermogravimetric analysis, Fourier transform infrared spectroscopy, X-ray diffraction, atomic force microscope, and field emission scanning electron microscope. Effects of water flow rate, pressure, and temperature were concurrently studied on CS-TEPA membranes through gas permeation. Almost twofold increase in CO_2 permeance (24.7 GPU) was detected in CS blend with 30% (w/w) of TEPA (CS70) as compared to pure CS membrane (12.5 GPU). CS70 yielded CO_2/N_2 selectivity of 80 whereas CS demonstrated a maximum of 54 at 90 °C. The membrane also exhibited improved stability at temperatures less than 120 °C which was evident from TGA isotherm trace. The proposed composite membrane can be a promising candidate for flue gas separation. © 2017 Wiley Periodicals, Inc. J. Appl. Polym. Sci. **2017**, *134*, 45206.

KEYWORDS: chitosan; CO_2/N_2 separation; composite membrane; flue gas; TEPA

Received 23 January 2017; accepted 10 April 2017
DOI: 10.1002/app.45206

INTRODUCTION

The CO_2 concentration in the atmosphere is increasing rapidly due to the human activity and witnessed 2 ppmv (parts per million by volume) increase per year in last decade, which has a significant effect on climate change across the world.[1,2] If appropriate measures are not taken at this crucial time, global CO_2 concentration will reach above 750 ppmv by 2100.[3] The contribution of CO_2 to world's annual emission of greenhouse gases is the maximum. Industry, transport, residential, natural gas processing, and biogas from anaerobic digestion are the primary sources of CO_2 emission. But flue gases from coal-fired power stations and natural gas processing, have become a primary target for reduction.[4] Adsorption, absorption, and cryogenic distillation are commonly used technology for CO_2 separation. However, research is oriented towards alternate technologies, which are energy efficient, cost-effective, having compact modular design and corrosion free. Amongst these, membrane technology is a preferred alternative for CO_2 separation because of their low cost and simple handling.

The separation of different gas mixtures have been investigated by polymeric membranes such as cellulose acetate,[5,6] polysulfone,[7] poly(arylene ether),[8] polyimides,[9] etc. These membranes suffer from truncated CO_2/N_2 separation factor, permeance, and some of these lack temperature stability. High gas permeance at high temperature reduces the cost of a membrane as it requires less membrane area to separate the same amount of gas while high selectivity increases the purity of the permeate gas. The membrane following solution-diffusion mechanism does not exhibit high permeance and selectivity. Hence, the membrane following facilitated transport mechanism is preferred due to high CO_2 permeance and selectivity.

Matsuyama *et al.*[10] studied CO_2/N_2 separation using poly(vinyl alcohol) blend with polyethyleneimine (PEI) at a CO_2 partial pressure of 0.065 bar and temperature of 25 °C. They achieved CO_2 permeability of 8.5×10^{-8} [cm^3 cm/(cm^2s cmHg)] with the CO_2/N_2 selectivity of 160. Similar facilitated transport of CO_2 on crosslinked poly(vinyl alcohol) blended with different amine for CO_2/N_2 separation at high temperature was reported previously in our lab by Mondal and Mandal.[11–13] Apart from poly(vinyl alcohol) blend membrane, another thermally stable biopolymer, chitosan (CS) has received attention of the researchers for CO_2 separation from flue gases.[14–23] Xiao *et al.*[14] studied the pure gas permeation of CO_2 and N_2 on CS membranes crosslinked with trimesoyl chloride and reported ideal separation factor of 42 with the CO_2 permeability of 163 Barrer at room temperature. Bae *et al.*[15] observed high CO_2 as well as N_2 sorption in swelled CS membrane than dry membrane due to plasticization effect. El-Azzami and Grulke[16] used CS for facilitated transport of CO_2 from ternary gas mixture (CO_2 10%, H_2 10%, and N_2 80%). They reported CO_2/H_2 and

Journal of Industrial and Engineering Chemistry 66 (2018) 419–429

Contents lists available at ScienceDirect

Journal of Industrial and Engineering Chemistry

journal homepage: www.elsevier.com/locate/jiec

Preparation and characterization of CO_2-selective facilitated transport membrane composed of chitosan and poly(allylamine) blend for CO_2/N_2 separation

Babul Prasad, Bishnupada Mandal*

Department of Chemical Engineering, Indian Institute of Technology Guwahati, Guwahati 781039, Assam, India

ARTICLE INFO

Article history:
Received 22 April 2018
Received in revised form 7 June 2018
Accepted 8 June 2018
Available online 18 June 2018

Keywords:
Chitosan
Membrane
Gas separation
PAA
Flue gas

ABSTRACT

This study involves the addition of poly(allylamine) (PAA) with chitosan (CS) for facilitated CO_2 transport. Detailed characterizations of the membranes including advance microscopic analysis, thermal stability, stiffness, etc. were investigated. The CO_2 separation studies from binary gas mixture indicated the superior CO_2 permeance and CO_2/N_2 selectivity of the PAA30 (70 wt% CS + 30 wt% PAA) membrane at 90 °C and feed absolute pressure of 2 bar. Further, CO_2 separation performance of PAA30 was gauged under varying conditions. The performance above the Robeson upper bound plot, displayed the potential of the PAA30 membrane for industrial flue gas separation.

Introduction

The energy requirement across the world is largely fulfilled by burning of coal which impacts the environment significantly. One of the major effects observed due to the emission of CO_2 is the global warming issue [1]. The ideal way to control the CO_2 emission is the separation and capture of CO_2 from various sources like fossil fuel combustion, coal gasification, and natural gas exploration. The CO_2 separation using membrane technology has received considerable attention over other technologies due to energy efficiency, low cost and corrosion free as compared to adsorption or absorption process [2]. Further, CO_2 separation by membrane offers other advantages like modular configuration, system compactness, simplicity and operational flexibility [3].

Most of the CO_2 separation membranes following facilitated transport involve the polymer poly(vinyl alcohol) (PVA) synthesis and thereof. But the major drawback of PVA is that it dissolves in water at temperatures above 70 °C [4]. Hence, crosslinking is a prerequisite to enable thermal stability of PVA based polymers that makes the synthesis process complex and time consuming. Polymer blending for CO_2 separation, instead of synthesis of new materials can be adopted owing to its simple and cost effective features. Chitosan (CS) is a biopolymer having amine group in its structure (Fig. 1a), is thermally stable without any crosslinking, possess good film forming ability and permits facilitated transport for CO_2 separation [5]. Chitosan membranes in a blend with other polymers or amines have been utilized for separation of CO_2 from pure gas [6], binary gas [7] and ternary gas mixtures [8]. El-Azzami and Grulke worked on pure CS and studied the swelling effect on CO_2 permeation using ternary gas mixture in the temperature of 25–150 °C and pressure of 1.5–5 atm [8]. They further used blend arginine salt as a mobile carrier with CS and observed a dramatic improvement in CO_2 permeability and selectivity [9]. However, in terms of carrier stability, fixed carriers are preferred over mobile carriers as covalently bonded fixed carriers prevents loss by leaching [10]. In our previous work, we observed that increasing amine content by adding tetraethylenepentamine (TEPA) to CS, increases the CO_2 separation performance than the pure CS alone, using solution casting technique [5]. The amine carrier serve the facilitated transport mechanism by reacting with CO_2 that can be described by the following Eqs. (1)–(5). CO_2 reacts with primary or secondary amines to form zwitterions as an intermediate and then the zwitterion is deprotonated by bases such as, the amine itself and H_2O to form the carbamate ion [26,27].

$$CO_2 + RNH_2 \leftrightarrow RNH_2^+COO^- \quad (1)$$

$$RNH_2^+COO^- + RNH_2 \leftrightarrow RNHCOO^- + RNH_3^+ \quad (2)$$

* Corresponding author.
E-mail addresses: p.babul@iitg.ernet.in (B. Prasad), bpmandal@iitg.ernet.in (B. Mandal).

https://doi.org/10.1016/j.jiec.2018.06.009
1226-086X/

Journal of Membrane Science 550 (2018) 416–426

Contents lists available at ScienceDirect

Journal of Membrane Science

journal homepage: www.elsevier.com/locate/memsci

Moisture responsive and CO_2 selective biopolymer membrane containing silk fibroin as a green carrier for facilitated transport of CO_2

Babul Prasad, Bishnupada Mandal*

Department of Chemical Engineering, Indian Institute of Technology Guwahati, Guwahati 781039, Assam, India

ARTICLE INFO

Keywords:
CO_2 separation
Blend membrane
Chitosan
Silk fibroin
Flue and syngas

ABSTRACT

The research quest in carbon dioxide (CO_2) separation technology through the polymeric membrane is intensive at this time of energy and environmental crisis. But, the pursuit of membranes with high selectivity and flux without trading it off for stability, still exists as a challenge. We report a novel membrane prepared by rational blending of two biopolymers: chitosan (CS) that acts as a matrix and silk fibroin (SF) that aids chitosan as a carrier for facilitated transport. The separation of binary gas mixture (CO_2/N_2) has been studied at temperature, feed absolute pressure and sweep water flow rate ranging from 60 to 120 °C, 2 to 5.93 bar and 0.01 to 0.07 ml/min, respectively. The optimum CO_2 permeance of 140 GPU and CO_2/N_2 selectivity of 103 for binary gas were observed at 90 °C and 0.05 ml/min of sweep water flow rate for the membrane containing 45 wt% of SF in blend with CS (SF45). The SF45 composite membrane exhibited CO_2 permeance of 123 GPU and selectivity of 93 and 60 for CO_2/N_2 and CO_2/H_2 respectively, in case of ternary gas mixtures ($CO_2/N_2/H_2$) at the similar operating conditions. The appreciable CO_2 separation performance tunable with temperature and moisture, displayed unprecedented stability for 30 days.

1. Introduction

Inevitable utilization of fossil fuel reserves exploited for economic growth is a pertinent issue with implications in environmental pollution and surge in carbon dioxide (CO_2) content in the atmosphere [1]. Various technologies for CO_2 separation are used among which, membrane technology has been accentuated in the current literature owing to energy efficiency, cost-effective and corrosion free compact modular design [2]. Various polymeric membranes such as cellulose acetate [3], polysulfone [4], poly(arylene ether) [5], polyimides [6] etc. have been studied for CO_2 separation from different gas mixtures. The performance of these membranes are limited by poor CO_2/N_2 separation factor, low permeance, and long-term stability [7]. High gas permeance diminishes the cost of the membrane and high selectivity intensifies the purity of the permeate gas. Membranes following solution-diffusion mechanism do not exhibit high permeance and selectivity. Hence, facilitated transport membranes prove to be the promising candidates for CO_2 separation [8].

Biopolymers are much sought-after materials because of their limited toxicity and biocompatibility. One such thermally stable biopolymer is chitosan (CS). CS is a semi-crystalline polymer having one hydroxyl group and one amine group present in its structure (Fig. 1a). These amine groups are responsible for the facilitated transport of CO_2. Swelled CS membranes exhibit higher CO_2 permeance than the CS membranes in dry conditions [9–11]. Various attempts have been made to improve the CO_2 permeance through CS membranes by incorporation of carriers such as triethanolamine [12], crosslinking of chitosan with trimesoyl chloride [13], blending with polymers like Pebax® [14] and through mixed matrix membranes using organic fillers [15–17]. However, the lack of steady performance with time is often mentioned as a major bottleneck of facilitated transport membrane, which is presumably due to loss of carrier [1].

To employ the membranes for practical use in CO_2 separation, fabrication of membranes with long-term stability, simultaneously with high permeance through eco-friendly and cost-effective materials is of utmost concern. The separation of CO_2/N_2 is a post-combustion step, to eliminate CO_2 from flue gases and the separation of H_2 from CO_2/H_2 is a pre-combustion processing from syngas [18]. Removal of CO_2 from syngas mixtures improves the H_2 purity that in turn enhances the fuel cell efficiency and curtails the pollution [19]. CO_2 separation from gas mixtures also becomes indispensable during fuel cell operation, as presence of CO_2 can lead to undesirable formation of CO via reverse water gas shift reaction that acts as a poison to platinum catalyst [19]. Additionally, during the production of carbon black by post-combustion method, tail gas is formed with following composition in vol%: 5.3% CO_2, 16.4% H_2, 60.5% N_2 and 17.9% CO [20]. To analyze the CO_2

* Corresponding author.
E-mail addresses: p.babul@iitg.ernet.in (B. Prasad), bpmandal@iitg.ernet.in (B. Mandal).

https://doi.org/10.1016/j.memsci.2017.12.061
Received 17 November 2017; Received in revised form 19 December 2017; Accepted 20 December 2017
Available online 21 December 2017

TH-2140_136107008

ACS APPLIED MATERIALS & INTERFACES

Research Article

Cite This: ACS Appl. Mater. Interfaces 2018, 10, 27810−27820

www.acsami.org

Graphene-Incorporated Biopolymeric Mixed-Matrix Membrane for Enhanced CO_2 Separation by Regulating the Support Pore Filling

Babul Prasad and Bishnupada Mandal*

Department of Chemical Engineering, Indian Institute of Technology Guwahati, Guwahati ,781039 Assam, India

Supporting Information

ABSTRACT: The CO_2 separation performance by a membrane is influenced essentially by film thickness, temperature, moisture, and pressure. Pore formation on the active layer and pore clogging of the membrane support are critical factors that impedes the CO_2 separation performance. This study involves the development of a novel nanocomposite membrane (CS/SF/GNP) consisting of chitosan (CS), silk fibroin (SF), and graphene nanoparticles (GNP). The CS acts as the matrix, SF contributes to the CO_2 facilitated transport by its inherent amines as carriers, and GNP helped in counteracting the support pore blockage during the gas separation test. The positive effect of GNP in the CS/SF/GNP was further apparent in the CO_2 permeance inconsequential drop of ∼7% during the initial 12 h in the presence of moisture and pressure. The detailed characterizations including FESEM, AFM, and swelling were performed for the membranes. The effect of sweep water flow rate, temperature, and feed absolute pressure on CO_2 separation performance from binary gas were performed. The CS/SF/GNP membrane exhibited CO_2 permeance of 159 GPU and CO_2/N_2 selectivity of 93 at 90 °C and a feed absolute pressure of 2 bar having a sweep side water flow rate of 0.05 mL/min. Further, when CS/SF/GNP membrane was tested to separate CO_2 from ternary gas mixture ($CO_2/N_2/H_2$), it displayed excellent CO_2 permeance of 126 GPU and selectivity for CO_2/N_2 and CO_2/H_2 as 104 and 52, respectively. The TGA isotherm and XPS analysis of CS/SF/GNP membrane suggested a thermal stability of the prepared membrane that establishes its suitability for the gas permeation at different temperature.

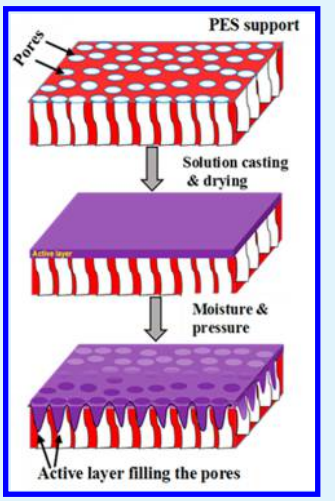

KEYWORDS: *CO_2 separation, membrane, biopolymer, chitosan, GNP*

1. INTRODUCTION

With the advent of increasing CO_2 levels in the atmosphere owing to global industrialization, the gas separation technique can be an adequate method due to its ease of processing and industrial application.[1] Use of polymeric membranes for CO_2 separation is preferred due to its desirable traits such as low cost and energy efficiency and being corrosion free.[2] A variety of polymers including cellulose acetate, polysulfone, poly(vinyl alcohol), and polyurethane have been explored for gas separation. However, some of these membranes lack thermal stability, long-term carrier stability, high permeance, and selectivity. Significant factors such as architectural structure, mechanical properties, and thickness of the active layer are to be attuned in order to acquire impressive CO_2 permeance and selectivity.

Chitosan (CS)-based membrane has received substantial consideration for CO_2 separation due to its low toxicity, temperature stability, and good film-forming abilities. Dry chitosan membranes exhibit lower permeabilities[3−6] than swollen chitosan membranes which demonstrated dramatically higher CO_2 permeabilities.[7−9] Ito et al.[7] observed that the humidifying feed gas increases CO_2 transport properties in the separation of CO_2/N_2 gas mixture through chitosan membranes. Bae et al.[8] reported that swelled chitosan membrane showed 15 times more CO_2 permeability and 11 times more N_2 permeability than the dry membrane. El-Azzami et al.[9] used CS membrane for facilitated transport of CO_2 for separation of the ternary gas mixture (CO_2 10%, H_2 10%, and N_2 80%). They reported CO_2/H_2 and CO_2/N_2 selectivities of 43 and 250, respectively, while CO_2 permeance was 7.4 GPU [1 GPU = 10^{-6} cm^3 (STP)/(cm^2 s·cmHg)] at 1.5 atm feed pressure and 110 °C temperature. Additionally, CS has been mixed with other synthetic amines like arginine salt[10] and triethanolamine (TEA)[11] to increase the concentration of carriers in the membranes. Further, chitosan membranes were prepared by cross-linking with 3-aminopropyltriethoxysilane (APTEOS),[12] trimesoyl chloride (TMC),[13] and an imidazole group[14] for CO_2 separation application. Also, chitosan was used in the blended form with other polymers like Pebax[15] and poly(vinyl alcohol) (PVA)[16] and showed a significant increase in CO_2 permeability. Hybrid ionic liquid-chitosan membrane has also been reported for CO_2 separation.[17] Water-soluble CS derivatives are also synthesized and used for CO_2 separation.[16,18−20] In spite of having CO_2 separation ability, most of the membranes are not commercially viable due to high cost, low permeance, and selectivity and most importantly their lack of long-term performance stability due to aging or leaching out of the carriers responsible for facilitated CO_2 transport. In addition to exploring new materials for a membrane, developing the requisite practical membrane geometry

Received: June 6, 2018
Accepted: July 30, 2018
Published: July 30, 2018

DOI: 10.1021/acsami.8b09377
ACS Appl. Mater. Interfaces 2018, 10, 27810−27820